OPPOSED JETS IN CROSSFLOW

by

Zafar Ayub Khan

Thesis submitted for the degree of
Doctor of Philosophy
in the Faculty of Engineering
University of London
and for the
Diploma of Membership
of Imperial College

Imperial College of Science and Technology
Mechanical Engineering Department

June 1982

To my parents, teachers and friends

ABSTRACT

This thesis describes measurements and calculations of rows of jets discharging normally into a confined crossflowing stream, and is relevant to the primary and dilution zones of gas turbine combustors.

Detailed turbulence and mean velocity measurements, obtained with Pitot-probes and a hot-wire anemometer, are presented for a single row of jets, rows of directly opposed and laterally staggered jets and single and opposed rows of jets with a downstream contraction. Measurements are also presented for the passive scalar field obtained by a helium trace concentration technique.

The single row of jets results showed that a jet-to-crossflow velocity ratio of 2, with a central jet asymmetry corresponding to the dimensional tolerances of gas turbine combustors, resulted in asymmetry of the velocity field; as the velocity ratio was decreased the velocity field asymmetry became less severe. With opposed rows of jets and pitch-to-diameter ratio of 2, the central jet asymmetry for one row of jets again resulted in severe asymmetries of the velocity field. For a pitch-to-diameter ratio of 4, however, the geometric asymmetry effects were less important. However, even with the jets symmetrically arranged, the opposing jets impinged and bifurcated to give large asymmetries.

A numerical scheme which solves the transport equations for velocity, pressure, turbulence kinetic energy and energy dissipation rate with a finite-difference formulation was used to calculate the flow downstream of a row of jets in a crossflow. The accuracy of the calculation scheme and the turbulence model used are discussed and the cause of discrepancies analysed. The predicted results gave

generally good qualitative agreement with the measurements; quantitative discrepancies exist and were probably due more to numerical than turbulence model errors.

ACKNOWLEDGEMENTS

There are many people who have helped me in the realisation of this thesis, and it gives me pleasure to acknowledge this.

I wish to acknowledge with gratitude, the guidance, valuable criticism and sound advice provided by my Supervisor, Prof. J. H. Whitelaw. His constant encouragement and support during some very unsettled times was invaluable in the presentation of this thesis.

I am indebted to Dr. J. J. McGuirk for his freely given help and advice, particularly with the computational aspects of the work.

Mr. K. Atkinson, Mr. I. Demirdzic, Dr. W. P. Jones, Dr. A. M. Taylor and Dr. N. Vlachos deserve a special mention for their many helpful discussions. I have also benefitted from my association with all my colleagues, particularly Mr. D. Arcoumanis, Mr. A. Bicen, Ms. G. Carvahlo, Ms. M. Founti, Dr. A. Green, Dr. Y. Levy, Mr. B. Thompson and Dr. M. Yianneskis.

My thanks go to Mr. A. Sotheran of Roll-Royce Ltd., Bristol, Mr. D. C. Dryburgh of Rolls-Royce Ltd., Derby and Mr. J. Bullard of the National Gas Turbine Establishment for their continued interest and advice throughout the course of research.

The technical staff of the Fluids section, Mr. G. Tindall and Ms. E. Archer have also been most helpful.

Dr. R. B. Dean and Dr. L. R. Wootton deserve a mention for their interest and encouragement during the completion of the thesis.

I thank Mrs. S. Gravestock for her speedy and efficient typing.

Finally, I gratefully acknowledge the financial support provided by the Science Research Council.

CONTENTS

		Page
ABSTRACT		3
ACKNOWLEDGEMENTS		5
CONTENTS		6
LIST OF TABLES		9
LIST OF FIGURES		10
NOMENCLATURE		16
CHAPTER 1: INTRODUCTION TO THE THESIS		20
1.1	The flows considered: Background and motivation	21
1.2	Previous related studies	24
	1.2.1 Plane jet in crossflow	25
	1.2.2 Round jets in crossflow	29
1.3	Objectives of present study	36
1.4	Outline of thesis	38
CHAPTER 2: EXPERIMENTAL CONFIGURATIONS AND MEASUREMENT TECHNIQUES		47
2.1	Introductory remarks	47
2.2	Description of the apparatus	48
	2.2.1 The mainstream air supply	48
	2.2.2 The jet air supply	48
	2.2.3 The test section and related details	49
2.3	Measurement techniques	52
	2.3.1 Mean velocity measurements	52

Page

2.3.2 Turbulence measurements 53

Hot-wire evaluation equations 53

Instrumentation 54

Experimental procedure 55

2.3.3 Concentration measurements 57

2.4 Accuracy of measurements 58

Mean velocity 58

Turbulence measurements 59

Concentration measurements 60

CHAPTER 3: PRESENTATION AND DISCUSSION OF EXPERIMENTAL RESULTS 61

3.1 Introduction 61

3.2 Single row of jets 64

3.3 Single row with a geometrical eccentricity 68

3.4 Directly opposed row of jets 70

3.5 Directly opposed and staggered rows of jets with a geometrical eccentricity 73

3.5.1 Mean velocity and scalar concentration characteristics 73

Pitch-to-diameter ratio of 2 75

Pitch-to-diameter ratio of 4 79

3.5.2 Turbulence characteristics 82

3.6 Row of jets in a crossflow with a downstream contraction 86

3.7 Conclusions and practical implications of the experimental investigation 89

Page

CHAPTER 4: CALCULATION OF JETS IN CROSSFLOW 93

4.1 Introduction 93

4.2 Calculation method 94

4.2.1 Equations to be solved 94

4.2.2 Turbulence models 95

The approach and choice of model 95

The k-ε turbulence model 98

4.2.3 The finite-difference method 102

4.2.4 Boundary conditions 104

4.2.5 Solution procedure 107

4.2.6 Accuracy of solution 109

4.3 Rows of jets in crossflow 110

4.3.1 Calculation details 111

Boundary conditions 111

Preliminary calculations 114

4.3.2 Comparison with measurements 117

4.3.3 Further calculations 120

4.4 Summary conclusions and general discussion 121

CHAPTER 5: CONCLUDING REMARKS 125

5.1 Experimental contribution 125

5.2 Theoretical contribution 128

REFERENCES 130

APPENDIX A 143

FIGURES 153

LIST OF TABLES

CHAPTER 1

Table 1.1 Experimental and Theoretical Investigations of a Plane Jet in Crossflow

Table 1.2 Experimental Investigation of Rows of Jets in Crossflow

Table 1.3 Theoretical Investigation of Round Jets in Crossflow

CHAPTER 2

CHAPTER 3

Table 3.1 Summary of Experimental Investigations

Table 3.2 Flow Conditions for the Measurements of Section 3.5

CHAPTER 4

Table 4.1 Values of Constants Appearing the the k-ε Turbulence Model

APPENDIX A

Table A1 Location of Domain Boundaries

Table A2 Variation of Recirculation Length with Grid Size

LIST OF FIGURES

CHAPTER 1

Figure 1.1 Apportioning the air flow

Figure 1.2 Schematic and co-ordinate system for plane (2D) jet in crossflow

CHAPTER 2

Figure 2.1 Schematic of wind tunnel

Figure 2.2 Working section and co-ordinate system for rows of jets in cross-flow

Figure 2.3 Schematic of opposed jets with a downstream contraction

Figure 2.4 Block diagram of data acquisition and processing arrangement

CHAPTER 3

Figure 3.1 Velocity and concentration profiles along centre-plane for pitch-to-diameter ratio (S/D) of 2 and duct height 4D

Figure 3.2 Velocity and concentration profiles along centre-plane for S/D of 2 and duct height 8D

Figure 3.3 Velocity and concentration profiles along centre-plane for S/D of 4 and duct height 4D

Figure 3.4 Velocity and concentration profiles along centre-plane for S/D of 4 and duct height 8D

Figure 3.5 Normalised velocity (U/U_∞) contours and concentration contours (θ/θ_j) at axial planes X/D = 4 and 8 for S/D of 2 and duct height 8D (central jet seeded)

Figure 3.6 Normalised velocity and concentration contours at axial planes X/D = 4 and 8 for S/D of 2 and duct height 4D

Figure 3.7 Normalised velocity and concentration contours at axial planes X/D = 4 and 8 for S/D of 4 and duct height 8D

Figure 3.8 Velocity and concentration contours at axial planes X/D = 4 and 8 for S/D of 4 and duct height 4D

Figure 3.9 Transverse velocity distributions at X/D = 6 for jets symmetrically arranged and jet-to-crossflow velocity ratios (V_j/U_∞); (a) 2.0, (b) 1.0, (c) 0.5

Figure 3.10 Concentration distributions at X/D = 6 with jets symmetric and velocity ratios (V_j/U_∞) of 2, 1 and 0.5 (central jet seeded only)

Figure 3.11 Transverse velocity distribution at X/D = 6 for V_j/U_∞ = 2.0 and central jet eccentric: (a) E/D = 0.1, (b) E/D = 0.25

Figure 3.12 Concentration distributions at X/D = 6 for V_j/U_∞ = 2.0 and central jet eccentric: (a) E/D = 0.1, (b) E/D = 0.25 (central jet seeded only)

Figure 3.13 Velocity distributions at X/D = 6 for V_j/U_∞ = 1.0 and 0.5 and central jet eccentricity of 0.1D and 0.25D

Figure 3.14 Concentration distributions at X/D = 6 for V_j/U_∞ = 1.0 and 0.5 and central jet eccentric E/D = 0.1 and 0.25 (central jet seeded)

Figure 3.15 Velocity and concentration profiles along centre-plane of duct with jets directly opposed and jets staggered by 1D for duct height 8D and S/D of 2 (central jet seeded)

Figure 3.16 Normalised contours of mean velocity and scalar concentration at axial planes X/D = 4 and 8 for S/D of 2, duct height 4D and V_j/U_∞ = 1.0

Figure 3.17 Normalised contours of velocity and concentration for S/D of 2, at axial planes X/D = 4 and 8, duct height 4D and V_j/U_∞ = 1.8

Figure 3.18 Normalised contours of mean velocity and scalar concentration for S/D of 4 at axial planes X/D = 4 and 8, duct height 4D and V_j/U_∞ = 1.8

Figure 3.19 Velocity distributions at X/D = 6 for directly opposed rows of jets with top central jet eccentricity E/D = 0, 0.1, 0.25, 0.5, S/D of 2 and V_j/U_∞ = 2.3

Figure 3.20 Velocity distributions at X/D = 6 for opposed rows of jets for S/D of 2 with floor jets staggered laterally by Z/D = 1 and central jet of top row (a) zero eccentricity and (b) E/D = 0.5

Figure 3.21 Velocity distributions at X/D = 6 for opposed rows of jets with S/D of 2 and ceiling jets staggered axially X/D = 1 (a) jets symmetric (b) central jet of top row E/D = 0.5

Figure 3.22 Concentration distributions at X/D = 6 for directly opposed jets with S/D = 2 and top central jet seeded only. (a) jets symmetric, (b) top central jet E/D = 0.25 (c) top central jet E/D = 0.5

Figure 3.23 Concentration distributions for opposed rows of jets with S/D of 2 and floor jets laterally staggered by Z/D = 1. Top central jet eccentricity E/D = 0.5 (top central jet seeded only)

Figure 3.24 Concentration distributions for opposed rows of jets with S/D = 2 and ceiling jets staggered axially by X/D = 1. Top central jet eccentricity E/D = 0.5 (top central jet seeded only)

Figure 3.25 Velocity distributions at X/D = 6 for directly opposed rows of jets with S/D of 4. (a) top central jet symmetric and (b) top central jet eccentricity E/D = 0.5

Figure 3.26 Velocity distributions at X/D = 6 for opposed rows of jets with S/D = 4 and floor jets staggered laterally by Z/D = 2 (a) top central jet symmetric, (b) top central jet eccentricity E/D = 0.5

Figure 3.27 Concentration distributions at X/D = 6 for directly opposed rows of jets with S/D of 4. Top central jet symmetric and eccentric, E/D = 0.5

Figure 3.28 Concentration distributions at X/D = 6 for opposed rows of jets with S/D of 4 and floor jets staggered laterally by Z/D = 2. (a) E/D = 0, (b) top central jet eccentricity E/D = 0.5

Figure 3.29 Axial mean velocity and turbulence intensity profiles along centre-plane for directly opposed jets with S/D of 2, H/D of 4 and V_j/U_∞ = 2.25

Figure 3.30 Normalised Reynolds-stress profiles at axial plane X/D = 6 for directly opposed jets and with top central jet eccentricity E = 0.5D for S/D of 2: V_j/U_∞ = 2.3. (a) Y/D = 3.0, (b) Y/D = 2.0, (c) Y/D = 3.0

Figure 3.31 Normalised Reynolds-stress profiles at axial plane X/D = 10 for directly opposed jets and with top central eccentricity E/D = 0.5 for S/D of 2: V_j/U_∞ = 2.3. (a) Y/D = 2.0, (b) Y/D = 1.0, (c) Y/D = 0.5

Figure 3.32 Normalised mean velocity and Reynolds-stress profiles at axial plane X/D = 6 for directly opposed jets with S/D of 2 and V_j/U_∞ = 1.5. (a) Y/D = 2.0, (b) Y/D = 1.0, (c) Y/D = 0.5

Figure 3.33 Normalised Reynolds-stress profiles at axial plane X/D = 6 for directly opposed jets and with top central jet eccentricity E/D = 0.5 for S/D of 4: V_j/U_∞ = 2.3. (a) Y/D = 3.0, (b) Y/D = 2.0

Figure 3.34 Normalised Reynolds-stress profiles at axial plane X/D = 6 for opposing row of jets with floor jets staggered laterally by Z/D = 2 and top central jet eccentricity E/D = 0.5 for S/D of 4: V_j/U_∞ = 2.3. (a) Y/D = 3.0, (b) Y/D = 2.0, (c) Y/D = 1.0

Figure 3.35 Normalised mean velocity and concentration contours at X/D = 6 for pitch-to-diameter ratios (S/D) of 2 and 4 and a downstream contraction with only floor jets blowing (floor central jet seeded only)

Figure 3.36 Normalised mean velocity and concentration contours at X/D = 6 for S/D of 2 and 4 and a downstream contraction with only ceiling jets blowing (top central jet seeded only)

Figure 3.37 Normalised mean velocity and concentration contours at X/D = 6 for directly opposed jets with S/D of 2 and a downstream contraction.

Figure 3.38 Normalised mean velocity and concentration contours at X/D = 6 for directly opposed jets with S/D of 4 and a downstream contraction (central floor jet seeded only)

Figure 3.39 Normalised mean velocity and concentration contours at X/D = 6 for the floor jets staggered laterally and S/D of 2 and 4 with a downstream contraction (floor central jet seeded only)

CHAPTER 4

Figure 4.1 Three-dimensional control volume

Figure 4.2 Jet exit velocity profile on centre-plane using constant total pressure condition

Figure 4.3 Tests for grid dependence. Centre-plane axial velocity profiles, S/D = 4, H/D = 4

Figure 4.4 Effect of boundary conditions at jet exit; axial velocity profiles on centre-plane for H/D = 4

Figure 4.5(a) Effect of boundary conditions at jet exit; axial velocity profiles on centre plane (Z/D = 0)

Figure 4.5(b) Effect of boundary conditions at jet exit; axial velocity profiles on mid-plane (Z/D = S/2)

Figure 4.6 Velocity profiles along centre-plane and mid-plane for duct height 4D and jet spacing 2D

Figure 4.7 Velocity profiles along centre-plane and mid-plane for duct height 4D and jet spacing 4D

Figure 4.8 Velocity profiles along centre-plane and mid-plane for duct height 3D and jet spacing 4D

Figure 4.9(a) Axial velocity profiles on centre-plane for blockage ratios of 4 and 2

Figure 4.9(b) Axial velocity profiles along Z/D = S/4 for blockage ratios of 4 and 2 with S/D = 4

Figure 4.9(c) Velocity contours at axial planes X/D = 4 and 8 for duct height 2D and S/D of 4

Figure 4.10(a) Axial velocity profiles on centre-plane for directly opposed rows of jets with H/D = 4, S/D = 4 and a single row of jets with H/D = 2 and S/D = 4

Figure 4.10(b) Axial velocity profiles along Z/D = S/4 for directly opposed rows of jets with H/D = 4, S/D = 4 and single row of jets with H/D = 2 and S/D = 4

NOMENCLATURE

Symbol	Meaning
A	Constant in King's law (Equation 2.1)
A	Area of control volume face
B	Constant in King's law (Equation 2.1)
b	Slot width
C	Scalar concentration
C_μ	
C_1	Constants in turbulence model
C_2	
D	Jet diameter
E	Jet eccentricity (Chapter 3)
E	Voltage fron hot-wire anemometer (Chapter 2)
E	Constant in "law of wall" (Chapter 4)
F	Weighting factor used in finite-difference equation
f	Under-relaxation factor
f_2	Function (Equation 1.2)
g	Mass flux into control volume across a face
H	Tunnel height
h	Pitch factor of hot wire
J	Jet-to-mainstream momentum ratio
k	Yaw factor of hot wire (Chapter 2)
k	Turbulent kinetic energy (Chapter 4)
L	Length of recirculation zone
ℓ	Local length scale
n	Constant in King's law (Equation 2.1)
P	Pressure
Pe	Local Peclet number

Symbol	Meaning
S	Sensitivity factor of hot-wire (Equation 2.2)
S_ϕ	Source term
S_p, S_u	Linearised source terms
S	Distance between adjacent jet centrelines
U_∞	Mainstream velocity
U^+	$U/(\tau_W/\rho)^{\frac{1}{2}}$ (Equation 4.17)
$\overline{U}$	Mean axial velocity
U_{eff}	Effective cooling velocity
U_I	Instantaneous velocity vector
U_n	Normal velocity component to hot wire
U_{n1}, U_{n2}	Orthogonal components of U_n
U_p	Axial velocity at near-wall node (Equation 4.19)
U_t	Tangential velocity component to hot wire
$\tilde{u}$	r.m.s. velocity
$\overline{V}$	Mean vertical velocity
V_j	Jet efflux velocity
$\tilde{v}$	r.m.s. velocity
$\overline{W}$	Mean lateral velocity
$\tilde{w}$	r.m.s. velocity
X,x	Axial ordinate
Y,y	Vertical ordinate
y^+	Characteristic parameter used in "law of wall"
Z,z	Lateral ordinate

Greek Symbol	Meaning
α	Angle between instantaneous velocity vector and normal to hot-wire
Γ	Exchange coefficient
δ	Distance between adjacent nodes
δ_{ij}	Kronecker delta function
Δ_x	Increment in axial direction
Δ_y	Increment in vertical direction
Δ_z	Increment in lateral direction
ε	Dissipation rate of kinetic energy
θ	Angle of inclination of jet (Chapter 1)
θ	Scalar concentration
κ	von Karman constant
μ_t	Isotropic eddy viscosity
ρ	Density
σ_ε	Constant Prandtl number in energy dissipation rate equation
σ_k	Constant Prandtl number in turbulence kinetic energy equation
τ_w	Wall shear stress
ϕ	Dependent variable

Subscript	Meaning
N,S,E,W,T,B	Nodal positions
eff	Effective value
i,j,k	Components of Cartesian tensor notation
j	Jet
new	New value of variable
old	Previous value
p	Wall adjacent node
u,v,w,p k,ε,ϕ	Notation for each variable
w	Wall

Superscript	
u,v,w,p k,ε,ϕ	Notation for each variable
*	Guessed value
'	Fluctuating value
-	Time averaged value
~	r.m.s. value

CHAPTER 1

INTRODUCTION TO THE THESIS

1.1 The Flow Considered: Background and Motivation

The research reported in this thesis is concerned with the mixing of a single or opposed rows of jet discharging normally into a confined cross-flowing stream.

Flow configurations consisting of single or multiple round jets discharging into cross-flowing streams are of interest because of their occurence in a multitude of engineering and environmental applications. When the jets discharge into a confined cross-flowing stream the practical relevance is to internal impingement cooling of turbine blades and to primary and dilution air jets in gas turbine combustion chambers, which are the emphases of the present study. The flow from jets discharging into an unconfined cross-stream is relevant to the dispersion of effluent from chimney stacks, cooling tower plumes and the jets of V/STOL aircraft in transition from vertical to forward flight.

In their application to primary and dilution zones of combustion chambers the outcome sought is of mixing the jet fluid rapidly and completely into the mainstream. In this effort, the cooler air jets are discharged radially into the combustion chamber through discrete circular holes in the chamber walls. In the primary zone*, near the head of the chamber, it is usual that the jets penetrate to the axis

---

* The various zones of the combustion chamber referred to in this thesis are illustrated by, for example, Poyser and Moxon (1969).

of the combustor, thereby locating the downstream end of the recirculation region which is used to anchor the flame. Some of the primary jet air travels upstream. The recirculation region so created acts to stabilise the flame by decreasing the velocity and introducing hot reaction products to form a source of continuous ignition. An additional advantage resulting from these jets is in blowing away from the chamber walls, and into the flame zone, fuel which runs along them and would otherwise be exhausted unburnt from the chamber. This is, clearly, a desirable outcome and is likely to result in increased combustion efficiency and a reduction in pollutant and smoke emissions. Further downstream, in the dilution zone of the combustion chamber, the purpose of the jets, arranged around the circumference, is to dilute the hot combustion products in such a way as to create a circumferentially uniform and acceptably low gas temperature at the exit of the chamber. This is of prime significance, both for the performance of the turbine and the expected life of the nozzle guide vanes and turbine blades.

The air supplied to the combustion chamber is, clearly, limited by design considerations of the engine and is apportioned between the various stages (see figure 1.1, taken from Rolls Royce Ltd, 1969). Typically, 10 per cent of the total air flow is used for the primary zone and about 30 per cent is used for the dilution purposes. Subject to the constraints on the length of the combustor and the amount of primary and dilution air available, these zones have to be designed to satisfy conflicting requirements. The primary zone needs to be designed with a view to providing stable recirculation zone to give efficient burning of the air and fuel mixture, without excessive temperature gradients. Combustion should be completed before the

dilution zone otherwise the dilution jets are likely to cool the flame and combustion will be incomplete with emission of unburnt hydrocarbons and other pollutants such as CO (Bahr, 1978). Efficient combustion, however, also means higher temperatures and this is an undesirable outcome as NO_x is produced at high temperatures.

The dilution zone needs to be designed with the aim of rapidly reducing, uniformly around the circumference, the temperature of the combustion products to a specified radial profile for optimum turbine blade life. The results of any asymmetries may be 'hot streaks' with subsequent performance loss and possible turbine blade failure. Further, the circumferential temperature distribution on the combustor walls is partly dependent on the arrangement of the dilution jets and any misalignment of these may result in local regions of high surface temperatures with possible cracking of the combustor walls (Sturgess, 1978).

In order to effect the above desired requirements in the performance of the primary and dilution zones and to eliminate the problems associated with 'hot streaks' and regions of high local surface temperatures an understanding of the aerodynamics of the mixing between the primary and dilution jets with the cross-flowing combustion products is essential.

One method of designing and improving the performance of combustion chambers has been to conduct experiments on real and model combustors and to amass data for different operating parameters and conditions. This data, combined with physical reasoning, was then used to produce correlations between, and estimates of, the more important design parameters. Lefebvre and Norster (1969) provide, in detail, examples of this approach as applied to the design of the

dilution zone in terms of the aerodynamic and geometric parameters. In a related manner, the work of Odgers (1979) includes the identification and use of calculations to describe the combustion effects. This type of approach is limited in its applicability in that the derived correlations are only useful for interpolating between the ranges of the experimental tests. Although some limited extrapolation may be possible, this is restricted to the type of combustors used in the experiments.

The more recent approach has been to predict the flow and reaction in combustor geometries by direct solution of the governing partial differential equations using finite-difference techniques. The turbulence and combustion aspects are represented by models of various levels of complexity allowing description of the turbulent stresses and fluxes, variable density and chemical kinetic effects. The numerical procedures are tested against data taken from experiments on real and model combustors with similar geometries. The results obtained are limited in their use to establishing trends and gross features of the flowfield in terms of variations in combustor geometry and the inlet conditions. Due to the complex nature of the geometry and the state of development of the turbulence and the chemical kinetics models the approach does not represent the quantitative features of the turbulence or the chemical kinetics sufficiently well. Mellor (1978) and, more recently Green (1981) have provided literature reviews on this type of approach.

Measurements of the flow properties in actual and model combustors are difficult and undesirable in terms of cost and time as the flow situation is extremely complex with three-dimensionality, regions of reverse flow and simultaneous heat and mass transfer.

Further, the results would be of limited value in improving the understanding of the fundamentals of jet mixing problems of a designer of primary and dilution systems. In an effort to enhance the understanding of the mixing of the jets with the cross-stream attention should be focussed on local effects associated primarily with the primary and dilution process and not the combustor as a whole, where the various different influences are difficult to isolate. Hence, for the purposes of the present research a simpler approach is adopted. An idealised isothermal flow configuration of single and opposed rows of jets discharging normally into a cross-flowing stream is considered. This geometry, although much simpler, still retains many of the complexities of the real configuration. Understanding of this simpler flow is essential for a better understanding of the more complex situation. Additionally, more detailed and precise measurements can be made in this geometry to allow a fuller assessment of any calculation schemes.

The foregoing discussion has attempted to outline the motivation behind the present research and the approach adopted. The following section provides a review of the relevant published work on the subject and, as a consequence, section (1.3) discusses the areas where information is lacking and provides details of the specific tasks undertaken in the research programme. Finally, section (1.4) provides an outline of the thesis.

1.2 Previous Related Studies

The review of previous related studies is concerned mainly with investigations directly related to rows of jets discharging into a crossflowing stream. The main interest of the present research is

focussed on the aerodynamics of the flow-field and consequently the literature pertaining to combusting flows is not reviewed here.

In the limiting case of the jets being closely spaced the flow approximates to the case of a plane jet discharging into the cross-stream. The other extreme is the single jet case, which is approached, when the pitch spacing of the jets is large. The understanding of these two limiting situations is important for a complete view of the row of jets problem and, consequently both are considered.

The single jet in crossflow has been examined by many investigators and a review of the previous work, as well as new measurements, is provided by Crabb et al (1981). In the present review, therefore, only a resume of previously published work for this configuration is presented. Additionally, the flow resulting from low jet-to-mainstream velocity ratios is appropriate to film cooling applications rather than combustors and the reader is referred to the reviews of Goldstein (1971) and Bergeles (1976) for further information.

1.2.1 Two-dimensional (2-D) Plane Jet in Crossflow

The 2-D plane jet geometry has been considered by many authors in connection with the cooling of turbine blade surface (lower velocity ratio); however, investigations of direct relevance to the present problem are scarce.

Table 1.1 provides a summary of the experimental and theoretical investigations of significance to the dilution problem. The detailed wind tunnel measurements of Rouse (1957), for a 2-D jet discharging at 90^{o} to an effectively unconfined cross-stream, is one of the first investigations of a flow related to the dilution problem. He measured some global properties of the flow, such as the length of the recirculation zone, L, (see figure 1.2) and the shape of the

recirculation bubble, for different values of the slot width (b) over a range of jet-to-crossflow velocity ratios (V/U). From his data Rouse concluded that the parameter (L/b) increases with the 3/2 power of the velocity ratio, ie,

$$(L/b) \quad \alpha \quad (V/U)^{3/2} \qquad (1.1)$$

Wygnanski and Newman (1968) made measurements of the reattachment length and surface static pressure for jets with initial inclination to the surface of 60^{o} and 70^{o}. In the combustor the jets may not enter at 90^{o} because of the annulus feed and hence these results are relevant to the present problem. The measurements accounted for variations in slot width, jet Reynolds number and jet-to-mainstream velocity ratio. The authors used these results and physical reasoning to propose a general relationship between velocity ratio, angle of inclination of jet (θ) and the ratio of reattachment length to slot width viz:

$$0.04 \left(\frac{L}{b}\right)\left(\frac{V}{U}\right)^2 = f_2 \frac{L}{b} \frac{\theta}{\sin \theta} - \cos \theta \text{ for } (V/U) < 100 \qquad (1.2)$$

where f_2 was obtained from the earlier experiments of Bourque and Newman (1960) for a plane jet reattachment to adjacent flat plate configuration. Comparison of the reattachment length from the experiments of Rouse (1957) for a velocity ratio of 2.9 and normal jet injection with the theoretical analysis of Wygnanski and Newman for the same condition give agreement to better than 5 per cent.

The penetration of the crossflow by the jet is an important parameter in the dilution problem. With this view, Kamotani and Greber (1973) conducted detailed measurements for a single jet, rows of jets and 2-D plane jets discharging normally into a confined cross-stream.

The main interest of the study was on the variation of the jet trajectory with the confinement by the wall lying opposite to the jet. The authors deduced the following empirical correlation for the velocity trajectory:

$$\frac{y}{b} = 2.0\ J^{0.28} \left(\frac{x}{b}\right)^{0.5} (1 - e^{-0.07\ H/b}) \qquad (1.3)$$

where x and y are the co-ordinates according to figure (1.2)
H is the tunnel height and
J is the ratio of the jet-to-mainstream momentum flux.

The 2-D plane jet has also been considered on a theoretical basis. Vizol and Mostinski (1965) provided an equation for the deflection of the axis of a laminar jet. They deduced this equation from the value of the drag represented by the jet. The theoretical curve compared reasonably well (with about 20 per cent discrepancy) with their experimental data. Similarly, Stek and Brandt (1976) provided an analytical solution for calculating the velocity and pressure distributions along the jet and also the trajectories of the streamlines emanating from the leading and trailing edges of the slot. In their analysis Stek and Brandt used empirical inputs to simplify the governing Navier-Stokes equations into a soluble form. The theoretical and experimental results were in good agreement.

The foregoing types of analytical solutions are dependent on experimental input and, in turn, do not provide a broad description of the flow-field. The approach adopted by White (1977) and McGuirk and Rodi (1978) does not suffer from such limitations. These authors solved the finite-difference form of the governing differential equations with a two-equation model of turbulence. White (1977)

presented numerical predictions of the experiments of Foster (1973) and found that the calculation procedure underpredicted the length of the recirculation region. This discrepancy became progressively worse with increasing velocity ratio and was as high as 30 per cent for the highest velocity ratio of White's predictions (V/U = 1.4). Also the calculations underpredicted the peaks in the velocity profiles downstream of the slot. McGuirk and Rodi (1978) were interested in the side discharges of effluent into open channel flow and also found that the calculation procedure underpredicted the length of the recirculation zone. Both White (1977) and McGuirk and Rodi (1978) attributed these discrepancies to shortcomings of the turbulence model.

Other authors have considered the plane-jet in connection with the side-discharge problem (McGuirk and Rodi, 1978) and these studies are also useful for the present problem; they are, however, complicated by the effects resulting from the free-water surface and the influence of friction at the river bed.

This section has provided a brief review of the previous experimental and theoretical studies related to the plane jet in crossflow problem with implications for primary and dilution jets of combustors. The experimental data is, clearly, scarce and that which is available lacks detail with previous authors providing only details of the global properties of the flow such as jet trajectory and length of the recirculation zone. It is questionable if satisfactory two-dimensional flow can be achieved for normal jet injection and this poses doubt on the accuracy of measurement of such parameters as the recirculation length which is highly dependent on the two-dimensionality of the flow.

The flow from a plane jet is useful for the understanding of the dilution problem as a limiting case of closely spaced row of jets. Although the two flow configurations exhibit similar characteristics, such as, for example, high pressure region upstream of the jet injection and a region of reverse flow behind the jet, there are also significant differences between them. For instance, the recirculation zone for the plane jet cases consists mainly of fluid originating from the jet whereas for the row of jets there is no true 'recirculation' zone and the back-flow which exists behind the jets is caused by entrainment into the low pressure region behind the jets and consists, therefore, mainly of the crossflowing stream.

In the next section a review of previous related studies for discrete round jets is given.

1.2.2 Round Jets in Crossflow

In this section previous investigations of the interaction between discrete round jets and a crossflow are reviewed. As mentioned earlier, Crabb et al (1981) have provided an extensive review of the literature related to the single jet and the following paragraphs are concerned mainly with rows of jets. For ease of presentation the experimental and theoretical investigations are reviewed under separate headings.

(i) Experimental Investigations

The single jet in crossflow has received considerable attention in the past and the range of parameters investigated by previous authors is extensive. Vogler (1963), Bradbury and Wood (1965) and Taylor (1977) have provided extensive measurements of the surface static pressure

distributions for normal and inclined jets to the cross-stream. These authors were motivated by a need to understand the lift losses associated with V/STOL aircraft in transition from vertical to forward flight and this data is limited in its applicability to the problem of primary and dilution jets of combustors where the main interests are the penetration and mixing of the jet and the crossflow.

In this connection, the jet trajectory is an important parameter and several authors have measured this and the effects of the various flow and geometric variables upon it. The effects of velocity ratio, density ratio and jet incident angle on the jet trajectory have been reported by, for example, Keffer and Baines (1963), Margason (1968) and Kamotani and Greber (1972). The main conclusions to emerge from these investigations were that the jet trajectory depended mainly on the ratio of the jet-to-crossflow momentum flux. In their further experiments, Kamotani and Greber (1973) found that, unlike the plane jet, the single jet trajectory was only mildly affected by the presence of an opposing wall unless the momentum ratio was sufficiently high to cause impingement.

Some understanding of the mixing between the jet and cross-stream flow can be gained from the investigations of McMahon et al (1971), Chassaing et al (1974) and Moussa et al (1977). These authors measured in the wake region of the jet and observed the existence of double vortices, caused by the jet entrainment of the crossflow and the high shear between the two flows. An understanding of these vortices and their development is important for the present flow as this effect may have implications for the high temperature streaks found in gas turbine practice.

From their detailed review Crabb et al (1981) concluded that there was a lack of detailed information in the initial mixing region and the previous measurements for this region were subject to uncertainty due to the type of instrumentation used. Also, except for the data of Bergeles (1976), there were no velocity measurements of the jet outlet profile. This is a required boundary condition in calculation procedures, to be discussed in Chapter 4. Crabb et al (1981) provided detailed measurements, made with a laser anemometer, of the initial mixing region ($0< X/D<6$), and hot-wire and Pitot-tube measurements further downstream. Their main conclusions were that the locus of maximum velocity did not correspond to fluid from the jet; the downstream regions of high velocity were mainly composed of cross-stream fluid accelerated around the jet. Further, they concluded that the flow was controlled mainly by pressure forces; these were responsible for the bending of the jet and the double-vortex structure.

The flow from a single jet is likely to be different from the row of jets in that the jet trajectory and vortex structure is expected to show greater dependence on the jet spacing and confinement by the opposing wall for the row of jets case. Unlike the single jet, the number of investigations pertaining to rows of jets with relevance to primary and dilution jets are much less abundant and table 1.2 provides a summary of these.

The investigation of Norgern and Humenik (1968) considered combustor exit-temperature profiles for a rectangular combustor geometry. The model combustor had a one-sided contraction and directly opposing or staggered rows of cold jets discharging into a hot cross-flowing stream. The flushed jet openings were either circular or rectangular and had an annular air feed. They found that

the type of dilution aperture was not important for the resulting temperature profile. Also, mixing of the two streams was improved for the rectangular shaped holes by enlarging the holes and increasing the spacing between them. These results are limited in their applicability as they are related to a particular geometry where the various different effects are difficult to isolate. Further, only laterally averaged temperature profiles are presented and no account of the transverse variations is provided.

Holdeman et al (1973) and Walker and Kors (1973) provide detailed temperature profiles downstream of a single row of cold jets discharging normally into a heated confined crossflow. These authors investigated the effects of flow variables such as the jet-to-mainstream momentum flux ratio and the jet-to-mainstream density ratio. Geometric variables such as jet orifice diameter and the pitch spacing was also considered. The results were discussed in terms of a mixing efficiency parameter based on the cross-stream and jet temperatures and the respective mass flow rates. The conclusions to emerge from the study were that the jet-to-mainstream momentum flux ratio was the most important flow variable influencing the mixing; density ratio variation, at constant momentum ratios, showed no significant change in the profiles or the mixing efficiency. In agreement with Norgern and Humenik (1968), these authors also concluded that, for a fixed jet exit area, fewer large jets provided better penetration than a large number of small jets.

Kamotani and Greber (1973) reported results of experiments on the effects of a confining wall on the characteristics of heated and unheated jets injected into a cold cross-stream. Longitudinal and transverse velocity and temperature distributions were presented for

various downstream planes. Also, trajectories of velocity maxima were presented for various ratios of jet-to-crossflow momentum flux and blockage ratios. Results showed that the structure and trajectories of a single row of jets are strongly dependent on both the momentum ratio and the spacing ratio. Temperature decay, for moderate spacing of the jets, was found to be similar to that for a single jet in the near-field of the jets exit and approached that of a two-dimensional jet in the downstream region. The transverse velocity distributions showed that for jet spacings of less than four diameters the vortex pair, found with the single jet, did not develop. The smoke flow visualization of the study indicated some flow asymmetry downstream of a row of symmetrically arranged jets. In a more detailed documentation of their experiments, Kamotani and Greber (1974) also provided velocity contours for two opposed jets and concluded that this flow situation could be represented by replacing the symmetry plane by an opposite wall. This is, certainly, questionable in the event of opposing jet impingement with a resulting asymmetric bifurcation. The non-uniform temperature distributions commonly found in the exit planes of combustors provided the motivation for the study of Crabb and Whitelaw (1979). These authors presented measurements of mean velocity and scalar concentration downstream of a row of jets, for a pitch-to-diameter ratio of 2 and jet-to-mainstream velocity ratio of 2.3, issuing normally into a confined cross-flow. The results were obtained to quantify the influence of a geometric asymmetry in the hole arrangement on the downstream mean-flow properties. The main conclusions to emerge from the investigation were that even a small asymmetry of the central jet (0.1D) resulted in a disproportionality large eccentricity of the velocity field. The eccentric jet, however, tended to return to a

symmetric position so far as the maximum value of the conserved scalar was concerned.

(b) Theoretical Investigations

Theoretical attempts for single or rows of jets have fallen into three main categories and Table 1.3 provides an outline of the theoretical investigations relevant to the present study. A common approach has been to amass experimental data for different flow and geometric conditions and derive correlations with this data as empirical input. For the single jet, equations for the jet trajectory derived using this approach by Ivanov (1952) and Shandrov (1957) {cited by Abramovich, 1963} compared favourably with experimental curves. Rajaratnam (1976) provides a summary of this type of analysis and its application to the single jet by other authors. For a row of jets, Holdeman and Walker (1976) and Cox (1976) derived correlations for predicting the temperature distribution downstream of a single row of cold jets discharging normally into a hot confined crossflow. These authors used the detailed experimental study of Holdeman et al (1973). This method is certainly useful when a large amount of data is available. Its applicability is, however, limited and any extrapolations have to be made with great circumspection.

Some theoretical approaches have involved the application of integral methods, for example, Schatzmann (1977) and Adler and Baron (1979). The first author presented, for a single jet, a model based on differential equations for the conservation of mass, momentum, concentration and thermal energy. The equations were transformed by vector operations in a streamwise co-ordinate system and integrated in the angular and radial directions using symmetry and similarity

assumptions. This method is limited in that an entrainment function needs to be specified and, further, the incorrect assumption of the jet cross-section being circular is made. Adler and Baron (1979) did not use the simple geometry assumption for the jet cross-section in their integral method. They successfully predicted the kidney-shaped region and their results compared favourably with the experimental single jet results of Kamotani and Greber (1972). These methods are, however, difficult to extend to rows of jets and confinement of the crossflow and are, therefore, of limited use for the present purposes.

The third, and less restrictive, approach has been to solve, using a finite-difference scheme, the time averaged forms of the Navier-Stokes equations together with a two-equation model of turbulence. Using this approach, Patankar et al (1977) calculated the flow for a single jet discharging normally into an effectively unconfined cross-flow. A 15 x 15 x 10 (X,Y,Z) finite grid was used and the calculated trajectories and decay of the maximum jet velocity were in good agreement with the experimental results of Keffer and Baines (1963) and Chassaing et al (1974). Further, reasonable qualitative agreement was obtained with the velocity profile measurements of Ramsey and Goldstein (1971). The accuracy of the calculations of Patankar et al is questionable as the grid used for the calculations is too coarse for this type of flow and resulting numerical errors may be large.

In the single and row of jets study of Crabb (1979) a 24 x 14 x 14 grid was used for the calculations. However, the calculation domain boundaries were set according to the dimensions of the experimental test rig and, as a result, the calculation grid was relatively coarse. The results reflect this with over-diffused velocity profiles and poor agreement between the calculations and the measurements.

The single round jet discharging into a confined cross-stream was calculated by Jones and McGuirk (1979) who used a 20 x 15 x 15 grid. The calculated results were compared with the measurements of Kamotani and Greber (1974) and found to be in good qualitative agreement. Comparison of temperature and velocity contours, however, showed only fair agreement. The discrepancies between the measurements and the calculations were attributed partly to the numerical error and, in part, to the turbulence model.

In their finite difference schemes, the previous authors employed either a simple constant velocity profile at the jet exit boundary condition or a profile based on a constant total pressure condition. In his study, of a single jet discharging normally into a confined crossflow, White (1980) extended the numerical procedure to calculate the distortion of the flow within the injection hole. Calculations were made for a range of jet-to-crossflow momentum flux ratios (0.4-2.3) and the distortion of the flow within the injection hole was found to have a significant affect on the calculated results. Comparison of the calculated results with the measurements of Crabb (1979), although a significant improvement over the calculations of Crabb, showed only fair agreement. The author concluded that with the finest grid of 25 x 15 x 15 nodes the calculation still showed some grid dependence.

1.3 Objectives of present study

The foregoing section has outlined the previous experimental and theoretical investigations related to the dilution zones of combustors. The single jet configuration is well documented both experimentally and theoretically. For a row of jets, the experimental data is by no

means plentiful but the more important flow and geometric parameters have been investigated and general trends established. The geometric eccentricity study of Crabb (1979) has revealed interesting results but these are limited to a single velocity ratio. Theoretical studies for rows of jets have, hitherto, been restricted to empirical correlations. Although the finite-difference schemes for direct solution of the governing equations have shown promise for the single jet configuration these have not been extended to rows of jets, except by Crabb (1979) where the chosen solution domain was too large with resulting coarse grids and consequently solutions with large numerical errors. Due to limitations of computer storage rows of jets need to be represented by a sector of the flow only. Effects of small geometric asymmetry can not be calculated in this way as the asymmetry cannot be represented by a small representative sector and these effects still need quantification by experiment.

Except for the isolated study of Kamotani and Greber (1974), the investigations on opposed rows of jets are virtually non-existent. For the design of annular combustors, understanding of the flow patterns resulting from rows of directly opposed and staggered jets are highly desirable; as indicated by, for example, Cox (1976).

The above brief remarks have given an indication of the areas where effort is still required. The specific objectives of the present research may be summarised as;

- To extend the range of velocity ratios for a single row of holes and demonstrate the influence of geometric asymmetry over this range.
- To provide measurements for directly opposed and staggered rows of jets and to demonstrate the influence of geometric and flow variables.

- To investigate the effect of a geometric eccentricity on directly opposed and staggered rows of jets.
- To apply a currently available prediction procedure to the problem of rows of jets discharging normally into a confined cross-stream and assess the accuracy to which the flows measured in this thesis may be simulated using currently available computer hardware.
- To apply the prediction procedure to calculate flow configurations outside the range of measurements.

1.4 Outline of thesis

The thesis is organised into five chapters. Chapter 1 has indicated the practical relevance of rows of jets in a cross-flow, reviewed previous studies and stated the specific objectives of the present research.

The experimental work is described in Chapters 2 and 3. The apparatus, experimental method and related errors are discussed in Chapter 2 and the results presented and discussed in Chapter 3.

Chapter 4, in three sections, is devoted to the numerical computation of selected experiments of Chapter 3. The first section of the chapter presents the partial differential equations to be solved and includes a brief description of the turbulence model used. The method of solution of the corresponding finite difference equations and consideration of the accuracy of the numerical solution are also outlined. In the second section of the chapter, results are presented and discussed for a single row of jets discharging into a confined crossflow and for opposing rows of jets. The final section of Chapter 4 presents conclusions of the theoretical study.

Chapter 5 relates the main findings of the present study to gas

turbine practice and provides suggestions for future work.

Calculations were also performed for a plane (2-D) jet discharging into a cross-flow and these are presented in Appendix A.

Table 1.1: Experimental and Theoretical Investigations of a Plane (2-D) Jet in Crossflow

Authors	Nature of Investigation	Comments
Rouse (1957)	Experimental investigation of jet injected normally into crossflow. Varied the slot width and jet-to-crossflow velocity ratio.	Measurements were made of the reattachment length as a function of the velocity ratio. An empirical relationship was provided, relating the ratio of the reattachment length and the slot width to the 3/2 power of the velocity ratio.
Wygnanski and Newman (1968)	Experimental investigation of jet injected at angles of 60° and 70° to the crossflow. A range of velocity ratios and slot widths were tested.	Measurements of reattachment length for different velocity ratios. Used 60° and 70° injection angle results to provide a relationship for calculating reattachment length for other jet angles.
Kamotani and Greber (1973)	Experimental investigation with jet injected normally. Varied velocity ratio and height of the duct.	Measurements of jet trajectory were made as a function of both the velocity ratio and the height of the duct. Correlation of trajectory is provided.

/Continued ...

Table 1.1 (concluded)

Authors	Nature of Investigation	Comments
Vizol and Mostinski (1965)	Theoretical investigation of deflection of jet axis.	Analytical solution of deflection of the jet axis given and based on considerations of the drag represented by the jet.
Stek and Brandt (1968)	Theoretical and experimental investigation for jet injected over a range of angles to the crossflow.	Used the experimental results to make simplifications to the governing Navier-Stokes equation such that they could be solved.
White (1977)	Theoretical study of jet injected normally for low jet-to-crossflow velocity ratios.	Numerical predictions with two-equation model of turbulence. Predicted results compared with measurements of Foster (1973). Poor agreement obtained between the predictions and measurements.
McGuirk and Rodi (1978)	Theoretical study of jet injected normally.	Numerical predictions of effluent disposal from a two-dimensional slot into an open channel. Reasonable agreement with a wide range of measurements. Length of recirculation zone underpredicted.

Table 1.2: Experimental Investigations of Rows of Jets in Crossflow

Authors	Nature of Investigation	Comments
Norgern and Humenik (1968)	Rows of opposing jets with converging section from lower surface. Annulus fed cool air jets with heated crossflow.	Measurements of temperature profiles at exit of test section were provided. The type of dilution aperture did not influence the profiles. Increasing the size of dilution holes and the spacing between them improved the mixing of the two streams.
Holdeman, Walker and Kors (1973)	Single row of cool air jets discharging normally into a hot crossflowing stream. Variations of momentum flux ratio and pitch-to diameter ratio.	Measurements of temperature profiles at various downstream planes. Jet-to-crossflow momentum flux ratio was found to be the most important operating variable influencing the jet penetration and mixing. For a constant value of pitch-to-diameter ratio the mixing improved as the jet diameter was increased.

/Continued ...

Table 1.2 (concluded)

Authors	Nature of Investigation	Comments
Kamotani and Greber (1973, 1974)	Heated and unheated single jet, row of jets and two opposed jet configurations discharging normally into a cool confined crossflow. Variations on momentum flux ratio and duct height.	Measurements of velocity and temperature contours and jet trajectory presented. Momentum ratio and jet spacing ratio found to determine the jet trajectory and structure.
Crabb and Whitelaw (1979)	Row of jets injected normally into a confined crossflow. Effect of a geometric eccentricity of one jet investigated.	Mean velocity and scalar concentration distributions presented. Large asymmetries resulted in mean velocity field from a small geometric eccentricity of one jet. Scalar field regained symmetry with downstream distance.

Table 1.3: Theoretical Investigations of Round Jets in Crossflow

Authors	Nature of Investigation	Comments
Ivanov (1952) and Shandrov (1957) {cited by Abramovich, 1963}	Determination of the equation for the axis of the jet using empirical input.	Empirical equation proposed for the axis of a single round jet. Equation relates the coordinates of the trajectory to the diameter of the jet, the angle of injection and dynamic pressures in the crossflow and the jet exit.
Cox (1976)	Prediction of temperature distribution downstream of a single row of jets using empirical input.	Derived correlations for predicting the temperature field as a function of the downstream distance and the main geometric and flow variables. Agreement between measurement and predictions was reasonable.
Holdeman and Walker (1976)	Same as Cox (above)	Same type of approach as Cox (1976), but used larger amount of data for derivation of the correlation equations. These correlations could be used for a wider range of independent variables.

/Continued ...

Table 1.3 (continued)

Authors	Nature of Investigation	Comments
Schatzmann (1977)	Calculation of spread and rise of buoyant jet by use of integral method.	Used symmetry and similarity assumptions and a round jet cross-section was also assumed. Empirical inputs used for simplification of equations. Method has limited application.
Adler and Baron (1979)	Prediction of single jet cross-section shape and jet trajectory using integral method.	Used fewer assumptions than Schatzmann's method. Predictions compared favourably with measurements of Kamotani and Greber (1971).
Patankar et al (1979)	Numerical predictions of single jet in crossflow by finite-difference solution techniques and a two-equation model of turbulence.	Used 15 x 15 x 10 grid (X, Y, Z directions). Calculation of trajectories and decay of maximum jet velocity in good agreement with experimental results.
Crabb (1979)	Numerical predictions of a single jet and row of jets.	24 x 14 x 14 grid used for calculations. Solution domain was too large and as a result, calculations were not grid-independent. Poor agreement between predictions and measurements.

/Continued ...

Table 1.3 (concluded)

Authors	Nature of Investigation	Comments
Jones and McGuirk (1979)	Numerical predictions of confined single jet in crossflow.	20 x 15 x 15 grid used. Predictions in good qualitative agreement with measurements of Kamotani and Greber (1974). Comparison of velocity and temperature contours showed only fair agreement.
White (1980)	Numerical predictions of single jet in confined cross-flow. Numerical procedure used to calculate flow within injection hole.	Used 25 x 15 x 15 grid. Comparison of predictions with measurements of Crabb (1979) showed only fair agreement. Concluded that predictions were not totally grid-independent.

CHAPTER 2

EXPERIMENTAL CONFIGURATIONS AND MEASUREMENT TECHNIQUES

2.1 Introductory Remarks

In this chapter the configuration and techniques used in the experimental program are described. The geometric tolerances of the apparatus, the limitations of the techniques and the precision of the measurements are stated and discussed.

The purpose of the experimental study was to provide a quantitative picture of the flow-field associated with rows of jets discharging normally into a crossflowing stream. Because of their practical importance, the effects of small geometric asymmetries and a downstream contraction of the working section were determined. The measurements comprised the mean velocity, the rms of velocity fluctuations and concentrations of a passive scalar which were made to provide an indication of the dilution of the jets by the crossflow and also serve to provide an analogy with the temperature of a jet and crossflow with different initial temperatures.

The chapter continues with section 2.2, which provides details of the air supplies to the mainstream and jets and construction of the working section and traversing apparatus. Section 2.3 gives details of the measurement techniques used and section 2.4 an assessment of the errors associated with the measurements.

2.2 Description of the Apparatus

2.2.1 The Mainstream Air Supply

The wind tunnel previously described by Rastogi and Whitelaw (1973),was used for the present investigation. Air supply for the mainstream was provided by a Gyro-flow centrifugal fan driven by a synchronomous motor through a belt and pulley arrangement which allowed the velocity of the fan to be varied. Fine control of the air velocity in the test section was achieved by throttling the air flow at the inlet to the fan by means of a slip valve.

The carefully constructed expansion and settling chambers and 12.1 contraction ratio section connected the fan to the working section. The screens and honeycomb placed in these sections, shown in figure 2.1, resulted in a free-stream turbulence intensity of 0.007 at the inlet to the working section for the velocity of 10.8m/s used in the experiments.

The contraction unit and the test section were each supported by steel frames with rubber pads to reduce vibration. The use of cloth tape to join the fan and the diverging section helped to render the effects of fan vibration insignificant.

2.2.2 The Jet air supply

The flow to the jets was generated by a separate fan and passed through an expansion chamber and connections to two separate, but identical, screened plenum boxes. The flow rate of air from the expansion chamber to the plenum boxes could be controlled by slip valves placed in the connectors. When a single row of holes was used,

one of the plenum boxes was isolated by closing one of these valves.

The flow to each of the ten jets passed through 0.76m long, straight, smooth pipes with 0.025 m internal diameter. Flexible polythene tubing was used to connect the plenum boxes and the straight pipes. The flow at the jet exit, measured with a Pitot-tube, could be set accurately by pinching the flexible pipes with hose clips.

2.2.3 The Test Section and Related Details

Three different arrangements of jets-in-crossflow were used in the present study:-

- Single row of jets
- Opposed rows of jets
- Rows of jets with downstream contraction of the test section.

The test section comprised a channel of nominal 300mm width and 200mm height with the five 25.4 mm holes located across the span of the roof and the same number of holes across the span of the floor with pitch of the holes of 50.8 mm. The arrangement, with relevant dimensions, is shown on figure 2.2. For the single row of jets, one row of holes was blanked off. A perspex plate was used to effect the contraction of the working section as shown by the line diagram 2.3. The floor of the tunnel could be raised to reduce the height of the working section to four jet diameters and with the single row configuration a splitter plate was used upstream of the jets to divide the flow from the contraction exit. The velocity of the mainstream was measured at this section, for this configuration, in the absence of the jets. A redistribution of the mainstream flow was caused by the operation of the jets. This was compensated for by adjustment of

the throttle valve at the fan inlet to achieve the same mainstream velocity as in the absence of the jets. For the remainder of the measurements, with the reduced duct height (H/D=4), a purpose-built steel plate contour was fitted in the existing contracting section and this effectively reduced the contraction section dimensions to those of the test section.

Sandpaper trips were fixed, at the upstream edge of the test-section, and resulted in boundary layers with momentum thickness Reynolds numbers of 2.65×10^2 at the location of the leading edges of the holes, in the absence of the jet flow. The shapes of these boundary layers conformed to a turbulent flow with identifiable logarithmic regions. Traverse mean velocity profiles were measured at various horizontal locations in the plane of the holes and confirmed the two-dimensionality of the mainstream within one percent of the free-stream value over the central 93 per cent of the channel. The walls of the test section were constructed from 10 mm thick perspex sheets and an array of static pressure tappings of 0.5 mm diameter were drilled in them.

The holes which formed the jets were arranged with a pitch-to-diameter ratio (S/D) of two; two holes on floor and roof could be blanked off to achieve S/D of four and the two opposed jet configuration. The mean flow at the exit planes of the jets were investigated for the two rows of jets separately and in the absence of the mainstream flow. The long length (30D) of the pipes ensured fully developed turbulent flow in the exit planes. The centreline velocity, at the exit plane, was adjusted for each pipe and the value for the ten pipes did not deviate by more than 0.5 per cent of the mean of the

ten values. Exit-plane profiles of mean velocity were measured for each jet across two orthogonal planes to check for symmetry. After some adjustment to the flexible piping, the profiles were made symmetrical to better than 3 per cent.

The central hole of the roof jets could be repositioned by means of slip gauges to allow investigation of hole eccentricity, and in addition, the top row of holes could be moved axially in relation to the floor holes. The jets could also be staggered laterally by moving the floor jets relative to the top row.

In view of the intention to investigate flow asymmetries, it is important to quantify tolerances of test section. The ten holes were measured in their exit planes and found to be round and of equal diameter within 0.05 mm. The pitch of the hole centrelines was identified within 0.02 mm and the distance between the floor and roof jets was uniform and within 0.5 mm. The alignment of the centrelines of the floor and roof jets could be achieved within 0.1 mm. These tolerances are considerably better than those found in the construction of gas turbine combustors and negligible when compared to the eccentricities investigated by the adjustment of the central roof hole, i.e. 2.54 mm, 6.35 mm and 12.70 mm. Two traverse mechanisms were employed and operated from the roof of the channel. The first, with access from the side walls, traversed the Pitot-probe in the exit plane of the jets and was used for measurement of mean velocity in this plane. The second (see Vasilic-Melling (1977) for details of construction and precision) with access from the roof of the channel, allowed measurement of the Pitot and hot-wire probes in the X, Y and Z directions, and was used for all the downstream measurements.

2.3 Measurement Techniques

Three types of measurement techniques, namely, Pitot-tube, hot-wire anemometry and scalar concentration measurement, were used in the experimental investigation, and are described in the following subsections.

2.3.1 Mean velocity measurements

Measurements of mean velocity were obtained with an impact probe of external and internal diameters 1.1 and 0.61 mm respectively, and an array of static pressure tappings located in the floor and side walls of the tunnel. The pressures were measured by a Furness Controls electronic transducer, capable of measuring pressure differences from 0.01 - 2000 mm H_2O, and were time-averaged by a Solartron voltmeter with typical averaging time per measurement point of 20 seconds. The reproducibility of the pressure measurements was better than ±1%.

Positioning of the probe, on the jet centreline, for measurement of velocity at jet exit was achieved by lining up the probe on the centreline of a disc placed in the pipe. For the downstream measurements, a thin line scribed along the centreplane of the tunnel and a grid of 0.3 mm pressure tappings on the floor were used for the zero transverse position. For the vertical location, zero positioning was assumed when the probe coincided with its mirror-image on the floor plate.

The Pitot-tube was aligned in the streamwise (X) direction of the flow and not with the local velocity vector. This can result in small errors at the measuring station (X/D = 4) closest to jets where

the flow from the jets may not have turned completely to become parallel with the alignment of the probe. However, as indicated by Ower and Pankhurst (1966), the Pitot-tube is insensitive to misalignment at large angles; at 20° yaw, for example, the measured pressure is only about one percent less than at zero yaw.

2.3.2 Turbulence Measurements

Turbulence quantities were measured by hot-wire anemometry and this section, in three subsections, considers the equations relating the signal from the anemometer with the velocity, a brief description of the instrumentation and details of the experimental procedure.

(i) Hot-wire evaluation equations

For constant-temperature operation of the hot-wire anemometer, the output voltage (E) is related to the effective velocity (U_{eff}) in the form:

$$E = A + BU_{eff}^{n} \qquad (2.1)$$

where A, B and n are constants dependent on the properties and dimensions of the hot-wire. With the use of a linearizer, the above equation can be transformed to the form:

$$E = SU_{eff} \qquad (2.2)$$

where S is the sensitivity factor of the hot-wire to be determined experimentally by calibration.

To relate the effective cooling velocity to the instantaneous velocity vector, Champagne et al (1967) confirmed experimentally the suggestion of Hinze (1959) that, for a linearized hot-wire,

$$E/S = U_{eff} = [U_n^2 + k^2U_t^2]^{\frac{1}{2}}$$
$$= U_I\ [\cos^2\alpha + k^2\sin^2\alpha]^{\frac{1}{2}} \qquad (2.3)$$

where U_n is the velocity component normal to the wire axis, U_t is the tangential component and α is the angle between the instantaneous velocity vector (U_I) and the normal to the wire axis.

Rodi (1971) and others suggested a modification of equation (2.3) to account for the disturbance from the wire supports. He reduced the normal velocity component U_n into two normal components, (U_{n1}) in the axis of the probe and (U_{n2}) in a plane normal to the plane of the prongs, giving:

$$U_{eff}^2 = U_{n1}^2 + hU_{n2}^2 + k^2U_t^2 \qquad (2.4)$$

where h is the pitch-factor to be determined from calibration of the wire. In the present investigation the simpler yaw law (equation 2.3) was adopted because the more complex method did not offer any distinct advantage for the added effort required.

The interpretation of the hot-wire signals was based on the evaluation method of Champagne and Sleicher (1967). This method uses a second order truncation of a series expansion, relating the anemometer output to the instantaneous velocity vector, to resolve for $\overline{U}$, $\tilde{u}$, $\tilde{v}$, $\tilde{w}$, $\overline{uv}$ and $\overline{uw}$ with signals from a cross-wire probe placed in the XY and XZ planes. A discussion of the errors associated with the technique are given in section (2.4).

(ii) Instrumentation

DISA crosswire probes (DISA 55P61) located in probe holders (DISA 55H2A) were used in conjunction with constant temperature

anemometers (DISA 55D01) operated at an overheat ratio of 0.8. The probe holders were located within stainless steel tubing to maintain constant sensor location when the probes were rotated about their own axis. The signal from the anemometer was linearized by DISA 55D10 type linearizers and passed to an analogue-to-digital convertor,A/D, (DECA862). The digitised signal was then processed on-line by a mini-computer (DEC PDP8E) to give values of the mean velocity and Reynolds stresses. The arrangement is shown in block diagram form in figure (2.4) and the system has been described in detail, previously by Ribeiro and Whitelaw (1975) and Crabb et al (1981).

(iii) Experimental Procedure

The anemometers were linearized and calibrated with the cross-wire probe placed in the potential core of a 50 mm diameter jet with turbulence intensity of less than 0.5 per cent. Each wire was linearized separately. The output from the linearizer was input to the mini-computer (PDP8E) via the analogue-to-digital convertor. This value was divided by the velocity measured by a Pitot-tube placed in the same axial plane as the hot-wire but 5 mm away, to minimise disturbance of the flow. The ratio of the linearizer output and the velocity measured by the Pitot-tube (E/U) was calculated, on-line by the PDP8E, for several values of the velocity over the range 3-25 m/s. Exponent and zero settings of the linearizer were adjusted until the ratios were within $\pm$2% of the mean value over the whole velocity range. Programs for calculation of the ratio (E/U) for linearization, calibration and sampling by the mini-computer, used in the present investigation are in a low level communication language (FOCAL) and

are described by Crabb (1979).

After linearization, the hot-wire was calibrated to determine the constant S and the yaw factor k of equation (2.3). This was achieved by locating the cross-wire at pairs of yaw angles of 30° and 60° to the mean velocity direction in the same jet core. For these angles (i.e. $\alpha_1 = 30°$, $\alpha_2 = 60°$), and in a manner similar to that of Ribeiro and Whitelaw (1975), values of S^2 and k^2 were calculated, on-line by the PDP8E, from the relationships:

$$S^2 = \frac{3E^2(30) - E^2(60)}{2U^2}$$

$$k^2 = \frac{3E^2(60) - E^2(30)}{-E^2(60) + 3E^2(30)} \qquad (2.5)$$

Each wire was calibrated separately, and the linearizer gains were then adjusted to make the calibration constant, S, the same for both sensors. The assumptions of low turbulence intensity and probe axis alignment with the mean flow direction in the evaluation procedure of Champagne and Sleicher (1967) necessitated that the measurements be made in the downstream region, where the V and W components of velocity were negligible. To produce the mean and rms quantities, at least 150,000 samples were taken at each measurement location.

The probes were cleaned and calibrated at the start of each measurement session and checked at regular intervals during the measurements, to ensure that the results were free from errors caused by dirt accumulating on the wires.

2.3.3 Scalar Concentration measurements

The impact probe with external and internal diameters of 1.1 and 0.61 mm, used for mean velocity measurements, was also used as a sampling probe.

A small quantity of helium, 1 per cent by volume, was injected into the flexible polythene tubing 40D upstream of the jet exit. The concentration of helium in the sample taken from the test-section was measured by a Servomex microkathorometer (Mk.158) of the flow-through type. This kathorometer was placed in an oven, kept at a constant temperature of $50^{o}C$, and consisted of two chambers containing platinum filaments which formed two arms of a Wheatstone bridge circuit. Atmospheric air was drawn through one chamber of the cell and the gas sample through the other by means of a vacuum pump connected to the outlet of the kathorometer. The optimum flow rate of 3ml/s through the chambers, found experimentally by Crabb (1979) to offer the minimum response time without affecting the results, was set by accurate rotameters. The resulting heat transfer rate at each filament was different because of the presence of helium in the sampled air. This causes the resistance of the filaments to change and a potential difference across the bridge results. Over the present range of concentrations, calibration of the kathorometer by Rastogi (1972) and Baker (1971) indicated a linear relationship between the output voltage of the bridge and the concentration of helium. A typical time taken for one concentration measurement was about 20 seconds.

2.4 Accuracy of Measurements

This section considers, briefly, the errors associated with the measurement techniques used in the experimental investigations for mean velocity, turbulence characteristics and scalar concentration measurements.

(i) Mean velocity

The errors associated with the measurement of mean velocity with a Pitot-tube are generally due to non-alignment of the probe with the mean flow direction and high turbulence levels in the flow. As indicated earlier, the error due to the non-alignment may be considered negligible for the present measurements.

High turbulence levels result in over-estimation of the total pressure. For the location of measurement at the plane nearest to the jet exit, turbulence levels as high as 0.2 were encountered, and it is this source of error which is likely to make the most significant contribution to inaccuracy in the measurement of the mean velocity. Ower and Pankhurst (1966) provide a means of calculating the error in the measured velocity if the turbulence effects are neglected. With the assumption of isotropic turbulence, the error in the mean velocity measurements is of the order of 2 per cent for the measurements when the turbulence intensity is around 0.2 with smaller values accompanying smaller intensities. For measurement locations closest to the jet exit plane, the turbulence intensity is higher, and consequently the error in the mean velocity is also higher, but it is still better than 6 per cent. The pressure transducer and time averaging voltmeter allowed reproducibility of the pressure measurements to better than ±1 per cent.

(ii) Turbulence Measurements

In the measurement of turbulence quantities, the errors can be classified as systematic errors in the approximated form of the response equation and random errors in linearization, calibration and measurement.

The evaluation method of Champagne and Sleicher (1967) used for the measurements is based on the assumption of low turbulence level. Following the rigorous analysis of Ribeiro (1972), the errors incurred by this assumption, as given by Crabb (1979), are $\overline{U}$ ± 0.8 per cent, $\tilde{u}/\overline{U}$ ± 2 per cent and $\overline{uv}/\overline{U}^2$ ± 5 per cent, for a typical turbulence level of 15 per cent. For turbulence levels above 25 per cent, the accuracy rapidly becomes unacceptable and measurements were taken in regions where this value was not exceeded. The other errors generated by the hot-wire system were in the linearization and calibration stages.

It was only possible to linearize the wire within ± 2 per cent of the actual velocity range, and the two sensors of the cross-wire were linearized to similar sensitivity within 1 per cent. In the calibration, the wires could be aligned to within ±0.5°, and this gives an accuracy limitation of 6 per cent on the measured values of the yaw factor, k. Summation of errors for the hot-wire due to truncation of the response equation, linearization and calibration give total probable errors of $\overline{U}/U_\infty$ ± 5 per cent, $\tilde{u}/U_\infty$, $\tilde{v}/U_\infty$, $\tilde{w}/U_\infty$ ±9 percent and $\overline{uw}/U_\infty^2, \overline{uv}/U_\infty^2$ ± 16 per cent for typical turbulence level of 15 per cent. Measurement of mean velocity with hot-wire and Pitot-tube at X/D of 6 indicated discrepancy of 2 per cent between the two with the hot-wire giving higher values.

(iii) Concentration Measurements

Outside regions of flow recirculation, the concentration measurements are precise to within $\pm$ 2 per cent of the maximum measured value at the jet exit. The precision of concentration measurements in regions of recirculation is difficult to quantify and these have been omitted in all cases.

CHAPTER 3

PRESENTATION AND DISCUSSION OF EXPERIMENTAL RESULTS

3.1 Introduction

Detailed measurements of mean velocity, turbulence characteristics and scalar concentrations are presented for a series of geometrical configurations of air jets, arranged transversely across a rectangular duct, discharging normally into a crossflowing air stream. The sequence of investigations, which is also the sequence of their presentation, is shown in table 3.1. This order of investigations is, firstly, an extension of the work of Crabb (1979) and others for a single row of jets and then an extension to more complicated arrangements of jets in crossflow. The aim throughout has been to enhance the understanding of the mixing mechanisms in the primary and dilution zones of gas turbine combustors.

The chapter is divided into seven sections of which this introduction is the first. Mean velocity and concentration profiles and contours for a single row of jets, arranged symmetrically, are presented in Section 3.2. This configuration has relevance to practical situations such as dispersal of plumes from chimney stacks, jets of V/STOL aircraft, cooling of turbine blades and the primary and dilution zones of gas turbine combustors which are the emphasis of the present study. The section extends the measurements of Kamotani and Greber (1973) to encompass the smaller ratios of duct height (H) to jet diameter (D) which are more akin to gas turbine systems. Section 3.3 supplements the results reported by Crabb and Whitelaw (1979) to

Sec	FLOW CONFIGURATION	GEOMETRIC VARIABLES	FLOW VARIABLES	COMMENTS
3.2	Single row of jets	H/D; 4 and 8 S/D; 2 and 4	Jet-to-cross velocity ratio (V_j/U_∞) = 2.3.	Centreplane and midplane mean velocity profiles at X/D = 4, 6, 8, 10. Mean velocity and concentration contours at X/D = 4, 8, Results presented in FS/81/9.
3.3	Single row of jets with eccentricity	H/D = 8, S/D = 2 Central jet eccentricity = 0.1D,0.25D	V_j/U_∞ = 0.5,1.0,2.0	Transverse distribution of mean velocity and velocity and concentration at X10 = 6. Report FS/79/16. Also published in J. Heat Trans., 102, 391 (1980).
3.4	Directly opposed rows of jets	H/D = 4 S/D = 2,4, ∞	V_j/U_∞ = 1.0, 1.8	Mean velocity, scalar concentration contours at X/D = 4,8. Results reported in FS/80/40, Also published J. Fluid Mech, 115, 493-504,(1982).
3.5	Directly opposed and staggered rows of jets with eccentricity	H/D = 4 S/D = 2,4 E/D = 0, 0.1	V_j/U_∞ = 2.25	Transverse distributions of mean velocity and concentration at various Y/D planes at X/D = 6. Results reported in FS/80/3. Also published Int. J. of Heat and Mass. Trans., 23, 1673 (1981)
3.6	Single and opposed rows of jets with downstream contraction.	H/D = 4 S/D = 2,4 contraction ratio 4:1	V_j/U_∞ = 5.75	Centreplane and midplane velocity and concentration profiles. Also velocity and concentration contours at X/D = 6.

Table 3.1: Summary of Experimental Investigations

cover a range of jet-to-mainstream velocity ratios from 2.0 to 0.5 for a single row of jets: it also demonstrates the influence of geometrical asymmetry of the central jet over this range.

General flow patterns associated with directly opposing rows of jets are reported in Section 3.4. The number of flow and geometric variables associated with rows of opposing jets are large and can include, for example, jet-to-mainstream velocity ratio, confinement of the crossflowing stream, jet incident angle, jet eccentricity and axial or lateral staggering of the opposed jets. In the present case, parameters were chosen to correspond to those of primary and dilution zones of combustion chambers. Thus measurements were made with directly opposed jets for a series of pitch-to-diameters ratios and two jet-to-mainstream velocity ratios. The simple arrangement was also useful from the point that the prediction method could be tested against the measurements. Crabb (1979) showed that, for a single row of jets discharging normally into a cross-stream, disproportionately large asymmetries resulted in the flow field as a consequence of small geometric asymmetries being introduced by moving the central jet out of symmetry. Due to limitations of computer storage, multi-jet flows are normally modelled by considering a representative sector of the flow and using symmetric or cyclic boundary conditions. With the introduction of a geometric asymmetry in a row of jets, the flow can no longer be represented by a sector. Thus, the effects of small geometrical asymmetries, within the range of dimensional tolerances found in practice, require experimental quantification. This is the philosophy underlying measurements reported in Section 3.5 where the single row investigation of Crabb (1979) is extended to opposing rows of jets in an effort to explain the contributions of geometrical effects to the

asymmetric outlet profiles found in practice. The influence of pitch-to-diameter ratio, central jet eccentricity for one row of jets and the lateral and axial staggering of one row of jets with respect to the opposing side are demonstrated. The measurements were made mostly for a single jet-to-mainstream velocity ratio but can be used in conjunction with those of the previous sections to establish the influences of varying this parameter. For ease and clarity of presentation the mean and turbulence characteristics of the flow are presented in separate subsections.

In gas turbine practice the downstream end of the combustor may take the form of a nozzle and the measurements of section 3.6 simulate this situation.

The final section, 3.7, discusses the practical relevance of the results reported in the previous sections and presents conclusions to the experimental study.

3.2 Single Row of Jets

The results reported in this section (figures 3.1 to 3.8) are for a single row of jet geometry, as described in detail in chapter 2, for the mainstream velocity of 10.8 m/s and a jet-to-mainstream velocity ratio (V_j/U_∞) of 2.3. Duct height to jet diameter ratios of 8 and 4 and pitch-to-diameter ratios of 2 and 4 are considered. The scalar concentration results were obtained with only the central jet containing the tracer of helium gas. In all cases, the velocities have been normalized by the freestream velocity in the absence of the jets and concentrations are normalized by the helium concentration at the jet-exit. Profiles shown in figures 3.1 to 3.4 were taken along the centerplane of the central jet.

Figures 3.1 and 3.2, for jet pitch-to-diamter ratio (S/D) of 2, illustrate the effect of increasing the duct height from 4D to 8D. As can be seen from both the velocity and concentration profiles, the jet penetrates further, by about 0.5D at X/D = 4, into the freestream with the increased duct height. This was expected since the close spacing of the jetsand the increase of the duct height result in a decrease in the pressure gradient across the jet and a consequent raising of its trajectory. In addition, the effect of the jet on the freestream flow is clearly demonstrated with H/D of 8; above Y/D of 5 the velocity profiles have become flat and the introduction of the jet fluid has resulted in the freestream velocity increasing to 1.2 U_∞. The non-dimensional concentration maxima of 0.6 at X/D of 2 have decayed to 0.2 at X/D of 8 for both duct heights indicating similar dilution rates of the jets for the two cases. The influence of increasing the jet spacing from 2 to 4D for H/D of 4 and 8 is demonstrated by figures 3.3 and 3,4 which show that the jet penetration of the freestream is similar to that for the smaller jet spacing, with the same duct height. This result can be explained by the investigation of Kamotani and Greber (1973) who demonstrated the effects of opposite wall location, jet-to-mainstream momentum ratio and jet spacing on the penetration of a row of jets in to the mainstream. They showed that, for a given jet-to-mainstream momentum ratio, the jet trajectory (or penetration) was controlled by

(i) pressure forces, and

(ii) the interaction of the adjacent jets.

With sufficiently close spacing, the jets combine to behave like a two-dimensional jet and 'throttle' the crossflow. This causes a large pressure difference across the jets with resultant supression of the jet

trajectory. Increase of the spacing between the jets allows the crossflow to pass between them, thus reducing the pressure gradient and resulting in a raising of the trajectory. If the confining wall is placed sufficiently far away, the blockage induced force effects due to the wall are reduced so that they are no longer significant and the influence of the jet interaction on trajectory can be considered in isolation. Starting with a very high single jet trajectory and considering the jet in crossflow as a pair of counter rotating vortices, it was shown that as the jet spacing was decreased, the jet interaction increased, with a lowering of the trajectory. With sufficiently close spacing, however, these vortices disappear and the jets start interfering with each others entrainment of the crossflow. This effect results in a slower decay of the upward momentum flux of the jets and, in turn, a raising of the trajectory as the two-dimensional jet case is approached. Trajectories are, thus, most suppressed for some intermediate value of jet spacing.

For the present set of results, increasing the jet spacing results in a reduction of the wake zone behind the jets with resulting decrease of the pressure gradient and an increase of the jet penetration. This effect is offset by the interaction of the jets, with the larger spacing, and consequently there is no resulting change in the jet penetration of the freestream. There are differences, however, in the two sets of velocity profiles (figures 3.3. and 3.4). Profiles for the larger jet spacing (S/D = 4) indicate secondary peaks near the floor of the tunnel. These peaks are due to the mainstream flowing between the jets. Similar peaks are also observed at the nearest measuring location to the jets (X/D = 4) for the smaller jet spacing but the greater lateral mixing of the jets for this case results in the mainstream being impeded from flowing bewteen the jets and consequently the secondary peaks are not

allowed to develop further downstream. The greater mixing of the jets, for the smaller pitch-to-diameter ratio, is also confirmed by the flatter concentration profiles.

Mean velocity and scalar concentration distributions in planes perpendicular to the crossflow are presented in figures 3.5 to 3.8. These contours were obtained by interpolation from a matrix of individual measurement points as indicated on figure 3.5. In each of the four cases, contours are presented at locations four and eight jet diameters downstream of the plane of the hole centrelines. Figure 3.5, for S/D of 2 and H/D of 8, shows that even at a downstream distance of 8D, the jet has retained its identity. At 4D, the near wall closed semi-circular velocity contours show the individual nature of the jets but this is no longer evident at 8D. The region of maximum velocity is not coincident with that of maximum concentration. This observation demonstrates the care needed in defining the jet trajectory. Loci of maximum velocity, Kamotani and Greber (1972)are usually considered as the jet trajectory although the locus of maximum temperature, see for example, Margason (1968), is also sometimes used. Further, the contours of mean velocity at the symmetry plane Z/D = 1, demonstrate and validate the $\partial U/\partial Z = 0$ boundary condition normally used in the prediction method. The concentration contours, however, do not show the expected $\partial C/\partial Z = 0$ condition on the same plane but this is due to the fact that only a single jet contains the tracer of helium.

Comparison of figures 3.5 and 3.6 confirm that, for S/D of 2, H/D of 4 and the present velocity ratio, the jets penetrate further into the crossflow for the larger duct height. Otherwise, the two flows are very similar and in considerable contrast with those obtained for a pitch-to-diameter ratio of 4, figures 3.7 and 3.8, where the ind-

ividual nature of the jets is apparent at both downstream stations. The overall lateral spread of the individual jets, as shown by the concentration contours, is similar for both S/D cases; with greater near wall spreading for the lower value of S/D and a greater spreading at larger S/D values, caused by the greater penetration of the jets, for the larger S/D case. The velocity maximum still tends to be associated with acceleration of the freestream fluid rather that with jet fluid. Superposition of tracer gas from each jet would, as expected, lead to regions of lower concentration along the gap between the jets for the higher pitch-to-diameter ratio, further demonstrating the reduced inter-jet penetration for this value of S/D.

3.3 Single Row of Jets with a Geometrical Eccentricity

This section demonstrates the influence of a geometrical eccentricity of the central jet on the flow-field for V_j/U_∞ ranging from 2.0 to 0.5 and for a jet spacing, S/D of 2. The measurements were made at a downstream distance of 6D from the plane of the jet centrelines and various horizontal planes above the floor. The freestream velocity was 20 m/s for V_j/U_∞ of 0.5 and 1 and 10 m/s for V_j/U_∞ of 2.0.

Figures 3.9 presents measured transverse distributions of mean velocity, normalized with the freestream velocity, for jet-to-mainstream velocity ratios of 2.0, 1.0 and 0.5 with the jets symmetrically arranged. The results indicate symmetry to better than 5% of the maximum velocity for the three velocity ratios and this is also confirmed by the concentration profiles of figure 3.10 where symmetry to better than 1% of the normalizing value is observed. Figure 3.11 shows the effect of the central-jet eccentricity, i.e., the central jet was moved to one side but in the same lateral plane as the other four jets, for

a velocity ratio of 2.0. Considering first the eccentricity of 0.1D (figures 3.11a) there is a disproportionately larger change in velocity behind the jet centrelines. At Y/D = 1 (near the floor) the velocity behind the jet adjacent to the eccentric jet has decreased from 0.3 U_∞, indicating a throttling of the mainstream flow, whereas on the other side between the jet centrelines, the velocity has increased from 0.35 U_∞ to 0.5 U_∞ and is due to the freestream passing between the slightly wider pitch. At Y/D = 3, the velocity behind the centreline of the eccentric jet and its more distant neighbour show peaks and between them a wake is observed. This indicates that the slight increase of distance between the jets has resulted in a supression of their trajectories. An increase in eccentricity to E = 0.25D, (figure 3.11b) results in the wakes of the eccentric jet and its near neighbour coalescing to form a common recirculation zone at Y/D = 1.0. In spite of the large asymmetry in the velocity field, it is clear from the concentration distribution of figure 3.12 that the eccentric jet has moved rapidly towards the initially symmetric (Z/D = 0) position and that, by 6D downstream, the maxima of the concentration distributions are very close to the geometrically symmetric position for both values of eccentricty. These results are generally in accord with those of Crabb (1979).

Figure 3.13 presents velocity distributions for central jet eccentricities of 0.1D and 0.25D for velocity ratios of 1.0 and 0.5. In contrast to the results for the higher velocity ratio, the asymmetries are much less severe and confined to near wall regions: no wake coalescence is observed. Figure 3.14 presents concentration distributions corresponding to the same eccentricities and velocity ratios as for the previous figure and for velocity ratio of 1.0, the distri-

butions show a tendency for the jet to move back towards the geometrically symmetric (Z/D = 0) position. For a velocity ratio of 0.5, however, the concentration distributions are symmetric about the centreline of the eccentric jet as the jets can not spread laterally to the same extent as for the higher velocity ratios and thereby the interaction between them is reduced.

3.4 Directly Opposed Rows of Jets

In this section, the effect of pitch-to-diameter ratio and jet-to-mainstream velocity ratio is considered for directly opposed rows of jets.

Preliminary measurements were made with the opposing jets separated by a distance of 8D and for the maximum velocity ratio possible with the present arrangement, i.e., 2.8. Figure 3.15 presents mean velocity and scalar concentration profiles along the centreplane (Z/D = 0) for directly opposed jets and laterally staggered (Z/D = -1) floor jets with S/D of 2 and H/D of 8. As is evidenced by the profiles, the staggering of the floor jets has no effect on the penetration or dilution of the opposing row of jets as the two sets of profiles are, within limits of experimental accuracy and scatter, identical. The spacing between the opposing jets was, consequently, reduced to 4D where it was expected that the opposing jets would interact and the remainder of the results presented in this section are for this duct height (4D) and a mainstream velocity of 10.82 m/s.

Figures 3.16 and 3.17 present contours of constant mean velocity and concentrations for velocity ratios of unity and 1.8 at downstream values of X/D of 4 and 8 and for a pitch-to-diameter ratio of 2. As with related results for S/D of 4, a lower (symmetric) quadrant of the

flow is presented in each case with velocity on the right and concentration on the left. With the lower velocity ratio there is, clearly, little interaction between the opposing jets and the flow from either row is separated by the midplane (H/D = 2). The freestream flow passes between the neighbouring jets and also accelerates, with maximum velocities of 1.1 U_∞ along the midplane. The minimum velocity, corresponding to the wake region, is nearly coincident with the region of maximum concentration, which represents the jet fluid. The substantial mixing between the adjacent jets has resulted in a reduction of the core concentration from 0.5 to 0.3 at the downstream plane. The results for the higher velocity ratio show a much increased velocity of the freestream of 1.4 U_∞ in the midplane. In contrast to the results for the lower velocity ratio, the concentration contours indicate a penetration of the jets beyond the midplane for the higher velocity ratio of 1.8. At the downstream location of 8D the interaction between the opposing jets has caused the velocity maximum to shift, with maximum velocity of 1.25 U_∞ , from the plane between the opposing jets (Y/D = 2) to the symmetry plane (Z/D = 1) between the neighbouring jets. As with the single row results, section 3.2, $\partial U/\partial Z = 0$ at the plane Z/D = 1, and the use of a symmetry boundary condition in the numerical procedure is justified.

Preliminary measurements for S/D of 4 and unity velocity ratio did not reveal characteristics which appeared to have any special significance and are, therefore, not presented. It appeared that, for the range of S/D under consideration, the jet trajectories with unity velocity ratio were not strongly dependent upon this parameter with the freestream accelerating between the opposing jets and inhibiting any mixing between them.

Figure 3.18 presents velocity and concentration contours for V_j/U_∞ of 1.8 and for the downstream distance Y/D of 4 and 8. The velocity contours show quite clearly the development of the flow over this distance in that the wake region has moved from halfway between the midplane and the wall at X/D of 4 to the midplane at X/D of 8. This is in accord with the acceleration of the freestream in the midplane at X/D of 4 and its tendency to move to a position between the adjacent jets with downstream distance (i.e., X/D of 8). The concentration contours are in contrast to the trends observed with the smaller S/D. They indicate a bifurcation, at X/D of 8, of the jets about the centreplane (Z/D = 0), to form four core regions of jet fluid which were already recognisable at X/D of 4 and do not appear to have moved closer to either the midplane (Y/D = 2) or the centreplane (Z/D = 0) at the downstream distance.

The limiting case of pitch-to-diameter ratio of infinity, i.e., of two opposing jets, was also considered and the results are reported in detail by Atkinson et al (1982). Again, with the unity velocity ratio no significantly different physical characteristics were observed and there was no interaction between the two jets. For the higher velocity ratio, however, the freestream was only able to accelerate around the jets. The concentration contours revealed the jet penetration to the midplane even at X/D of 2 with concentration maxima on either side of the centreplane and forming two core regions of jet fluid.

Thus we have three general flow configurations which arise from opposed jets in crossflow. The situation obtained with the unity velocity ratio where the opposing jets retain their identities and the midplane can be replaced by a wall (also observed by Kamotani and Greber, 1974). The two jet cores found with two opposed jets and the higher velocity ratio and the four cores implied by figures 3.18 for the

V_j/U_∞ of 1.8 and S/D of 4.

With a single row of jets, symmetry of the flow was readily achieved for all velocity ratios. For the opposed rows of jets and a pitch-to-diameter ratio of 2, symmetry similar to that of the single row could be achieved for velocity ratios of unity and 1.8. With an increased velocity ratio of 2.3, however, considerable difficulty was experienced in achieving symmetric flow, although great care was exercised to achieve equal mass flow rates through the individual pipes. This question of flow asymmetry and those resulting from a geometric eccentricity of the central jet of one row is considered in detail in the following section.

3.5 Directly Opposed and Staggered Rows of Jets with a Geometrical Eccentricity

Measurements of mean velocity, scalar concentrations and turbulence characteristics were made for directly opposed and laterally and axially staggered rows of jets. In order that the results could be easily compared with results for a single row of jets and those of Crabb (1979) the measurements were made at a downstream distance of 6D from the jet centrelines and for a jet-to-mainstream velocity ratio of 2.3 and duct-height of 4D. The mean and turbulence characteristics are presented under separate headings for ease and clarity of presentation.

3.5.1 Mean Velocity and Scalar Concentration Characteristics

Measurements of mean velocity and scalar concentration have been obtained for the geometric arrangements shown on table 3.2 and are presented here in a sequence which conforms to that of the table;

		Positions of the Opposing Jets	Eccentricity of top central jet	Y/D								
				3.5	3.0	2.5	2.25	2.0	1.75	1.5	1.0	0.5
Pitch-to-diameter ratio (S/D) = 2	Velocity Profiles	Jets Opposing	E = 0	*	*			*			*	*
			E = 0.1D	*						*		
			E = 0.25D	*	*			*			*	*
			E = 0.5D	*		*		*			*	
		Floor jets staggered laterally (ie Z = - 1.0D)	E = 0	*	*			*			*	*
			E = 0.5D	*			*	*	*			*
		Ceiling jets staggered axially (X = 1.0D)	E = 0		*			*			*	
			E = 0.5D		*			*			*	
	Concentration Profiles	Jets Opposing	E = 0	*	*			*				
			E = 0.25D	*	*			*		*		
			E = 0.5D	*	*			*		*		
		Floor jets staggered	E = 0.5D	*		*				*		
		Ceiling jets staggered	E = 0.5D	*				*		*		
Pitch-to-diameter ratio (S/D) = 4	Velocity Profiles	Jets Opposing	E = 0	*				*			*	
			E = 0.5D	*				*			*	
		Floor jets staggered laterally	E = 0	*	*			*			*	*
			E = 0.5D	*	*			*			*	*
	Concentration Profiles	Jets Opposing	E = 0	*	*			*		*		
			E = 0.5D Top central Seeded	*	*			*		*		
			E = 5D Floor central Seeded	*	*			*		*		
		Floor jets staggered laterally	E = 0	*				*			*	
			E = 0.5D	*				*			*	

Table 3.2 Flow conditions for the measurements of Section 3.5

(* indicates measurement taken)

the results for S/D of 2 and 4 are presented separately. In the figures, individual measured values are presented to indicate the detail and scatter of results and smooth lines are drawn to represent and interpolate the measured values.

(i) Pitch-to-Diameter Ratio (S/D) of 2

Mean velocity values, measured at various distances above the duct floor, are shown on figures 3.19 to 3.21. Figure 3.19 corresponds to directly opposed jets, figure 3.20 to floor and roof jets staggered in the lateral (Z) direction by one jet diameter and figure 3.21 to floor and jets staggered axially (x-direction) by one diameter. The influence of the lateral displacement of the central roof jet, with respect to its neighbours, is shown on all these figures.

The general nature and symmetry of the flow may be deduced from figure 3.19(a) which shows, for the symmetric case (E/D=0) that the free-stream flow accelerates between the adjacent jets with velocities in excess of 1.5 U_∞ in the midplane (Y/D = 2). The influence of the opposing jets extends to the midplane as is evidenced by the wakes behind the jet centrelines, at X/D of -2,0 and 2. At Y/D of 3.5 and 3.0 the velocity maxima between the neighbouring jets exhibit differences of about 4% but, at Y/D of 2 and below the midplane, the two maxima are within 1% of each other. This result is due to the discrepancy (less than 2%) in the velocities issuing from the roof jets for this series of measurements. This discrepancy was reduced to an acceptable value (as discussed in Chapter 2) for all subsequent measurements. The series of figures 3.19(b), (c) and (d) demonstrate the influence of geometric asymmetries of 0.1D, 0.25D and 0.5D of the central jet for the top row. With the smallest eccentricity, the

velocity maximum between the displaced jet and its close neighbour has decreased to 1.0 U_∞ from the earlier value of 1.15 U_∞ for the symmetric case. On the other side (Z/D = -1), the velocity maximum has remained unchanged at 1.1 U_∞ . The eccentricity effect has not penetrated to the midplane (Y/D = 2) where the profile has remained unaltered.

The influence of a further increase of eccentricity to 0.25D is, as was the case with the single row of jets of the earlier subsection, to increase the velocity maximum in the larger gap between the neighbouring jets and to reduce the velocity maximum behind the two more closely neighbouring jets. Near the top wall there is evidence of wake coalescence of the jets, with a common wake at Y/D = 3.5 but this is not present at Y/D = 3.0. For the largest eccentricity (E/D = 0.5) the velocity maximum is increased from 1.25 U_∞ to 1.45 U_∞ at Z/D of -1.0 and reduced from 1.25 U_∞ to 0.92 U_∞ at Z/D of 1.0 in the vertical plane corresponding to Y/D of 3.0. Wake coalescence of the close neighbouring jets, with eccentricity of 0.25D, has occurred and is evident at Y/D of 3.0. For a single row of jets and with eccentricity of 0.25D the eccentric jet and its close neighbour had combined and a recirculation zone was found behind the combined jet at X/D of 6. In the opposing jet case, even with the largest eccentricity of 0.5D, no negative velocities were encountered. The penetration of the effects of the asymmetry to the lower half of the flow is not important except for the case of 0.5D eccentricity where the velocity maximum at Z/D = -1 has been increased by around 10% due to the two closely neighbouring roof jets presenting a barrier to the free-stream which is accelerated between the wider gap between roof jets, as previously discussed, and between the midplane (Y/D = 2) and the floor.

Figure 3.20 corresponds to roof and floor holes staggered in the Z-direction by one diameter and also shows the effect of an eccentricity of 0.5D of the central roof hole. Figure 3.20 corresponds to roof and floor jets staggered in the lateral (Z) direction by one jet diameter. Figure 3.20(b) shows, in addition, the effect of 0.5D eccentricity of the central roof jet. The velocity distributions with no eccentricity of the central jet, figure 3.20(a) are similar for planes equi-distant from the floor and the roof, i.e. Y/D of 0.5 and 3.5 and Y/D of 1.0 and 3.0, but displaced laterally by Z/D of 1 and should be uniform at Y/D of 2.0. The lack of uniformity suggests that flow asymmetries considered negligible at Y/D planes above and below the midplane (Y/D = 2) have been magnified to become significant at Y/D of 2.0. Again, the free-stream has tended to accelerate between the jets to give a midplane average value of around 1.3 U_∞. The non-uniformity of the midplane velocity distribution may, in part, reflect the preference of the free-stream to yield maximum velocities at locations of equal velocities at lower and higher values of Y. The effect of hole eccentricity is even larger than on figure 3.19(d) at Y/D values above the midplane but is of similar magnitude at Y/D of 0.5. The velocity distributions for both zero and 0.5D eccentricity show large deviation from symmetric flow below the midplane and are clearly associated with the asymmetry of the floor hole arrangement, with respect to the tunnel walls.

The velocity results for the axially staggered case, figure 3.21, reflect the different effective X-values of the measurements above and below the midplane. Thus, the velocities of the lower half, figure 3.21(a), corresponding to X/D of 6, are lower than those of the upper half which correspond to X/D of 7. This accounts for the slightly hi-

gher velocities of the figure when compared to those of figure 3.19(a). The effect of the 0.5D eccentricity, figure 3.21(b), is however much larger than can be explained by the X-value alone. The larger wake region and the pronounced asymmetry, in comparison to the directly opposed case, at the midplane is due to the floor jets causing the freestream to accelerate towards the roof when it encounters a second row of jets, this time emerging from the roof and with eccentricity.

The non-dimensional concentration profiles of figures 3.22-3.24 were obtained with the helium tracer in the ceiling central jet only. Figure 3.22 correponds to directly opposed jets. The profiles of figure 3.22(a), for symmetrically arranged jets, exhibit a slight asymmetry close to the wall, i.e. at Y/D of 3.5. In common with the velocity distributions the profiles become symmetric away from the wall and have a maximum value on the jet centreline at the midplane (Y/D = 2) and lower values in the near wall region. The lateral spread of the jet indicated by the distributions is similar to that for the single row case of section 3.3. This suggests the non-dependence of the lateral spreading of the jet on the confinement due to either the position of opposing wall or the presence of the jets issuing from it. Figures 3.22(b) and (c) demonstrate the effect of the central jet eccentricity of 0.25D and 0.5D respectively. With both values of eccentricity the near-wall values of concentration show a rapid return of the jet fluid to the initially symmetric (Z/D = 0) position. On the midplane and beyond (at Y/D = 1.5) the symmetry remains but with an axis corresponding to that of the eccentric jet. Thus, it appears that the close neighbour of the eccentric jet tends to push it towards the initially symmetric position but the opposing jet has the effect of countering this action and aids the eccentric jet in maintaining

its asymmetry.

Figure 3.23 shows the effect of a 0.5D eccentricity of the top central jet for laterally staggered floor and roof jets. In contrast to the results for the directly opposed jets, with the same eccentricity, the eccentric jet is symmetrical about its newaxis (z/D = 0.5) for the Y/D of 3.5. For values of Y/D near the midplane (Y/D = 2.5) and beyond (Y/D = 1.5) the results indicate a tendency of the jet fluid to return to a symmetric distribution about the centreline of a corresponding non-eccentric jet (i.e. Z/D = 0). This is probably due to the combined action of the close neighbour of the eccentric jet and the staggered opposing jet acting together to cancel the effects due to the geometric asymmmetry. Figure 3.24, for axially staggered roof jets and with top central jet eccentricity of 0.5D, exhibits characteristics which are identical to those for directly opposed jet with the same value of eccentricity which have been discussed above. Thus, and in contrast to the velocity characteristics, the influence of the scalar quantity, for pitch-to-diameter ratio of 2, extends beyond the midplane and to an important extent.

(ii) Pitch-to-Diameter Ratio (S/D) of 4

Figure 3.25 presents results for directly opposed jets and the effect of 0.5D eccentricity of the top central jet. The resulting flow asymmetry is drastically reduced from the previous S/D of 2 case. This stems from the ability of the free-stream to better penetrate the gap between the two neighbouring jets where they are separated by 3.5D rather than the 1.5D for S/D of 2. The geometric eccentricity has, however, resulted in a shifting of the wake region to behind the eccentric jet and a wider wake region at the midplane (Y/D = 2),

due to the impingement and greater lateral spread of the jets on that plane. The tendency for asymmetry, even with the nominally symmetric arrangement of holes, should be noted on figure 3.25(a) and will be discussed further in relation to the corresponding concentration profiles (figure 3.27a) which confirm that the opposed jets tend to diverge in opposite directions from the hole centreline. The results of figure 3.26a, for laterally staggered jets and zero eccentricity, suggest that the non-uniformity of the midplane velocity values for the similar arrangement with S/D of 2 (figure 3.20a) do result from the freestream accelerating more in regions of equal velocity above and below the midplane. The series of wakes present at Y/D of 3 and Z/D of $\pm$ 2 indicate that the floor jets have penetrated far beyond the midplane. The penetration of the ceiling jets to Y/D of 1.0 is also indicated in the figure but the ceiling jet is not able to penetrate beyond the midplane as strongly or to the same extent and this is probably associated with the reduction in total mass injected from the floor surface and the preference of the freestream to follow this route for its reduced resistance. The eccentric jet results of figure 3.26(b) follow the expected pattern with significant influence beyond the midplane, but becoming diminished by Y/D of 0.5.

The non-dimensional concentration results of figure 3.27(a) for directly opposed jets show, for symmetric arrangement of jets, that the expected symmetry does not exist and that the fluid from the seeded roof jet has tended to bifurcate and in an asymmetric manner. This observation is consistent with the small asymmetries revealed by the velocity distributions of figure 3.25(a) and is important in its implication that, with opposed jets unconstrained by surrounding jets or walls, with a geometrically symmetric arrangement flow symmetry cannot be achieved

with the dimensional tolerances of the present arrangement. Figure 3.27(b) demonstrates the influence of the top central jet eccentricity of 0.5D. The concentration distributions for near wall regions (Y/D = 3.5, 3.0) reveal two peaks which are symmetric about the centrelines of the eccentric jet. On and beyond midplane, however, only single concentration maxima are observed at Z/D of 1.5. Thus, it appears that the introduction of an eccentricity of 0.5D has led to the opposing jets 'slipping' past each other with concentration peaks being displaced by 1.0D. This is confirmed by the results of figure 3.27(c), which corresponds to the same conditions as those of figure 3.27(b) but with the floor central jet carrying the helium trace where single concentration maxima are again observed on and beyond the midplane but this time are displaced to the opposite side of the jet centreline, i.e. at Z/D of - 1.0.

The results of laterally staggering the jets for S/D of 4 are demonstrated by figure 3.28. With the jets symmetric, figure 3.28(a), the concentration distributions are, generally, symmetric about the centreline of seeded jet, although small deviations from symmetry are found in the near-wall region (Y/D of 3.0). Figure 3.28(b) demonstrates the effect of top central jet eccentricity of 0.5D. Unlike the smaller S/D case, there is little effect of the close neighbour on the eccentric jet with the concentration distribution showing nominal symmetry about the centreline of the displaced jet at Y/D of 3.0. The distributions show a tendency of the jet fluid to return to a symmetric distribution about the centreline of a corresponding non-eccentric jet (Z/D = 0) and this is probably due to the staggered jet of the opposing row influencing the eccentric jet to regain symmetry about the centreplane (Z/D = 0).

3.5.2 Turbulence Characteristics

The turbulence measurements reported here were obtained with the hot-wire anemometry system described in chapter 2. Due to the inability of the system to give accurate measurements in regions of high turbulence intensity, i.e. greater than 25 per cent, the measurements were conducted at and downstream of 6 diameters from the jet centrelines and are subject to errors discussed in chapter 2.

In order to be consistent with the mean velocity and concentration measurements the detailed turbulence measurements were made at the downstream plane X/D = 6. In all cases, only a sample of the measurements is presented and has been chosen to demonstrate the different and more important flow features.

Centreplane profiles of the mean and rms values of the axial velocity, for a pitch-to-diameter ratio of 2 and jet-to-crossflow velocity ratio of 2.3, are presented on figure 3.29. Values of the rms fluctuations in excess of 35 per cent were observed at X/D of 4 and the accuracy of any hot-wire measurements at this plane would, certainly, be questionable. At the nearest measurement position (X/D = 4) the mean velocity profiles show a maximum at the symmetry plane (Y/D = 2) due to the acceleration of the crossflow between the floor and ceiling jets. Also a large wake region, caused by the jet injection is observed. Further downstream, (X/D of 6 and beyond) the velocity maximum decays and the wake region is filled in by the mainstream fluid flowing between the opposing and the adjacent jets and the flow shows a tendency towards two-dimensionality. The maximum of the rms fluctuations coincides with the point of inflexion in the mean velocity profile at X/D of 4 and the fluctuations show a rapid decay with downstream distance which is consistent with the mean velocity profiles. It is interesting to note

that the maximum of the rms fluctuations coincides with that of the scalar concentration which is found in the wake region.

The lateral distributions of the turbulence characteristics showing rms values of the three velocity components and two shear stresses ($\overline{uv}/U_\infty^2$, $\overline{uw}/U_\infty^2$) for directly opposed jets and for directly opossed jets with top central jet eccentricity of 0.5D are presented in figures 3.30. The normal stresses are generally of equal magnitude at this downstream location for the three measured horizontal planes. The ($\overline{uw}/U_\infty^2$) correlation has maximum values which are associated with the largest gradients shown in the mean velocity profiles. The positive values of $\overline{uw}$ are probably due to the high velocity fluid elements moving into the wakes (u and w positive) and the negative values are produced in a similar manner but the w- direction is in the negative sense for these. The zero $\overline{uw}$ shear stresses are found behind the jet centrelines and between the centres of the neighbouring jets. This is expected, due to the inability of the two streams to penetrate each other to this extent. As with the mean flow data, there are deviations from symmetry in the turbulence measurements for geometrically symmetrical arrangement of the jets. The ($\overline{uv}/U_\infty^2$) correlation has all positive values at the plane Y/D of 3, due to the transfer of momentum from the faster moving fluid in the lower planes to the slower moving fluid of the plane Y/D = 3 (u and v both positive). In contrast, the ($\overline{uv}/U_\infty^2$) values are all negative, but generally of the same magnitude, on the plane Y/D = 1. This was expected since the transfer of momentum below the symmetry plane (Y/D = 2) was from the higher planes to the lower ones (u positive, v negative) and the same outcome was also implied by the mean velocity profile.

The effect of a 0.5D asymmetry of the top central jet are also demonstrated on figure 3.30. In accord with the measured mean velocity profiles (figure 3.19d) the $(\overline{uw}/U_\infty^2)$ correlations are strongly affected at the measured plane nearest the upper wall (Y/D of 3) but only slight deviations, from the symmetric case, are observed at the lower horizontal planes Y/D of 2 and 3. The $(\overline{uv}/U_\infty^2)$ correlations, however, exhibit large changes from the symmetric case, on the symmetry plane (Y/D = 2). These probably resulted from the crossflow being accelerated upwards, through the wider gap, by the floor jets on one side of the eccentric jet and the eccentric jet and its close neighbour combining to accelerate the crossflow downwards, between the symmetry plane (Y/D = 2) and the floor jets, on the other side. The effects of the large geometric asymmetry are not reflected in the turbulence measurement on the lowest horizontal plane Y/D = 1.

Measurements similar to those of figure 3.30, and for the same conditions, are presented on figure 3.31 for a downstream distance of 10D for symmetrically opposed jets on the horizontal planes Y/D = 2, 1 and 0.5. The normal stresses for the three directions are generally of equal magnitudes and show little variation in the transverse plane. The near-zero shear stresses indicate that the two streams have mixed to a greater extent and the flow has become two-dimensional.

As discussed earlier, considerable difficulty was experienced in achieveing symmetric flow for geometrically symmetrical opposed jets with the higher velocity ratio (V_j/U_∞ = 2.3). This asymmetry in the mean flow results was also reflected by the turbulence measurements. The series of figures 3.32 (a), (b) and (c) show the effect of reducing the velocity ratio to 1.5, directly opposed jets with a pitch-to-diameter ratio of 2. With this velocity ratio there is little interaction

between the opposed jets. The mean velocity profile of figure 3.32(a) for the mid-plane (Y/D = 2) is nearly flat with an average value of 1.3 U_∞. Thus, the crossflow has accelerated between the opposed jets which have turned without penetrating to the midplane (Y/D = 2); the shear stresses $\overline{uv}$ and $\overline{uw}$ are both zero on this plane. There is symmetry of the mean flow in the plane Y/D = 2 (figure 3.32 (b)) and this is also reflected by the $(\overline{uw}/U_\infty^2)$ correlation. The three normal stresses are again, generally of equal magnitudes and the $\overline{uv}/U_\infty^2$ correlation shows symmetry within the limits of experimental scatter. The same trends are also observed on the near-wall plane Y/D = 0.5, except for the $(\overline{uv}/U_\infty^2)$ correlation which is approaching zero due to the proximity to the wall and the consequent decay of the momentum transfer in the vertical direction.

Measurements were also obtained for the same conditions as for figures 3.32 but with the floor jets staggered laterally by one diameter with respect to the ceiling jets. Above and below the mid-plane at Y/D of 3 and 1 the results were similar to the opposed jet configuration but displaced by one diameter below the mid-plane. On the mid-plane (Y/D = 2), however, the turbulence results indicated non-uniformities similar to those found in the mean velocity profiles and the introduction of top central jet eccentricity of 0.5D did not produce any significant changes on this plane.

The effect of increasing the pitch-to-diameter ratio to 4 for directly opposed jets is demonstrated by figure 3.33 for horizontal Y/D of 3 and 2. Measurements were also obtained at Y/D of 1 and were similar to those at Y/D of 3. The increase of the spacing between the adjacent jets has resulted in a decrease of the lateral velocity gradients and is shown but the smaller values of the $(\overline{uw}/U_\infty^2)$ correlation at Y/D of 3.

On the mid-plane (Y/D = 2), however, the increase of jet spacing has resulted in impingement of the jets and a large wake region and this effect is clearly demonstrated by the $(\overline{uw}/V_\infty^2)$ correlation where large values are observed at Z/D of $\pm$ 5 and are indictive of the strong shear between the jets and the crossflow. The $\overline{uv}$ shear stress is very small on this plane and suggests the lack of momentum transfer in the vertical direction. As with the mean velocity and concentration distributions, the turbulence characteristics are not as strongly affected by the top central jet eccentricity of 0.5D for the S/D of 4 as they are for the smaller pitch-to-diameter ratio of 2.

Measurements for S/D of 4 and with the floor jets staggered laterally by two diameters with respect to the ceiling jets are presented by figure 3.34. As with the directly opposed jets at Y/D of 3 and 1, the $(\overline{uw}/U_\infty^2)$ correlations are small on the planes Y/D of 3, 2 and 1 due to the reduction of the lateral velocity gradients. The $(\overline{uv}/U_\infty^2)$ correlations are much larger and this increase, over the directly opposed case results from the strong shear between the jets from the opposing walls penetrating beyond the mid-plane and interacting with each other. Effects of geometric eccentricity are not severe on the turbulence characteristics for this larger value of pitch-to-diameter ratio and with the jets from the opposing wall staggered laterally.

3.6 Rows of Jets in Crossflow with a Downstream Contraction

The result presented here quantify the variations in mean velocity and a conserved scalar as a function of hole arrangements with a downstream contraction similar to that found in the downstream region of some annular combustors. The present arrangement has been described in chapter 2. The single-sided contraction had an area ratio of 4 and this

led to a decrease of the crossflow velocity to 4.3 m/s, in the plane of the jets, and to a jet-to-crossflow velocity ratio of 5.75. Most measurements were obtained at the downstream location X/D of 6 with pitch spacings of 2 and 4 diameters. Results are presented for floor and ceiling jets, blowing separately and with both rows blowing simultaneously for directly opposed and laterally staggered arrangements.

Figure 3.35 presents normalised velocity and concentration contours for the case where only the jets on the lower surface were blowing and for pitch-to-diameter rations of 2 and 4. The mean velocity distribution for the lower S/D value shows a strong tendency towards two-dimensional behaviour. Without the contraction the individual nature of the jet was still apparant in the form of wakes at X/D of 6 but with its addition the wake regions have disappeared. Velocity measurements taken in the absence of the jets indicated a recirculation region of 0.5D on the lower surface at the entrance of the convergent section but no regions of reverse flow were detected when the jets were blowing. The velocity results for the larger pitch-to-diameter ratio, in contrast to those for S/D of 2, indicate the individual nature of the jets with the crossflow accelerating between and above the jets and low velocity regions appearing behind the jet centrelines. The concentration results were obtained with only the central jet containing the helium tracer and indicate, for a pitch-to-diameter ratio of 2, the penetration of the jet to the top wall with a single concentration core. The lateral spread of the jet fluid is similar to the single sided injection results in the absence of the contraction. For the larger value of S/D the jet fluid has, again, penetrated to the top wall but has also bifurcated with regions of maximum concentration occurring off the centreline of the jet at Z/D of 1.25. These trends are very different from the

results without the contraction and are due wholly to the presence of the converging section.

Figure 3.36 shows results for the same flow conditions as above but this time only the upper row of jets are in use. As before, the jet fluid is present in the vicinity of the wall opposite to the jets. The mean velocity contours indicate regions of higher velocities near the upper surface with smaller values appearing on the floor side. Thus it appears that the effect of the pressure gradient, caused by the convergence, is stronger than any blockage effect caused by the jets.

In practice, it is more usual to have both rows in use with the jets directly opposed and figure 3.37 provides related results with helium tracer in the central jet of the upper or the lower row for a pitch-to-diameter ratio of 2. The velocity contours correspond closely to a two-dimensional boundary layer and there is no evidence of the individual jets. As before, the higher velocities resulting from the convergent section are located nearer the upper surface. The concentration contours with only the floor jet containing the tracer indicate regions of high concentration near the upper surface, again caused by the contraction, and those with the tracer in the ceiling jet show a more even distribution between the upper and lower surfaces. Contours obtained by adding the results from measurements with the two central jets separately containing the helium tracer are near vertical lines with regions of maximum concentration in the plane of the jet centrelines and those of low concentrations appearing between the adjacent jets of each row.

Measurements were also made for the same flow conditions as figure 3.37(a) but with a pitch-to-diameter ratio of 4 and the results are presented in figure 3.38. The velocity results are similar to those for the lower value of S/D, except that the high velocity values

have been displaced near the top surface to appear on the plane between the ceiling jets. The concentration contours, with only the floor central jet containing the tracer, indicate regions of maximum concentration near the upper surface. The local concentration values are smaller with the increased S/D and this is due to the greater lateral spreading of the jet in this case. Thus, it appears that with directly opposed jets the opposing jets impinge and combine to form a single jet which is forced to move towards the upper surface by the pressure gradient resulting from the convergence of the lower surface.

Figure 3.39 presents results with the opposing rows staggered laterally, so that the axes of the upper jets lay between those of the lower jets, for S/D values of 2 and 4. The resulting velocity field for the lower pitch-to-diameter ratio again tends towards two-dimensionality but, for the larger S/D value, the individual nature of the jets is still evidenced by the low velocity region on the plane of the jet centreline. Concentration contours show a small degree of bifurcation of the jet with the smaller jet spacing and a much larger bifurcation occurs for S/D of 4 with a shifting of the concentration peak to Z/D of 1.25, as was observed with the single rows for the same pitch-to-diameter ratio. On the evidence of the present results it is difficult to assess whether the directly opposed or the laterally staggered configuration provides a better mixing of the jets with the crossflow.

3.7 Conclusions and Practical Implications of the Experimental Investigation

This chapter has examined the nature of flows resulting from various jets-in-crossflow arrangement. This section considers, in summary form, the main conclusions to emerge from the various configurations considered. This is followed by a more general discussion of the

practical implications of the present experimental study.

(i) Single row of jets

The mean velocity and concentration profiles downstream of a row of jets issuing normal to a crossflow, and with uniform pitch-to-diameter ratio, are symmetrical.

The effect of reducing the pitch-to-diameter ratio from 4 to 2 is a rapid lateral coalescence, loss of individual jet identity and appearance of practically two-dimensional flow by 6D downstream of the jet injection.

For high jet-to-crossflow velocity ratios, the introduction of a geometric asymmetry leads to a highly eccentric velocity field, but the passive scalar field tends to return to symmetry about the centreline of the non-eccentric jet (Z/D = 0), with downstream distance. With lower velocity ratios, however, the asymmetry of the velocity field becomes less pronounced and the passive scalar field is no longer able to regain symmetry.

(ii) Opposing rows of jets

For pitch-to-diameter ratio values of 2, 4 and ∞ (i.e., two opposing jets) and jet-to-crossflow velocity ratio of unity the opposing jets do not impinge to any great extent and, as a result, retain their identities at downstream stations with single concentration maximum for each jet.

With the higher velocity ratio (V_j/U_∞ = 1.8) the jets impinge and can bifurcate in three different ways; i.e. retaining their identities with single jet cores as for S/D of 2, with two jet cores per jet as for S/D of 4 or mixing to form two mixed-jet cores as for S/D $\rightarrow \infty$.

The introduction of a geometric asymmetry for one row of jets, for jet-to-crossflow velocity ratio of 2.3, results in large flow asymmetries for S/D of 2. With the larger pitch-to-diameter ratio, however, even with

geometric symmetry the jets bifurcate with large asymmetries; the flow is not affected strongly by any geometric asymmetry of the central jet for one row.

The pressure forces are more dominant than any turbulence effects and this is especially true for the smaller pitch-to-diameter ratio.

(iii) Row of jets with a downstream contraction

For a single row of jets, the jet fluid is present in higher concentrations in the vicinity of the wall opposite to the jets. In addition, for S/D of 4 the jets bifurcate to give a maximum concentration value which is shifted to a plane between centrelines of the adjacent jets.

With opposed rows of jets the mixing of the jet fluid and the cross-flow is more uniform than for the single row case.

The present experimental results, although obtained from simple geometric configurations, have implications for the design of dilution zones of practical combustion chambers. For instance, the directly opposed jets results showed that with the high velocity ratios and pitch-to-diameter ratios of 2 and 4 - a combination present in some combustor arrangements - the jets bifurcated. The multiple maxima in scalar concentrations will correspond to cool streaks with consequent implications for design. These streaks were persistent as was witnessed by their presence in results obtained with higher velocity ratios (up to 2.3) even though significant asymmetries were present.

The results also showed that geometric asymmetries gave rise to important flow asymmetries and that, particularly for the lower value of pitch-to-diameter ratio, these are relevant to the manufacturing tolerances of gas-turbine combustors and to the resulting flow uniformity.

With the larger pitch-to-diameter ratio the opposed jets bifurcated asymmetrically and engineering tolerances were of lesser importance.

The results for the contracting section implied that dilution jets located upstream of a contraction give rise to regions of cool gas between the adjacent jets with the hotter regions found behind the jet centerlines. These results supported the observations made with tests on model combustors by industry, Sotheran (1980).

In addition to their relevance to engineering practice, the results are important for the development of calculation methods in that they quantify the effect of the common assumption of symmetric flow boundary conditions. Clearly, assumptions of this type can give erroneous results if a geometric asymmetry exists or, as in the case of S/D of 4, impinging jets bifurcate asymmetrically. In the next chapter the properties of some of the flows examined in the present experimental study will be calculated. The asymmetric bifurcation of jets, however, is not likely to be successfully calculated in the immediate future.

CHAPTER 4

CALCULATIONS OF JETS IN CROSS FLOW

4.1 Introduction

This chapter describes the calculations of jets in crossflow for selected cases of Chapter 3. The calculation approach is based on the solution of finite-difference forms of the partial differential equations representing conservation of mass and momentum and transport of kinetic energy and dissipation rate.

The following section, 4.2, gives details of the calculation method including the equations to be solved, the turbulence model, the procedure for the numerical integration of the equations in finite-difference form, the boundary conditions and discussion of the limitations of the calculation approach. Section 4.3 presents details of the specific boundary conditions used for a single row of jets, rows of directly opposing jets and presents comparison and discussion of calculated results with selected measurements of Chapter 3. Calculations are also presented outside the range of measurements to quantify the influence of the blockage parameter on the flow development for a single row of jets discharging normally into the crossflow and for opposed rows of jets.

The final section, 4.4, presents a more generalised discussion summarising the main conclusions of the present theoretical study and its implications for future work.

Calculations were also performed for the plane (2-D) jet in crossflow case of Rouse (1957). These were undertaken to improve

understanding of the computational method, with a computationally more economic case. Details of the boundary conditions and comparison and discussion of calculated results with the measurements of Rouse are appendicised at the end of the thesis (Appendix A).

4.2 Calculation Method

The basic features of the calculation method have previously been described in detail by several authors; see for example Gosman and Pun (1973), and only a brief description is included here. The discussion concentrates on the specific requirements of the calculations for jets-in-crossflow.

4.2.1 Equations to be solved

The conservation equations for mass and momentum (Navier-Stokes equations), see for example Schlichting (1968), are solved here in time-averaged form. The instantaneous form of the equations forms a closed set and with provision of boundary conditions and a suitable formulation of the numerical scheme, may be solved both for laminar and turbulent flow. However, for the turbulent flows considered in this thesis, the spatial resolution required the resolution of a range of length scales which is far greater than can be accommodated in available computer storage. Thus the equations were recast in Reynolds-averaged form, as indicated below, to retain the characteristics of engineering interest and permit their numerical solution.

Assuming steady, constant density flow, the Reynolds-averaged form of the conservation equations of mass and momentum may be written

in cartesian tensor notation (see Hinze, 1959), as:

Mass conservation

$$\frac{\partial \overline{U}_i}{\partial x_i} = 0 \qquad (4.1)$$

Momentum conservation

$$\frac{\partial(\overline{U}_i\overline{U}_j)}{\partial x_j} = -\frac{1}{\rho}\frac{\partial \overline{P}}{\partial x_i} - \frac{\partial}{\partial x_j}(\overline{u_i u_j}) \qquad (4.2)$$

In the present calculations the Reynolds number of the flow is considered to be sufficiently large such that the laminar transport effects in equation (4.2) are negligible in comparison to the turbulence effects. This will not be true near walls, and a special treatment, described in Section (4.2.4), is necessary.

The process of time-averaging, however, means that the equations (4.1 - 4.2) no longer form a closed set (that is, the number of unknowns exceeds the number of equations) and the Reynolds stress tensor $\overline{u_i u_j}$ must be represented by additional equations to allow closure of the equation set. The mathematical process of effecting this closure is referred to as turbulence modelling, and this is considered next.

4.2.2 Turbulence Model

(i) The approach and choice of model

Turbulence models generally fall into two main categories (Launder and Spalding (1972) and Bradshaw et al (1981)).

(a) Eddy-viscosity models

(b) Reynolds-stress models

The first approach relies upon the "eddy viscosity" concept of Boussinesq (1877) where the Reynolds stress is related to the mean rate of strain via:

$$-\rho\overline{u_i u_j} = \mu_t \left(\frac{\partial \bar{U}_i}{\partial x_j} + \frac{\partial \bar{U}_j}{\partial x_i}\right) - \frac{2}{3}\rho k\, \delta_{ij} \qquad (4.3)$$

with μ_t the isotropic eddy or turbulent viscosity

k the turbulent kinetic energy ($\equiv \frac{1}{2}(\overline{u_i u_i})$

and δ_{ij} the Kronecker delta function

Attention is then focussed on relating μ_t to known or calculable quantities. Models falling into this category vary in complexity from the simple algebraic equations for mixing length ("zero equation" level) such as that of Prandtl (1925), the one-equation models of Prandtl (1945) and Nee and Kovasznay (1969) to the numerous two-equation models (for example, Kolmogorov (1942), Jones and Launder (1972) and Saffman, 1974). The mixing length model is limited to its use to boundary layer type flows where a characteristic length scale of the turbulent motion (the mixing length) can easly be prescribed.

The lack of universality of the mixing-length model led to the introduction of effects of local turbulence properties, as well as the mean-flow properties, into the Reynolds stress relations. In a one-equation model, the turbulent viscosity is related to a typical length scale and the kinetic energy of turbulence, k, with the solution of a transport equation for k and the length scale defined empirically.

More complicated flows, such as these considered here, have regions of recirculation, and for this type of flow the length scale is difficult to specify empirically. The two-equation models overcome this problem by solving an equation for the dissipation rate, ε, of the turbulence energy which may be related to the length scale.

The second category of turbulence models do away with the concept of turbulent viscosity and, instead, solve equations for the individual Reynolds stresses, for example, Hanjalić and Launder (1972) and Launder et al (1973). In the present three-dimensional recirculating flow situation, this approach would require differential equations to represent the six Reynolds stresses and the turbulence energy dissipation rate. As well as being computationally more expensive, the Reynolds stress approach places demands on the available computer storage such that a reduction in the number of finite-difference grid nodes would be required in order to accommodate all the equations. In addition, and perhaps even more important, numerical inaccuracies which may be present in the calculation of the present flows are likely to cancel any advantages gained from the use of these more sophisticated models. In their study of flow behind a baffle, for example, Pope and Whitelaw (1976) showed that the simpler two-equation model performed as well as the Reynolds-stress models. Although Taylor (1981) has raised doubts about the accuracy of these results, the overall conclusions of Pope and Whitelaw (1976) are nevertheless noteworthy.

For present purposes, the two-equation eddy-viscosity models appear to offer the best compromise between accuracy and economy. Of the many two-equation models that have been proposed, the k-ε model

has been chosen for the present calculations as this has previously been extensively used and tested for two-dimensional flows with recirculation, for example, by McGuirk and Rodi (1978), Neilson et al (1978), Durst and Rastogi (1979), Habib and Whitelaw (1980) and others. Three-dimensional flows with recirculation have also been calculated with some success by, for example, Jones and McGuirk (1979), Crabb (1979), White (1980) and Gosman et al (1980). In general, the model has allowed the qualitative trends of the flows to be represented adequately. Details of the k-ε turbulence model are presented next.

(b) The k-ε Turbulence Model

As discussed earlier, the Reynolds stress is related to the eddy viscosity, μ_t, which is a spatial variable. This variation is given by the Prandtl-Kolmogorov expression (see, for example, Launder and Spalding, 1974):

$$\mu_t = C_\mu \rho k^{\frac{1}{2}} \ell \tag{4.4}$$

where C_μ is an empirical constant

k is the kinetic energy of turbulence

and ℓ is a characteristic length scale of the turbulence

The length scale, ℓ, may be related to a local turbulence property of the flow, namely, the rate of dissipation of turbulence energy, ε, (Jones 1971), by:

$$\varepsilon = \frac{k^{\frac{3}{2}}}{\ell} \tag{4.5}$$

Equations (4.4) and (4.5) can now be combined to give:

$$\mu_t = \frac{C_\mu \rho k^2}{\varepsilon} \tag{4.6}$$

The above equation (4.6) give the variation of the eddy viscosity in terms of the kinetic energy of turbulence and its dissipation rate*, which can be represented by their own transport equations. Details of the transport equation for k have been given by, for example, Hanjalic (1970) and for ε, Harlow and and Nakayama (1968) and Daly and Harlow (1970) have provided the required derivation. Rodi (1970) gives the modelled equations for these two quantities (for high Reynolds number flows) as:

The k-equation

$$\frac{\partial \rho \overline{U}_i k}{\partial x_i} = \frac{\partial}{\partial x_i}\left(\frac{\mu_t}{\sigma_k}\frac{\partial k}{\partial x_i}\right) \qquad \text{turbulent diffusion}$$

$$+ \mu_t \frac{\partial \overline{U}_i}{\partial x_j}\left(\frac{\partial \overline{U}_i}{\partial x_j} + \frac{\partial \overline{U}_j}{\partial x_i}\right) \qquad \text{generation}$$

$$- \rho\varepsilon \qquad \text{viscous dissipation} \tag{4.7}$$

---

* $\varepsilon \equiv \nu \overline{\left(\frac{\partial u_i}{\partial x_j} \cdot \frac{\partial u_i}{\partial x_j}\right)}$

The ε-equation

$$\frac{\partial \rho \bar{U}_j \varepsilon}{\partial x_j} = \frac{\partial}{\partial x_j}\left(\frac{\mu_t}{\sigma_\varepsilon}\frac{\partial \varepsilon}{\partial x_j}\right) + \frac{\varepsilon}{k}\left[C_1 \mu_t \frac{\partial \bar{U}_i}{\partial x_j}\left(\frac{\partial \bar{U}_i}{\partial x_j} + \frac{\partial \bar{U}_j}{\partial x_i}\right) - C_2 \rho \varepsilon\right] \quad (4.8)$$

where the parameters C_μ, C_1, C_2, σ_k and σ_ε are empirical constants.

Launder et al (1972) made extensive examinations of free turbulent flows and, as a result, recommended the values of the constants appearing in equations (4.6) - (4.8) as given in Table 4.1:

C_μ	C_1	C_2	σ_k	σ_ε
0.09	1.44	1.92	1.0	1.3

Table 4.1: Values of constants appearing in the k-ε turbulence model

This form of the turbulence model is valid only for fully turbulent flow. Near walls, where viscous effects dominate turbulent ones, the model needs modification (Jones and Launder, 1973). The use of a modified form, however, incurs a high penalty in the increased grid fineness required to resolve the rapid variation of the variables in this region, and the associated long computing times required to obtain converged solutions. The "wall function" approach, (described by, for example, Patankar and Spalding, 1970) which is based upon physical reasoning and empirical data, avoids the low Reynolds number region by bridging the sub-layer with special functions which connect

conditions at its outer edge to those at the wall. This approach is described in Section (4.2.4). The wall function approach, however, imposes limitations on the accuracy of the present predictions as the technique was formulated for boundary layer type flows with zero pressure gradient. For flows with separation and recirculation regions, such as those considered here, the wall functions may not adequately represent the local mean velocity gradients since the pressures may vary.

The investigation of Chieng and Launder (1980) for a backward facing step, compared the accuracy of predictions obtained using the low-Reynolds number form of the k-ε model and the wall function approach with experimental data. They concluded that the wall function approach gave reasonable agreement with experimental data and the results obtained using the low-Reynolds number form of the k-ε model gave, for example, heat transfer rates in the vicinity of the reattachment point that were five times too large. The dissipation equation was held responsible for these large discrepancies as it gave physically unacceptably large length scales close to the wall. The evidence from the study of Chieng and Launder (1980) suggests that with the current state of development of the low-Reynolds number form of the k-ε model, no distinct advantage would be gained from its use.

The other turbulence model related deficiencies of the present calculations concern the use of a scalar eddy viscosity. This is used to represent momentum diffusion in all three directions. In highly anisotropic flows it is unlikely that scalar eddy viscosity will represent adequately the differing rates of momentum transfer parallel and perpendicular to the walls as observed by, for example, Bergeles (1976).

Additionally, for flows with streamline curvature the additional strain rates caused by the curvature (Bradshaw, 1973, cited by Green, 1981) are not accounted for, and this is also likely to result in erroneous predictions.

In addition, the k-ε model under-predicts the length of the recirculation region (Vasilic-Melling, 1977), implying that the predicted turbulent viscosity is too high in recirculating flows. Although in this context the question of numerical truncation errors cannot be ignored as the additional "numerical" viscosity will contribute to shortening of the recirculating length and this point will be returned to in discussion of the results.

4.2.3 The finite-difference method

The calculation procedure adopted here uses finite-difference forms of the partial differential equations for each of the dependent variables over a discretized calculation domain. This transformation is brought about by integrating the equations over a non-uniform "staggered" grid arrangement, similar to that of Harlow and Welch (1965).

In developing the finite-difference version of the conservation equations for the transport of momentum, k, ε and a passive scalar, C, it will be convenient to consider a common form of equation for any dependent variable, ϕ, written in general form:

$$\frac{\partial \rho U_j \phi}{\partial x_j} = \frac{\partial}{\partial x_j} \left(\Gamma_\phi \frac{\partial \phi}{\partial x_j} \right) + S_\phi \qquad (4.9)$$

where ϕ is a surrogate variable standing for either U, V, W, k, ε or C,

Γ_ϕ is the diffusion coefficient, and

S_ϕ is a "source" term (Patankar, 1980)

Integration of equation (4.9) over a control volume yields a finite-difference which relates the value of the variable at a point P to those of its neighbours. For a three-dimensional control volume (Figure 4.1), this can be expressed in the following manner:

$$C_P\phi_P = C_W\phi_W + C_E\phi_E + C_N\phi_N + C_S\phi_S + C_T\phi_T + C_B\phi_B + S_U^\phi \qquad (4.10)$$

with $C_W = A_W g_W(F_W - 1)$ (4.11)

$$C_E = A_E g_E F_E \qquad (4.12)$$

where A_E is the area of <u>east</u> face of control volume

g_E is <u>east</u> face mass flux ($\rho_e \overline{U}_e$)

$$C_P = C_E + C_W + C_N + C_S + C_T + C_B - S_P^\phi \qquad (4.13)$$

S_U^ϕ and S_P^ϕ are the source term coefficients such that:

$$S_\phi \Delta x\, \Delta y\, \Delta z = S_U^\phi + S_P^\phi \phi_P \qquad (4.14)$$

The left-hand side of equation (4.14) represents the integration of the source term over the control volume. F_W and F_E etc. are factors (defined below) dependent upon the differencing used. Central differencing is used except when Peclet numbers exceed |2| and result in difficulties in achieving converged solutions; in this case upwind differencing is introduced, i.e.:

$$F_W = (1 + 2Pe_W^{-1})/2 \quad |Pe_W| < 2 \qquad \text{central}$$

$$F_W = \begin{cases} 1 & Pe_W \geq 2 \\ 0 & Pe_W \leq 2 \end{cases} \qquad \text{upwind} \qquad (4.15)$$

with $P_e = g_W \, \delta/\Gamma_W^{\phi}$, a ratio of the convective flux to diffusive flux, δ is the distance between nodes and Γ_W^{ϕ} is the mean exchange coefficients at neighbouring nodes. Runchal (1972) has shown that this hybrid-differencing scheme is stable for all Peclet numbers. The upwind differencing scheme is not as accurate as the central differencing, however, and errors associated with the upwind scheme are discussed in detail in Section 4.2.6.

In the finite-difference equations for momentum transport, pressure gradient enters as a source term, but does not appear explicitly in the equation for the conservation of mass. The determination of pressure requires special treatment and this will be considered in Section 4.2.5.

4.2.4 Boundary Conditions

For solution of the transport equations, specificiation of variables at the boundaries of the solution domain are required. The general types of boundaries and the dependent variable treatment are now discussed briefly.

(i) Inlet Boundary

The distribution of the variables U, V, W, k and ε at each grid node at the inlet plane were obtained from experiment wherever possible;

otherwise distributions based on "plug profiles" were used.

(ii) Outlet Plane

This boundary was chosen at a downstream distance sufficiently large to ensure that the flow was parabolic in nature and the location of the boundary had no influence on the upstream domain. Zero axial gradients were thus assumed, i.e.:

$$\frac{\partial U}{\partial x} = \frac{\partial V}{\partial x} = \frac{\partial W}{\partial x} = \frac{\partial k}{\partial x} = \frac{\partial \varepsilon}{\partial x} = 0 \qquad (4.16)$$

The accuracy of this assumption will be discussed later.

(iii) Symmetry Plane

The gradients of the variables normal to the symmetry plane and the normal velocity to the plane were set to zero.

(iv) Wall Functions

Wall functions were utilised to solve the problem of steep gradients at wall boundaries.

In the calculation procedure, the logarithmic law of the wall (see, for example, Townsend, 1980) is used to introduce a fictitious wall value for the diffusion coefficient, Γ_ϕ for the velocity component parallel to the wall and the scalar quantities k and ε. For elliptic flows, the standard form of the logarithmic law of the wall poses numerical problems at stagnation or reattachment points where the wall

shear stress, τ_w, is zero (i.e. $\ell n(o) \rightarrow \infty$). Launder and Spalding (1974) recommended the form of the law of the wall given by:

$$U^+ = \frac{1}{K} \ell n\ (Ey^+) \tag{4.17}$$

with $K = 0.41$ and $E = 9.0$

$$\text{where } U^+ = U_p \rho C_\mu^{\frac{1}{4}} k^{\frac{1}{2}} / \tau_w \tag{4.18}$$

$$\text{and} \quad Y^+ = \rho \Delta y C_\mu^{\frac{1}{4}} k^{\frac{1}{2}} / \tau_w \tag{4.19}$$

where Δy is distance of grid node from wall

and U_p is the velocity at the near wall node

With this form, there is no problem of $\ell n(o)$, as τ_w may be zero at stagnation or reattachment points but k is not. For local equilibrium boundary layer type flows:

$$\left(\frac{\tau_w}{\rho}\right)^{\frac{1}{2}} = C_\mu^{\frac{1}{4}} k^{\frac{1}{2}} \tag{4.20}$$

so that Y^+ and U^+ reduce to the standard forms. Thd diffusion coefficient for the velocity component parallel to the wall is then set as:

$$\Gamma_\phi = \frac{\mu\ k\ y^+}{\ell n\ (Ey^+)} \tag{4.21}$$

The source term in the equation of this velocity component is modified to the form:

$$S_U^\phi + S_p^\phi \phi_p - \frac{\Gamma_\phi\ A}{\Delta y} \tag{4.22}$$

where A is the area of the control volume face.

In applying a boundary condition for the turbulent kinetic energy the exchange coefficient, Γ_ϕ is set to zero as the diffusion of k near a wall is assumed to be negligible. The generation term in the equation for k is still assumed to be important and this is taken account of in the source term, which is modified to the form:

$$S_\phi = \frac{C_\mu^{\frac{1}{2}} \rho k \, Up}{\Delta y \, \ell n \, (Ey^+)} \tag{4.23}$$

In the near wall region, an exchange coefficient is not calculated for ε; instead the value of ε for the near-wall node is prescribed by a length scale as:

$$\varepsilon_W = C_\mu^{\frac{3}{4}} k^{\frac{3}{2}} / K\Delta y \tag{4.24}$$

This formula may be obtained with the assumption that the turbulence is in local equilibrium in the near-wall region.

4.2.5 Solution Procedure

The set of finite-difference equations for the dependent variables were solved by an iterative solution algorithm, previously described by Patankar and Spalding (1972) and Caretto et al (1973). Briefly, the procedure proceeds by using a guessed value of the pressure field, P*, and using this value to solve for $\overline{U}$, $\overline{V}$ and $\overline{W}$ from the momentum transport equations. These velocities will not, in general, satisfy the local continuity equation (local here means the finite-difference form of the continuity equation written for the control volume surrounding each grid node), but produce a net mass source for the point P. Pressure

corrections are then made such that the resulting velocity corrections will reduce the mass source to zero. The corrected pressure is then used to obtain new values of $\overline{U}$, $\overline{V}$ and $\overline{W}$. The remaining equations, for k and ε do not pose any problem and are solved next. This completes one iteration and the process is repeated until a converged solution is obtained. The criterion used to assess the extent of the convergence of the solution was based on the imbalance between the mass flow evaluated from the boundary conditions and that calculated from the continuity equation. Additionally, the change in the value of the dependent variables was checked at locations where steep gradients were expected. The exact details for the two and three-dimensional calculations are given in the relevant sections. The individual equations were solved for each variable with the line-by-line application of the tri-diagonal matrix algorithm (TDMA) described by, for example, Patankar and Spalding (1970) and Roache (1976).

The use of an iterative scheme for solving a set of non-linear coupled equations requires the use of under-relaxation, to prevent large changes from one iteration to the next, inducing divergence and numerical instability. This under-relaxation took the form:

$$\phi = f\,\phi_{new} - (1-f)\,\phi_{old} \qquad (4.25)$$

where f is an under-relaxation factor with a typical value of 0.5. ϕ_{new} is the new value of the variable and ϕ is the value taken forward to the next iteration.

4.2.6 Accuracy of Solution

The accuracy of the numerical approach is dependent on the degree of convergence of solution and the error associated with representing the partial differential equations by their finite-difference analogues, referred to as truncation errors. The use of sufficiently large number of iterations (typically 200 iterations for 2-D and 300 iterations for 3-D calculations) ensured that the iteration error was negligible. Truncation errors, therefore, formed the bulk of the numerical error in the solution. As discussed in Section 4.2.3, the type of differencing used in the present calculations was the hybrid scheme where "central" differencing (second-order accurate with respect to grid size) was used for local mesh Peclet numbers, Pe, of less than $|2|$ and "upwind" differencing (first-order accurate) was used for Pe greater than $|2|$. Of the two differencing formulations, the central differencing approximation is more accurate, but is numerically unstable to iterative solution for Peclet numbers greater than 2. The limits on available computer time and storage do not allow the use of fine grids for which Pe can be reduced to less than two everywhere in both 2D and 3D elliptic flow problems, and, in order to procure stable solutions, the upwind formulation is used. Although the upwind scheme gives stable solutions it introduces an error in the form of an artificially increased diffusion coefficient (Raithby, 1976). This "false diffusion" may result in predictions with gradients of the dependent variables which are locally smoothed-out not only by turbulent diffusion, but also by unphysical numerical diffusion; this sort of error can only be reduced by grid refinement. As discussed by Patankar (1980), for

example, this problem is particularly serious when the resultant velocity vector is skewed to the finite-difference grid.

In the type of flows considered here, there are two main problems: firstly, the geometrical configuration of jets-in-crossflow means that the flow is of necessity skewed across the grid nodes in some regions of the solution domain, so that significant numerical errors in these regions may be expected. Secondly, because of the 3D nature of the flow, and the consequent need thus to solve 3D elliptic partial differential equations, computer storage limitations provide an upper limit to the number of grid lines that can be used in each direction.

The approach which has been adopted in the calculations is to use non-uniform grid spacing and to concentrate grid lines in regions where numerical errors may be expected to be largest - i.e. regions with strong gradients or regions where the flow was at a large angle to the grid-lines. The location of these suspect regions was judged from calculations with a coarser grid. This process was repeated until the maximum grid-size on the available computer was reached. For each flow, an attempt has been made to judge which regions and what aspects of the flow are still influenced by numerical error and which features are believed to be predicted without being dominated by false-diffusion effects; these points are discussed further below.

4.3 Rows of Jets in Crossflow

This section is concerned with calculations of rows of round jets discharging normally into a confined cross-flowing stream. The

numerical scheme, as embodied in the computer code PACE (Jones, 1975), was used for these predictions. The section is divided into three sub-sections. The first (4.3.1) provides calculation details, including the boundary conditions used for a single row of jets and for directly opposed jets. Subsection (4.3.2) compares measured and predicted results for a single row of jets. The final subsection (4.3.3) presents calculations outside the range of measurements for a single row of jets and selected cases of directly opposing rows of jets.

4.3.1 Calculation Details

(i) Boundary Conditions

The solution domain for the present configuration may be represented by a rectangular box whose upper and lower walls coincide with the roof and floor of the wind tunnel; boundary conditions along these solid walls employed the wall function approach described earlier (Section 4.2). For opposed rows of jets the upper wall was replaced by a plane of symmetry. With the assumption of an infinitely long row of holes, the flow is symmetric about vertical planes through a hole centre (hereafter referred to as the centre-plane) and through the line bisecting the space between two holes (hereafter called the mid-plane). The upstream boundary condition corresponded to the measured mean axial profile at X/D = -5.5 with the cross-stream velocity components presumed zero, and k and ε determined assuming a turbulence intensity of one per-cent and a length scale equal to the duct height; the results obtained here were found, by numerical experiment, to be

insensitive to these assumptions and the location of the upstream plane. A similar approach was taken with the downstream boundary condition where the axial gradients of the dependent variables were assumed zero; the influence of the position where this assumption was imposed was evaluated by comparing results for the downstream boundary located progressively further away from the jets. The boundary condition was eventually assigned at X/D = 12.5 and had no influence on the results presented.

The final boundary condition was that imposed over the jet exit plane. Apart from the special treatment necessary in the regions where the semi-circular hole boundary intersected the rectangular finite-difference control volume surface areas, two types of conditions were tested. The first, and simplest form, assumed the efflux velocity ($\overline{V}_j$) to be constant over the hole, with zero U and W velocities and k and ε calculated with turbulence intensity value of 3 per-cent and length scale based on the jet diameter. Since it is known, see for example, Bergeles (1976) and Andreopoulos (1980), that the flow within a hole subjected to a crossflow at reasonably low values of jet-to-crossflow velocity ratios, is distorted due to the strong pressure gradients which are set up over the jet exit plane, the constant velocity boundary condition was considered to be a possible source of error with the present velocity ratio of 2.3. An alternative condition, based on the assumption that the velocity profile across the injection hole is consistent with a constant total pressure condition was also considered and, on inspection, gave results which were closer to the measurements. This boundary condition was prescribed by starting the calculation with zero static pressures everywhere within

the flow-field and a constant jet velocity, V_j, enabling the total pressure to be calculated initially:

$$P_{tot} = \tfrac{1}{2} \rho V_j^2 \qquad (4.26)$$

On subsequent iteration cycles, the static pressure over the hole had changed, and this enabled the vertical velocity within the injection hole to be updated using the equation:

$$P_{tot} = P_{stat} + \tfrac{1}{2} \rho V_j^2 \qquad (4.27)$$

An additional constraint was that the total mass flow from the slot was the same as in the constant velocity case. The velocity profile produced using this treatment over the jet exit is compared on the centre-plane for S/D = 2, H/D = 4 in Figure 4.2 to the profile measured by Andreopoulos (1980). The data of Andreopoulos was not taken in exactly the same configuration, but were measured in a single jet in crossflow at a slightly lower velocity ratio of 2.0 and the jet fed from a plenum chamber rather than through long supply tubes. Nevertheless, the qualitative trend of a low velocity at the front end of the jet and a higher than bulk mean velocity at the rear edge is reproduced; the predicted shape shows the maximum velocity too near to the rear of the hole, but is closer to the measured shape than the constant velocity condition. For the other variables in this boundary condition, U and W were set to zero. The boundary conditions on the turbulent quantities were based on fully-developed pipe flow as the length of the jet supply pipe was sufficiently long for this assumption to be valid; accordingly, the turbulence intensity level, which fixed the k value, was taken as 7 per-cent, which is a value

representing the area averaged turbulence level in fully developed pipe-flow, the jet diameter was used as the length scale in calculating ε.

(ii) Preliminary Calculations

The results presented in the next sub-section (4.3.2) were obtained with a finite-difference grid consisting of 20 x 20 x 30 nodes (in the y, z, x directions respectively). Non-uniform spacing was used in an attempt to cluster grid nodes in regions where rapid variations were expected. Because of the relatively small dimensions of the solution domain in the y-z plane, it was decided to use uniform spacing in these directions, but a finer grid was adopted in the axial direction near the hole and increased geometrically in the up and downstream directions; for the S/D = 4 calculation, a total of 16 grid nodes lay within the half-hole inside the solution domain, and this number increased to 35 for S/D = 2. Because of the complex three-dimensional flow-field and the use of upwind differencing, which is known to introduce numerical diffusion errors on coarse grids, it is necessary to investigate the extent to which the solutions are grid-independent.

The results of grid-independence tests are presented in Figure 4.3 in the form of axial velocity profiles on the centre-plane for S/D = 4, H/D = 4 for grid sizes 10 x 10 x 20, 15 x 15 x 20 and 20 x 20 x 30 (y, z and x directions respectively). It can be seen that the solutions are particularly sensitive to changes in the grid size in close to jet-discharge region; this is most apparent in the growth of the wake region behind the jet which does not extend to the X/D = 4 location

in the coarse grid case and shows an appreciable negative velocity region with the finest grid run. In addition, noticeable peaks in the maximum axial velocities at X/D = 2,4 start to appear as the grid is refined. Both these features are symptomatic of a reduction in numerical diffusion, which tends to smear out peaked profiles and leads to additional diffusion of momentum from high momentum to low momentum regions such as the wake. Although it can be presumed, on the evidence of Figure 4.3, that the addition of extra grid nodes in the near jet-discharge region would have brought about still further changes in the profiles, it can also be seen from the figure that the solutions downstream of X/D = 4 are not very dependent on the grid size, so that trends observed in the results at these locations are not strongly influenced by numerical errors. Further grid refinement was impossible as the 20 x 20 x 30 calculation employed the maximum accessible core-store on the IBM 360/195 machine used. A typical calculation involved 300 iterations to converge using 1200 K bytes of core and about 80 minutes CPU time. The convergence criterion was based upon the ratio of the magnitude of the overall continuity error to the total mass flow rate and the solution was considered to be converged when this ratio dropped below 0.5 per-cent.

Figure 4.4 indicates that the two jet exit boundary conditions yield very similar results for the S/D = 4, H/D = 4 configuration. The distortion of the exit velocity produced in the constant total pressure case was such that the jet velocity decreased at the leading edge and in the front portion of the hole by about 20 per-cent from its mean value (lowest velocity ≃ 20 m/s) and increased at the edge of the hole and towards the rear by about the same amount (maximum velocity ≃ 30 m/s).

This distorted profile produces different values of the local strain rates which were observed to be higher in the constant total pressure case; these larger velocity gradients generate more turbulence and hence lead to larger values of the turbulent viscosity than in the solution assuming constant jet velocity. Consequently, the axial velocity profiles show a smaller wake region and a slightly decreased penetration of the jet (more rapid diffusion of the vertical momentum) for the constant total pressure condition.

It was also confirmed that the higher levels of turbulence energy are produced predominantly by the extra generation effect described above and not due to the increased prescribed level of turbulence energy at the jet exit used in the constant total pressure condition. The same observations hold for the changes produced by altering the jet exit conditions for the case of a pitch-to-diameter ratio of 2, but now the effects are larger. Figure 4.5(a) presents the axial velocity profiles at four locations downstream of the jet discharge plane for the centre-plane and Figure 4.5(b) similar results for the mid-plane conditions. In the case of constant jet velocity, the lateral mixing is not rapid enough to prevent the free-stream penetrating between the jets, although some distortion of the profile can be observed in the appearance of wake-regions on the mid-plane at X/D = 4 and 8; the centre-plane profiles exhibit, however, the same inverted S-shape as was observed in the S/D = 4 calculations. The imposition of the constant total pressure condition produces a markedly different behaviour. The increased strain-rates induced by the distorted jet exit profiles (the efflux velocity variations are approximately the same) are enhanced now by the proximity of the jets. The

additional mixing enables the jets to coalesce rapidly in the lateral direction as can be seen from the nearly identical shapes of the profiles at X/D = 4 on the centre-plane and mid-plane. This trend towards a two-dimensional jet implies that the free-stream can no longer penetrate the gaps between the holes and must be accelerated over the jets, causing the maximum axial velocity to lie near the upper wall in the constant total pressure case. The additional turbulent mixing has also caused the wake region behind the jets to become very much smaller (it lies completely upstream of X/D = 2) and the inverted S-shape profile is no longer observed. The sensitivity of the calculations to the usually unknown profiles at the jet exit for low values of the pitch-to-diameter ratio is an undesirable feature which will be returned to in the next section.

It must be stressed however, that the changes in the solution described above, have not been brought about due to any changes in the effective momentum flux ratio or velocity ratio (jet-to-freestream) implied by the switch from one boundary condition to the other. An evaluation of the momentum mean velocity in the jet using the constant total pressure condition ($\int_{jet} \rho V^2 dA / \int_{jet} \rho V dA$) showed that the effective velocity ratio had only increased by about one per-cent from the value of 2.3 used in the constant velocity boundary condition calculation.

4.3.2 Comparison with Measurements

Figures 4.6 to 4.8 present comparisons between predicted and measured velocity profiles on the centre-plane for four transverse planes X/D = 4, 6, 8 and 10 and for three combinations of duct height-

to-diameter and pitch-to-diameter ratios; at two planes X/D = 4 and 8, a comparison is also presented for the profiles on the mid-plane. The results in all cases were obtained with the constant total pressure boundary condition at the jet exit. In Figure 4.6 the case of S/D = 2, H/D = 4 shows the worst agreement in that the shape of the profile is incorrectly predicted at X/D = 4, although the proximity of the flow to two-dimensionality is correctly predicted. The measurements still exhibit the inverted S-shape at X/D = 4, although in this low pitch-to-diameter ratio case, this has all but disappeared by X/D = 8; it persists in the other cases at the furthest downstream stations (see Figures 4.7 and 4.8). The increased rate of mixing in the calculations is unlikely to be caused predominantly by truncation error since it was brought about by a change in boundary conditions with a fixed grid. It is probable that the turbulence model has overestimated the level of mixing causing with the effects of stronger lateral mixing, and the tendency to jet coalescence and two-dimensional flow, also stronger vertical mixing which causes the wake region to shrink and the inverted S-shape profile to disappear much more rapidly than in the measurements. It is impossible to separate these two effects with the present level of turbulence closure which uses a scalar eddy viscosity and hence increased lateral mixing must be accompanied by increased vertical mixing. It must also be said, however, that the sensitivity to the jet exit boundary conditions for this case calls into question the validity of the assumptions made in implementing the constant total pressure condition (particularly the assumption that the U and W velocities are both zero). Examination of the profiles for S/D = 2, H/D = 4 reveals a discrepancy in mass flow rates between measurements and cal-

culations (seen most clearly at X/D = 8). This is due to the assumed value of the free-stream velocity used in the calculations; subsequent checks indicated that for this flow U_∞ had been somewhat lower, and hence the velocity ratio had assumed a slightly higher value of 2.6. It may also be noted that the lack of correspondence between measurements and calculations at the downstream stations (but not upstream) is almost entirely due to this mass-flow discrepancy; this did not occur in the other cases measured where the free-stream velocity was confirmed to be constant at 10.8 m/s.

The effect of increasing jet spacing is shown in Figure 4.7, and the agreement between predictions and measurements is satisfactory. The free-stream penetration through the gaps between the adjacent jets can be clearly seen in both predicted and measured mid-plane profiles of X/D = 4 and 8 and the shape of the centre-plane profile is predicted correctly. This inverted S-shape is typical of the strongly three-dimensional flow generated by rows of jets in confined cross-flow; the vertical flow structure takes on a three-layered nature with the acceleration of the free-stream causing the upper velocity peak, the wake behind the jets causing the low velocity region and the re-developing boundary layer on the bottom wall representing the fluid sucked into the low pressure region behind the holes but not totally entrained by the jets themselves. The peak in velocity caused by free-stream acceleration is underpredicted at X/D = 4. It is possible that this local peak has been smeared out by numerical diffusion errors in the upstream, near-discharge region, although it is believed that the general shape of the profile is not adversely affected by this problem. The rate at which the profile flattens-out in the vertical

direction as we proceed from X/D = 4 to 10 is well predicted, being if anything, slightly too slow.

Figure 4.8 allows comparisons for the case where H/D is increased to 8 at a constant pitch-to-diameter ratio of 4. Once again, the inability to resolve local velocity peaks can be identified at X/D = 4 and 6 and this is almost definitely due to numerical diffusion errors, since a uniform grid distribution in the vertical direction with only 20 points is certainly not suitable for this flow, which remains within Y/D = 4 over the whole downstream distance. A comparison of the location of the velocity maxima with Figure 4.6 indicates slightly greater jet penetration which is to be expected for an increase in H/D. Once more, the overall rate of smoothing of the vertical profiles with increasing downstream distance is reasonably well-predicted.

4.3.3 Further Calculations

The calculation procedure was applied to geometric configurations outside the range of measurements. Figures 4.9(a), (b) and (c) demonstrate the effect of decreasing the tunnel height to an H/D value of 2. The profiles on the centre-plane may be compared, Figure 4.9(a), with the predicted results for H/D = 4 and Figure 4.9(b) compares the same two configurations for the profiles at an off centre-plane location (Z/D = S/4). It is clear from the profiles for H/D = 4 that the whole region, which corresponds to the jet fluid, rises above the Y/D = 2 level, but this is of course impossible when the tunnel roof is brought down to H/D = 2. In this case, jet bifurcation occurs, as shown by Figure 4.9(c), when the wake region itself impinges on

the upper wall downstream of X/D = 4 causing an enhancement of the secondary flow in the cross-stream plane which results in a stronger tendency for two-dimensionality near the upper wall and for the maximum velocities to lie near the bottom wall and at off centre-plane location. At a velocity ratio of 2.3 however, even with the upper wall at 2D distance, impingement occurs some distance downstream of the discharge plane and is not strong enough to cause backflow velocities near the upper wall as observed in the single jet case of Kamotani and Greber (1974) and Jones and McGuirk (1979) at higher velocity ratios.

Finally, Figure 4.10 presents results for rows of directly opposed jets with H/D of 4. Also shown on the figure are the predicted results for a single row of jets with a duct height of 2D. The difference in the numerical procedure lies in the treatment of the upper boundary of the solution domain; in the case of opposing jets the no-slip conditions representing a wall are replaced by the zero-gradient conditions representing a plane of symmetry. These changes are also reflected by the results, with significant differences between the two sets of results appearing only on the upper boundary where the conditions have been fixed.

4.4 Summary Conclusions and General Discussion

This chapter has considered the numerical predictions of rows of jets discharging normally into a confined cross-flowing stream. This section considers, in summary form, the specific conclusions to emerge from the various geometrical configurations considered and

this is followed by a more general discussion on the computational approach and implications of the present study.

The main conclusions to emerge from the present theoretical study were:

- Grid-dependence tests using a range of finite-difference grids showed that even with the finest grid of 20 x 20 x 30 nodes, the results were not grid-independent in the near-discharge ($0 \leqslant X/D \leqslant 4$) region; further downstream they were not strongly affected by numerical errors.

- The rapid jet coalescence and trend toward two-dimensional behaviour were predicted in the lower pitch-to-diameter ratio case (S/D = 2) only when a constant total pressure boundary condition was used at the jet exit. In this calculation it is also believed that the turbulence model, which uses a scalar eddy viscosity, overestimated the rate of mixing in the vertical direction and caused the profile shapes in the near-field to be wrongly predicted.

- The calculation for the S/D = 2 flow was shown to be very sensitive to the boundary condition at the jet exit and further work is required here to investigate a method for calculating these boundary conditions more accurately.

- The calculated results for the S/D = 4 case were in good agreement with the measurements for both ratios of H/D = 4 and 8; apart from the failure to resolve the locally peaked shape of the velocity profile in the near-field which was

probably due to numerical diffusion problems.

- A lowering of the tunnel roof to a height of 2 jet diameters produced impingement of the jets which could clearly be identified in the calculated results. The impingement even at this H/D value was however fairly far downstream and the solution indicated no region of reverse flow near the tunnel roof.

The predictions of this chapter have shown that the qualitative trends of jets in crossflow can be represented adequately and that the technique can be applied to investigate effects of varying the geometric parameters on the flow-field.

The calculations used the hybrid differencing scheme where upwind differencing was used for cell Peclet numbers greater than |2| and the more accurate central differencing elsewhere. Due to computer core storage limitations it was not possible to refine the grid sufficiently such that central differencing could be used everywhere. The use of upwind differencing resulted in numerical errors with over-diffused peaks in the velocity profiles. This problem can be remedied by using much finer meshes, but this is not the most cost-effective approach to adopt as the type of meshes required for grid-independent solutions in three-dimensional flows far exceeds the core storage limitations of present-day computers. Even if fine grids could be accommodated, there are still problems related with obtaining converged solutions using presently available fluid flow solution algorithms. Use of higher-order accurate schemes is an approach which has been pursued in order to obtain more accurate solutions. The main difficulty with such

shcemes is that they generate non-physical oscillations in the vicinity of steep gradients, which makes converged solutions difficult to obtain and which can also violate the boundedness properties of positive definite quantities such as the turbulence kinetic energy. Han et al (1981) have demonstrated that one such scheme, namely the quadratic-upstream differencing shceme of Leonard (see, for example, Leonard et al, 1978), can be manipulated to give "satisfactorily rapid convergence" and provide results which have greater numerical accuracy than those obtained with the hybrid scheme. This is encouraging as the development of more accurate schemes, such as Leonard's, offers long-term advantages in terms of calculations of complex turbulent flows such as jets in cross-flow on reasonably-sized meshes which are free from numerical error.

Only when it has been demonstrated that the predictions are free from numerical error and independent of the grids used can the performance of the turbulence model be accurately appraised and modifications made.

CHAPTER 5

CONCLUDING REMARKS

The main conclusions that have emerged from the present experimental and theoretical investigations have been stated and discussed previously, at the end of the relevant chapters and are not repeated here. The paragraphs which follow indicate, under separate headings for the experimental and theoretical aspects, some implications of the results for gas turbine practice and put forward views on the way in which further work should proceed.

5.1 Experimental Contribution

Detailed mean velocity and scalar concentration measurements have been obtained for a single row of jets and the effects of a small geometric asymmetry for a range of jet-to-crossflow velocity ratios demonstrated. THese results are directly relevant to the design and operation of dilution zones where small geometric asymmetries may exist due to manufacturing tolerances and larger ones as a result of dilution ports burning and enlarging asymmetrically. In this case, the results imply that, for high velocity ratios (or momentum ratios) encountered in the dilution zone, the scalar field (i.e. temperature) downstream of the asymmetric jet will regain symmetry with downstream distance and the resulting radial temperature profile at the turbine entry will not be strongly affected by the asymmetry. In contrast, the velocity field is likely to retain its asymmetry with consequent non-uniform forces on the turbine components. The lower velocity ratio results suggest that

if similar geometric asymmetries are present in the arrangement of film cooling holes, arranged with discrete holes for total coverage cooling, local regions of high surface temperature will result since the scalar field does not regain symmetry.

The results obtained with opposed jets demonstrate the flow-field dependence on the velocity ratio and pitch spacing of the jets. For close spacing of the jets (S/D = 2) the opposed jets were not able to penetrate to the centre-line of the duct. Clearly, this type of arrangement would not be practical for the primary zone of a combustor where the jets are required to impinge upon each other and to bifurcate with some primary jet fluid flowing upstream to help to stabilise and anchor the flame. With an increased pitch spacing (S/D = 4) the opposing jets impinged and bifurcated in an asymmetric manner. This arrangement in the dilution zone could be undesirable as the non-uniform nature of the velocity and scalar fields would manifest themselves in the form of hot streaks which are generally detrimental to the performance and life of the nozzle guidevanes and turbine blades. A further shortcoming of the larger pitch spacing in the dilution zone would be the passage of hot combustion gases between the adjacent jets with resulting high surface temperatures in these regions; this is less likely when the jets are closely spaced, as the free-stream is forced to accelerate over rather than between the adjacent jets. The opposed rows of jets with a geometrical asymmetry in one row suggested, in contrast to the single row results, that the velocity and passive scalar fields were not able to regain symmetry with downstream distance for the smaller pitch-to-diameter ratio and this implies that the temperature profile at the turbine inlet would be non-uniform. However, for the S/D = 4 case, engineering tolerances

were of lesser importance as the jets bifurcated asymmetrically even with a symmetric arrangement.

Most gas turbine combustors have a convergent cross-section in the dilution zone and this was represented in the present study by the addition of a perspex plate downstream of the jets. The results from this configuration showed that the jets bifurcated with the concentration maxima appearing between the centre-lines of the adjacent jets. These results imply that the hot streaks would be found behind the jet centre-lines and this observation is supported by tests on model combustors by Industry. The results of the investigation with the downstream contraction do not, however, provide conclusive evidence of the causes of the jet fluid between the centre-lines of the adjacent jets. The realisation of this effort in gas-turbine combustors could explain some aspects of non-uniform temperature distributions and further work is required to provide better explanations.

The link between the present results and gas-turbine combustors depends on the assumption that the uniform density flows are representative of the non-uniform density flows of practice. It is likely that the results will scale with momentum ratio, but it is undoubtedly desirable for a small series of tests to be carried out at realistic velocity and density ratios. This is best done with gases of different density rather than with temperature variations.

In addition, the present geometric configurations are very much simpler than those found in practice. The absence of film cooling rings, the plunged form of primary and dilution holes and of the upstream recirculations and swirl must have detailed implications for the value of the present results. It is expected that they will be small, but

sample checks must be obtained in realistic arrangements. The explanations of the flows are sufficient for many practical purposes, except for the region of the contraction, but different hole arrangements and especially those with different diameters and pitch of holes on opposing sides are worthy of further investigations of the present type.

5.2 Theoretical Contribution

The calculations of Chapter 4 have demonstrated that a row of jets-in-crossflow can be represented adequately, in qualitative terms, by the present calculation method with its assumed conservation equations, numerical method, turbulence model and boundary conditions.

The validity of the technique can be further appraised, by extending the investigation to examine by calculation, the range of flows recommended for future experimental investigations in the preceding section. The detail of the proposed measurements, and the range of configurations to be examined experimentally can be very much reduced by making use of the calculation procedure to interpolate and extrapolate the measured results. Thus, the two investigations should be carried out in an interactive manner to minimise the amount of effort, and particularly new hardware configurations, required.

In the longer-term, further development of the numerical technique is desirable in order to increase the degree of confidence in the calculated results. The effort should be directed towards reducing the effects of numerical diffusion and other grid related problems, as discussed earlier in Chapter 4. It will involve investigations of more accurate finite-difference schemes and solution algorithms, in-

itially with emphasis on flow configurations simpler than those considered here.

The calculation method can, and should, be extended to assist the better understanding of the flows which exist in gas turbine combustors. This involves the representation of for example, film cooling rings, internal boundaries, and the complex geometry at the head of the combustor. The first steps in this extension are to allow the representation of the combustor geometry, from assigned coordinates, and to generate an appropriate finite-difference grid, and efforts of this type are already in progress, and show considerable promise. The incorporation of the effects of film cooling rings are readily represented by local sources of cooling air but, in the longer-term, are likely to be best represented by linking the solutions of the elliptic Navier-Stokes equations to solutions of the parabolic boundary-layer equations with the latter solved for the wall, and film cooled, region.

The designer of primary and dilution zones is also faced with the additional complications introduced by combustion. To be used as a design tool, the numerical technique needs the incorporation of combustion models of adequate precision. The early results of related investigations carried out in parallel to this one suggest that, in most regions of combustors, the accuracy of the calculations of combusting flows is limited more by numerical and turbulence assumptions than by the assumptions of the combustion model. Nevertheless, improvements to existing combustion models are desirable and, as in the present work, should involve a coordinated program of numerical and experimental work.

- - - o o 0 o o - - -

REFERENCES

ABRAMOVICH, G. N. (1963)
"The Theory of Turbulent Jets"
M.I.T. Press

ADLER, D. and BARON, A. (1979)
"Prediction of a three-dimensional circular turbulent jet in crossflow"
AIAA Journal, 17, 168

ATKINSON, K. N., KHAN, Z. A. and WHITELAW, J. H. (1982)
"Experimental investigation of opposed jets discharging normally into a cross-stream"
J. Fluid Mech. 115, 493

BAHR, D. W. (1978)
"Gas turbine engine emissions abatement - status and needed achievements"
Project SQUID Workshop on Gas Turbine Combustor Design Problems

BAKER, R. J. (1971)
"The turbulent boundary layer with streamwise pressure gradient and foreign gas injection"
Ph.D Thesis, University of London

BERGELES, G. (1976)
"Three-dimensional discrete-hole cooling processes. An experimental and theoretical study"
Ph.D Thesis, University of London

BOURQUE, C. and NEWMAN, B. G. (1960)
"Reattachment of a two-dimensional incompressible jet to an adjacent flat plate"
Aero. Quart, 11, 201

BOUSSINESQ, J. (1877)
"Theorie de l'ecoulment tourbillant"
Mem. Acad. Sci. 23, no. 46

BRADBURY, L. J. S. and WOOD, M. N. (1965)
"The static pressure distribution around a circular jet discharging normally from a plane wall into an air stream"
ARC CP822

BRADSHAW, P. (1973)
"The effect of streamline curvature on turbulent flows"
AGARD, no. 169

BRADSHAW, P., CEBICI, T. and WHITELAW, J. H. (1981)
"Engineering Calculations Methods for Turbulent Flow"
Academic Press, London

CARETTO, L. S., GOSMAN, A. D., PATANKAR, S. V. and SPALDING, D. B. (1973)
"Two calculation procedures for steady three-dimensional flows with recirculation"
Proc. Third Int. Conf. Num. Meth. in Fluid Mech. II 60.
Springer-Verlag, Heidelberg

CHAMPAGNE, F. H. and SLEICHER, C. A. (1967)
"Turbulence measurements with inclined hot-wires. Part 2. Hot wire response equations"
J. Fluid Mech. 28, 177

CHAMPAGNE, F. H., SLEICHER, C. A. and WEHRMANN, O. H. (1967)
"Turbulence measurements with inclined hot-wires. Part 1. Heat transfer experiments with inclined hot wires"
J. Fluid Mech. 28, 153

CHASSAING, P., GEORGE, J., CLARIC, A. and SANANES, F. (1974)
"Physical characteristics of subsonic jets in a cross stream"
J. Fluid Mech. 62, 41

CHIENG, C. C. and LAUNDER, B. E. (1980)
"On the calculation of turbulent heat transport downstream from an abrupt expansion"
Num. Heat Transfer, 3, 189

COX, G. B. (1976)
"Multiple jet correlations for gas turbine engine combustor design"
J. of Eng. for Power, 98, 265

CRABB, D. (1979)
"Jets in Crossflow"
Ph.D Thesis, University of London

CRABB, D., DURAO, D. F. and WHITELAW, J. H. (1981)
"A round jet normal to a crossflow"
J. Fluids Eng. 103, 142

CRABB, D. and WHITELAW, J. H. (1979)
"The influence of geometric asymmetry on the flow downstream of a row of jets discharging normally into a free-stream"
J. Heat Transfer, 101C, 183

DALY, B. J. and HARLOW, F. H. (1970)
"Transport equations of turbulence"
Phys. Fluids, 13, 2634

DURST, F. and RASTOGI, A. K. (1979)
"Turbulent flow over two-dimensional fences"
2nd Symp. on Turbulent Shear Flows, London

FOSTER, R. C. (1973)
"Experimental study of boundary layer and heat transfer in the region of separated flow downstream of normal injection slots"
Ph.D Thesis, University of Texas

GEHRIG, W., JURISCH, R. and LEMMIN, U. (1976)
"Ausbreitung bei Ein leitung von Strahlen in Gerinneströmungen"
University of Karlsruhe report SFB,80/ETM/76

GOLDSTEIN, R. J. (1971)
"Film cooling" Advances in heat transfer, Vol. 7

GOSMAN, A. D. and IDERIAH, F. J. (1976)
"TEACH-T: A general computer program for two-dimensional, turbulent, recirculating flows"
Unpublished work

GOSMAN, A. D., NIELSEN, P. V., RESTIVO, A. and WHITELAW, J. H. (1980)
"The flow properties of rooms with small ventilation openings"
J. Fluids Engng., 102, 316

GOSMAN, A. D., and PUN, W. M. (1973)
"Lecture notes for a course entitled "Calculation of Recirculating Flows"
Imperial College, London

GREEN, A. S. (1981)
"Isothermal models of combustion chamber flows"
Ph.D Thesis, University of London

HABIB, M. A. and WHITELAW, J. H. (1980)
"Measured velocity characteristics of confined coaxial jets with and without swirl"
J. Fluids Engng., 102, 47

HAN, T., HUMPHREY, J. A. C. and LAUNDER, B. E. (1981)
"A comparison of hybrid and quadratic-upstream differencing in high Reynolds number elliptic flow"
Computer Methods in Appl. Mech. and Eng., 29, 81

HANJALIĆ, K. (1970)
"Two-dimensional asymmetric turbulent flow in ducts"
Ph.D Thesis, University of London

HANJALIĆ, K. and LAUNDER, B. E. (1972)
"A Reynolds stress model of turbulence and its application to thin shear flows"
J. Fluid Mech., 52, 609

HARLOW, F. H. and WELCH, J. E. (1965)
"Numerical calculation of time-dependent viscous incompressible flow of fluid with free surface"
Phys. of Fluids, 8, 2182

HARLOW, F. H. and NAKAYAMA, P. (1968)
"Transport of turbulence energy decay rate"
LA-3854, Los Alamos Science Lab., University of California

HINZE, J. O. (1959)
"Turbulence"
McGraw-Hill, New York

HOLDEMAN, J. D. and WALKER, R. E. (1976)
"An empirical model for the mixing of a row of dilution jets with a confined crossflow"
AIAA paper 76-48

HOLDEMAN, J. D., WALKER, R. E. and KORS, D. L. (1973)
"Mixing of multiple dilution jets with a hot primary airstream for gas turbine combustors"
NASA TMX - 71426

JONES, W. P. and LAUNDER, B. E. (1972)
"The prediction of laminarization with a two-equation model of turbulence"
Int. J. of Heat Mass Transfer, 15, 301

JONES, W. P. and LAUNDER, B. E. (1973)
"Prediction of low-Reynolds number phenomena with a two-equation model of turbulence"
Int. J. of Heat Mass Transfer, 16, 1119

JONES, W. P. and McGUIRK, J. J. (1979)
"Computation of a round jet discharging into a confined crossflow"
2nd Symp. on Turbulent Shear Flows, London.

KAMOTANI, Y. and GREBER, I. (1972)
"Experiments on a turbulent jet in a crossflow"
AIAA paper 72 - 149

KAMOTANI, Y. and GREBER, I. (1973)
"Experiments on confined turbulent jets in crossflow"
AIAA paper 73 - 647

KAMOTANI, Y. and GREBER, I. (1974)
"Experiments on confined turbulent jets in crossflow"
NASA CR - 2392

KEFFER, J. F. and BAINES, W. D. (1963)
"The round turbulent jet in a cross wind"
J. Fluid Mech., 15, 481

KHAN, Z. A., McGUIRK, J. J. and WHITELAW, J. H. (1981)
"A row of jets in a crossflow"
AGARD Conf. Proc. No. 308

KHAN, Z. A. and WHITELAW, J. H. (1980)
"Mean velocity and concentration characteristics of rows of jets in a crossflow"
J. Heat Transfer, 102, 391

KHAN, Z. A. and WHITELAW, J. H. (1980)
"Vector and scalar characteristics of opposing jets discharging normally into a cross-stream"
Int. J. Heat Mass Transfer, 23, 1673

KOLMOGOROV, A. N. (1942)
"Equations of turbulent motions of an incompressible turbulent fluid"
Izv. Akad, Nauk. SSSR Ser. Phys. VI, 56

LAUNDER, B. E., MORSE, A., RODI, W. and SPALDING, D. B. (1972)
"The prediction of free shear flows - A comparison of the performance of six turbulence models"
Proc. NASA. Conf. on Free Shear Flows, Langley

LAUNDER, B. E., REECE, G. J. and RODI, W. (1975)
"Progress in the development of a Reynolds stress turbulence closure"
J. Fluid Mech., 68, 537

LAUNDER, B. E. and SPALDING, D. B. (1972)
"Mathematical Models of Turbulence"
Academic Press, London

LAUNDER, B. E. and SPALDING, D. B. (1974)
"The numerical computation of turbulent flows"
Computer Methods in Appl. Mech. and Eng., 3, 269

LEFEBVRE, A. H. and NORSTER, E. R. (1966)
"A design method for the dilution zones of gas turbine combustion chambers"
Cranfield Note. Aero. No. 169

LEONARD, B. P., LESCHZINER, M. A. and McGUIRK, J. J. (1978)
"Third-order finite-difference method for steady two-dimensional convection"
Proc. of 1st Int. Conf. on Numerical Meth. in Laminar and Turbulent Flow, Eds. C. Taylor et al, Pentech Press, London

LESCHZINER, M. A. and RODI, W. (1980)
"Calculation of annular and twin parallel jets using various discretization schemes and turbulence-model variants"
University of Karlsruhe Report SFB 80/T/159

McGUIRK, J. J. and RODI, W. (1978)
"A depth-averaged mathematical model for the near field of side discharges into open channel flow"
J. Fluid Mech., 86, 761

McGUIRK, J. J., TAYLOR, A. M. K., WHITELAW, J. H. (1981)
"The assessment of numerical diffusion in upwind-difference calculations of turbulent recirculating flows"
3rd Symp. on Turbulent Shear Flows, Davis, U.S.A.

McMAHON, H. M., HESTER, D. D. and PALFREY, J. G. (1971)
"Vortex shedding from a turbulent jet in a cross-wind"
J. Fluid Mech., 48, 73

MARGASON, R. J. (1968)
"The path of a jet directed at large angles to a subsonic free stream"
NASA TN D-4919

MELLOR, A. M. (1978)
"Turbulent combustion interaction models for practical high intensity combustors"
17th Int. Symp. on Combustion, Leeds

MOUSSA, Z. M., TRISCHKA, J. W. and ESKINAZI, S. (1977)
"The near field in the mixing of a round jet with a cross stream"
J. Fluid Mech., 80, 49

NEE, V. W. and KOVASZNAY, L. S. G. (1966)
"The calculation of incompressible turbulent boundary layer by a simple theory"
Phys. of Fluids, 12, 473

NEILSON, P. V., RESTIVO, A. and WHITELAW, J. H. (1978)
"The velocity characteristics of ventilated rooms"
J. of Fluids Eng., 100, 291

NORGERN, C. T. and HUMENIK, M. (1968)
"Dilution-jet mixing study for gas-turbine combustors"
NASA TN D-4695

ODGERS, J. (1979)
"Combustion modelling with gas turbine engines; some applications and limitations"
AGARD Conf. Proc. No. 275

OWER, E. and PANKHURST, R. C. (1966)
"Measurements of Air Flow" 4th Ed.
Pergamon Press

PATANKAR, S. V. (1980)
"Numerical Heat Transfer and Fluid Flow"
Hemisphere, New York

PATANKAR, S. V., BASU, D. K. and ALPAY, S. A. (1977)
"Prediction of the three-dimensional velocity field of a deflected turbulent jet"
J. Fluids Eng., 99, 758

PATANKAR, S. V. and SPALDING, D. B. (1970)
"Heat and Mass Transfer in Boundary Layers"
2nd Edn. Intertest Books, London

PATANKAR, S. V. and SPALDING, D. B. (1972)
"A calculation procedure for heat, mass and momentum transfer in three-dimensional parabolic flows"
Int. J. Heat Mass Transfer, 15, 1787

POPE, S. B. and WHITELAW, J. H. (1976)
"The calculation of near-wake flows"
J. Fluid Mech., 73, 9

POYSER, J. R. and MOXON, H. B. (1969)
"Evolution of the RB162 combustion system"
Proc. Cranfield Int. Symp. Vol 11

PRANDTL, L. (1925)
"Berich uber Untersuchungen zur ausgebildeten turbulenz"
ZAMM, 5, 136

PRANDTL, L. (1945)
"Über ein neues formalsysten für die ausgebildete turbulenz"
Nachrichten von der Akad. der Wissenschaft in Gottingen

RAITHBY, G. D. (1976)
"A critical evaluation of upstream differencing applied to problems involving fluid flow"
Comp. Meth. Appl. Mech. Engng., 9, 75

RAJARATNAM, N. (1976)
"Turbulent Jets" Elsevier, Amsterdam

RAMSEY, J. W. and GOLDSTEIN, R. J. (1971)
"Interaction of a heated jet with a deflecting stream"
J. Heat Transfer 93, 365

RASTOGI, A. K. (1972)
"Effectiveness and heat-transfer downstream of three-dimensional film cooling slots"
Ph.D Thesis, University of London

RIBEIRO, M. M. (1972)
"Turbulent mixing of co-axial jets"
M.Sc. Thesis, University of London

RIBEIRO, M. M. and WHITELAW, J. H. (1975)
"Statistical characteristics of a turbulent jet"
J. Fluid Mech., 70, 1

ROACHE, P. J. (1976)
"Computational Fluid Dynamics" Revised Ed.
Hermosa Pub., N. Mexico

RODI, W. (1970)
"Basic equations for turbulent flows in Cartesian and cylindrical coordinates"
Imperial College, Mech. Eng. Dept. report BL/TN/A/36

RODI, W. (1971)
"A new method for analysing hot wire signals in highly turbulent flow and its evaluation in a round jet"
Imperial College, Mech. Eng. Dept. ET/TN/B/10

ROLLS ROYCE LTD. (1969)
"Jet Engine"

ROUSE, H. (1957)
"Diffusion in the lee of a two-dimensional jet"
9th Conf. Int. Méc. Appl., Univ. Bruxelles

RUNCHAL, A. K. (1972)
"Convergence and accuracy of three finite difference schemes for a two-dimensional conduction and convection problem"
Int. J. Num. Meth. Engng., 4, 541

SAFFMAN, P. G. (1974)
"Model equations for turbulent shear flow"
Stud. appl. Math. 53, 17

SCHATZMANN, M. (1977)
"A mathematical model for the prediction of plume rise in stratified flows"
1st Symp. Turbulent Shear Flows, Penn. State Univ.

SCHLICHTING, H. (1968)
"Boundary Layer Theory"
McGraw-Hill, New York

SOTHERAN, A. (1980)
Private communication

STEK, J. B. and BRANDT, H. (1976)
"Aerodynamic throttling of a two-dimensional flow by a thick jet"
Aero. Quart., 27, 229

STURGESS, G. J. (1978)
"Liner durability"
Project SQUID Workshop on Gas Turbine Combuster problems

TAYLOR, A. M. K. (1981)
"Confined isothermal and combusting flows behind axisymmetric baffles"
Ph.D Thesis, University of London

TAYLOR, P. (1977)
"An investigation of an inclined jet in a crosswind"
Aero. Quart. 28, 51

TOWNSEND, A. A. (1980)
"The Structure of Turbulent Shear Flows"
2nd Ed. Cambridge Univ. Press

VASILIC-MELLING, D. (1977)
"Three-dimensional turbulent flow past rectangular bluff bodies"
Ph.D Thesis, University of London

VIZOL, Y. M. and MOSTINSKI, Z. G. (1965)
"Deflection of a jet injected into a stream"
J. of Eng. Physics, 8, 160

VOGLER, R. (1963)
"Surface pressure distributions induced on a flat plate by a cold air jet issuing perpendicularly from the plate and normal to a low-speed free-stream flow"
NASA TN D-1629

WALKER, R. E. and KORS, D. L. (1973)
"Multiple jet study final report"
NASA CR-121217

WHITE, A. J. (1977)
"The numerical prediction of film cooling from angled flush slots"
Rolls Royce Private Data

WHITE, A. J. (1980)
"The prediction of the flow and heat transfer in the vicinity of a jet in crossflow"
ASME paper 80-WA/HT-26

WYGNANSKI, I. and NEWMAN, B. G. (1968)
"The reattachment of an inclined two-dimensional jet to a flat surface in streaming flow"
CASI Trans. 1, 3

APPENDIX A: PLANE (2-D) JET IN CROSSFLOW

This appendix presents predictions of the plane (2-D) jet in crossflow measurements of Rouse (1957). This simpler geometry was chosen mainly to gain experience with the location of grid nodes and an appreciation of the related errors. The numerical scheme described in Chapter 4, and as embodied in the computer code TEACH-T (Gosman and Ideriah, 1976), was used for the predictions of this section.

The appendix is divided into two sections. The first (A.1) provides a description of the boundary conditions and other details of the calculations. The final section (A.2) presents a comparison of the predictions with the measurements of Rouse and discusses the possible sources of errors in the predictions, including those associated with upwind differencing.

A.1 Calculation Details

The boundary conditions discussed previously (Chapter 4, Section 4.2.4) were taken mainly from experimental conditions and are summarised in Table A1.

Boundary	Location (b = slot width)
Upstream of slot	25 b
Downstream of slot	150 b
Wall opposite slot	500 b
Slot exit	Const. total pressure condition

Table A1: Location of Domain Boundaries

Preliminary calculations were performed with a range of finite difference grids to find the dependence of the results on the number and location of grid nodes. The grid nodes were concentrated in the vicinity of the slot where large gradients were expected, and expanded geometrically in the up and downstream directions (see Figure A.1). The grid also expanded from the floor to the roof of the solution domain. The variation in the length of the recirculation region with grid size for jet-to-crossflow velocity ratio of 2.92 is shown below in Table A2. This parameter was used for the assessment of the performance of the various grid sizes as an experimental value of 100 b was available for comparison.

Grid		Recirculation length (L) (b = slot width)
X-direction	Y-direction	
22	22	37.2 b
32	22	50.4 b
48	22	50.6 b
47	42	57.6 b
47	52	57.8 b

Table A2: Variation of Recirculation Length with Grid Size

Clearly for even the finest grids used, the recirculation length was grossly under-predicted. The increase of grid size from 32 x 22 to 47 x 52 grid node resulted in only a 7 per-cent increase in accuracy but this was accompanied by a four-fold increase in the number of iterations that were required for convergence and an associated increase in computing costs. The 32 x 22 grid was eventually chosen as the best compromise between accuracy and economy, and used for all

subsequent calculations. The core storage requirements for this grid were 25 K words on a CDC 6600 computer and the solution required about 190 seconds (for 200 iterations) to converge.

A.2 Presentation of Results and Comparison with Experimental Data

The calculated streamline pattern for a velocity ratio of 2.92 is shown in Figure A.1. Also shown, in the figure, is the distribution of the grid nodes; not all of the grid points have been shown for reasons of limited space. The streamlines show the general features of a jet in crossflow; the mainstream fluid is forced to accelerate over the jet while the low pressure region behind the jet causes the jet to bend and reattach to the surface, from which it emerged. The influence of the opposing wall location was also explored by progressively lowering it; even for a channel height of 100 b, no significant changes were observed in the length of the reverse-flow region or the flow pattern, for this value of velocity ratio. As discussed earlier, the reattachment length was grossly under-predicted (by 50 per-cent). This was partly due to the numerical error caused by the use of insufficient grid nodes in the downstream region. It was not possible to concentrate grid nodes throughout the recirculation region due to core storage limitations. An addition of 16 extra grid lines in the downstream region, resulting in a 50 per-cent decrease in grid spacing in the recirculation region, did not provide any distinct advantage; only a 0.2 b increase of the recirculation region was achieved. It has been observed that in recirculating flows the k-ε model over-predicts values of the eddy viscosity and hence the turbulent shear stresses. This results in an over-prediction of the turbulent diffusion of momentum,

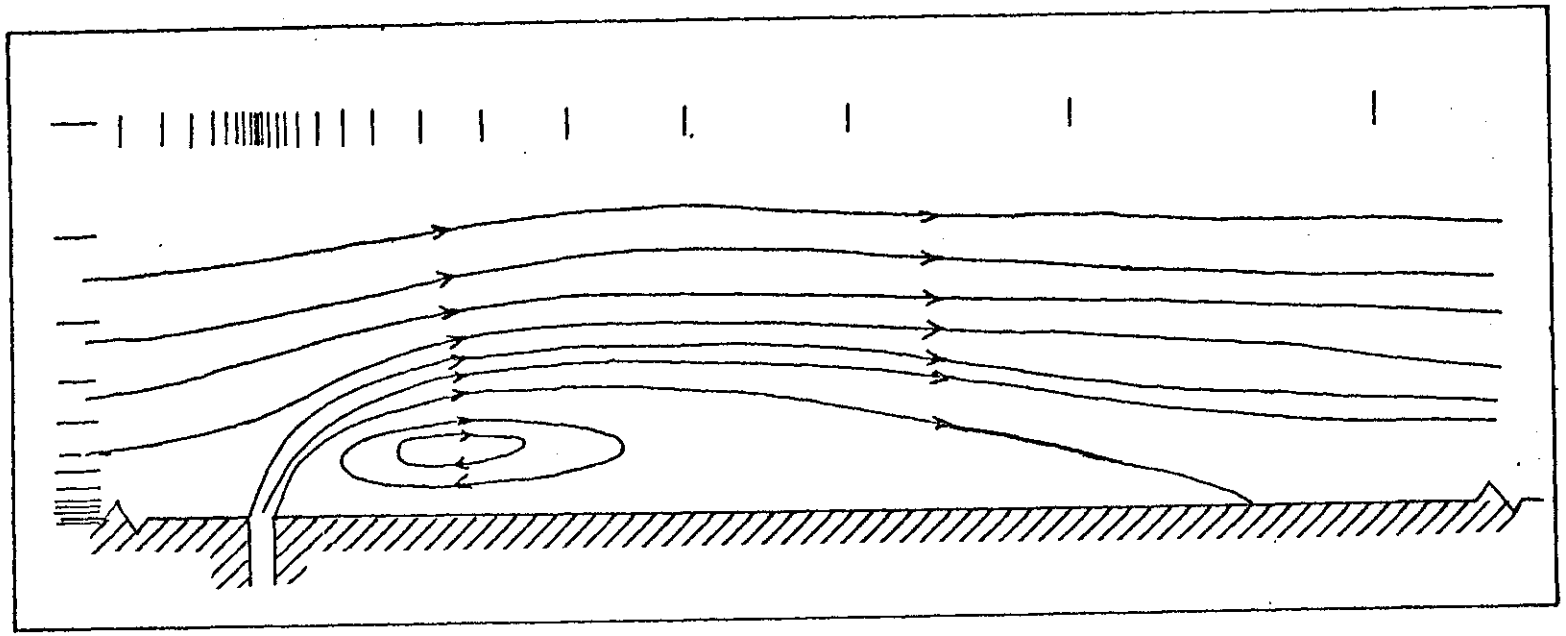


Figure A.1: Streamline plot for velocity ratio of 2.92 (grid size: 32x22)

from the shear layer bordering the recirculation into the negative velocity region, which manifests itself in a reduction of the reverse flow region.

The form of the k-ε model employed in the current predictions does not account for the effects of the extra strain rates caused by the curvature of the streamlines. The physical effect of these extra strain rates in the present flow is to reduce the turbulent transport of momentum and thereby to elongate the recirculation length. This is a deficiency of the model and is partly responsible for the discrepancy between the predicted and measured values. Leschziner and Rodi (1980) and others have proposed modifications to the k-ε model to account for the streamline curvature and these modifications have resulted in improved predictions for the unconfined flows examined by the authors. These modifications were not incorporated for the present predictions as these were not considered to be sufficiently grid-independent for the turbulence model modifications to be of any significance. A further possible cause for the large disparity between the measurements and the predictions may lie in erroneous measurements caused by three-dimensionality of the experimental set-up. In the experience of the author, a 2D jet-in-crossflow situation is difficult to achieve experimentally and excursions from the ideal situation lead to a shortening of the reverse flow region on the edges and an increase of this length in the central region where, presumably, the measurements were taken. Unfortunately other, more precise, measurements were not available for a more reliable comparison.

Correlations of velocity trajectories for various channel heights and a velocity ratio of 6.5 are shown in Figure A.2. The jet trajectory, here and elsewhere in the thesis, has been defined as the locus of

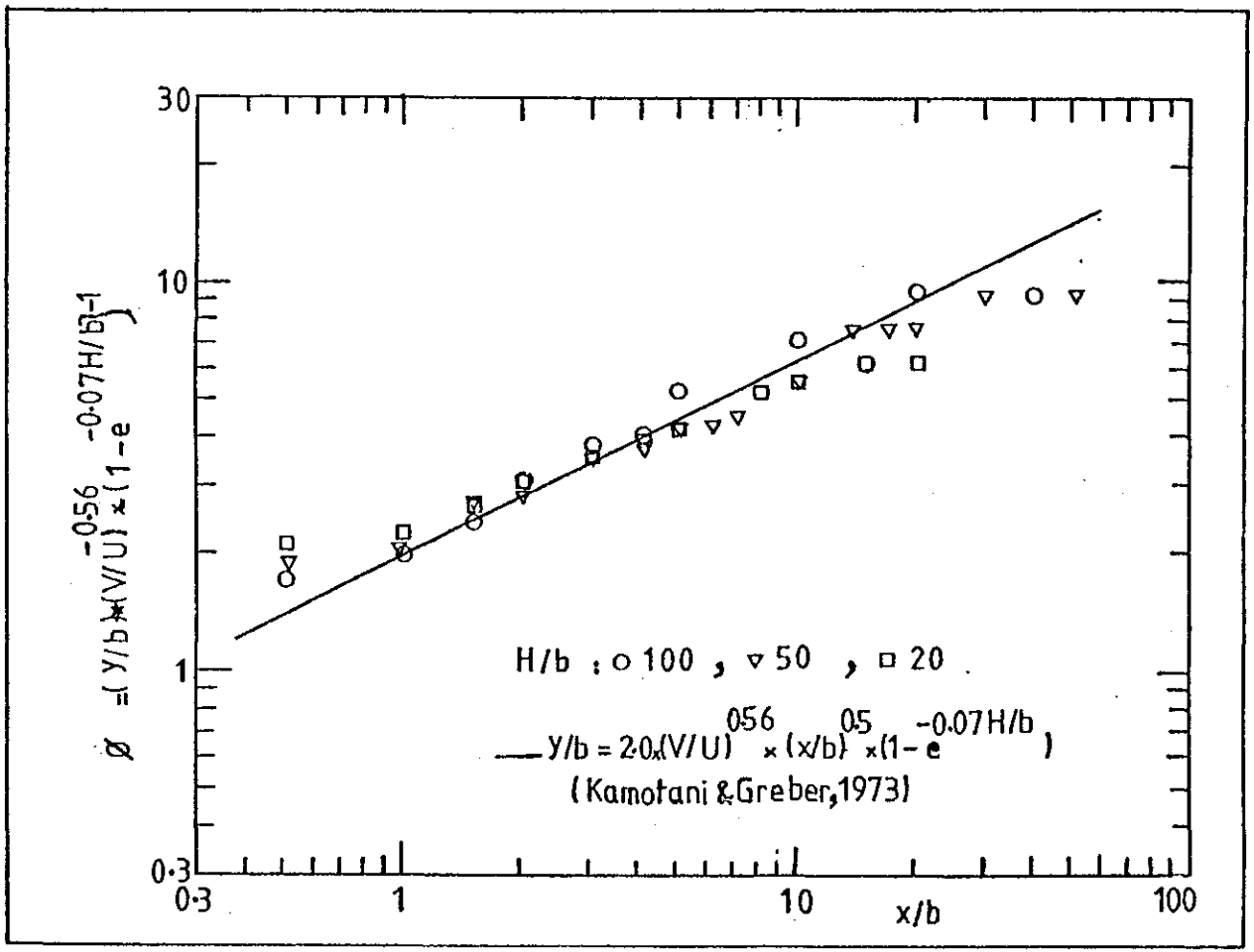


Figure A.2: Correlations of velocity trajectories of various channel heights for a velocity ratio of 6.5

maximum velocity of the velocity profiles. The predictions were correlated by using the relationship suggested by Kamotani and Greber (1973). The predicted results are in good agreement, with the proposed equation, in the near field region. This indicates that the initial bending of the jet has been well predicted. Further downstream, however, the predicted results show deviations from the correlation equation, with the predicted values appearing below the line. This is to be expected since the correlation is only accurate for the region of the jet where the trajectory is increasing. When the jet begins to bend, the height of the trajectory will decrease and this is not represented in the correlation, which shows a monatonic increase for the whole of the downstream region.

The variation of the reattachment length with velocity ratio is shown in Figure A.3. Also shown on the figure are the experimental results of Rouse (1957), Foster (1973), Gehrig et al (1976) and Wygnanski and Newman (1968). These are compared with the present predictions and those of White (1977), for low jet-to-crossflow velocity ratios. The other experimental results show a good correlation with the equation proposed by Rouse, which relates the ratio of the reattachment length and the slot width to the 1.5 power of the velocity ratio. The predictions, however, give a relationship with a 1.15 power. The results of White show reasonable agreement with the measurements. A 33 x 24 grid was used for these predictions and due to the reduced length of the solution domain (much shorter recirculation lengths are expected) a greater number of grid nodes could be clustered in the recirculation region to reduce the numerical diffusion there. The predictions were, however, still not grid-independent; with over-diffused peaks in the

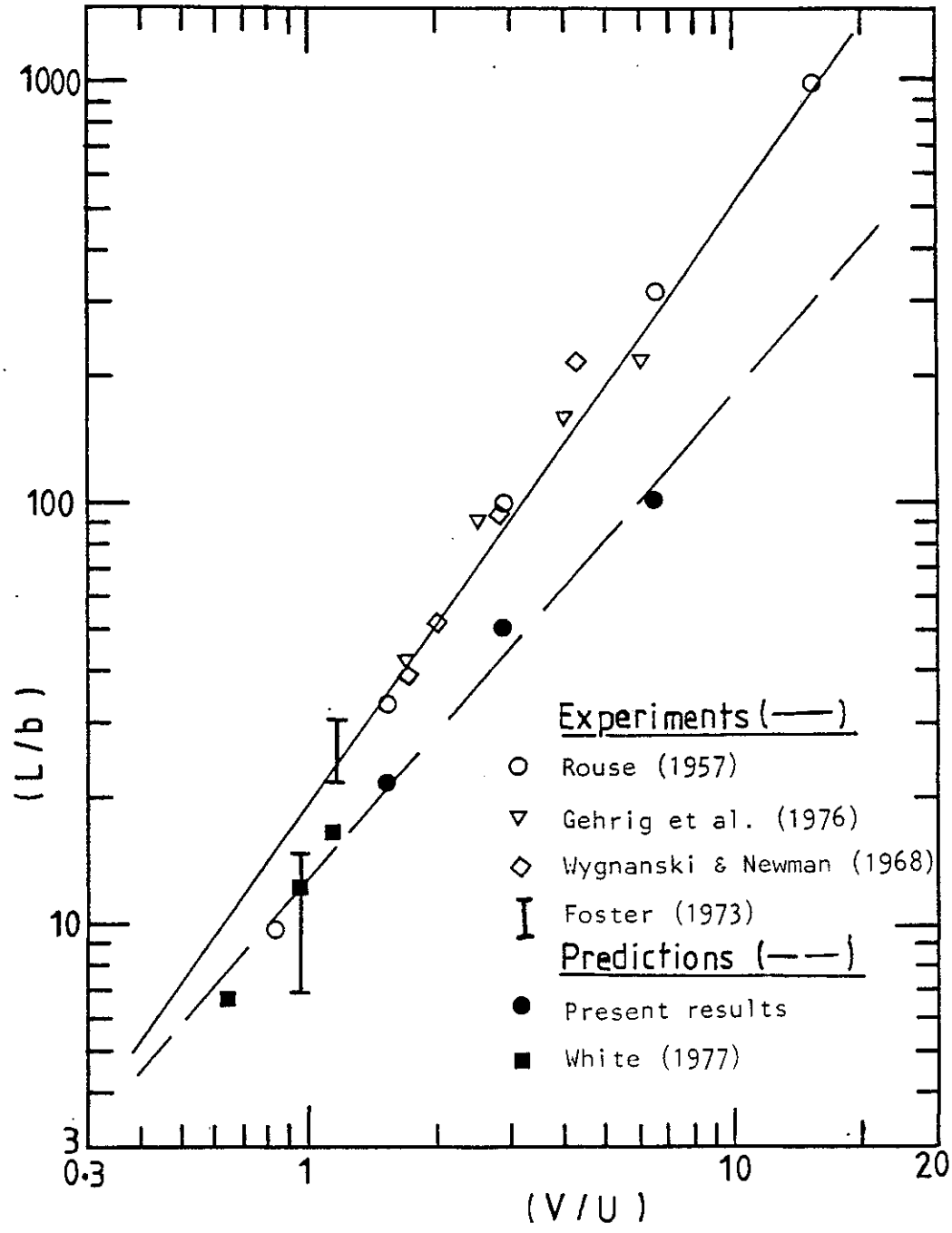


Figure A.3: Reattachment length as a function of velocity ratio

velocity profiles.

Clearly, the predicted results are not in good agreement with the measurements. It was outside the scope of the present research objectives to consider this two-dimensional problem in greater detail but it is expected that the accuracy of the predictions could be improved by applying the technique of McGuirk and Rodi (1978) and McGuirk et al (1981) to identify regions where the numerical error was particularly serious and to improve grid refinement in these local regions.

FIGURES

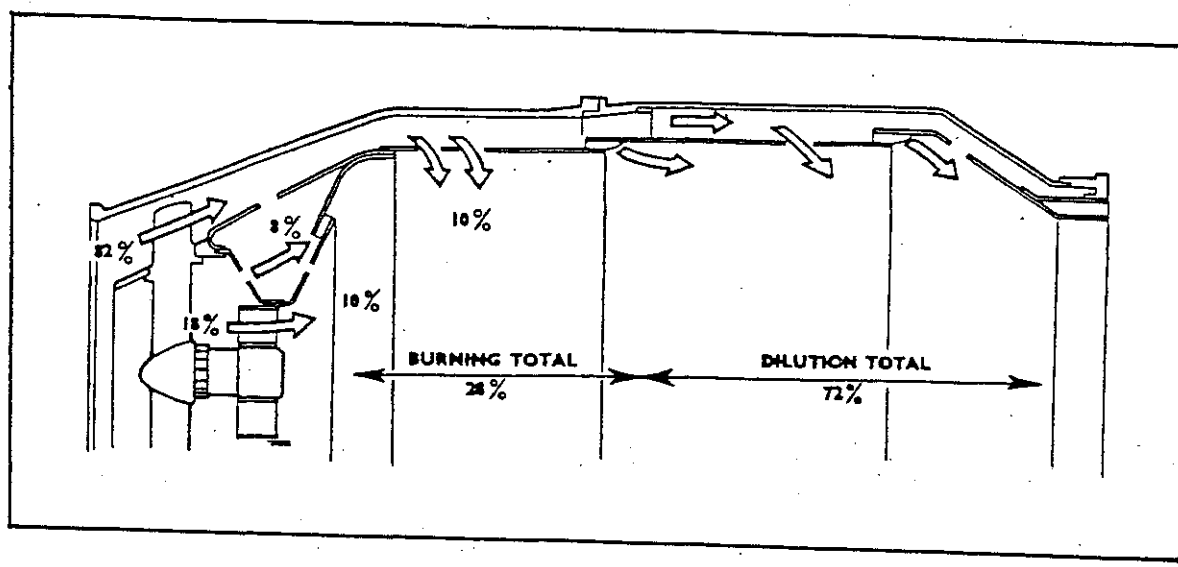


Figure 1.1: Apportioning the air flow

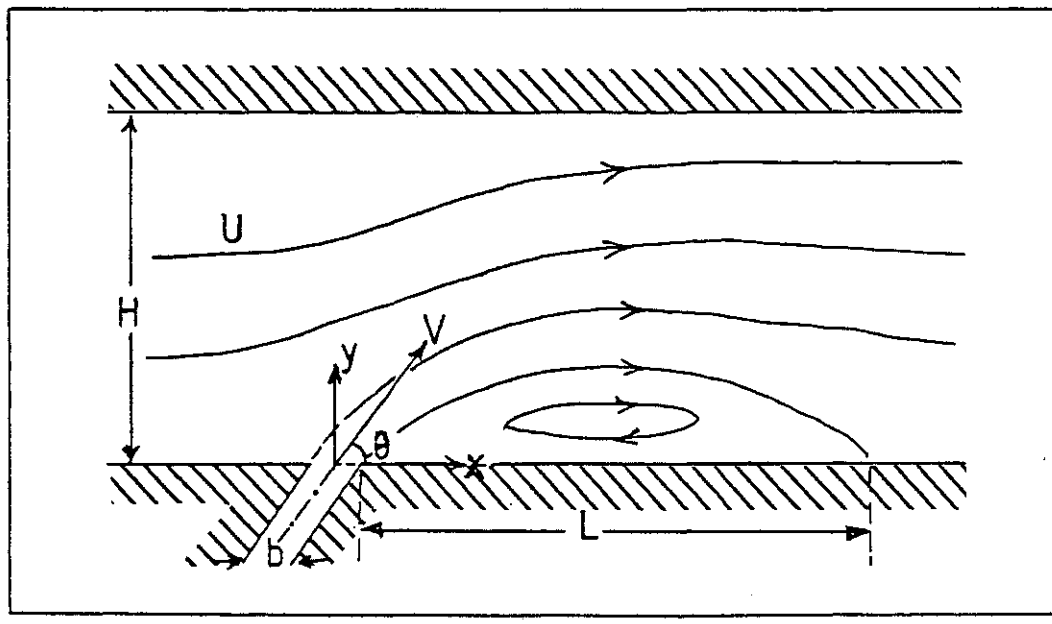


Figure 1.2: Schematic and coordinate system for plane (2D) jet in crossflow

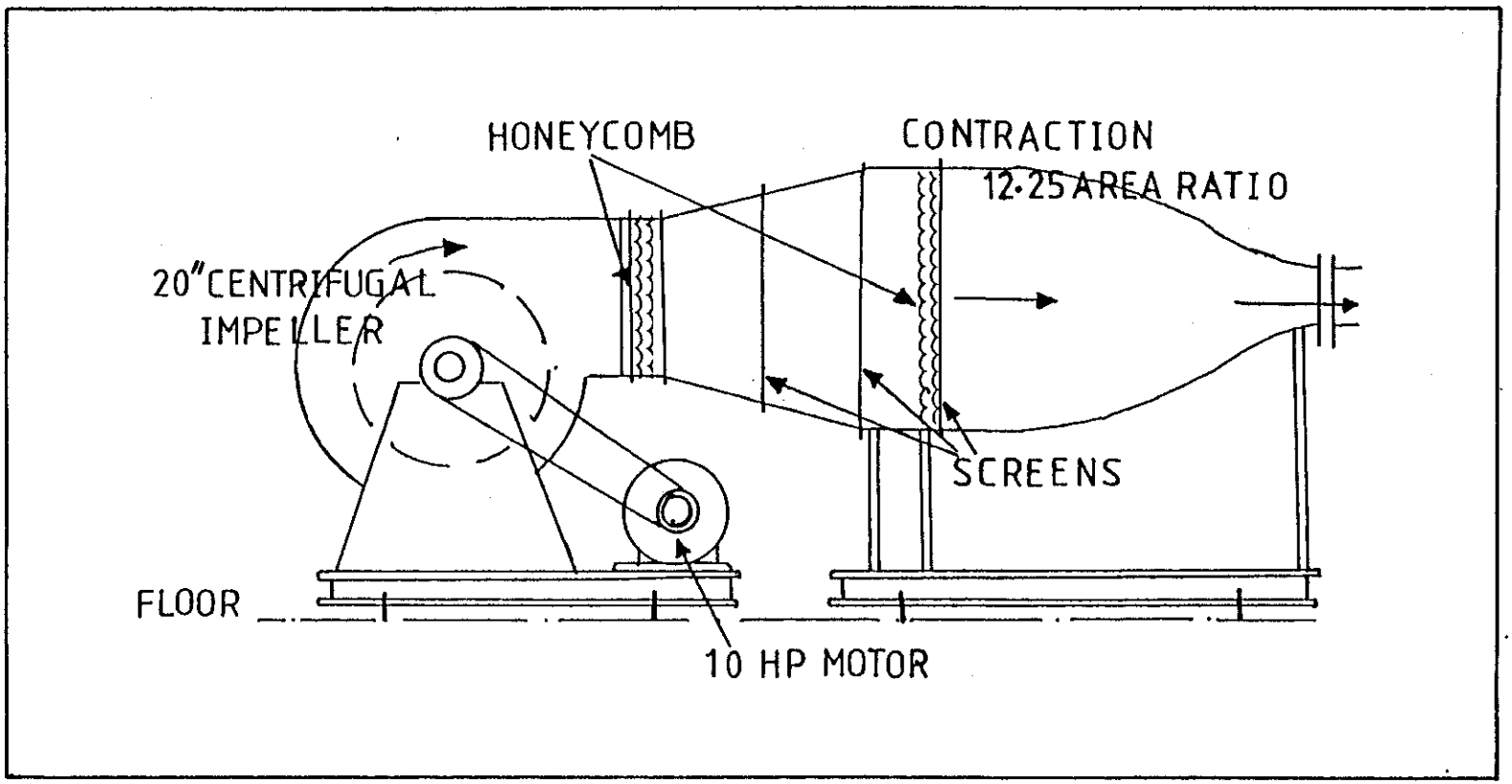


Figure 2.1: Schematic of wind tunnel

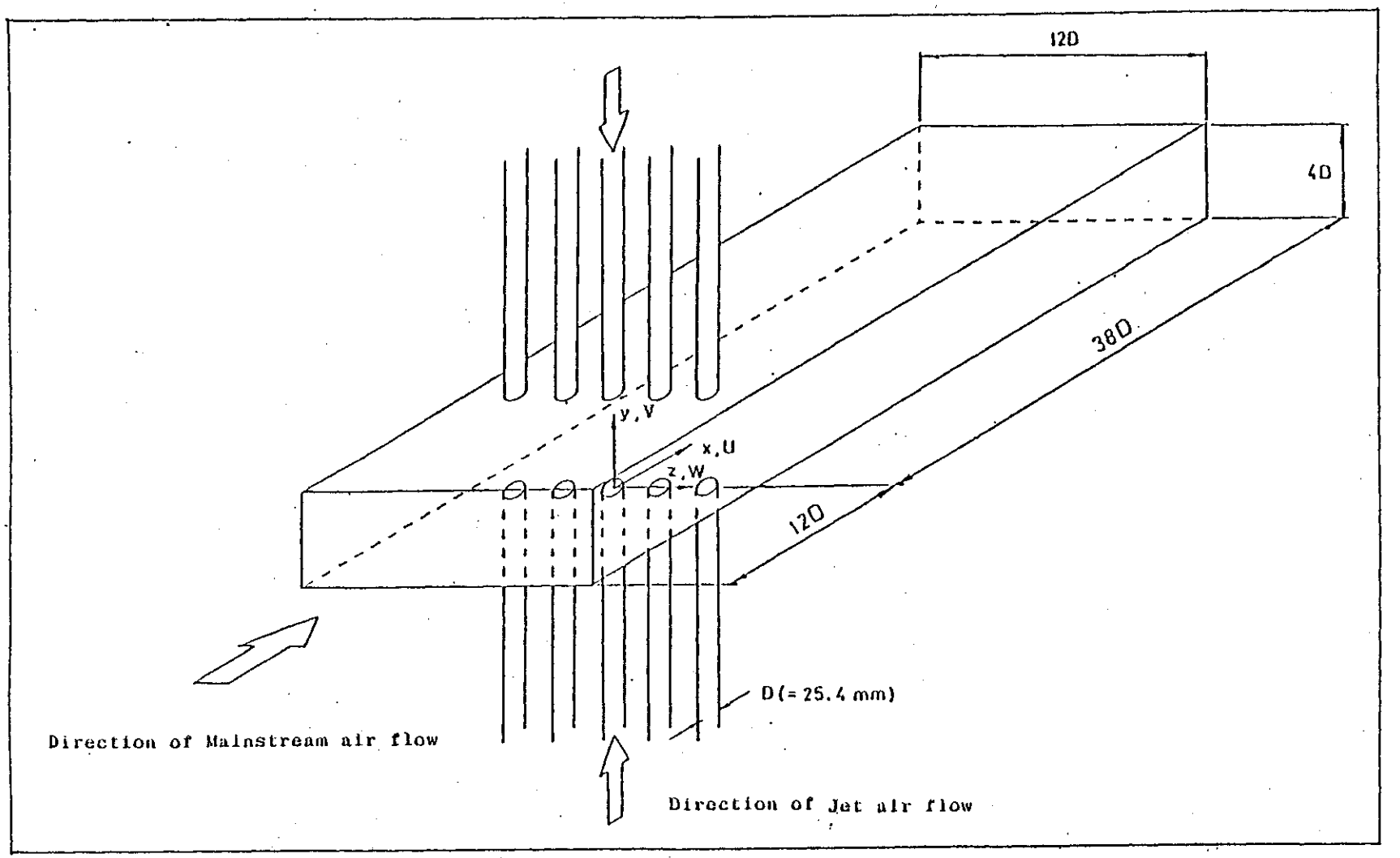


Figure 2.2: Working section and coordinate system for rows of jets in cross-flow

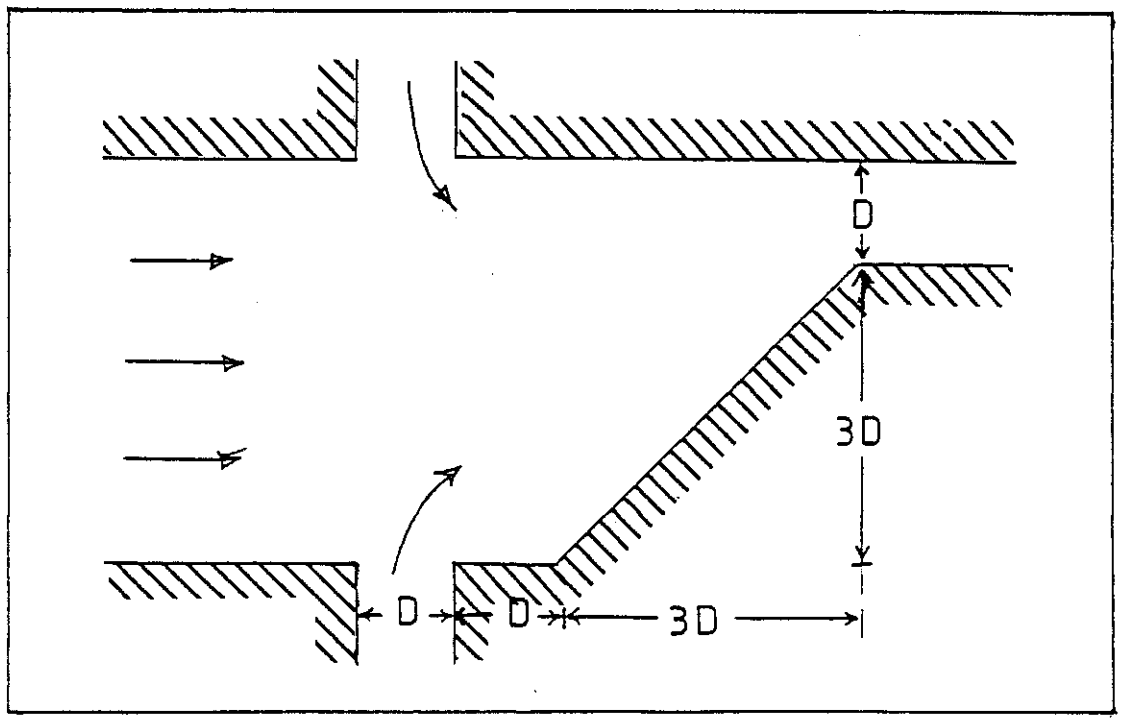


Figure 2.3: Schematic of opposed jets with a downstream contraction

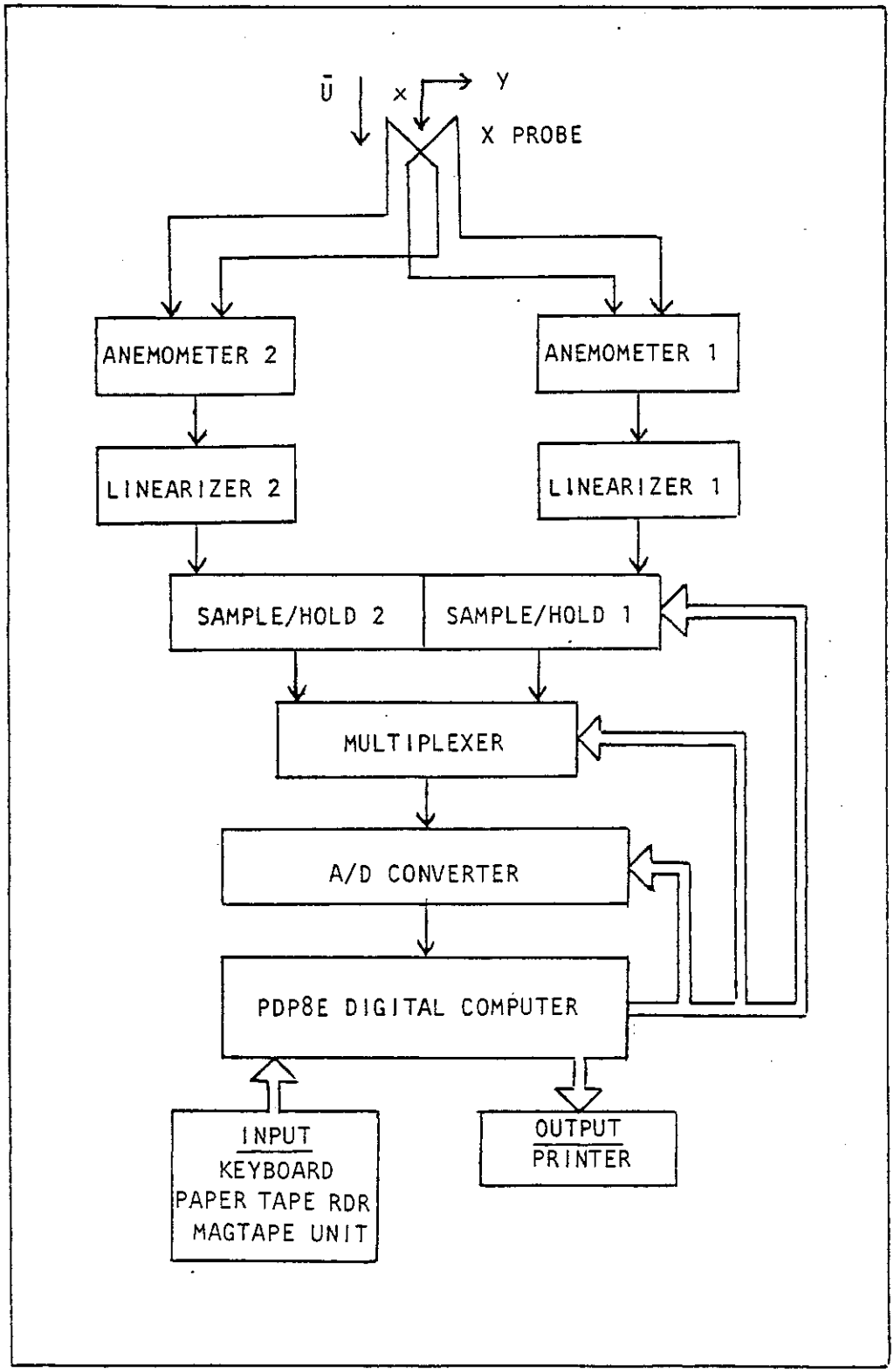


Figure 2.4: Block diagram of data acquisition and processing arrangement

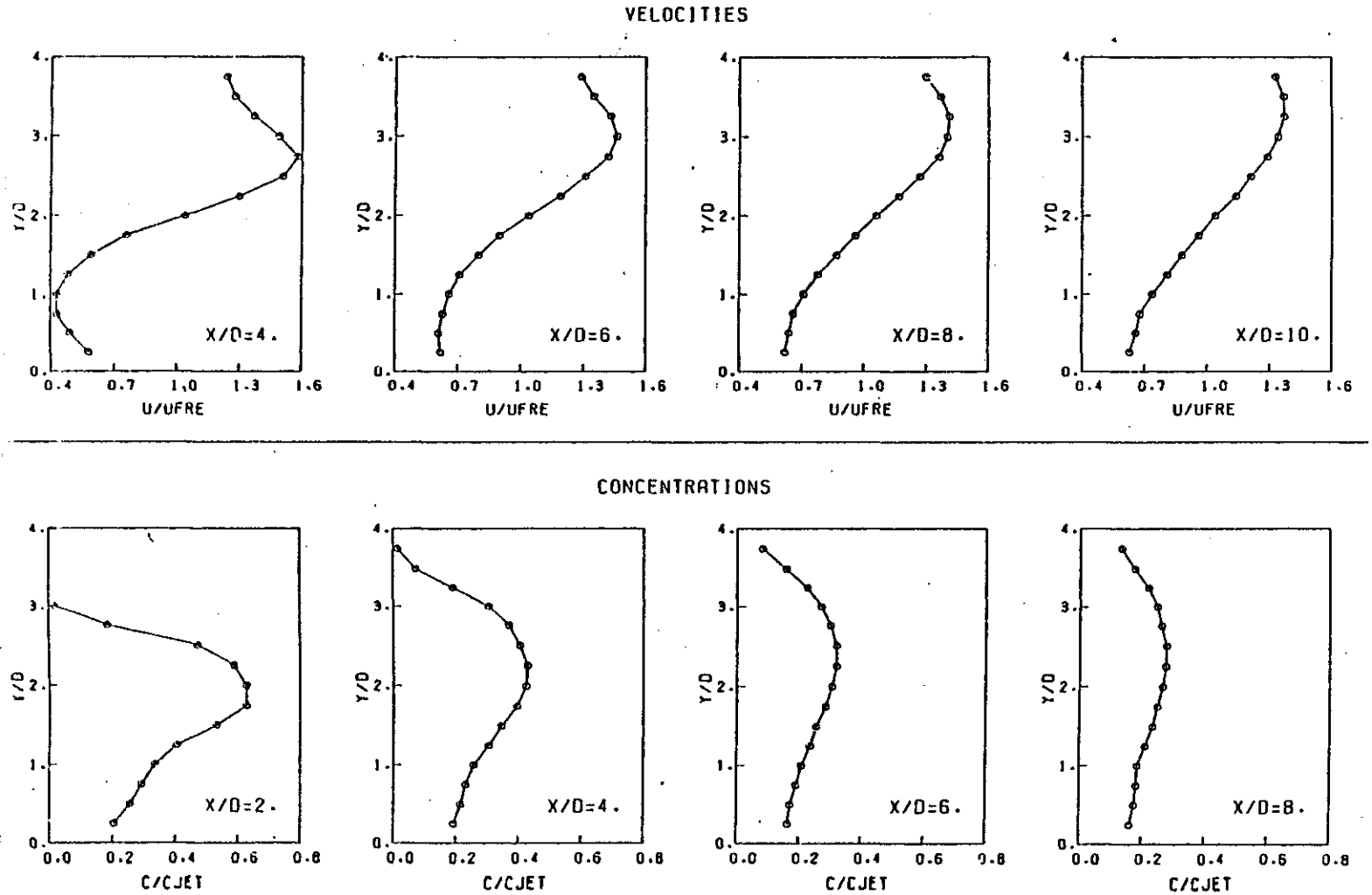


Figure 3.1: Velocity and concentration profiles along centre-plane for pitch-to-diameter ratio (S/D) of 2 and duct height 4D

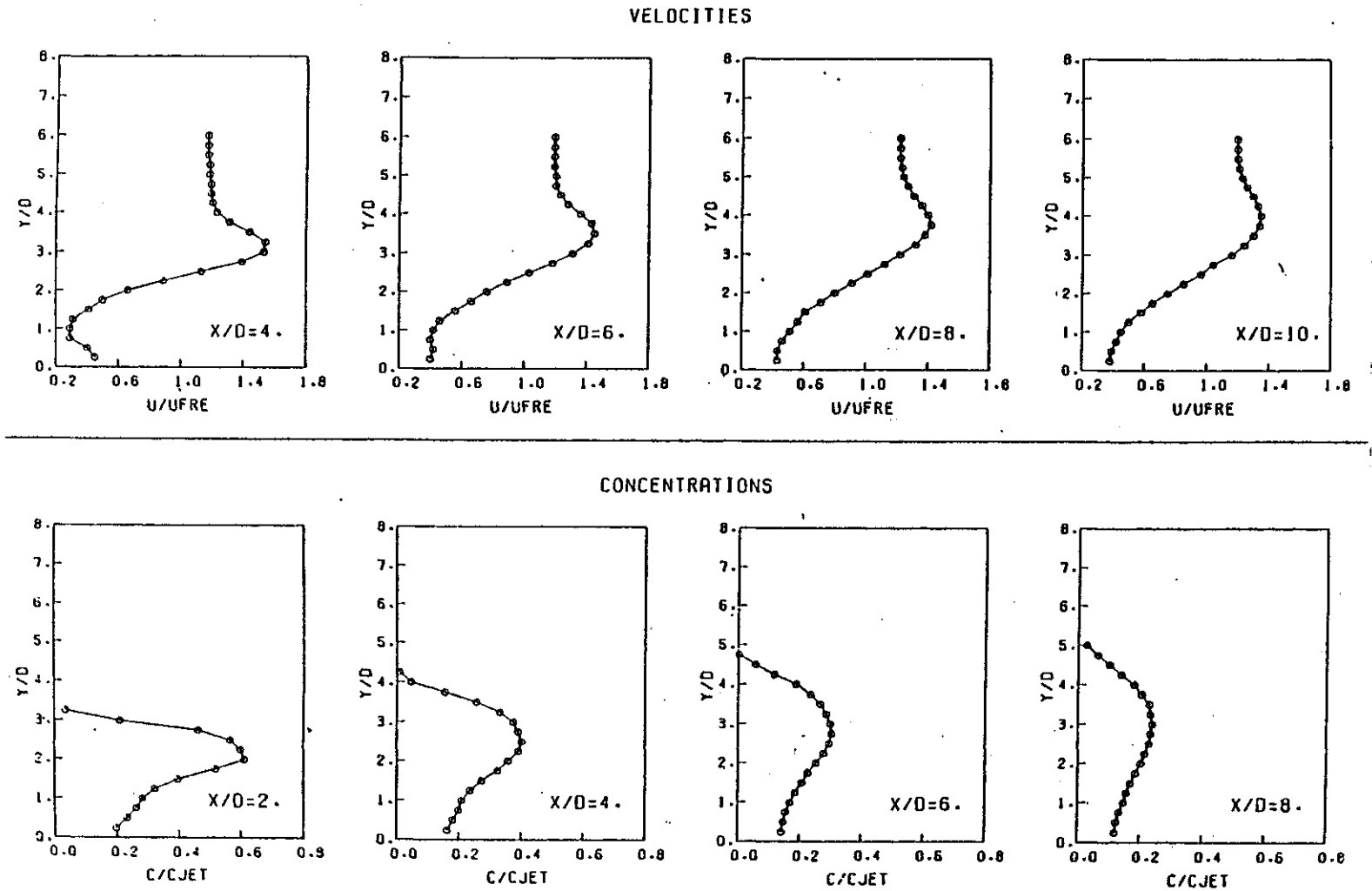


Figure 3.2: Velocity and concentration profiles along centre-plane for S/D of 2 and duct height 8D

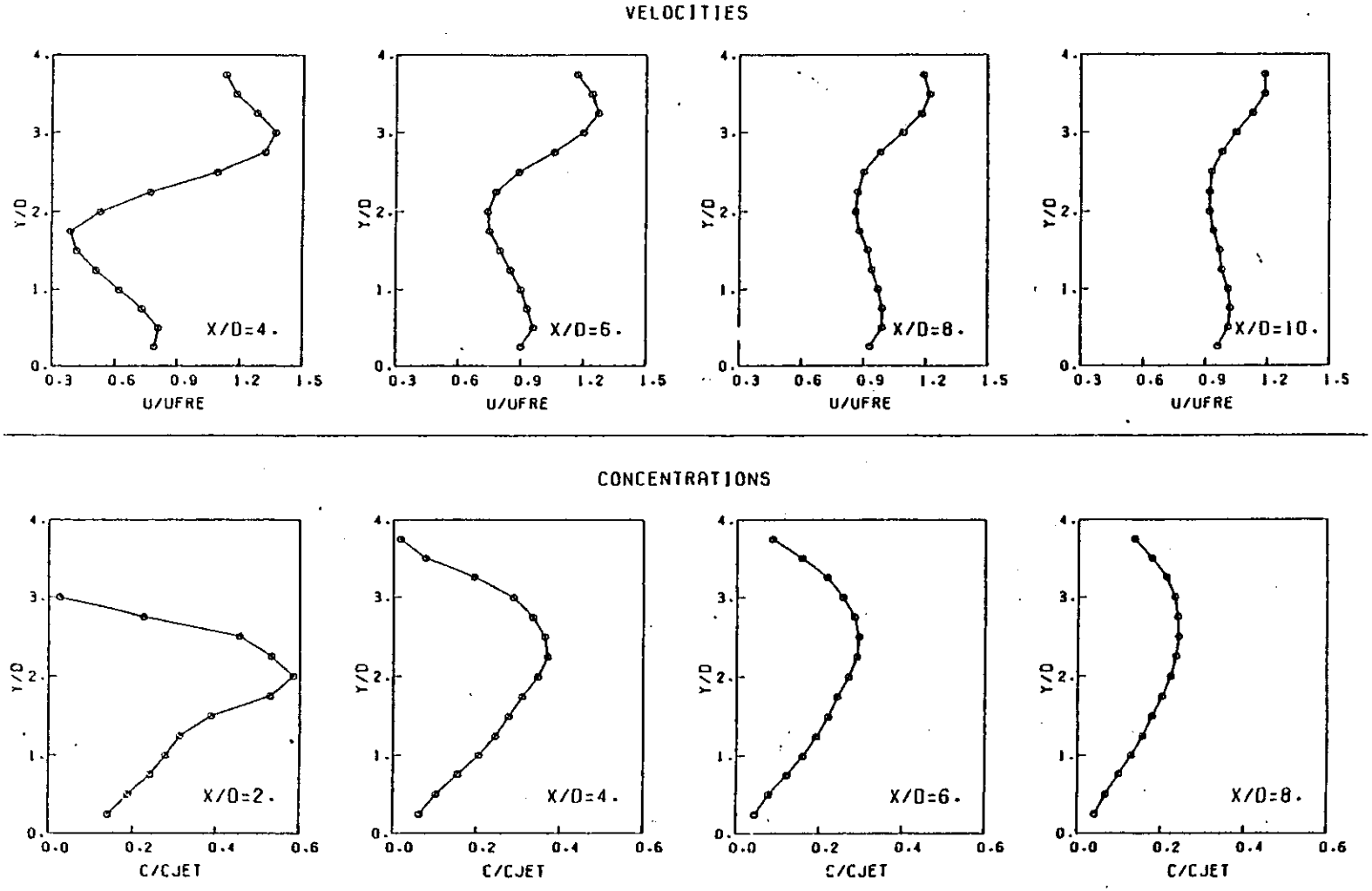


Figure 3.3: Velocity and concentration profiles along centre-plane for S/D of 4 and duct height 4D

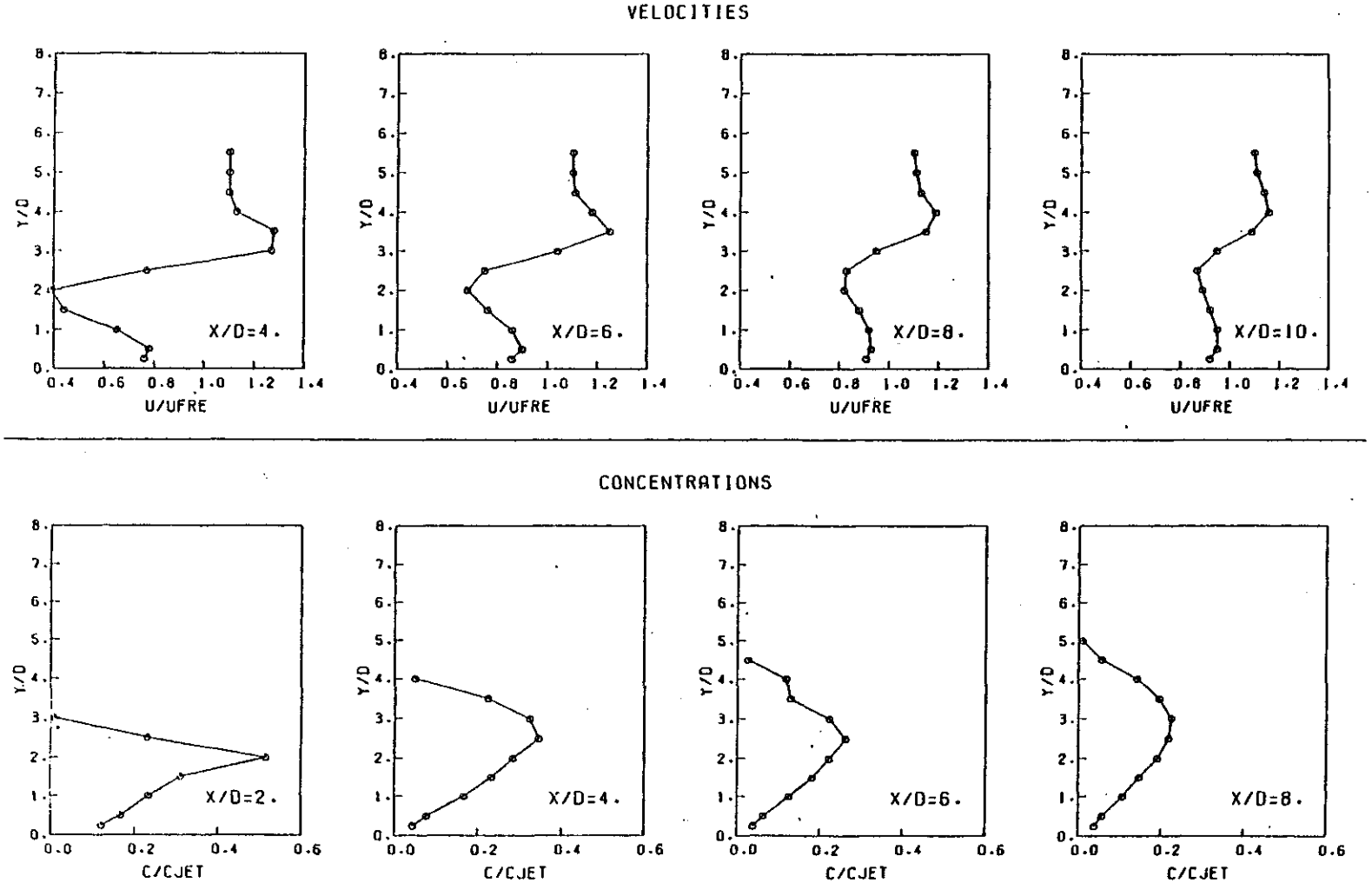
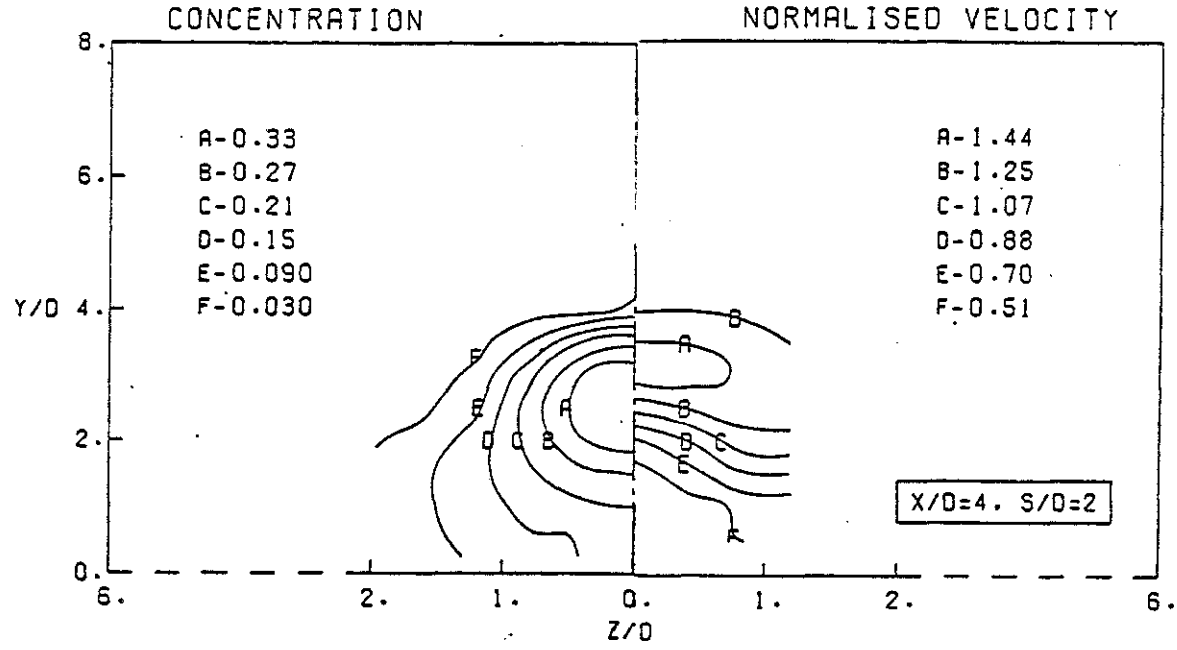


Figure 3.4: Velocity and concentration profiles along centre-plane for S/D of 4 and duct height 8D



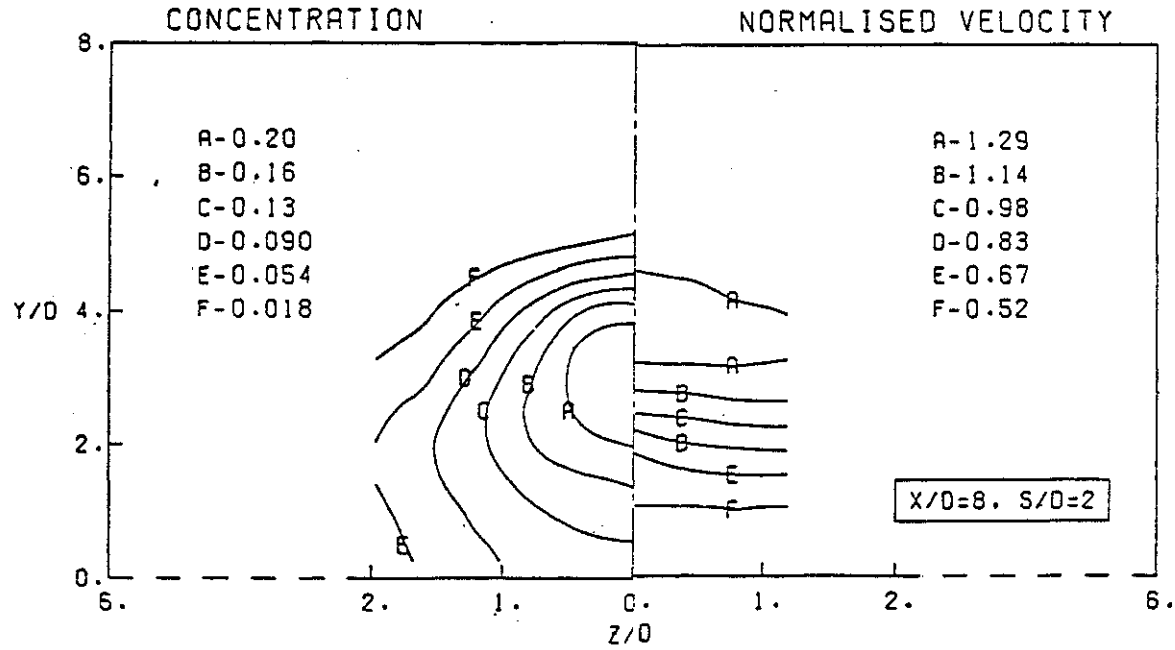


Figure 3.5: Normalised velocity (U/U_∞) contours and concentration contours (θ/θ_j) at axial planes X/D = 4 and 8 for S/D of 2 and duct height 8D (central jet seeded)

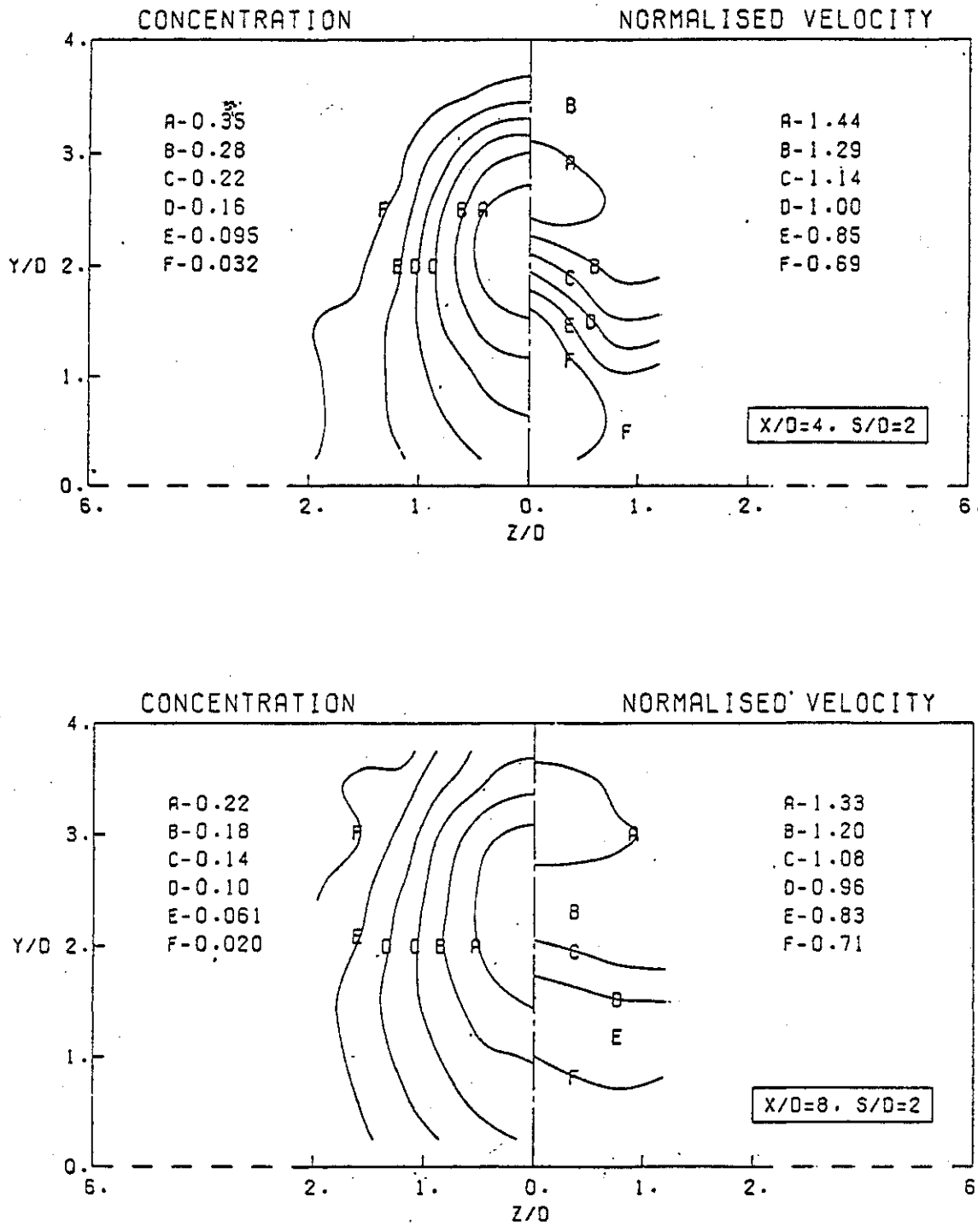
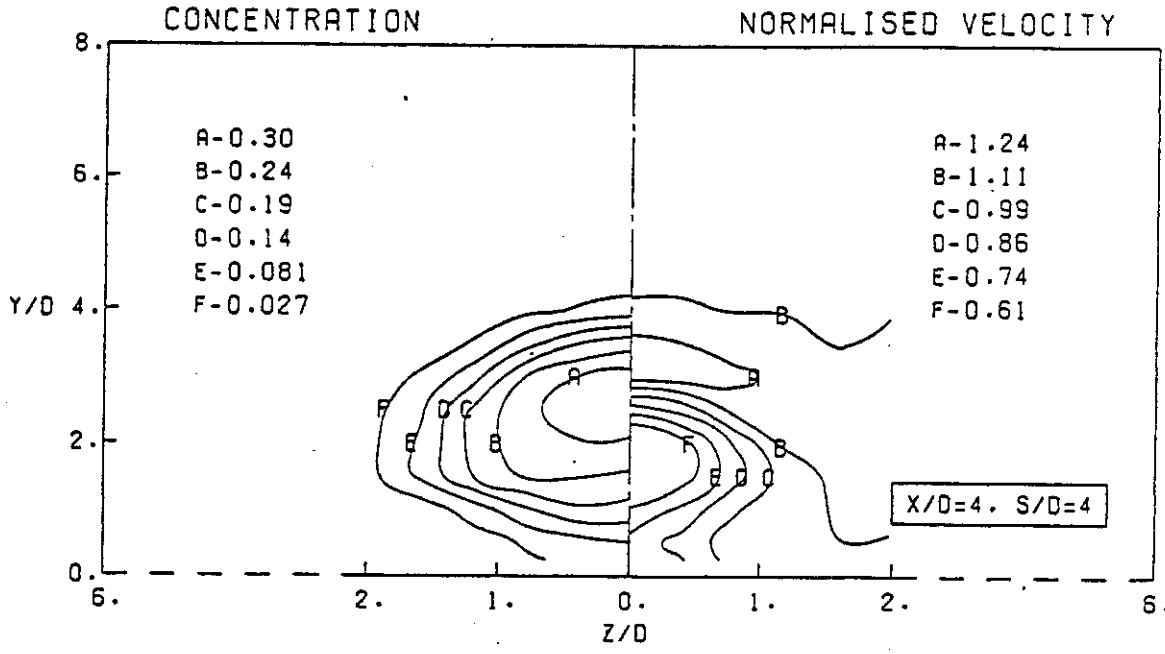


Figure 3.6: Normalised velocity and concentration contours at axial planes X/D = 4 and 8 for S/D of 2 and duct height 4D



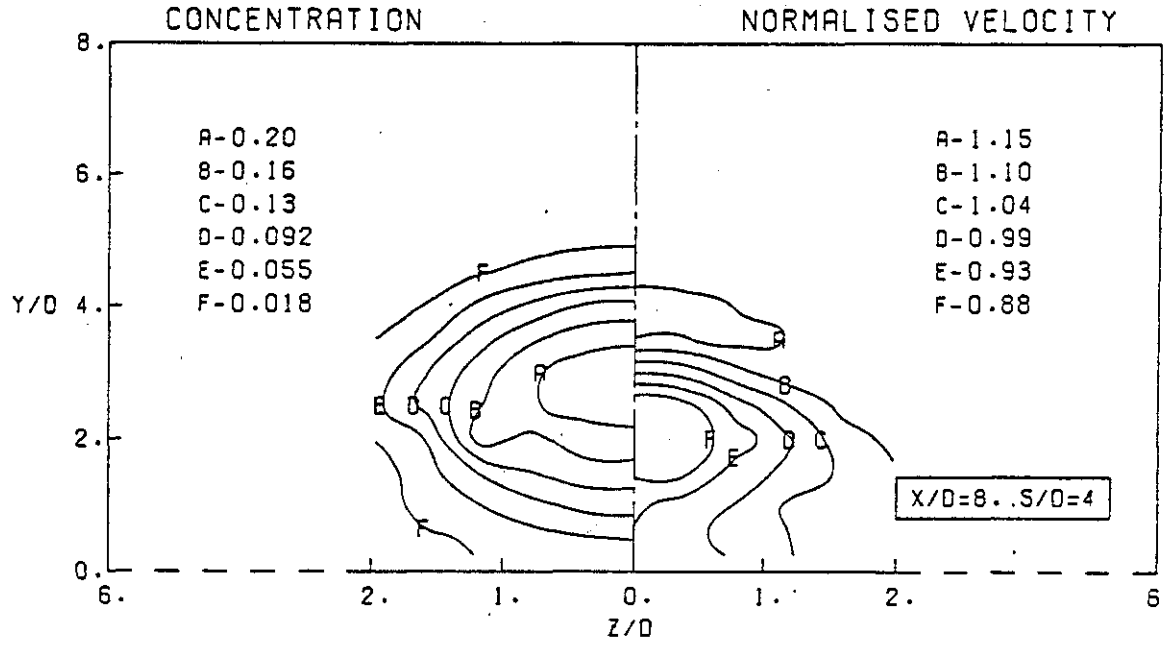
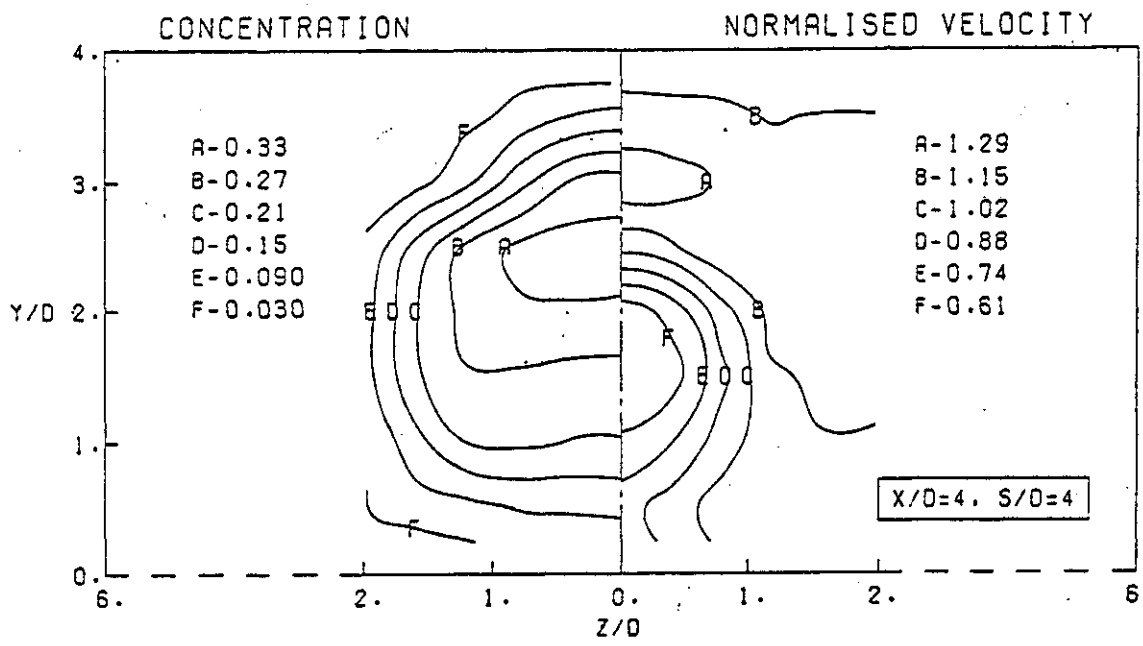


Figure 3.7: Normalised velocity and concentration contours at axial planes X/D = 4 and 8 for S/D of 4 and duct height 8D



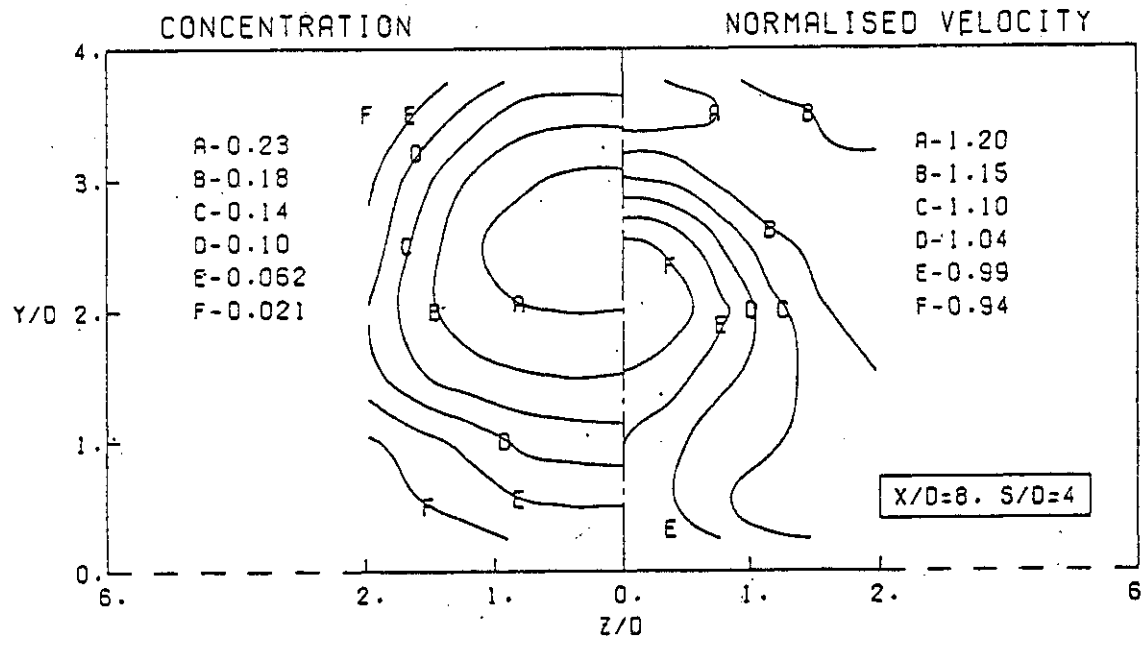
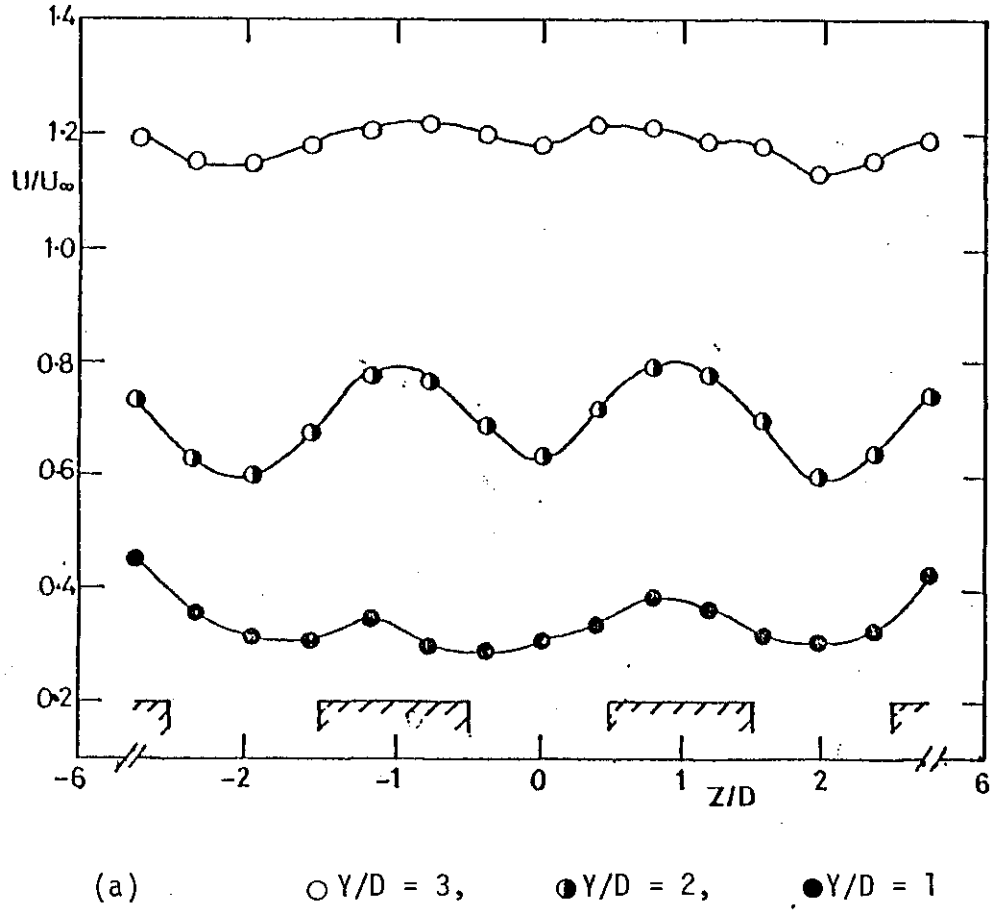
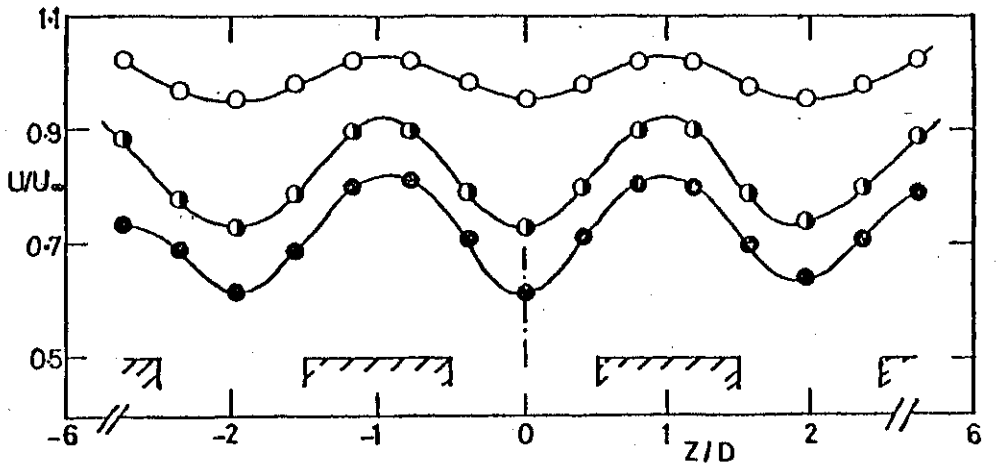


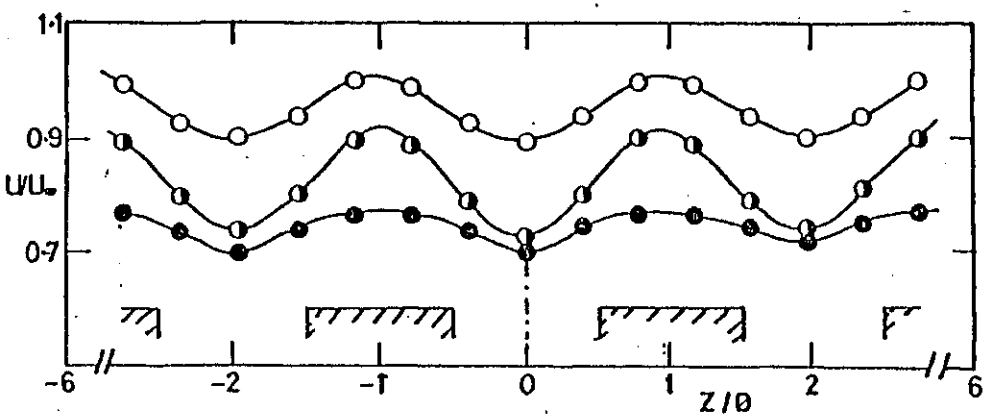
Figure 3.8: Velocity and concentration contours at axial planes X/D = 4 and 8 for S/D of 4 and duct height 4D



(a) ○ Y/D = 3, ◑ Y/D = 2, ● Y/D = 1

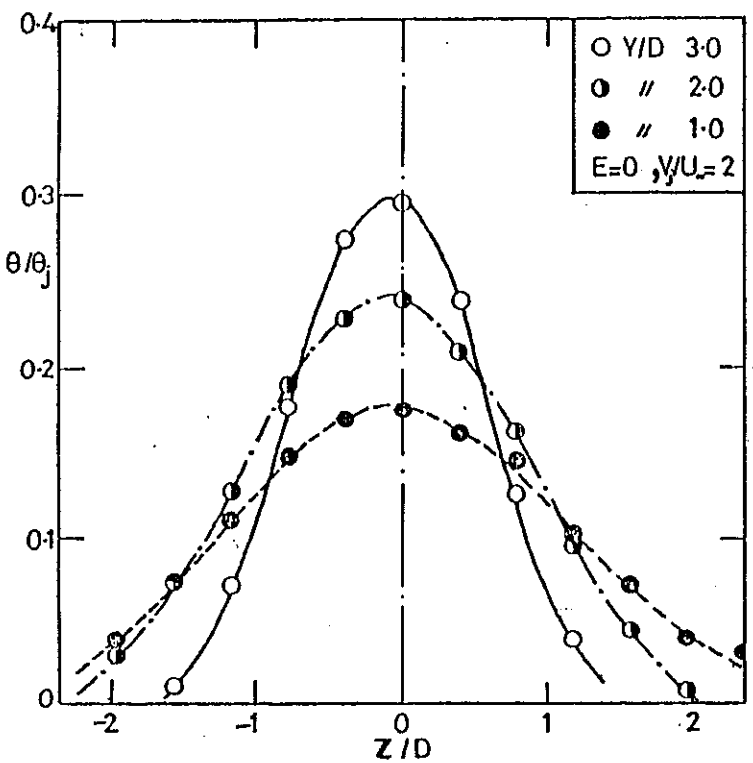


(b) ○ Y/D = 1.5, ◑ Y/D = 1, ● Y/D = 0.5

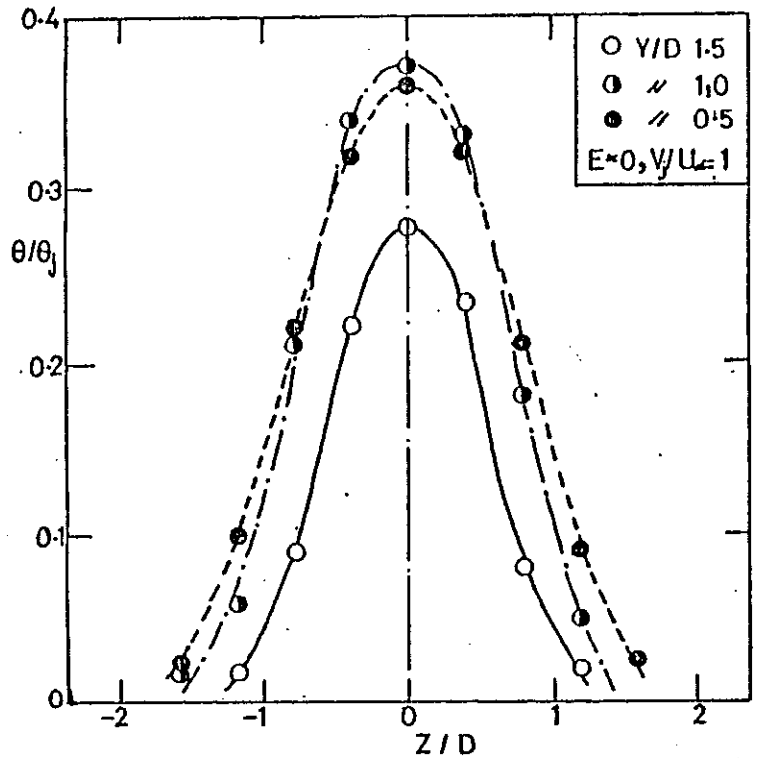


(c) ○ Y/D = 1, ◑ Y/D = 0.5, ● Y/D = 0.25

Figure 3.9: Transverse velocity distributions at X/D = 6 for jets symetrically arranged and jet-to-crossflow velocity ratios (V_j/U_∞); (a) 2.0, (b) 1.0, (c) 0.5

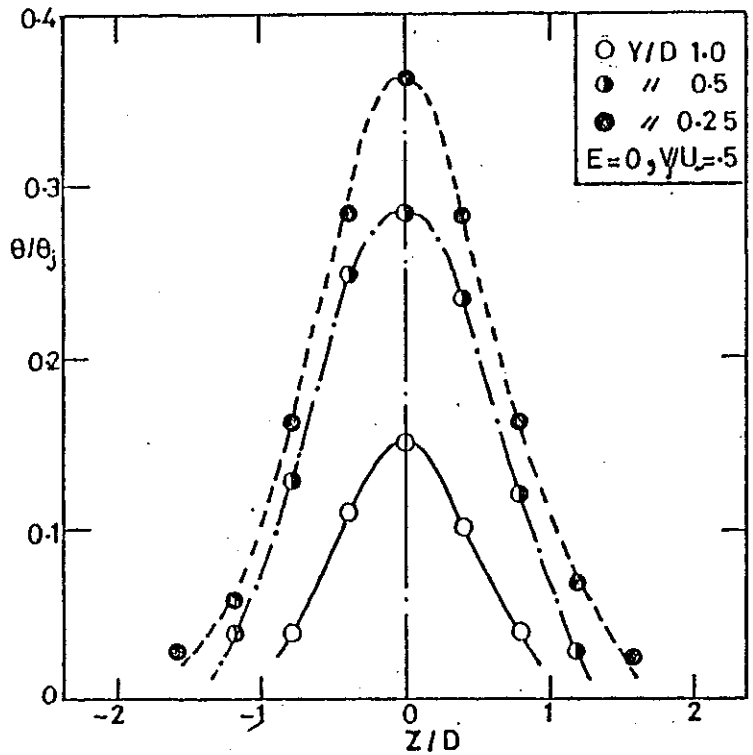


(a) V_j/U_∞ = 2.0



(b) V_j/U_∞ = 1.0

Figure 3.10: Concentration distributions at X/D = 6 with jets symmetric and velocity ratios (V_j/U_∞) of 2, 1 and 0.5 (central jet seeded only)



(c) $V_j/U_\infty = 0.5$

Figure 3.10 (concluded)

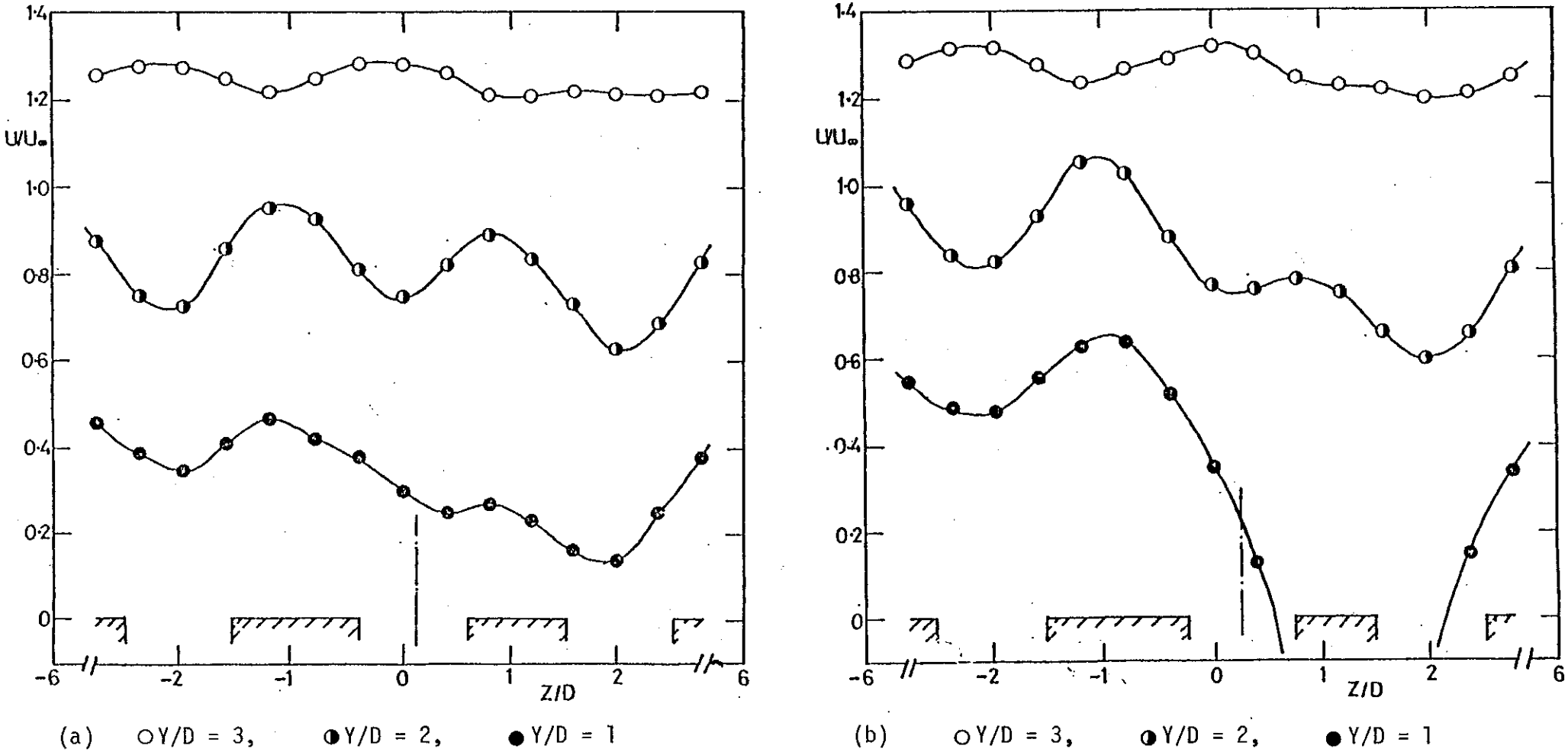
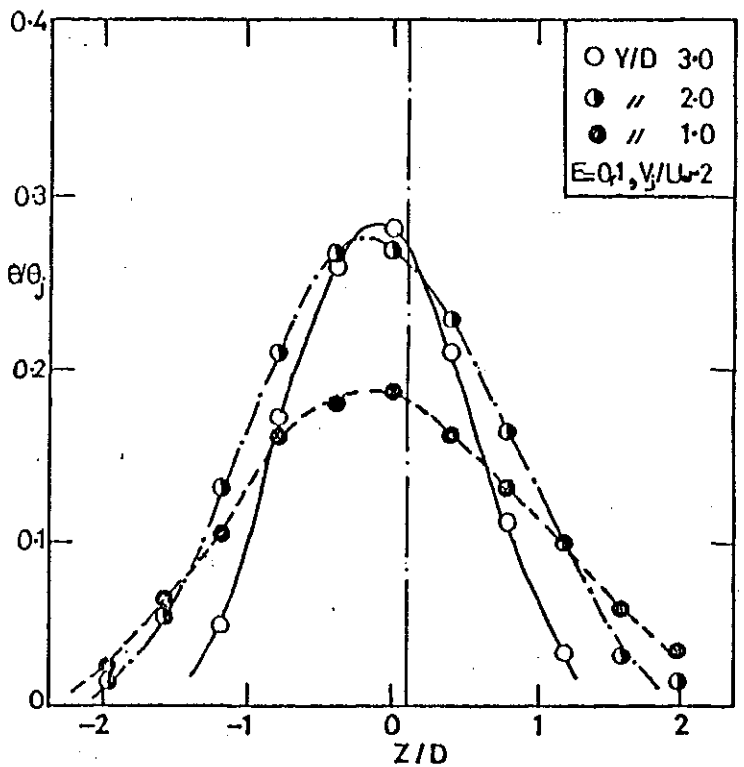
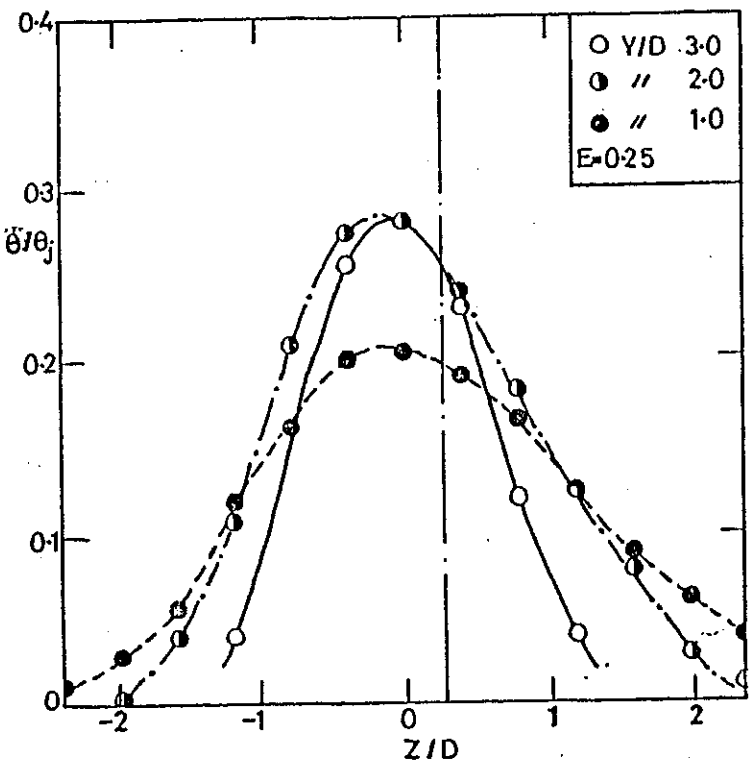


Figure 3.11: Transverse velocity distributions at X/D = 6 for V_j/U_∞ = 2.0 and central jet eccentric: (a) E/D=0.1, (b) E/D=0.25

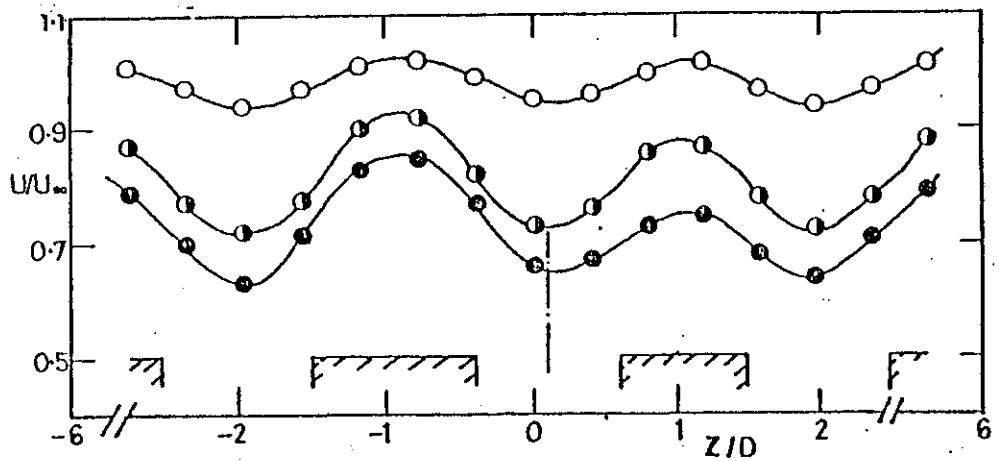


(a) E/D = 0.1



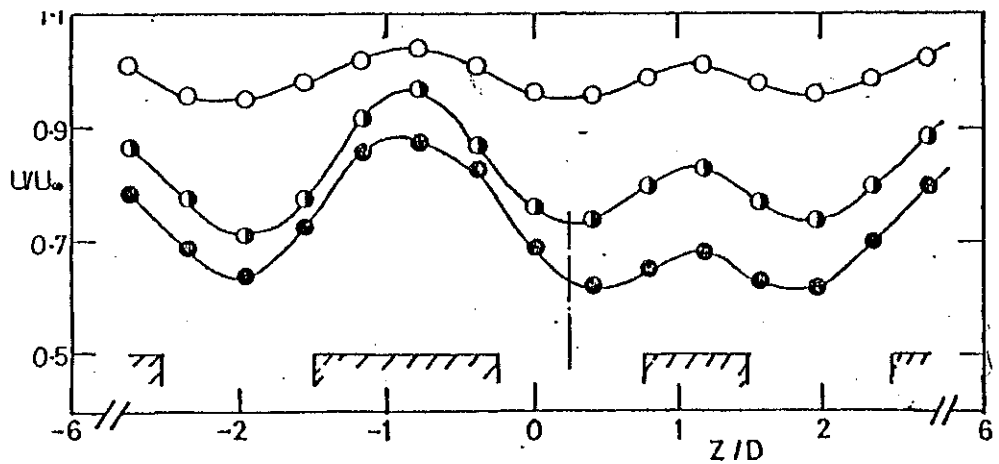
(b) E/D = 0.25

Figure 3.12: Concentration distributions at X/D = 6 for V_j/U_∞ = 2.0 and central jet eccentric: (a) E/D = 0.1, (b) E/D = 0.25 (central jet seeded only)

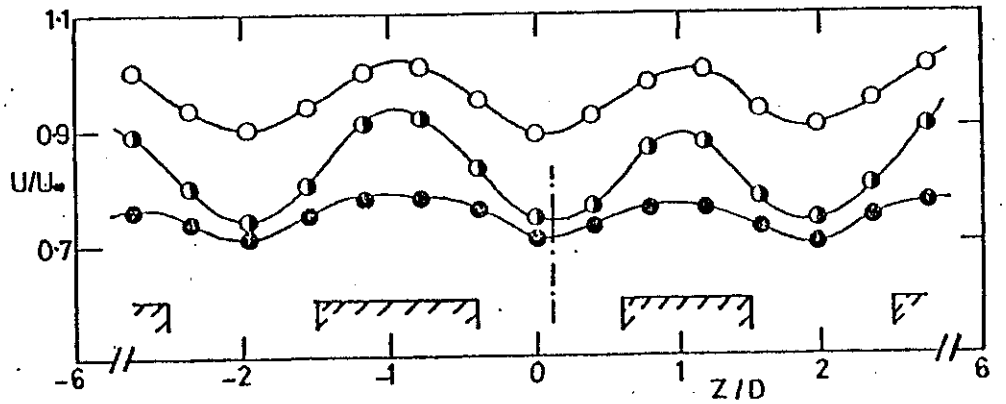


(a) V_j/U_∞ = 1.0, E/D = 0.1

○ Y/D = 1.5, ◑ Y/D = 1.0, ● Y/D = 0.5

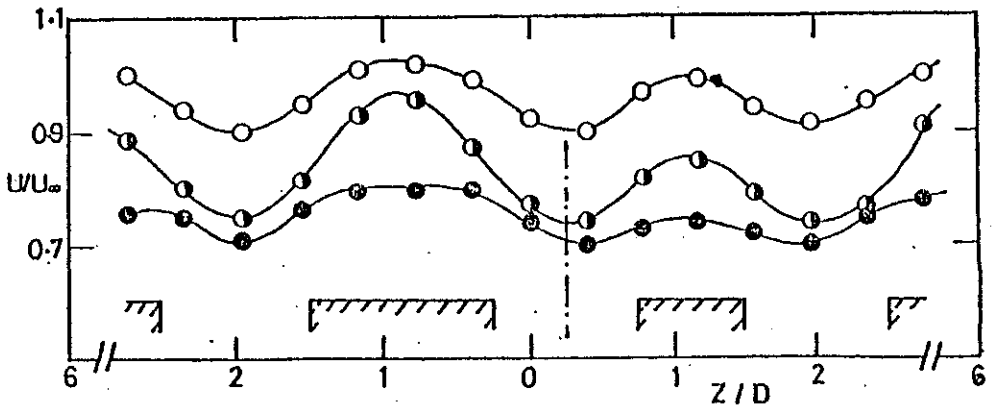


(b) V_j/U_∞ = 1.0, E/D = 0.25



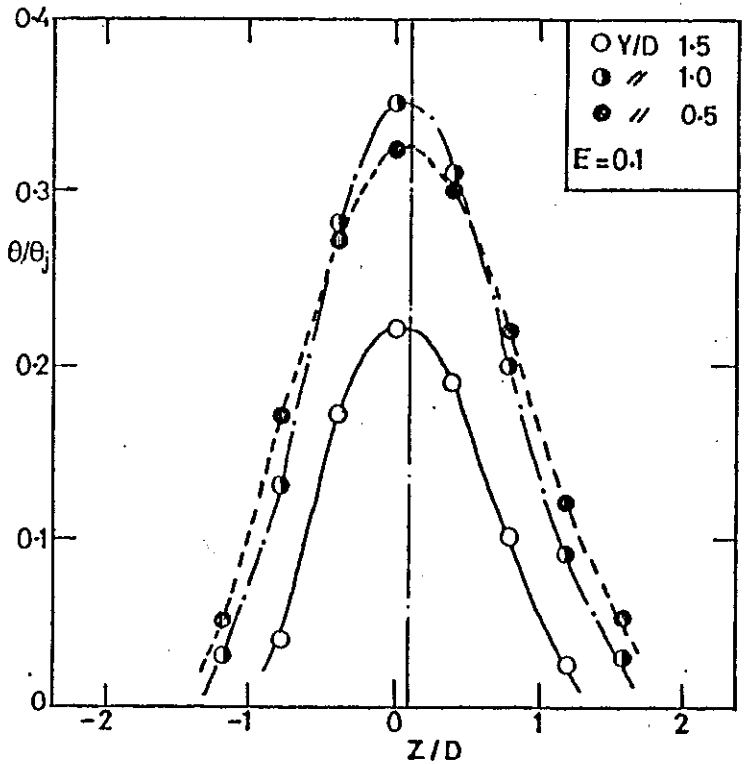
(c) V_j/U_∞ = 0.5, E/D = 0.1

○ Y/D = 1, ◑ Y/D = 0.5, ● Y/D = 0.25

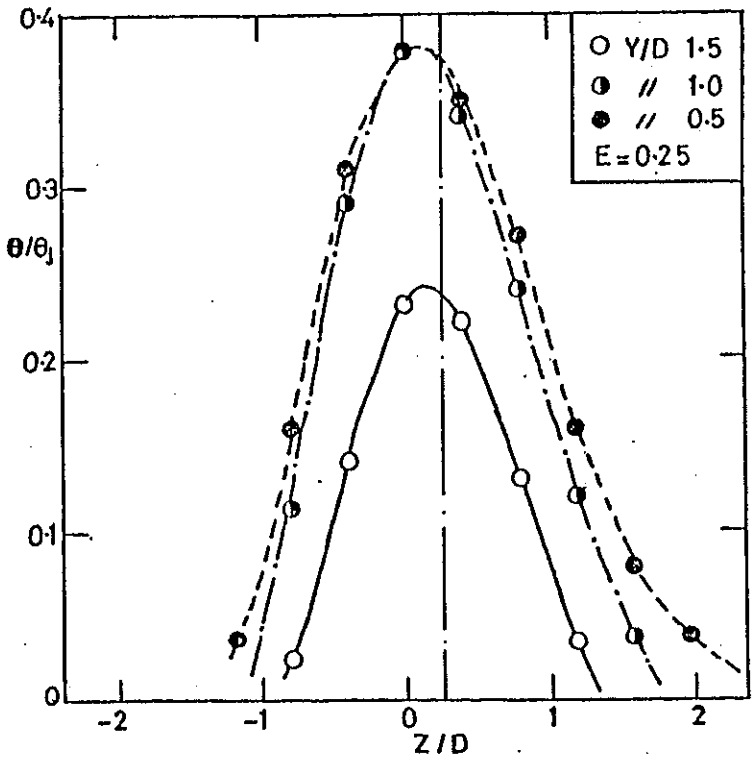


(d) V_j/U_∞ = 0.5, E/D = 0.25

Figure 3.13: Velocity distributions at X/D = 6 for V_j/U_∞ = 1.0 and 0.5 and central jet eccentricity of 0.1D and 0.25D

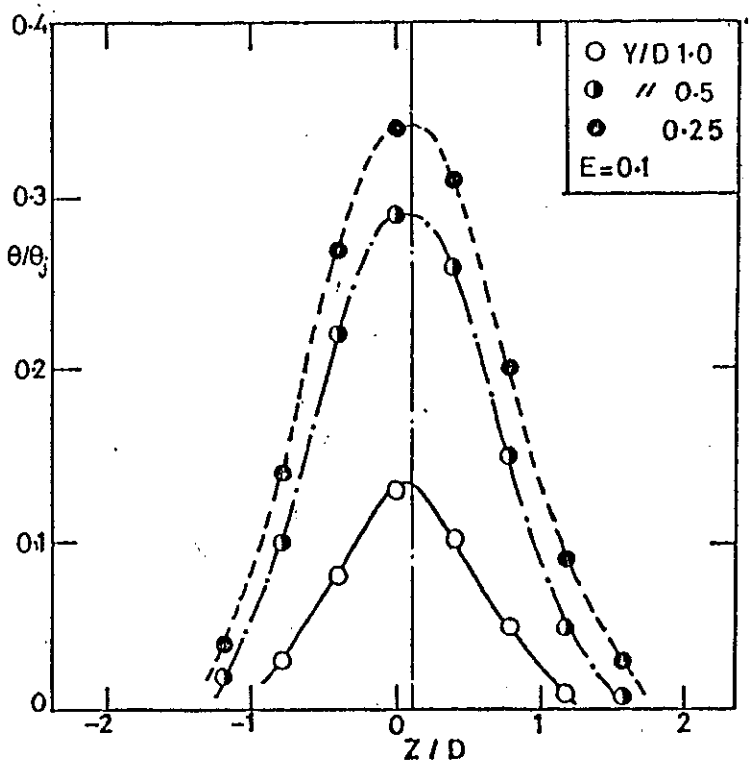


(a) V_j/U_∞ = 1.0, E/D = 0.1

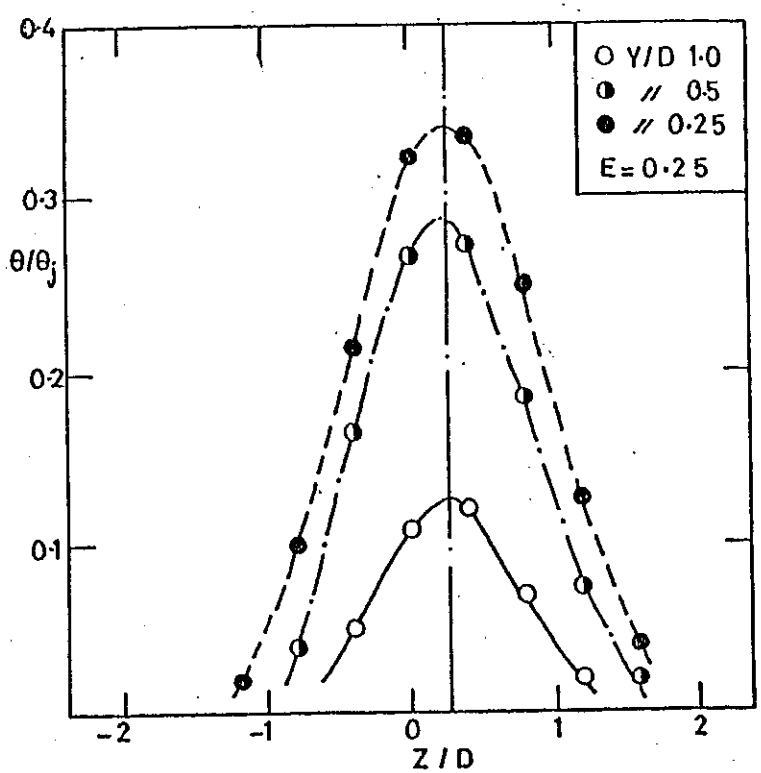


(b) V_j/U_∞ = 1.0, E/D = 0.25

Figure 3.14: Concentration distributions at X/D = 6 for V_j/U_∞ = 1.0 and 0.5 and central jet eccentric E/D = 0.1 and 0.25 (central jet seeded)



(c) V_j/U_∞ = 0.5, E/D = 0.1



(d) V_j/U_∞ = 0.5, E/D = 0.1

Figure 3.14 (concluded)

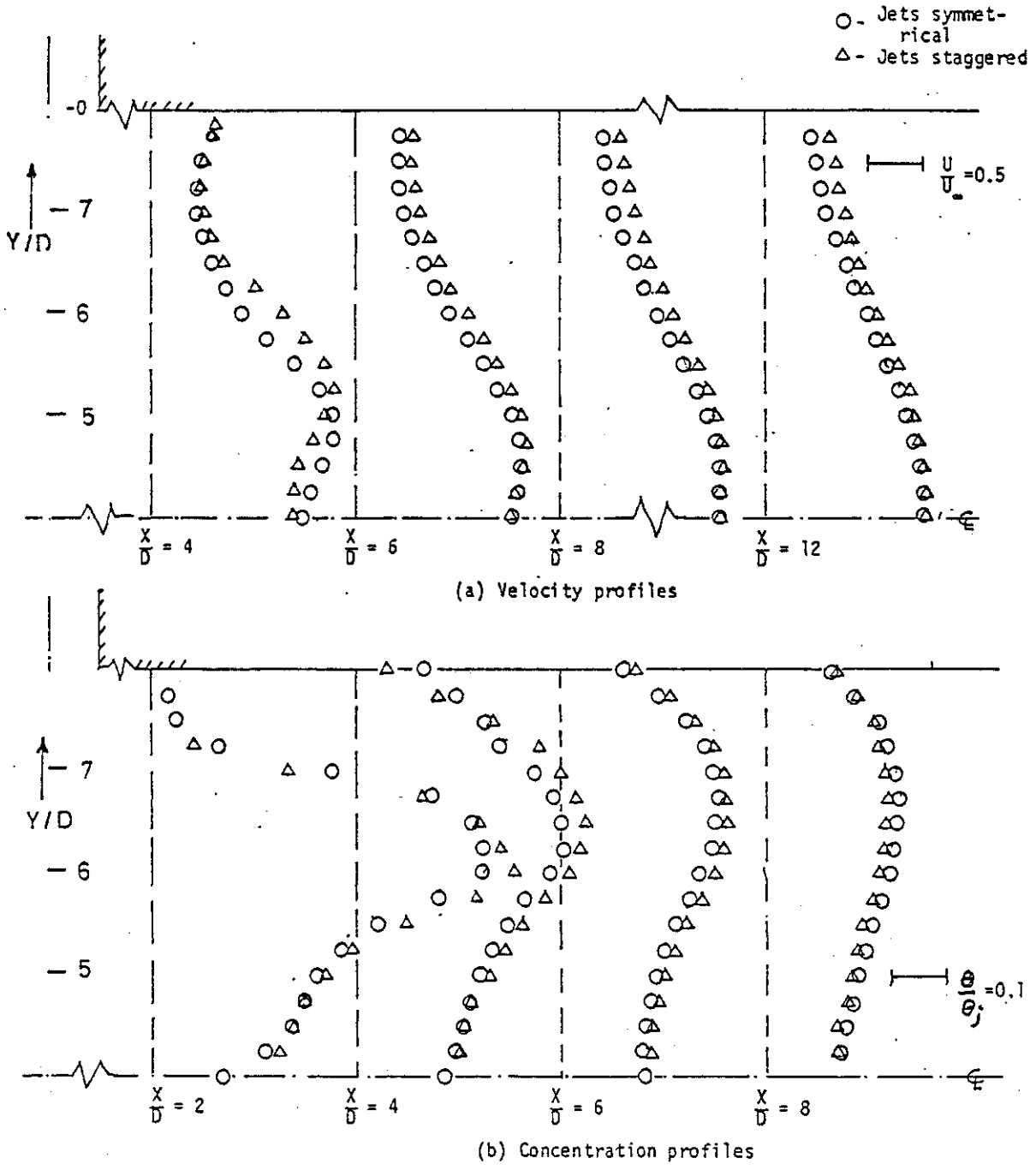


Figure 3.15: Velocity and concentration profiles along centre-plane of duct with jets directly opposed and jets staggered by 1D for duct height 8D and S/D of 2 (central jet seeded)

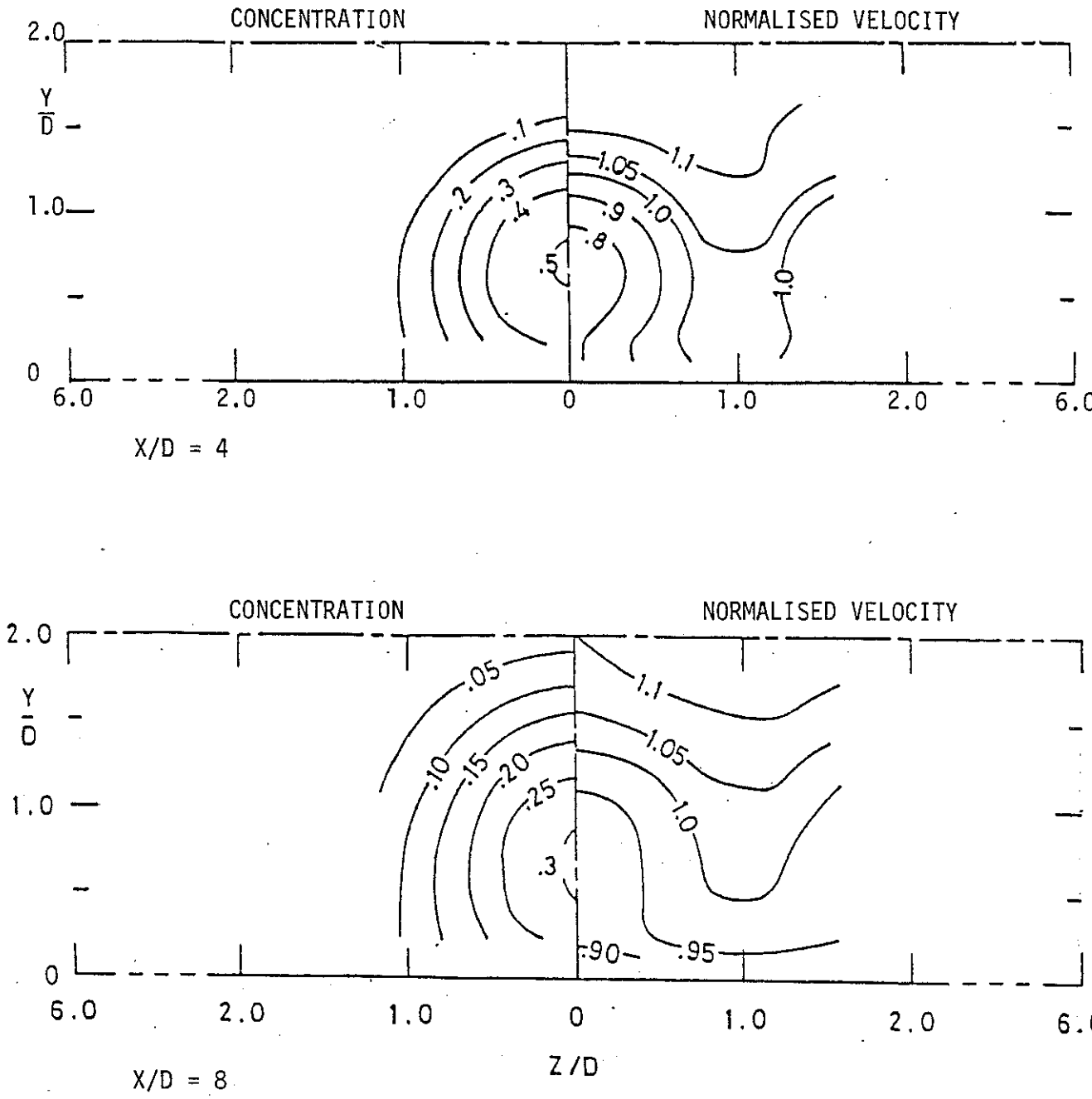


Figure 3.16: Normalised contours of mean velocity and scalar concentration at axial planes X/D = 4 and 8 for S/D of 2, duct height 4D and V_j/U_∞ = 1.0

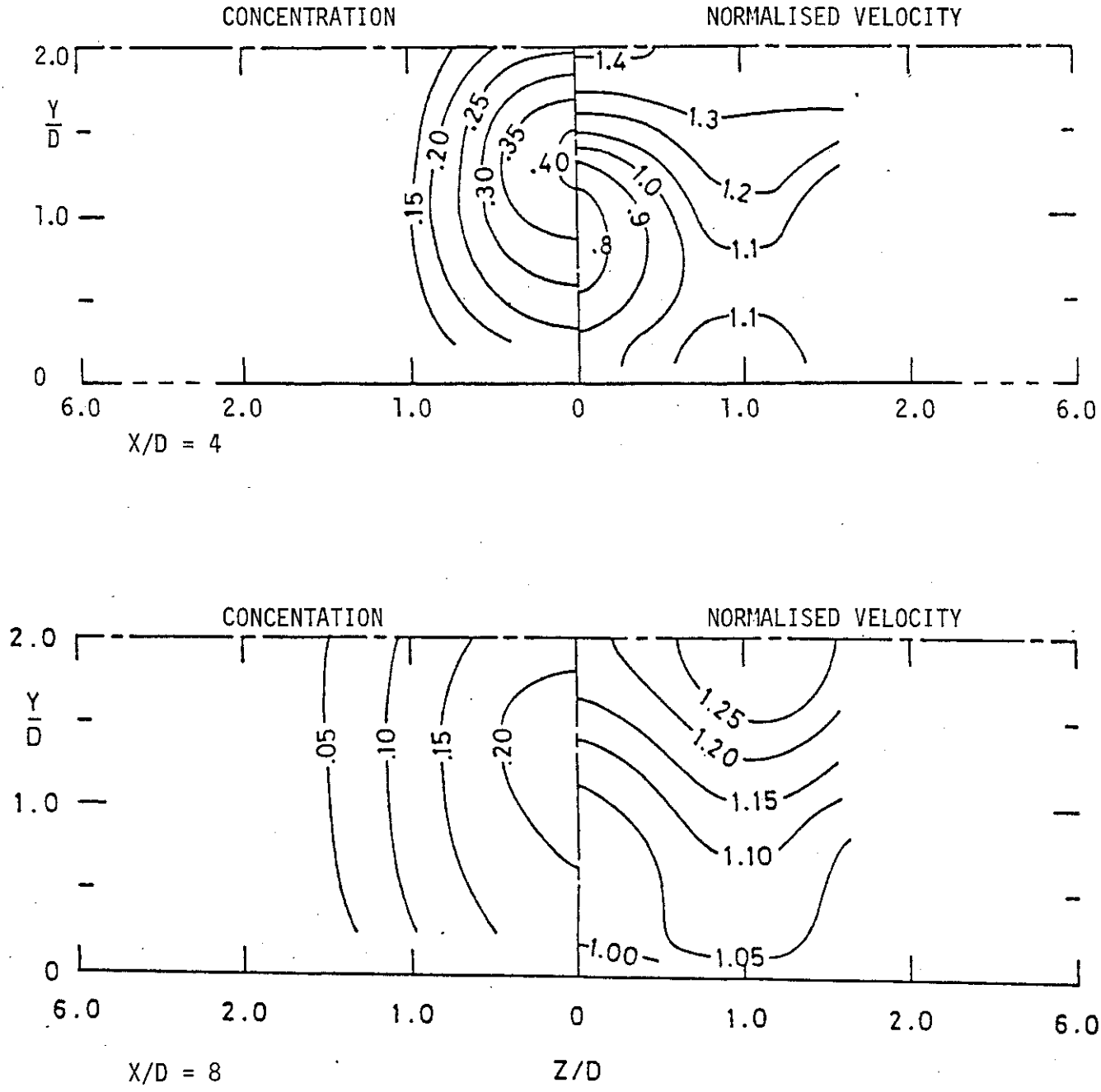


Figure 3.17: Normalised contours of velocity and concentration for S/D of 2 at axial planes X/D = 4 and 8, duct height 4D and V_j / U_∞ = 1.8

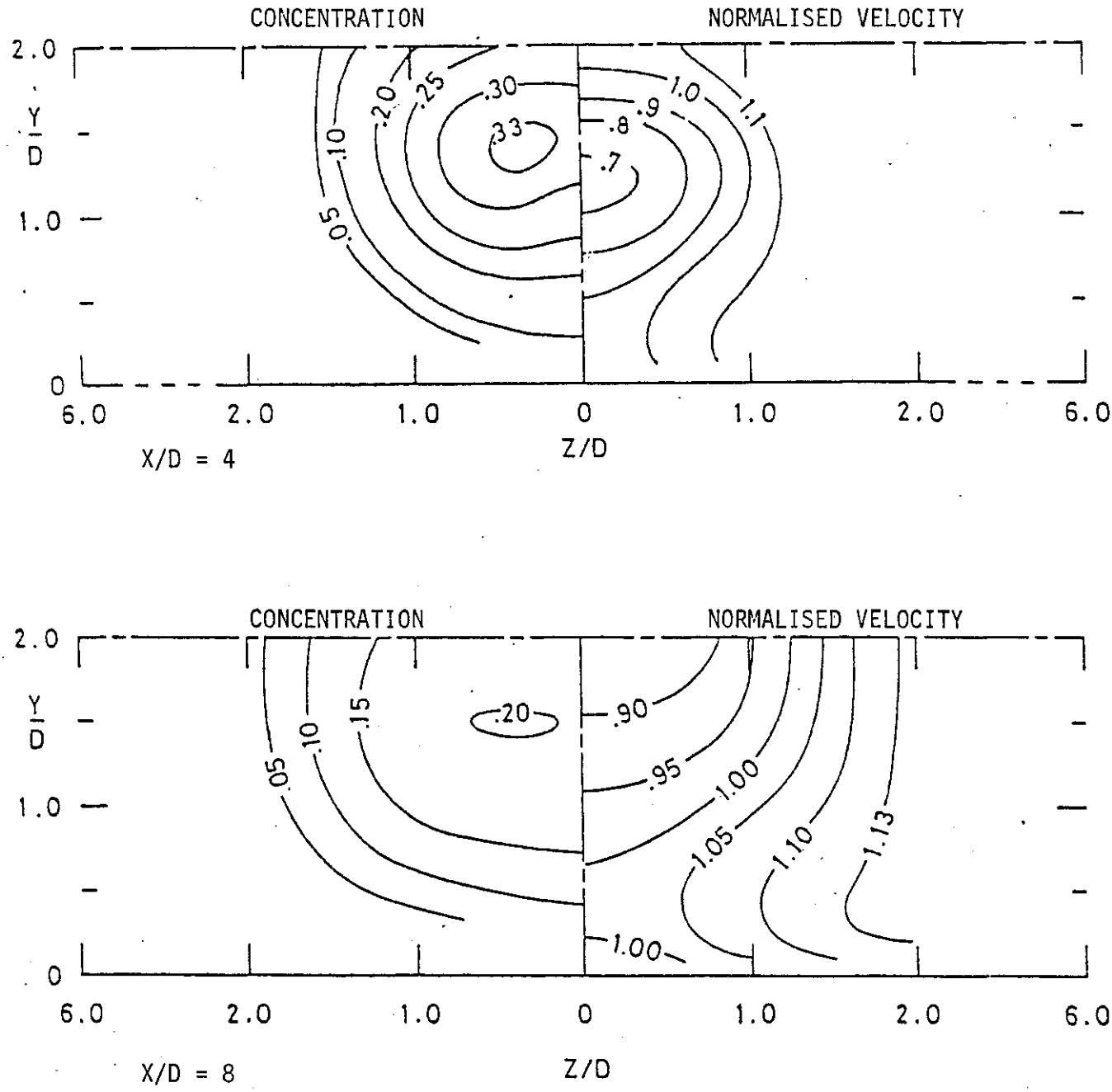
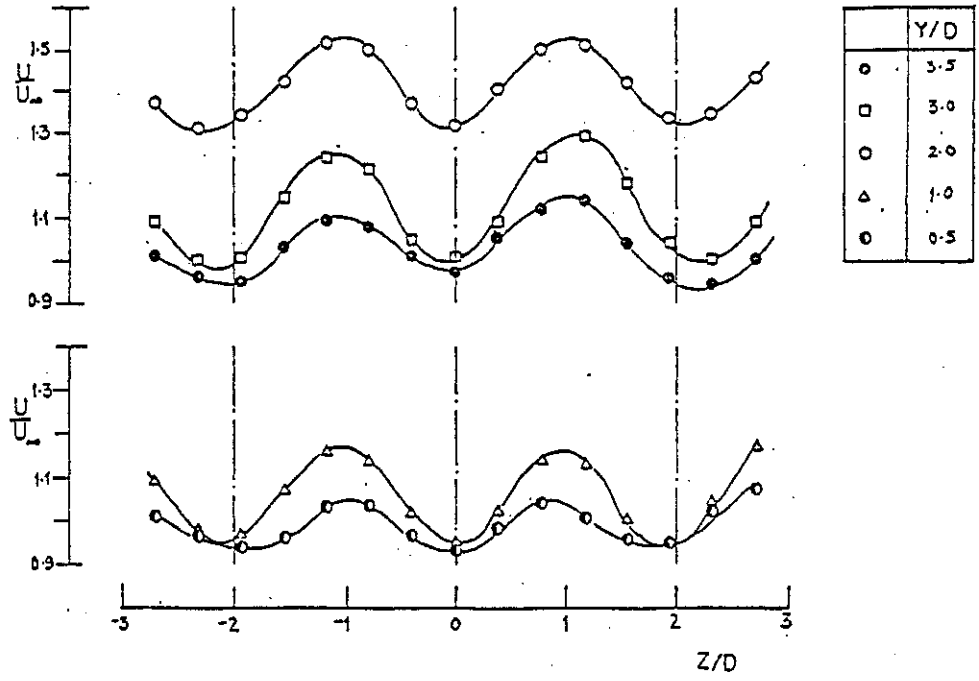
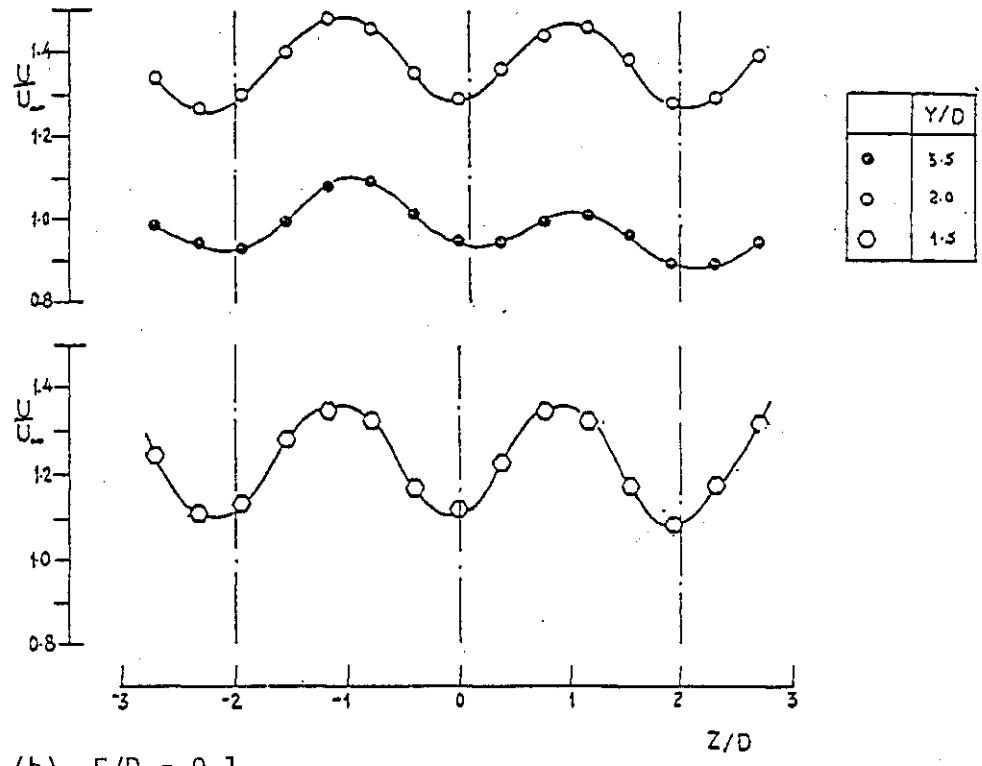


Figure 3.18: Normalised contours of mean velocity and scalar concentration for S/D of 4 at axial planes X/D = 4 and 8, duct height 4D and V_j/U_∞ = 1.8

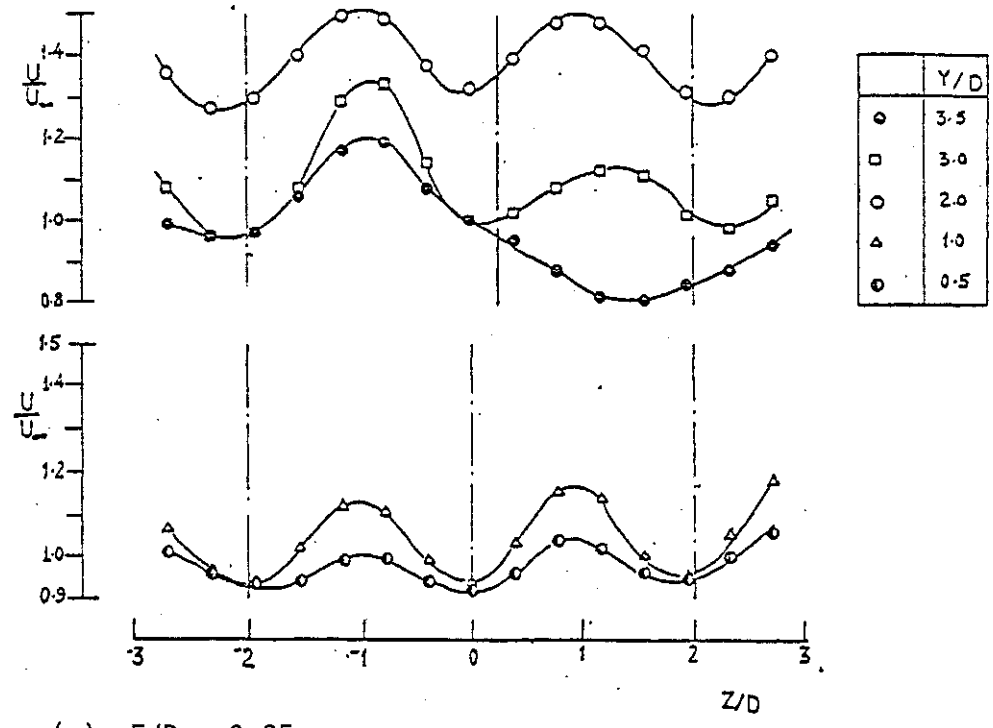


(a) E/D = 0

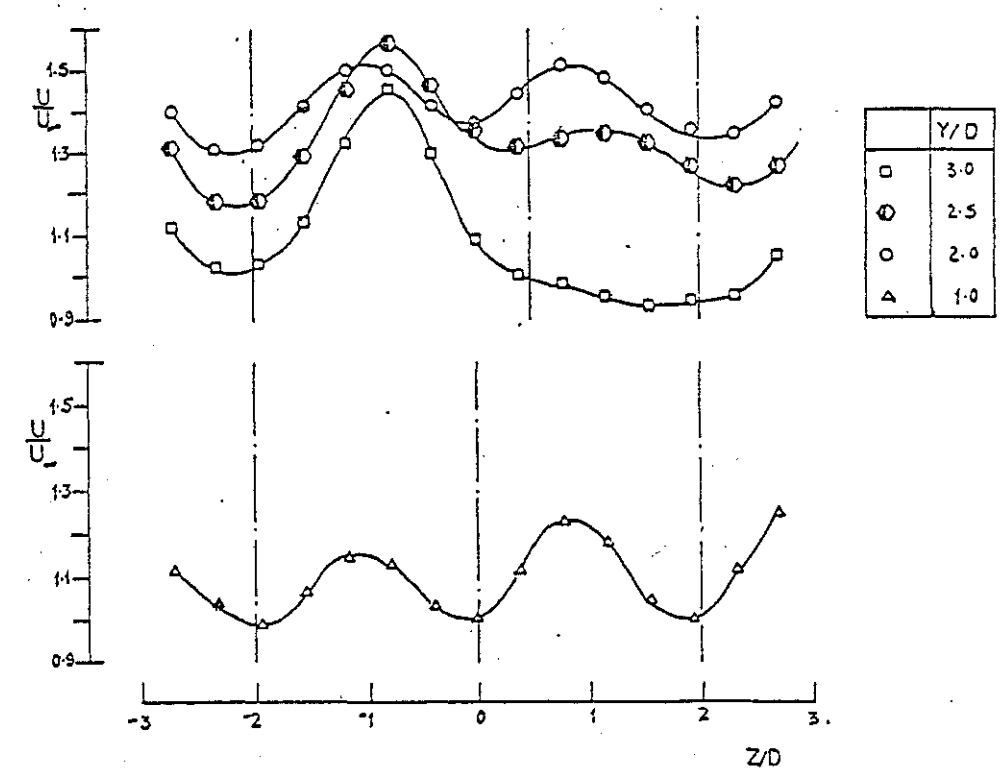


(b) E/D = 0.1

Figure 3.19 Velocity distributions at X/D = 6 for directly opposed rows of jet with top central jet eccentricity E/D = 0, 0.1, 0.25, S/D of 2 and V_j/U_∞ = 2.3

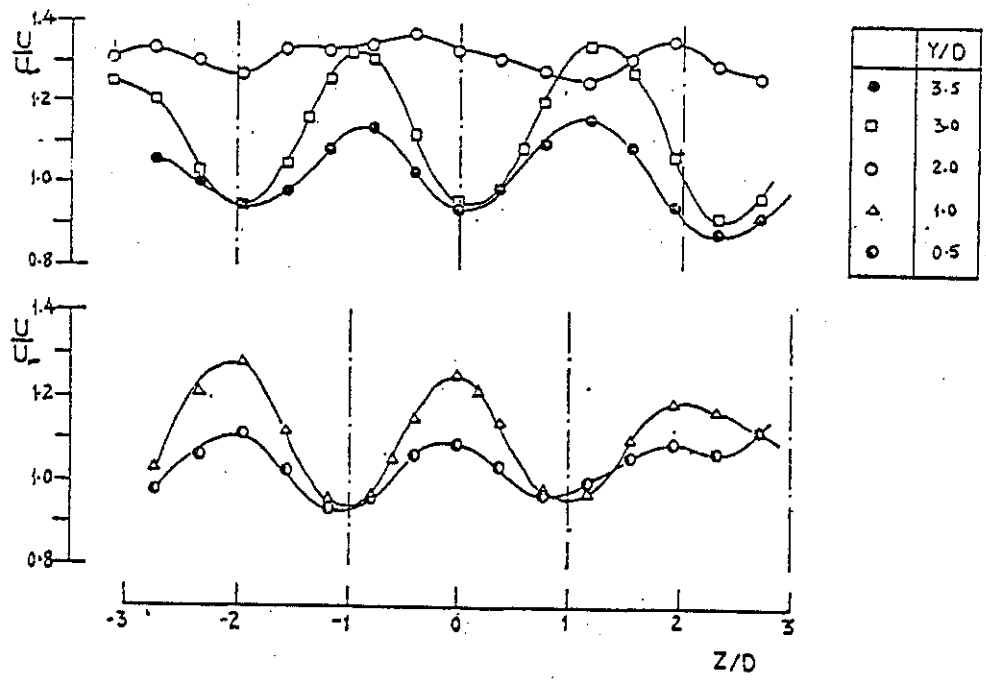


(c) E/D = 0.25

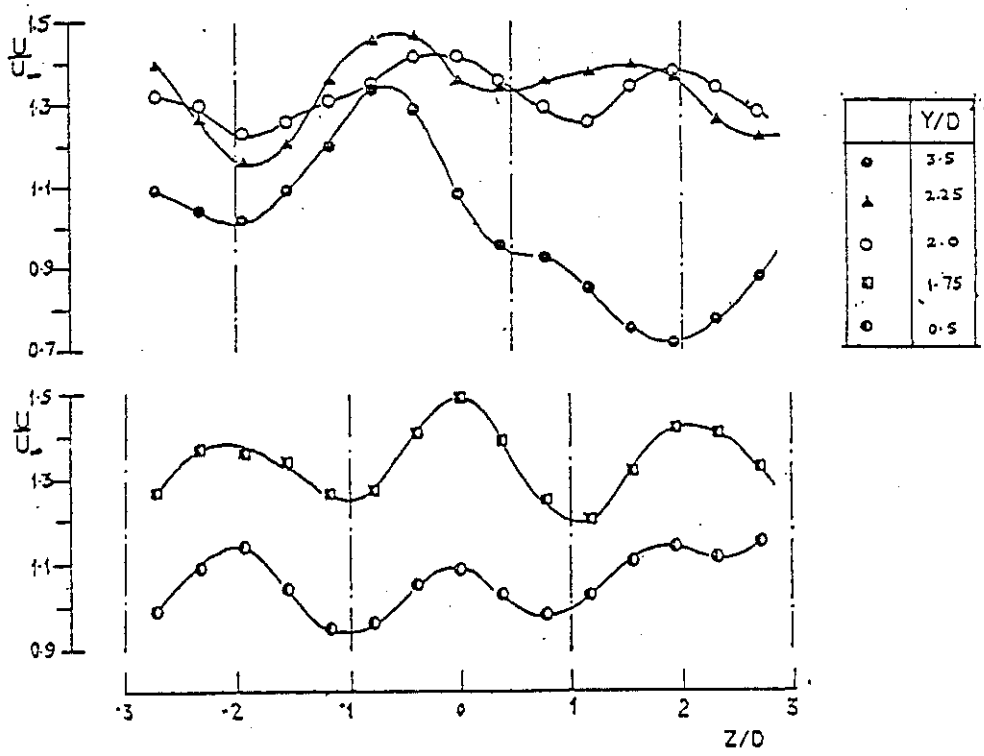


(d) E/D = 0.5

Figure 3.19 (concluded)

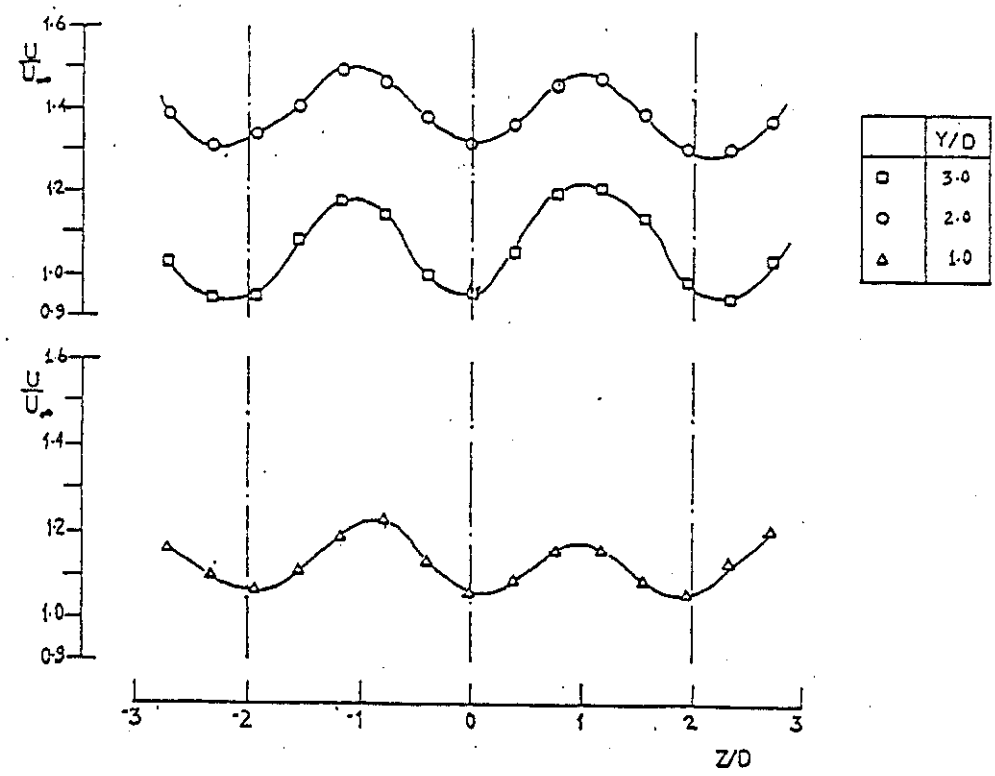


(a) E/D = 0

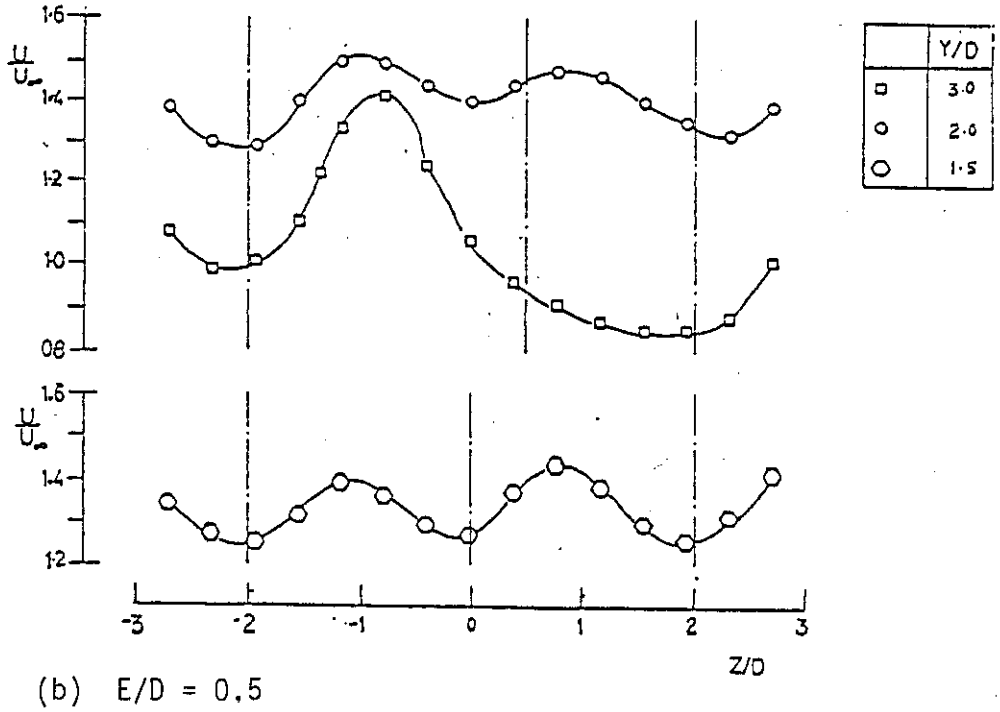


(b) E/D = 0.5

Figure 3.20: Velocity distributions at X/D = 6 for opposed rows of jets for S/D of 2 with floor jets staggered laterally by Z/D = 1 and central jet of top row (a) zero eccentricity and (b) E/D = 0.5

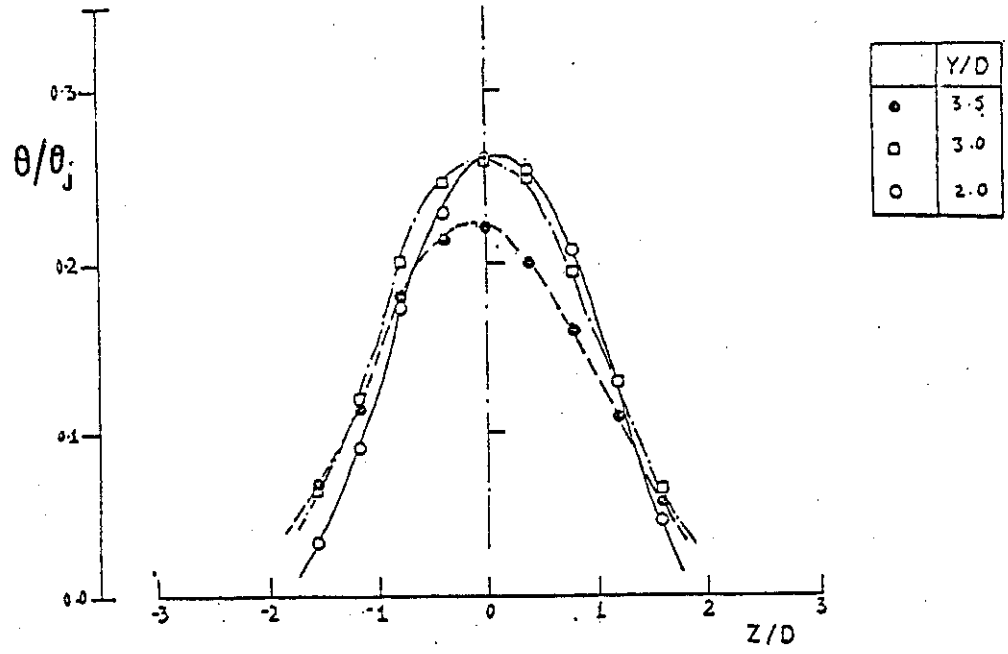


(a) E/D = 0

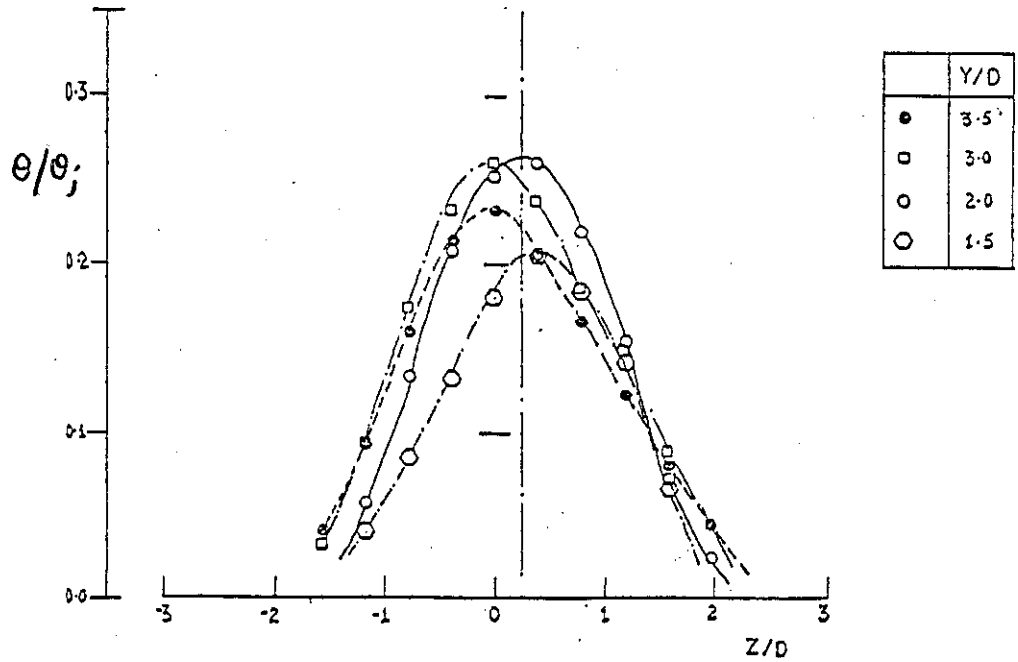


(b) E/D = 0.5

Figure 3.21: Velocity distributions at X/D = 6 for opposed rows of jets with S/D of 2 and ceiling jets staggered axially by X/D = 1. (a) jets symmetric (b) central jet of top row E/D = 0.5

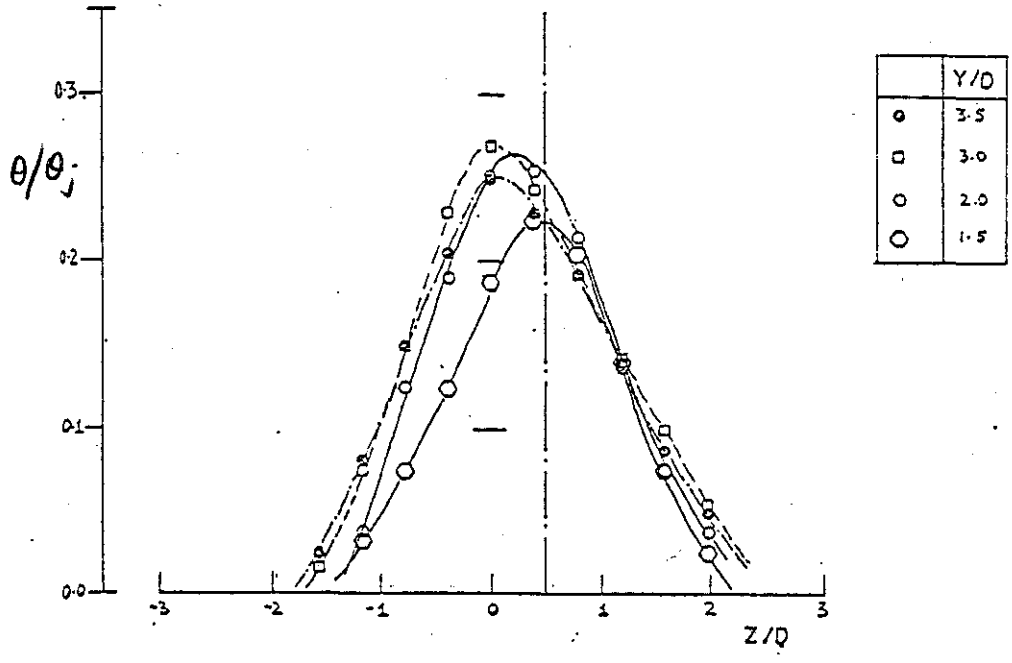


(a) E/D = 0



(b) E/D = 0.25

Figure 3.22 Concentration distributions at X/D = 6 for directly opposed jets with S/D = 2 and S/D = 2 and top central jet seeded only. (a) jets symmetric, (b) top central jet E/D = 0.25, (c) top central jet E/D = 0.5



(c) E/D = 0.5

Figure 3.22 (concluded)

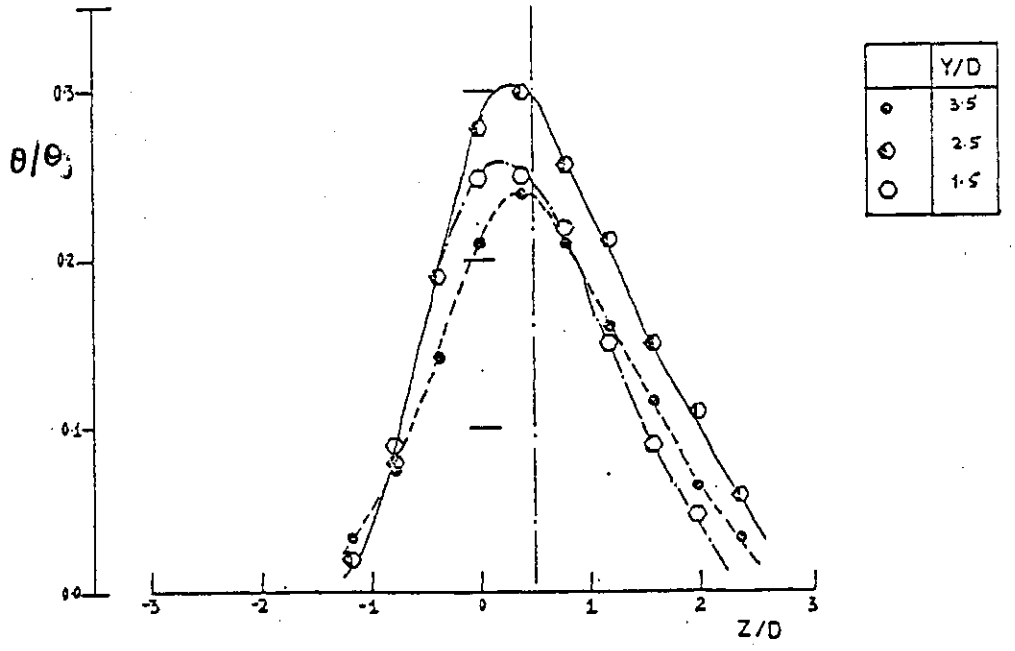


Figure 3.23: Concentration distributions for opposed rows of jets with S/D of 2 and floor jets laterally staggered by Z/D = 1. Top central jet eccentricity E/D = 0.5 (top central jet seeded only)

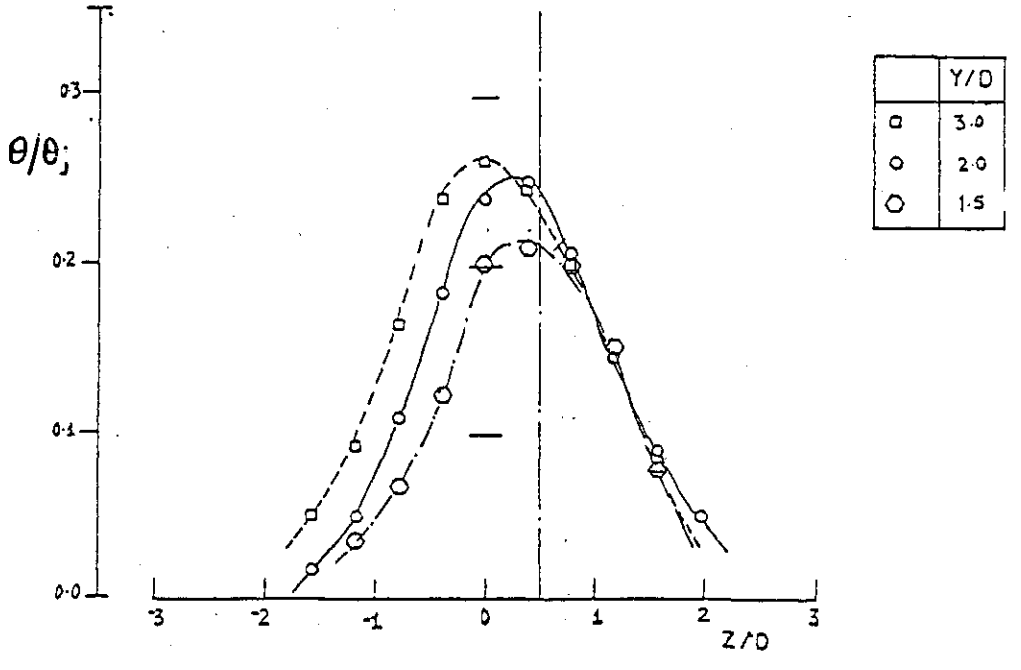
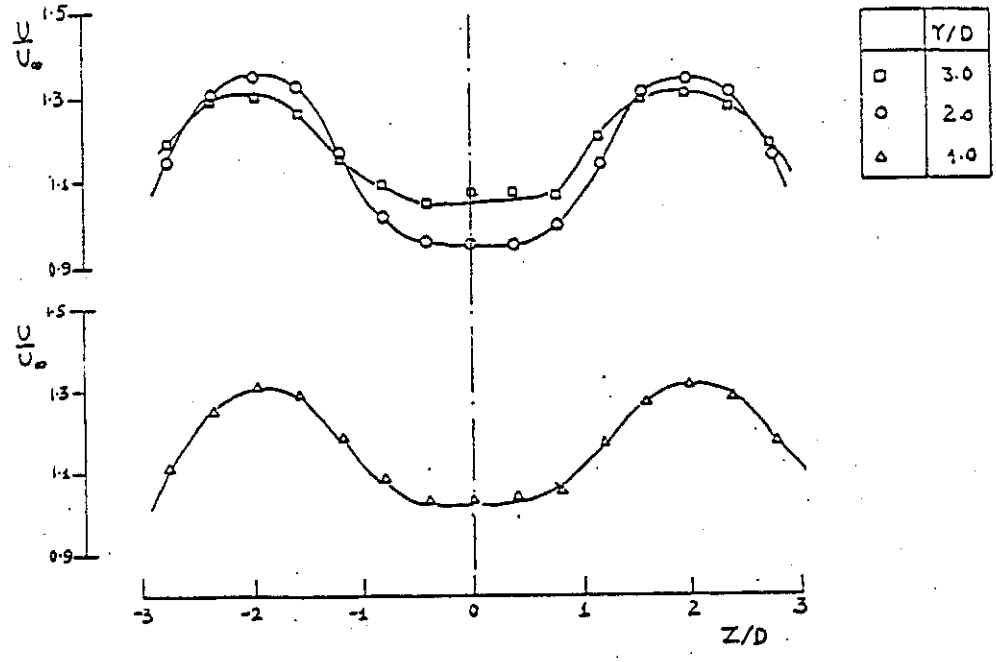
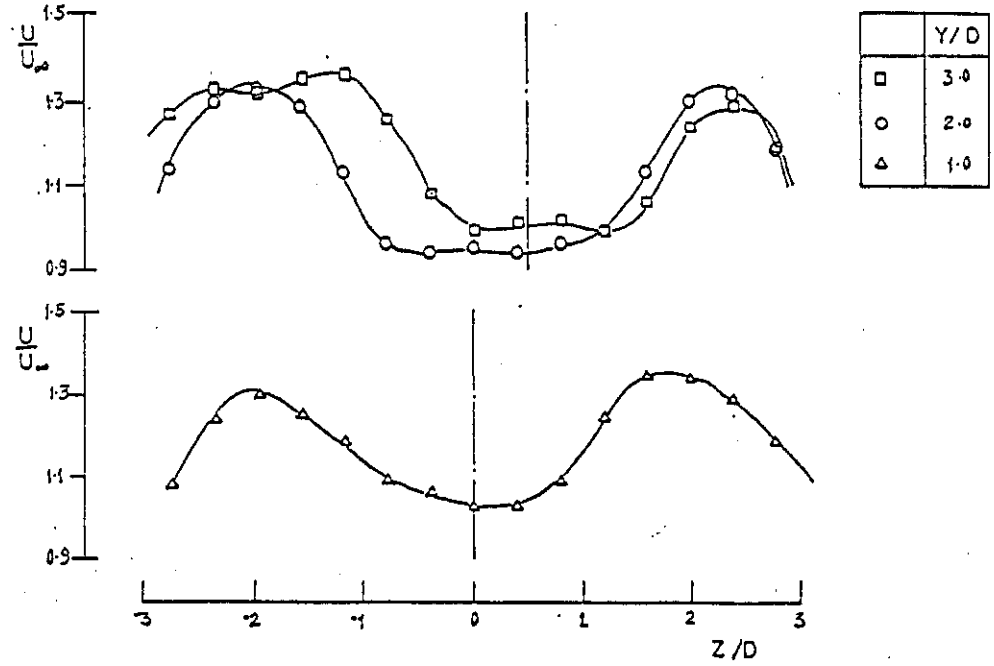


Figure 3.24: Concentration distributions for opposed rows of jets with S/D = 2 and ceiling jets staggered axially by X/D = 1. Top central jet eccentricity E/D = 0.5 (top central jet seeded only)

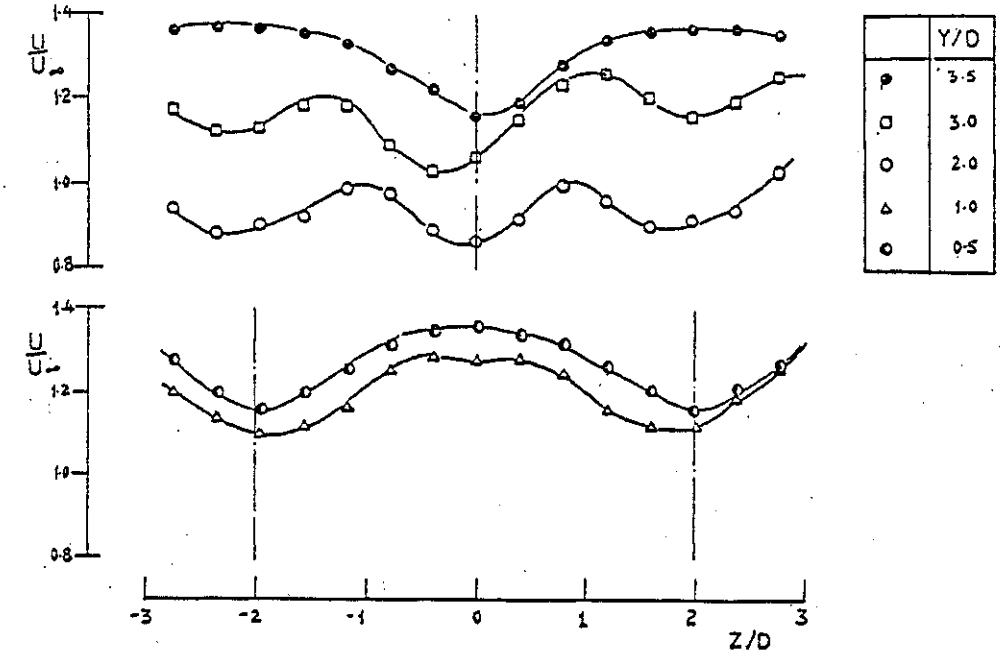


(a) E/D = 0

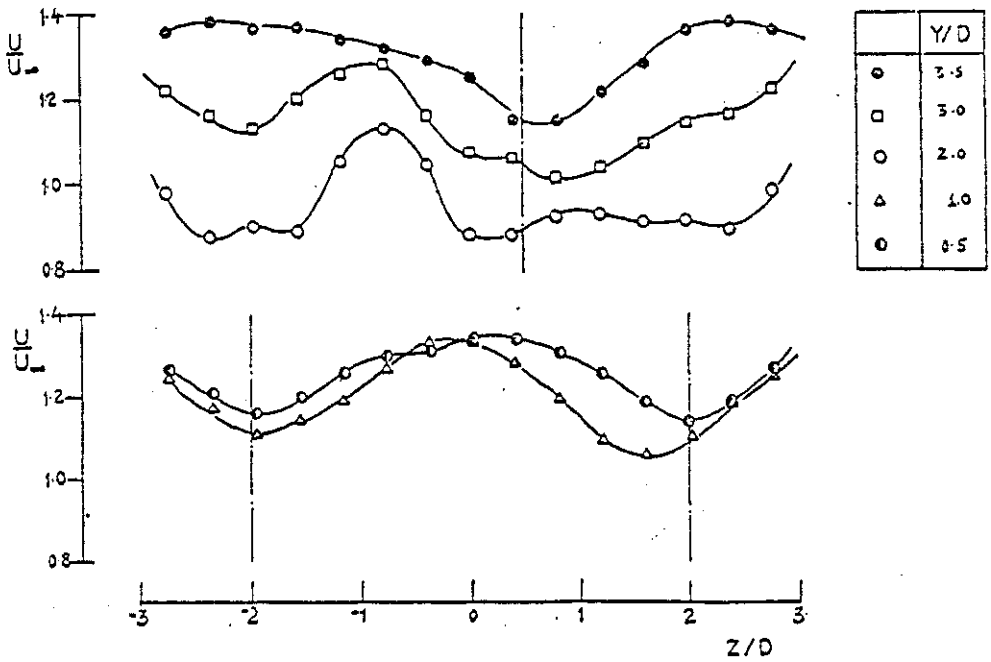


(b) E/D = 0.5

Figure 3.25: Velocity distributions at X/D = 6 for directly opposed rows of jets with S/D of 4. (a) Top central jet symmetric and (b) Top central jet eccentricity E/D = 0.5

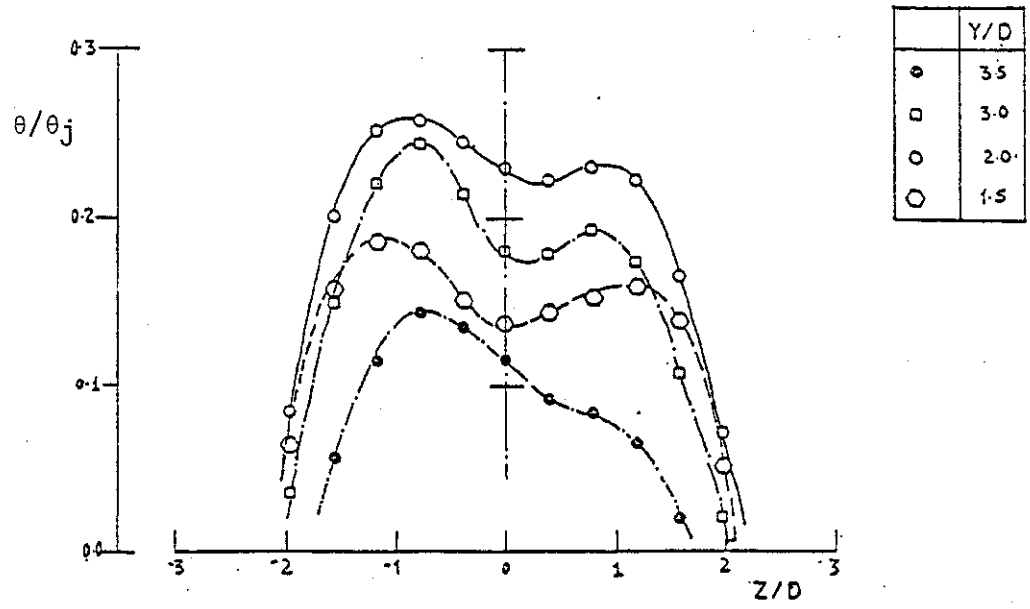


(a) E/D = 0

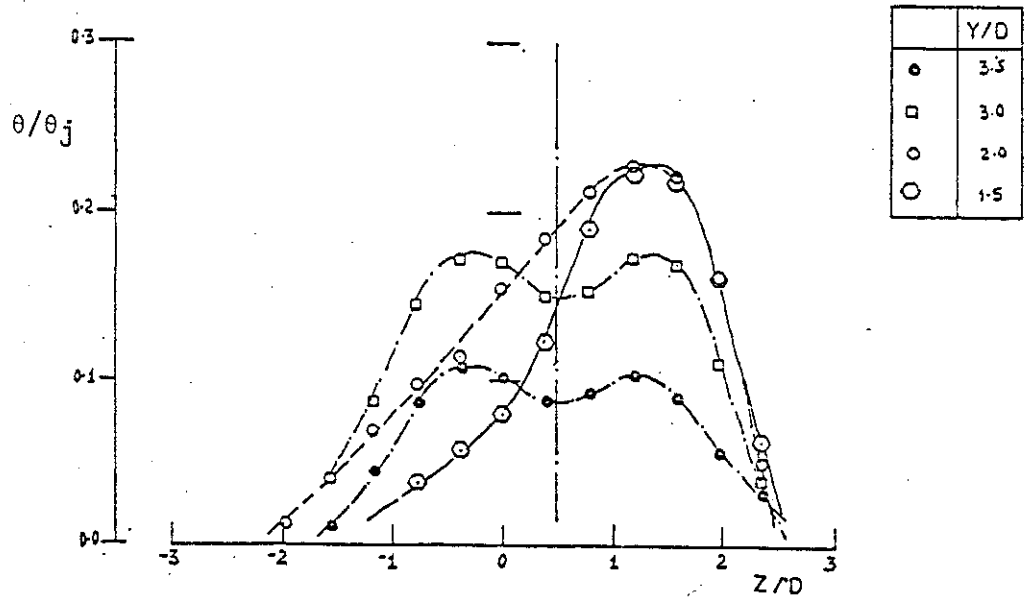


(b) E/D = 0.5

Figure 3.26: Velocity distributions at X/D = 6 for opposed rows of jets with S/D = 4 and floor jets staggered laterally by Z/D = 2. (a) Top central jet symmetric (b) Top central jet eccentricity E/D = 0.5

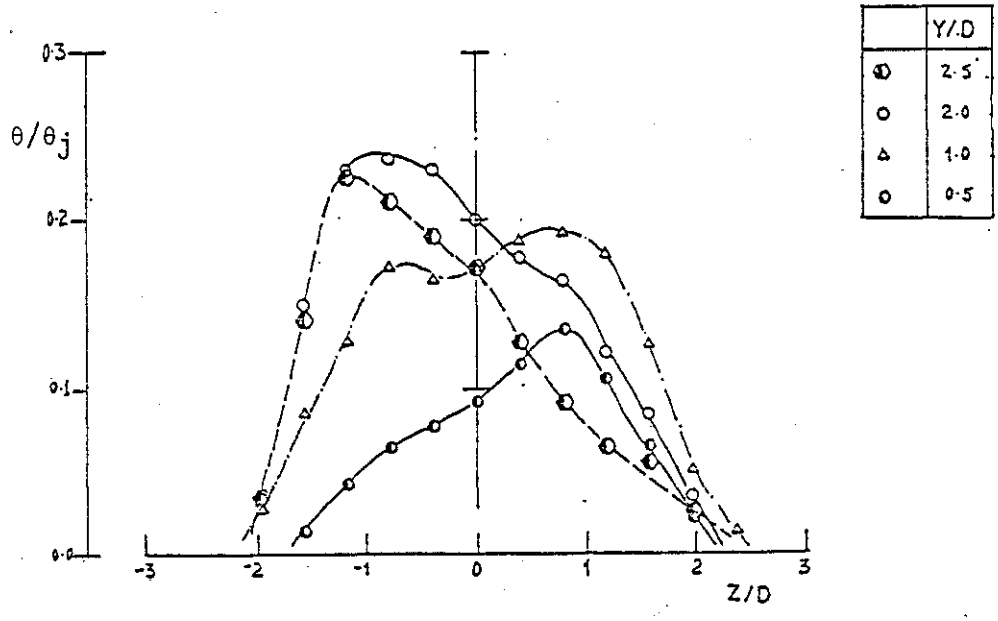


(a) E/D = 0 Top central jet seeded only



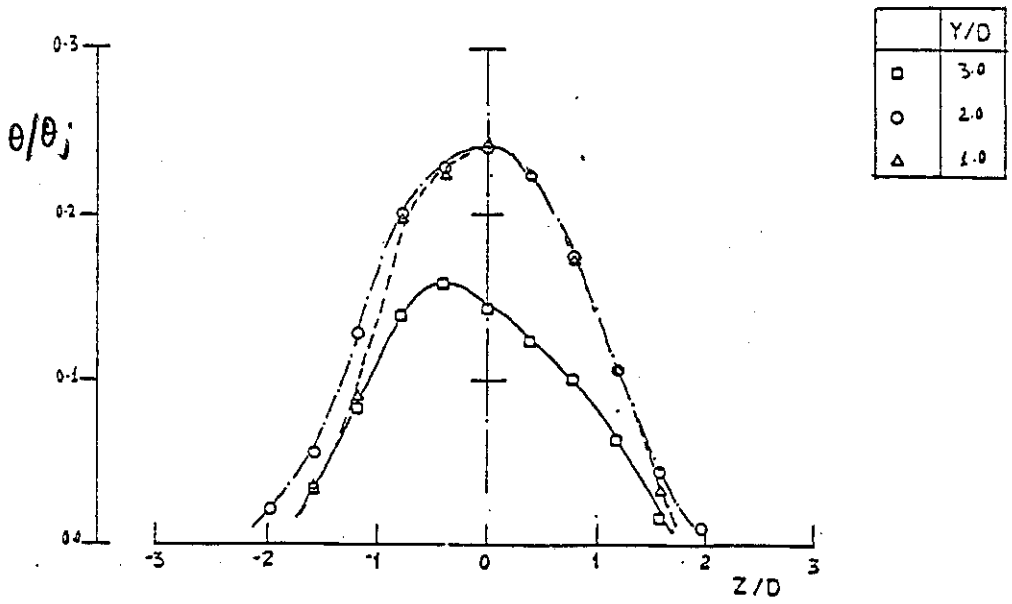
(b) E/D = 0.5 Top central jet seeded only

Figure 3.27 Concentration distributions at X/D = 6 for directly opposed rows of jets with S/D of 4. Top central jet symmetric and eccentric, E/D=0.5

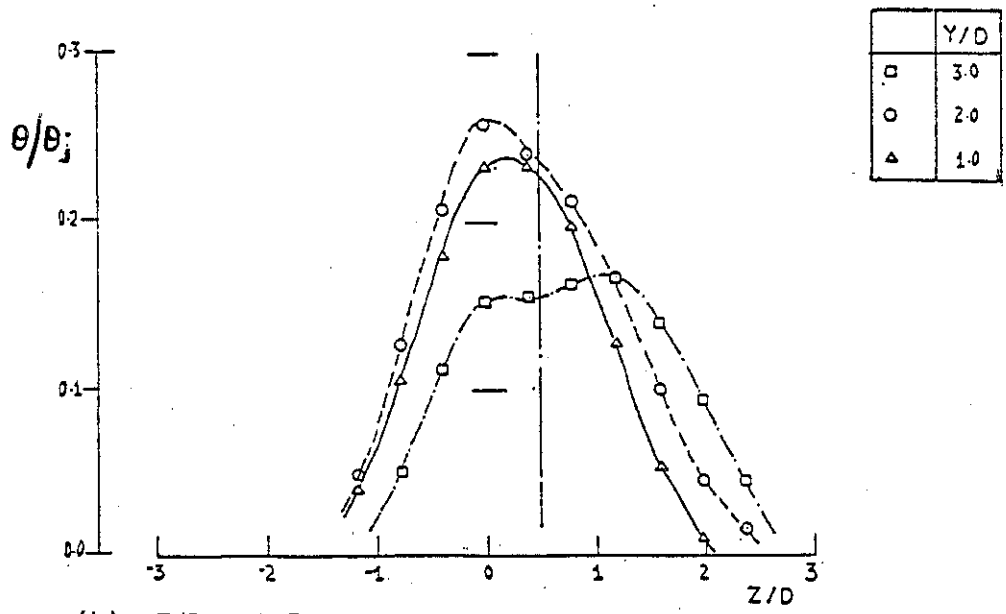


(c) Top central jet eccentricity E/D = 0.5
Floor central jet seeded only

Figure 3.27 (concluded)



(a) E/D = 0 Top central jet seeded only



(b) E/D = 0.5 Top cental jet seeded only

Figure 3.28 Concentration distributions at X/D = 6 for opposed rows of jets with S/D of 4 and floor jets staggered laterally by Z/D = 2.
(a) E/D = 0, (b) Top central jet eccentricity E/D = 0.5

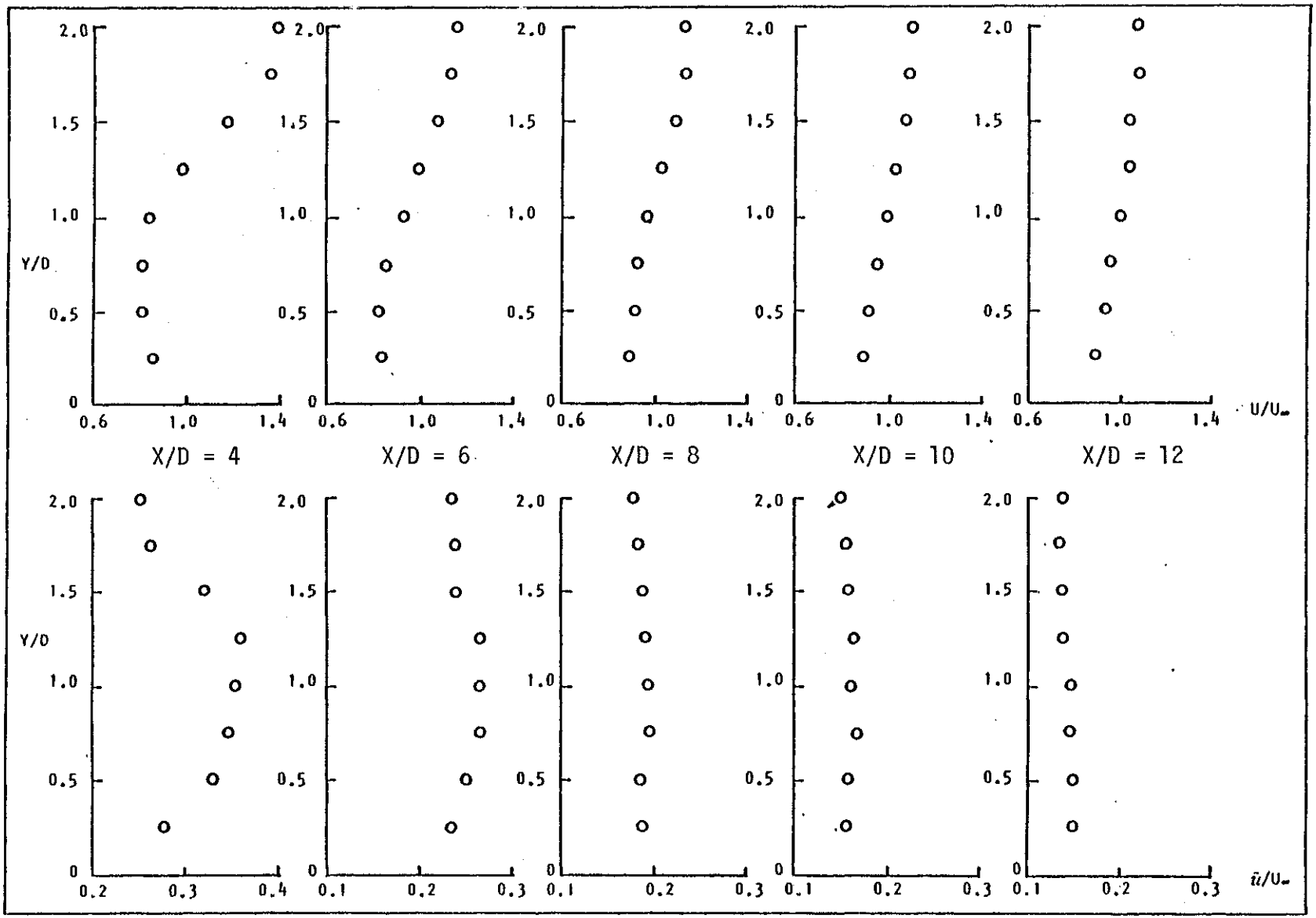


Figure 3.29 Axial mean velocity and turbulence intensity profiles along centre-plane for directly opposed jets with S/D of 2, H/D of 4 and V_j/U_∞ = 2.25

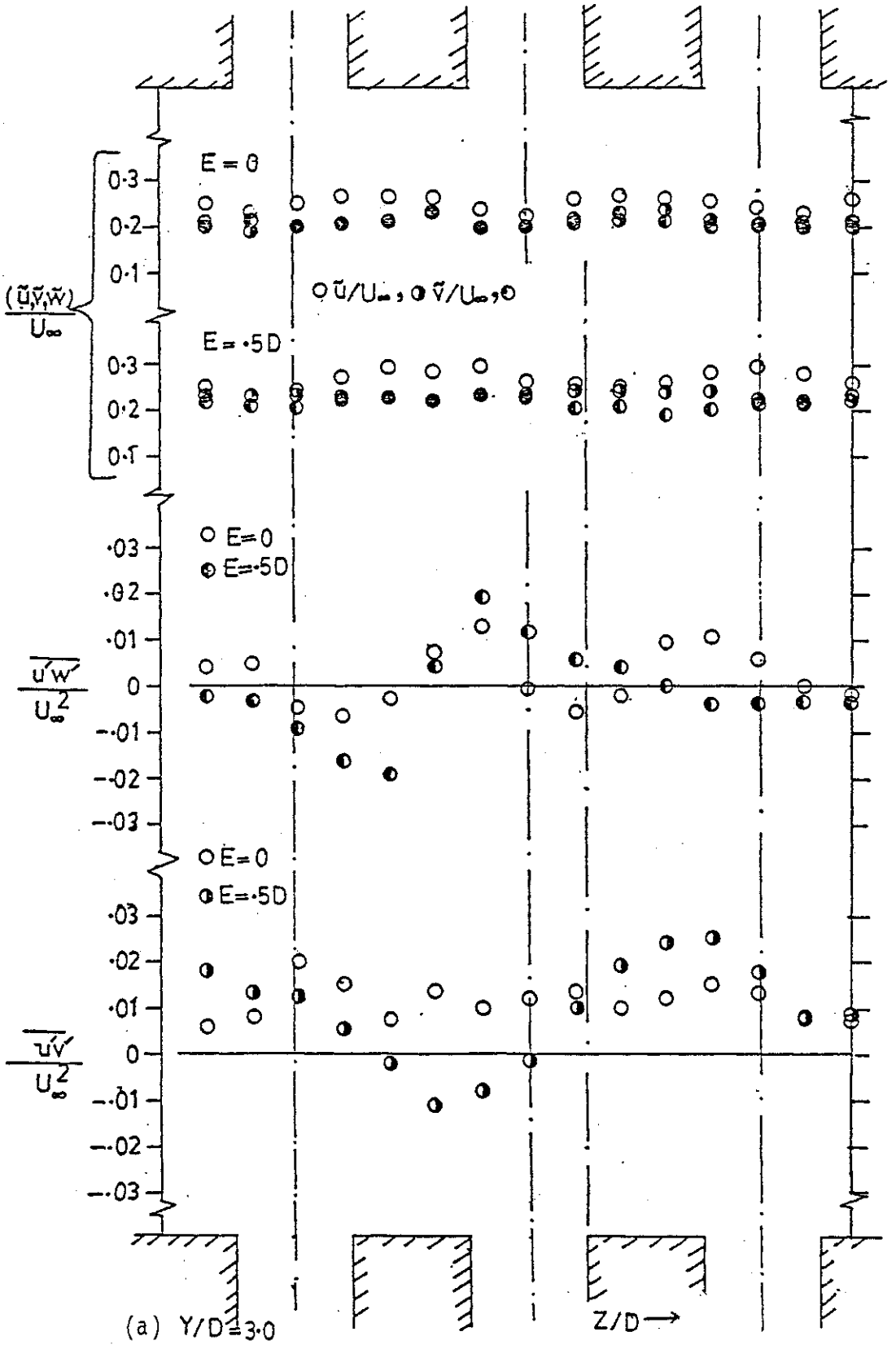


Figure 3.30: Normalised Reynolds-stress profiles at axial plane X/D = 6 for directly opposed jets and with top central jet eccentricity E = 0.5D for S/D of 2: V_j/U_∞ = 2.3 (a) Y/D = 3.0, (b) Y/D = 2.0 (c), Y/D = 3.0

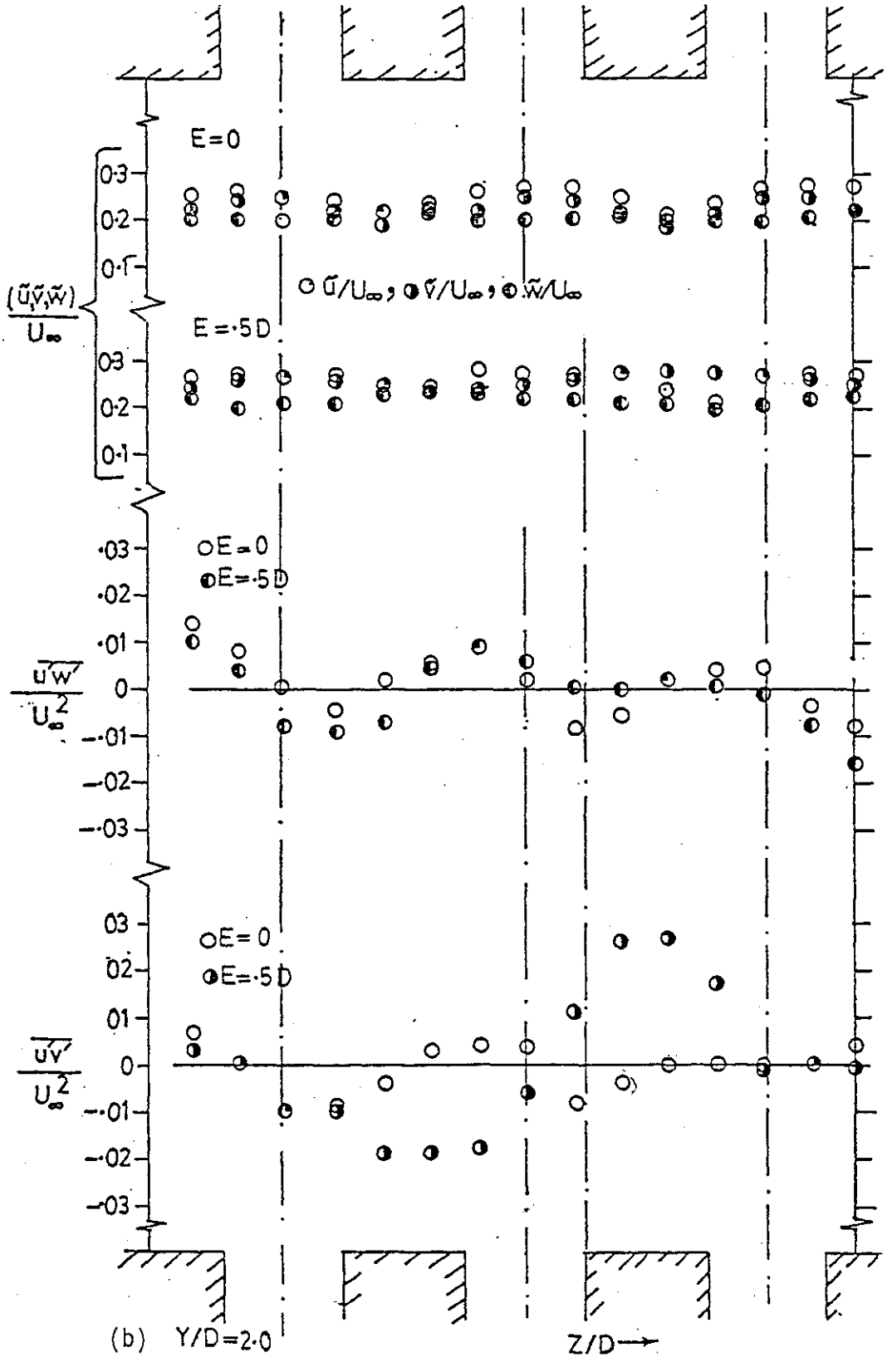


Figure 3.30 (continued)

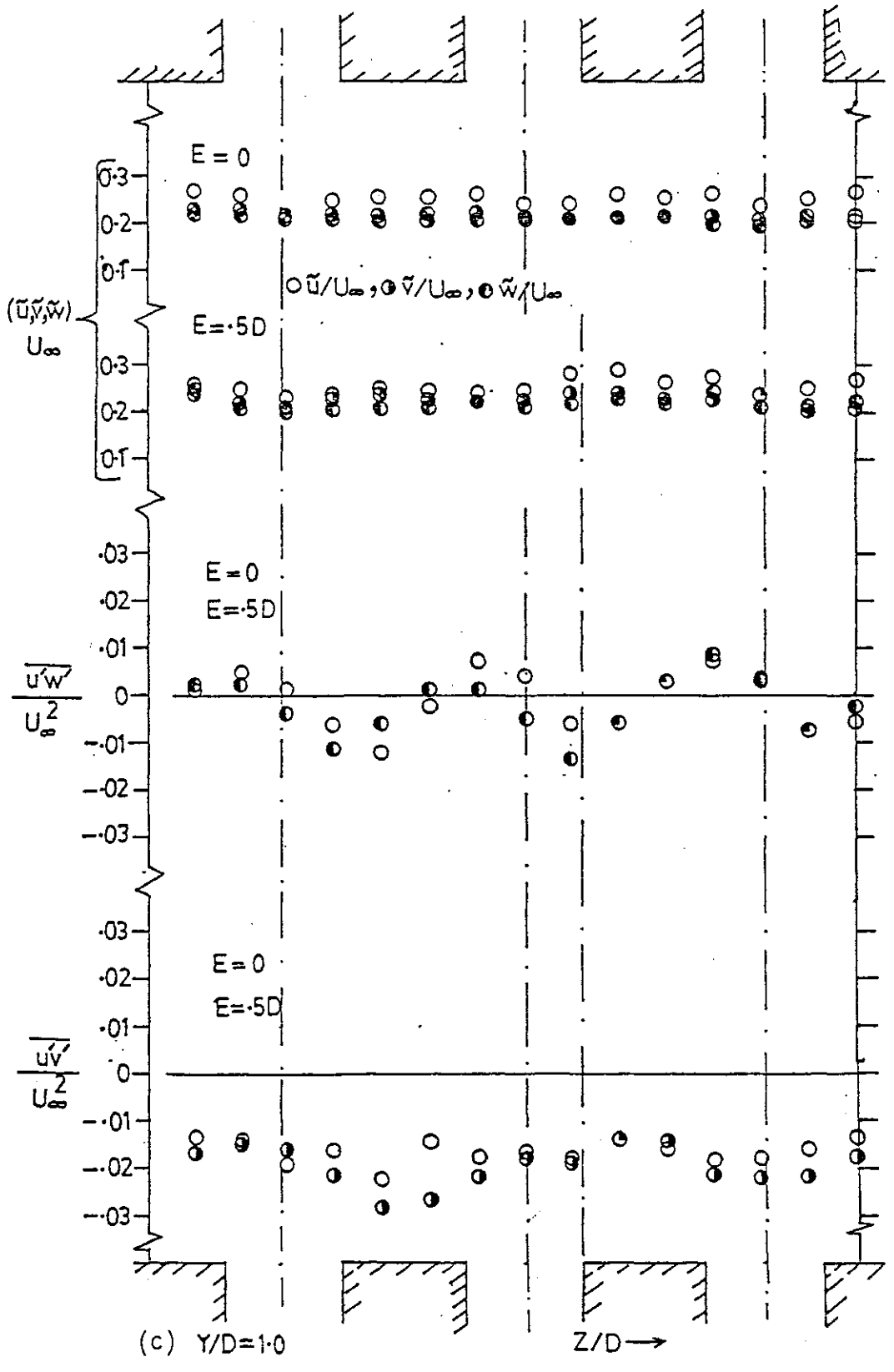


Figure 3.30 (concluded)

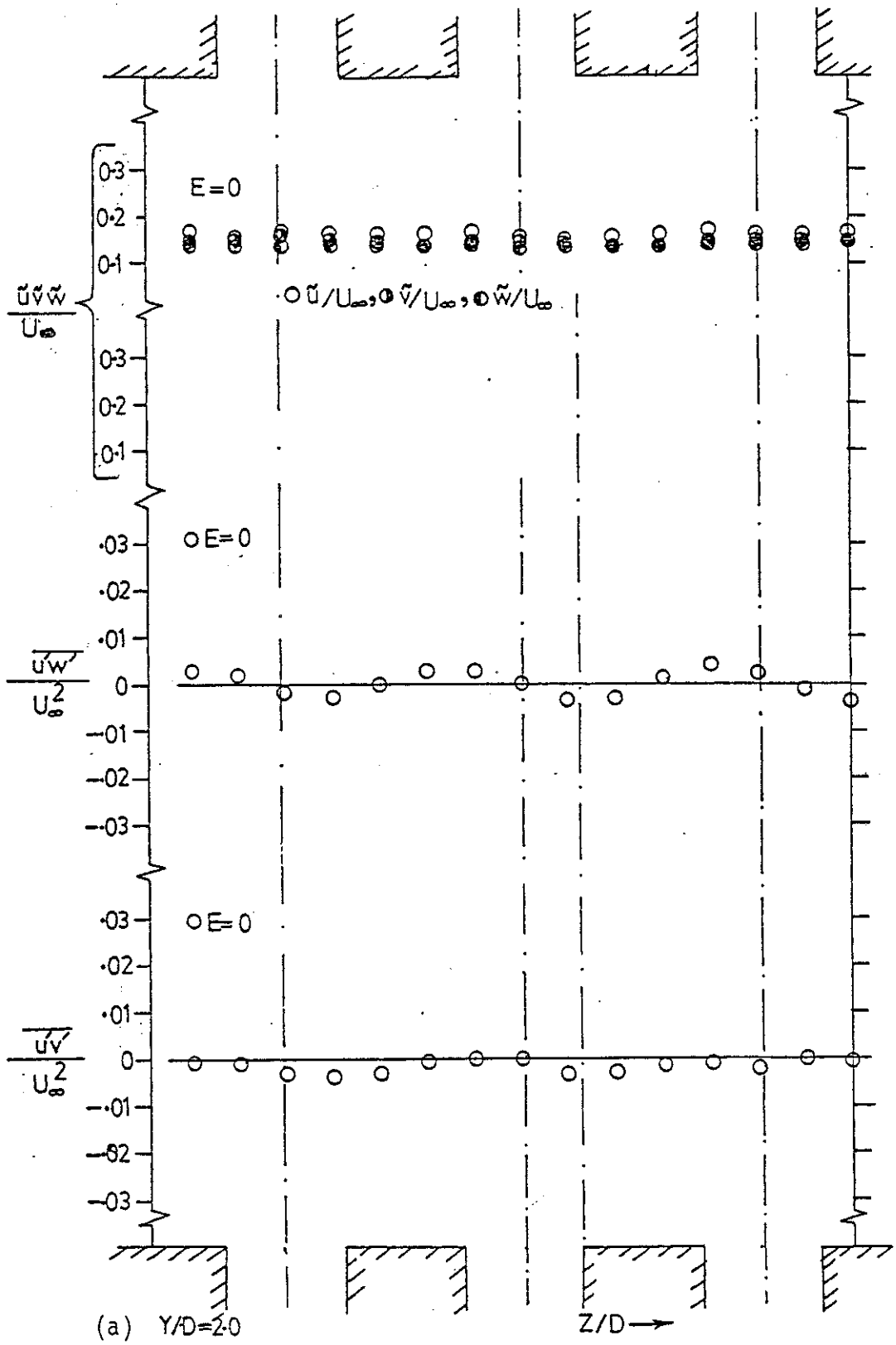


Figure 3.31: Normalised Reynolds-stress profiles at axial plane X/D = 10 for directly opposed jets and with top central eccentricity E/D = 0.5 for S/D of 2: V_j/U_∞ = 2.3 (a) Y/D = 2.0, (b) Y/D = 1.0, (c) Y/D = 0.5

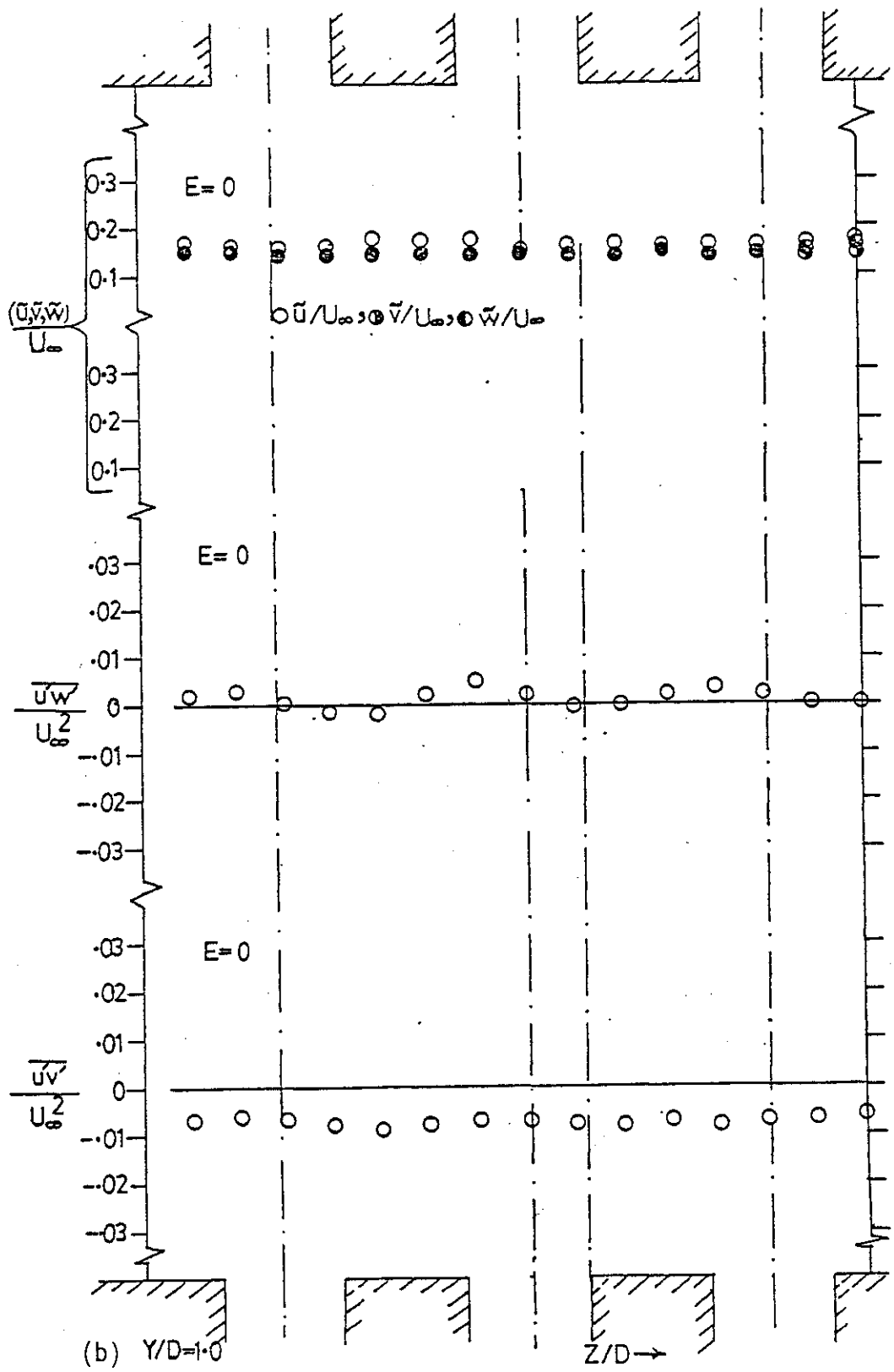


Figure 3.31 (continued)

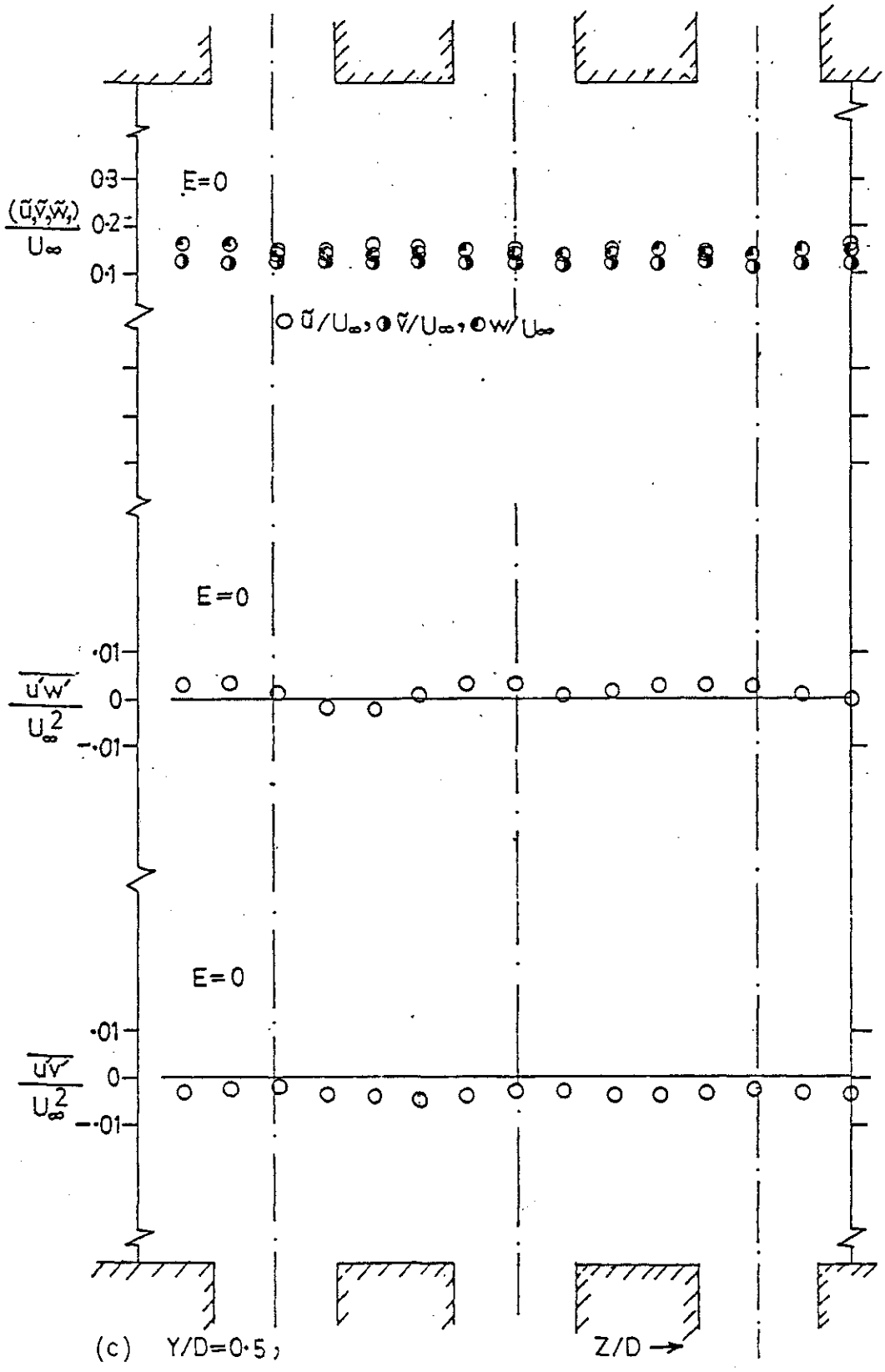


Figure 3.31 (concluded)

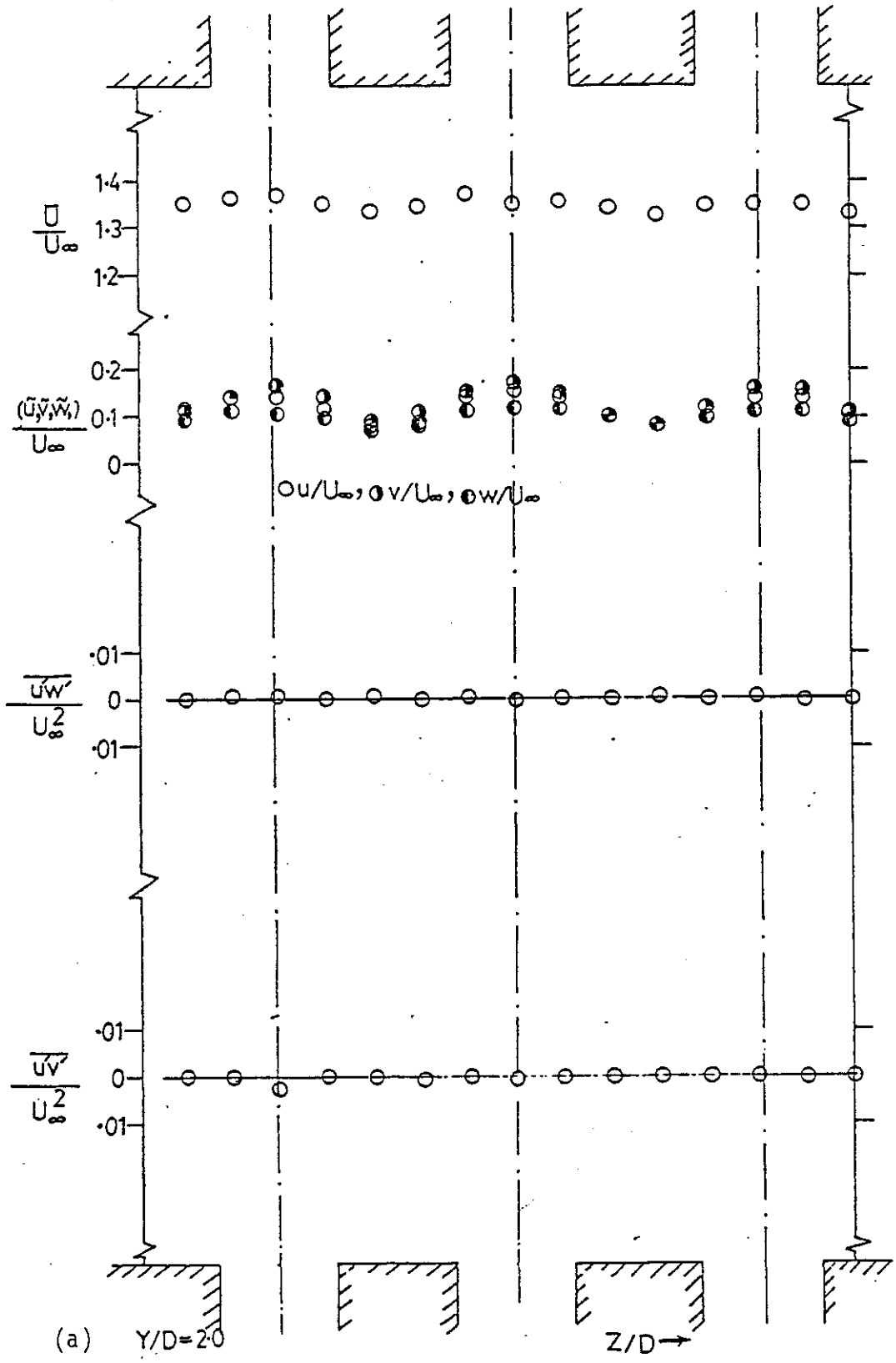


Figure 3.32: Normalised mean velocity and Reynolds-stress profiles at axial plane X/D = 6 for directly opposed jets with S/D of 2 and V_j/U_∞=1.5 (a) Y/D = 2.0, (b) Y/D = 1.0, (c) Y/D = 0.5

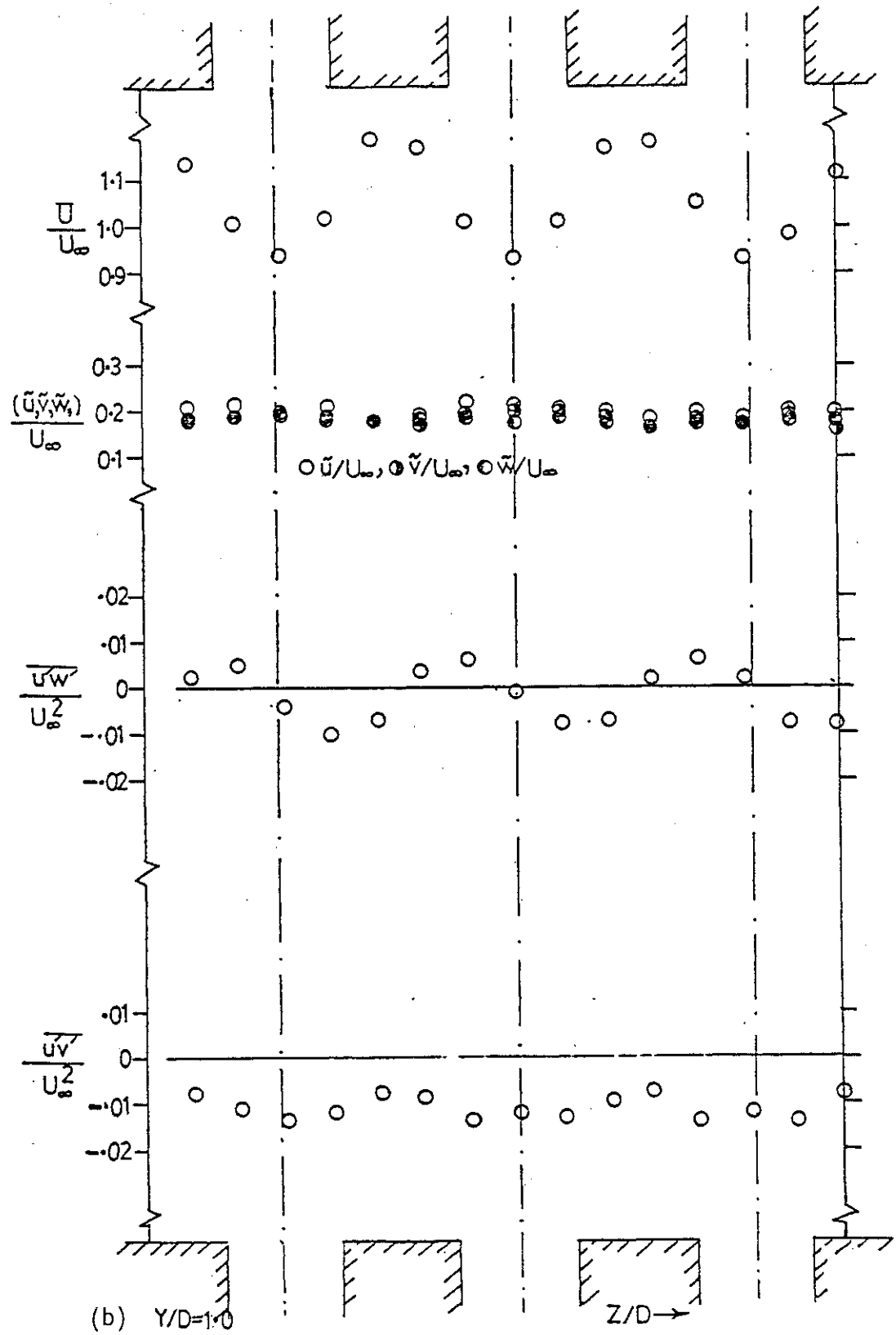


Figure 3.32 (continued)

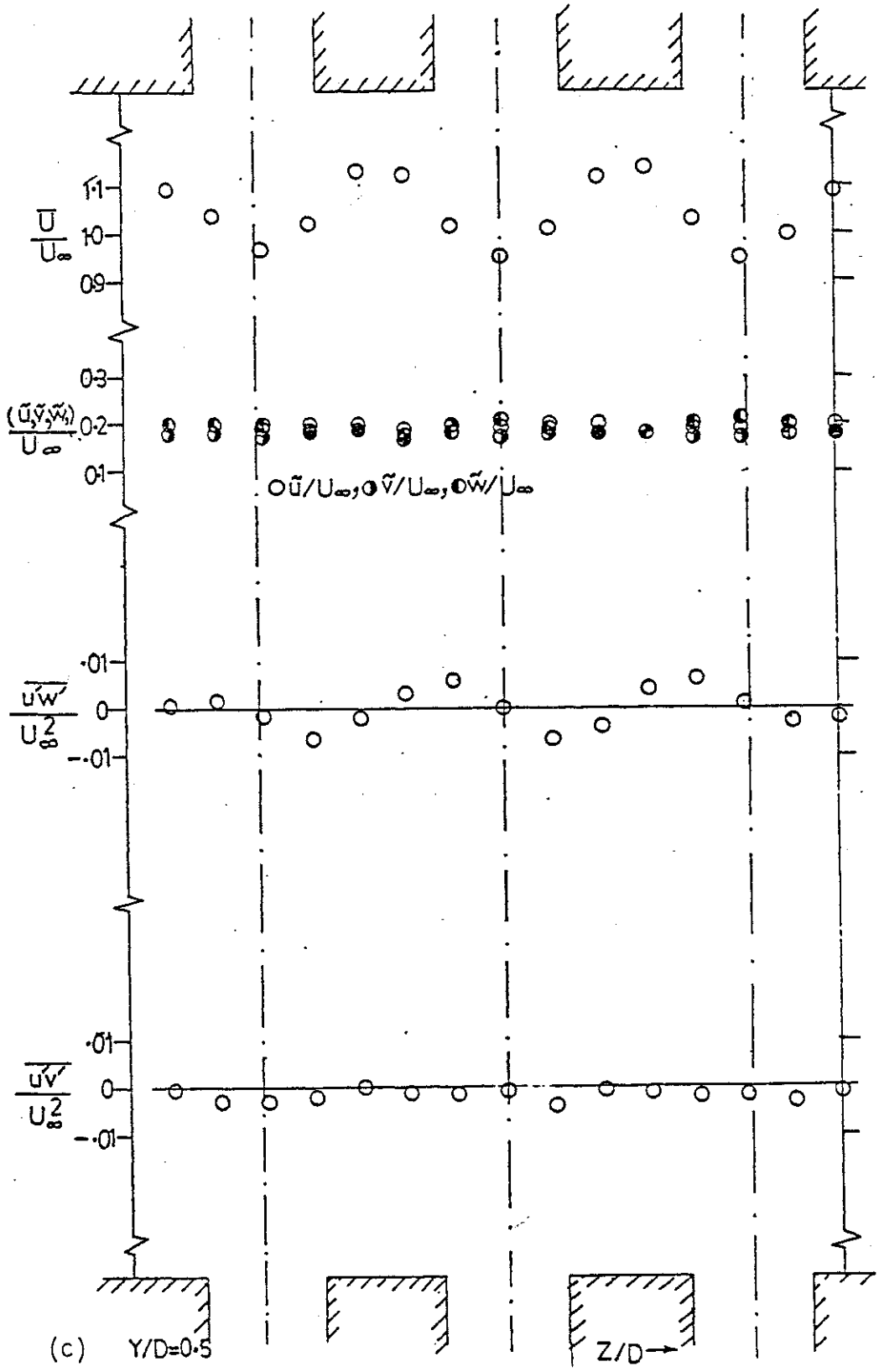


Figure 3.32 (concluded)

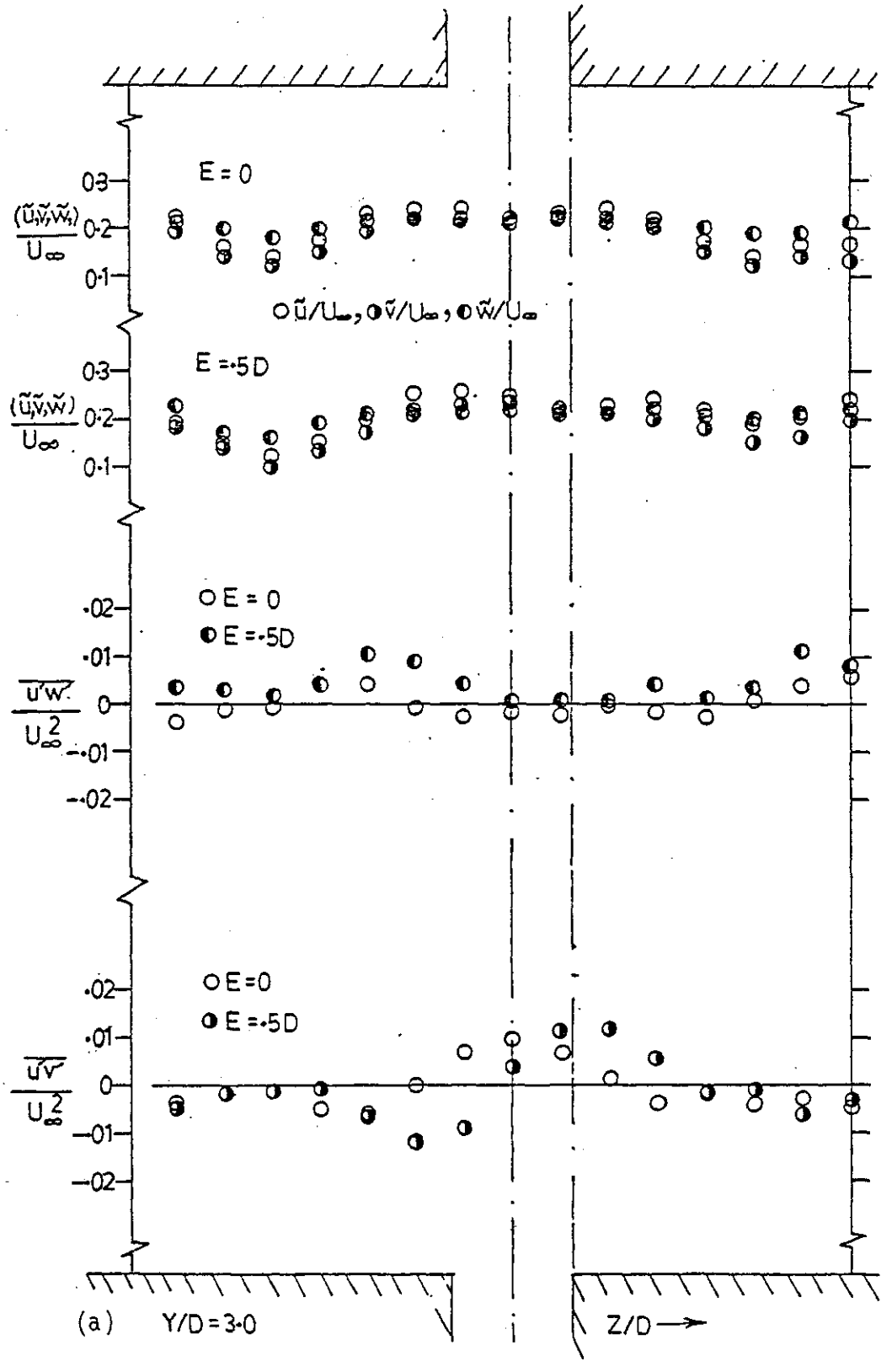


Figure 3.33: Normalised Reynolds-stress profiles at axial plane X/D = 6 for directly opposed jets and with top central jet eccentricity E/D = 0.5 for S/d of 4: V_j/U_∞ = 2.3 (a) Y/D = 3.0, (b) Y/D = 2.0

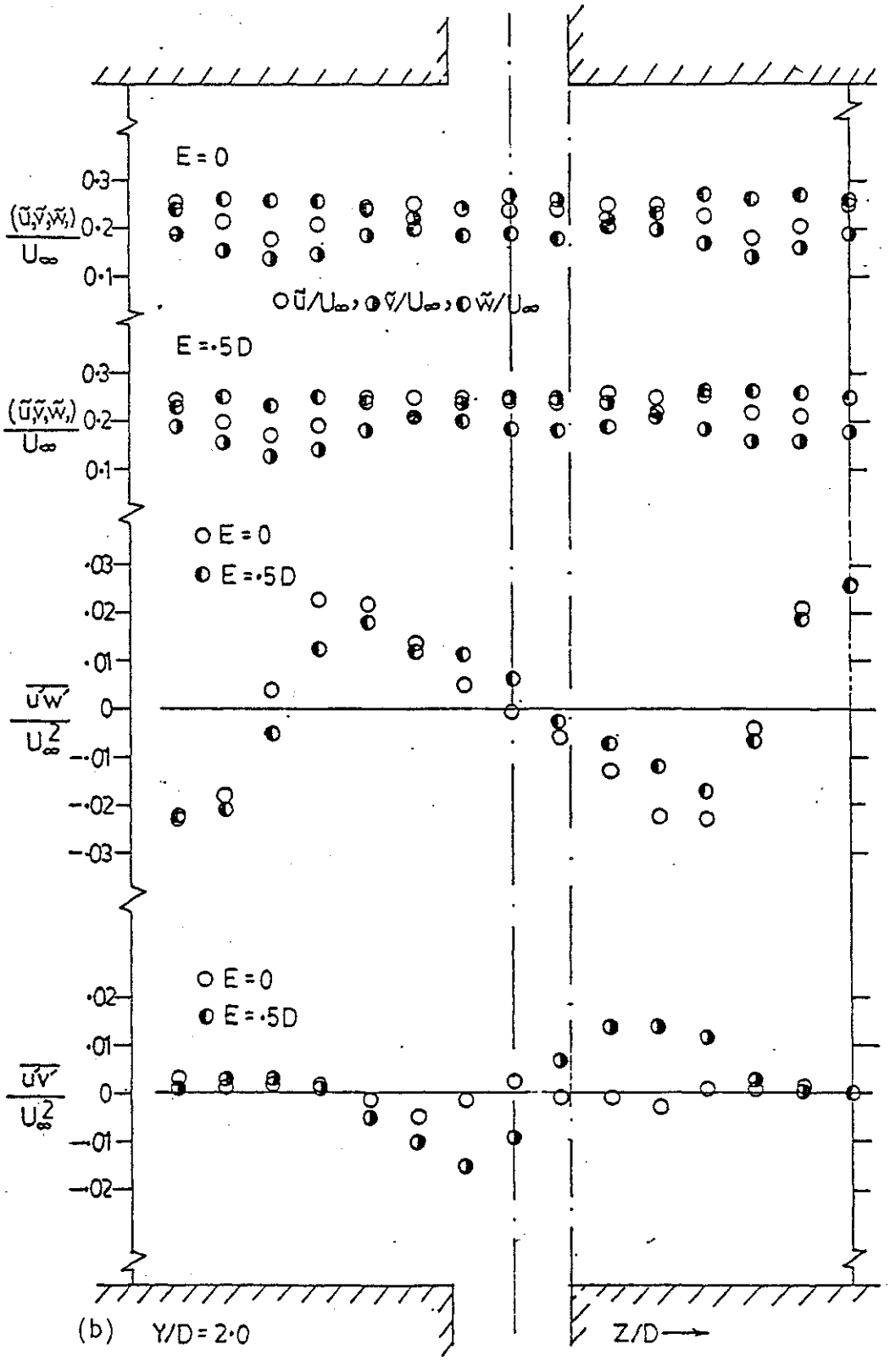


Figure 3.33 (concluded)

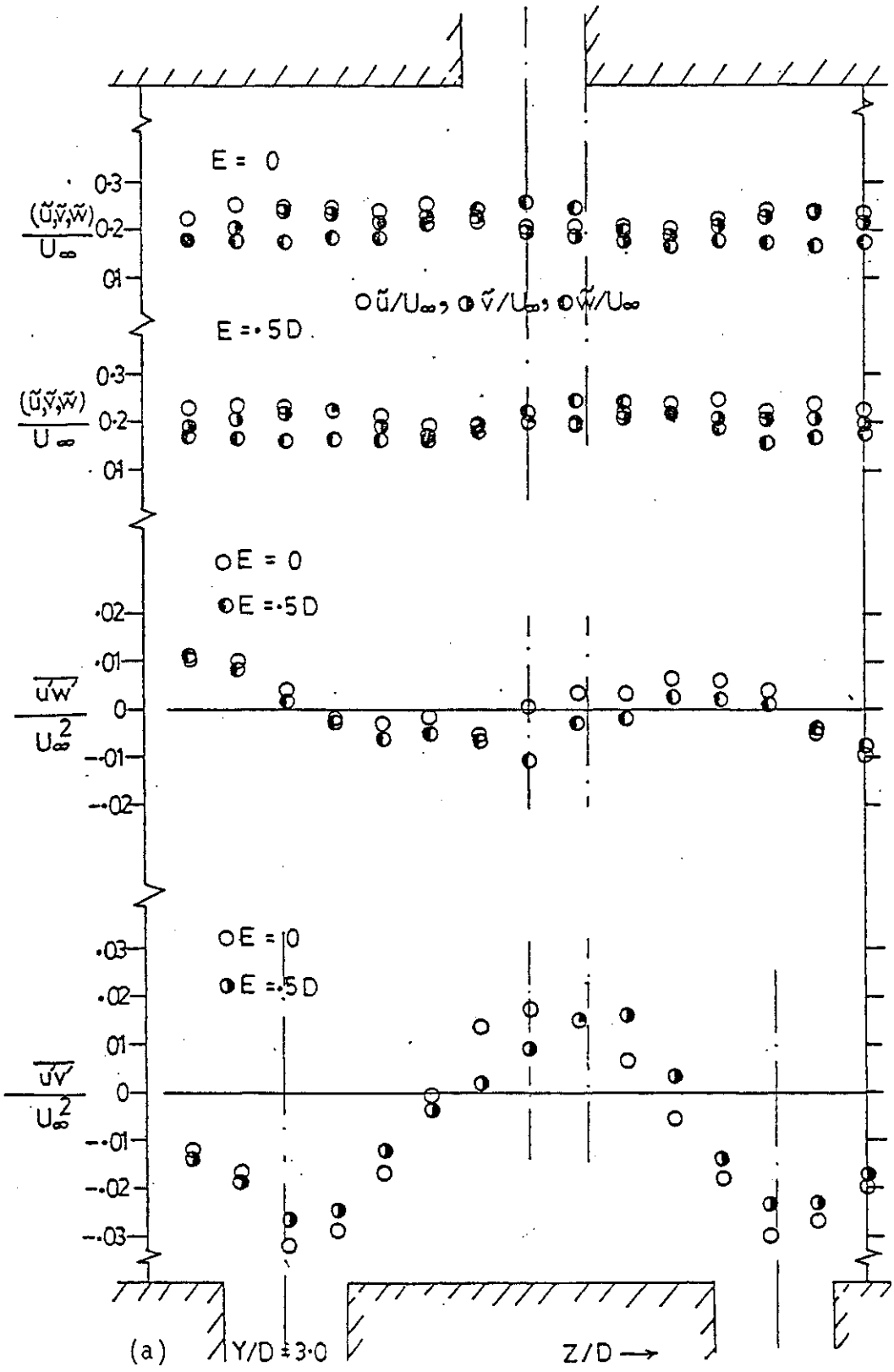


Figure 3.34: Normalised Reynolds-stress profiles at axial plane X/D = 6 for opposing row of jets with floor jets staggered laterally by Z/D = 2 and top central jet eccentricity E/D = 0.5 for S/D of 4: V_j/U_∞ = 2.3
(a) Y/D = 3.0, (b) Y/D = 2.0, (c) Y/D = 1.0

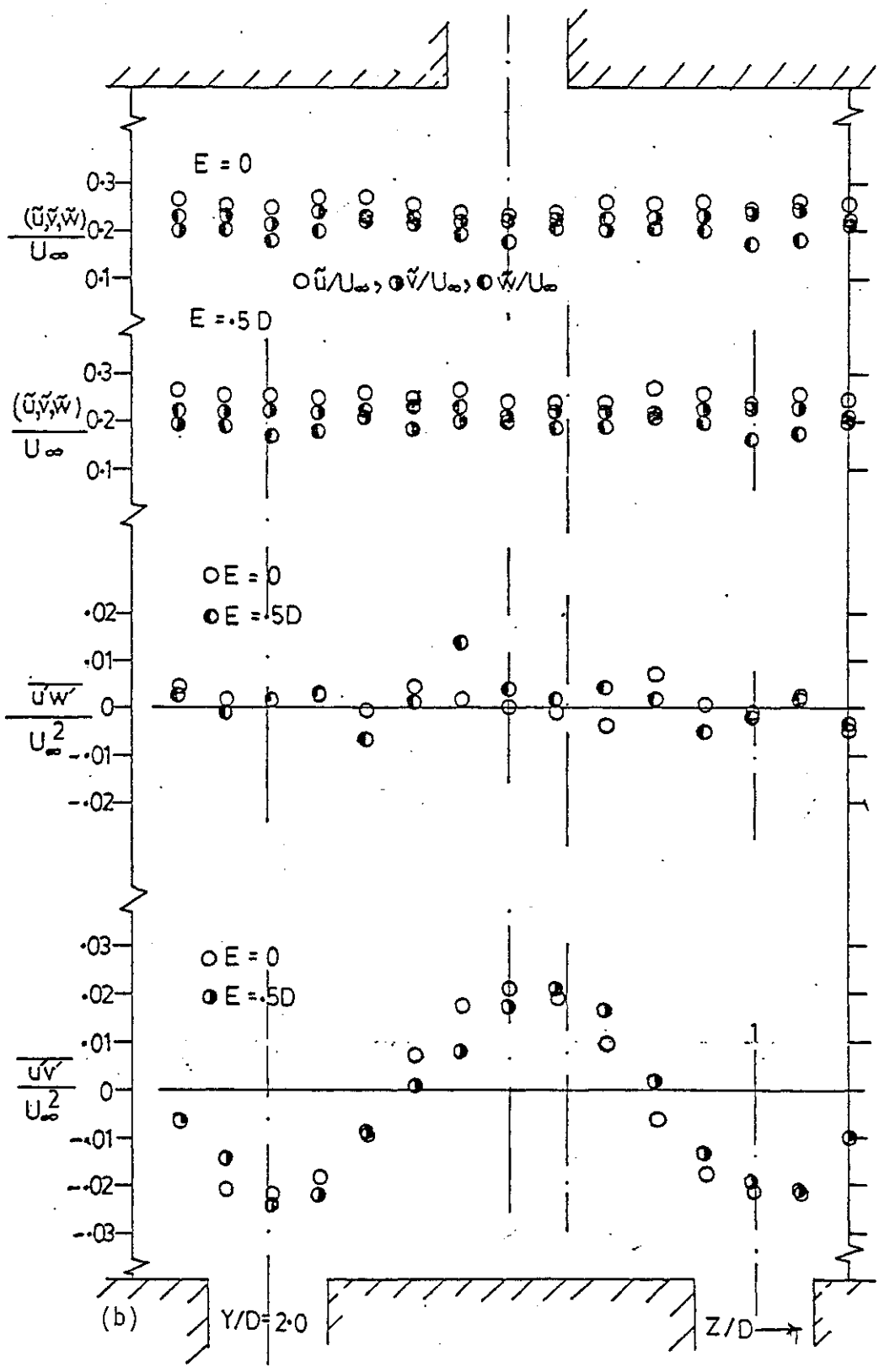


Figure 3.34 (continued)

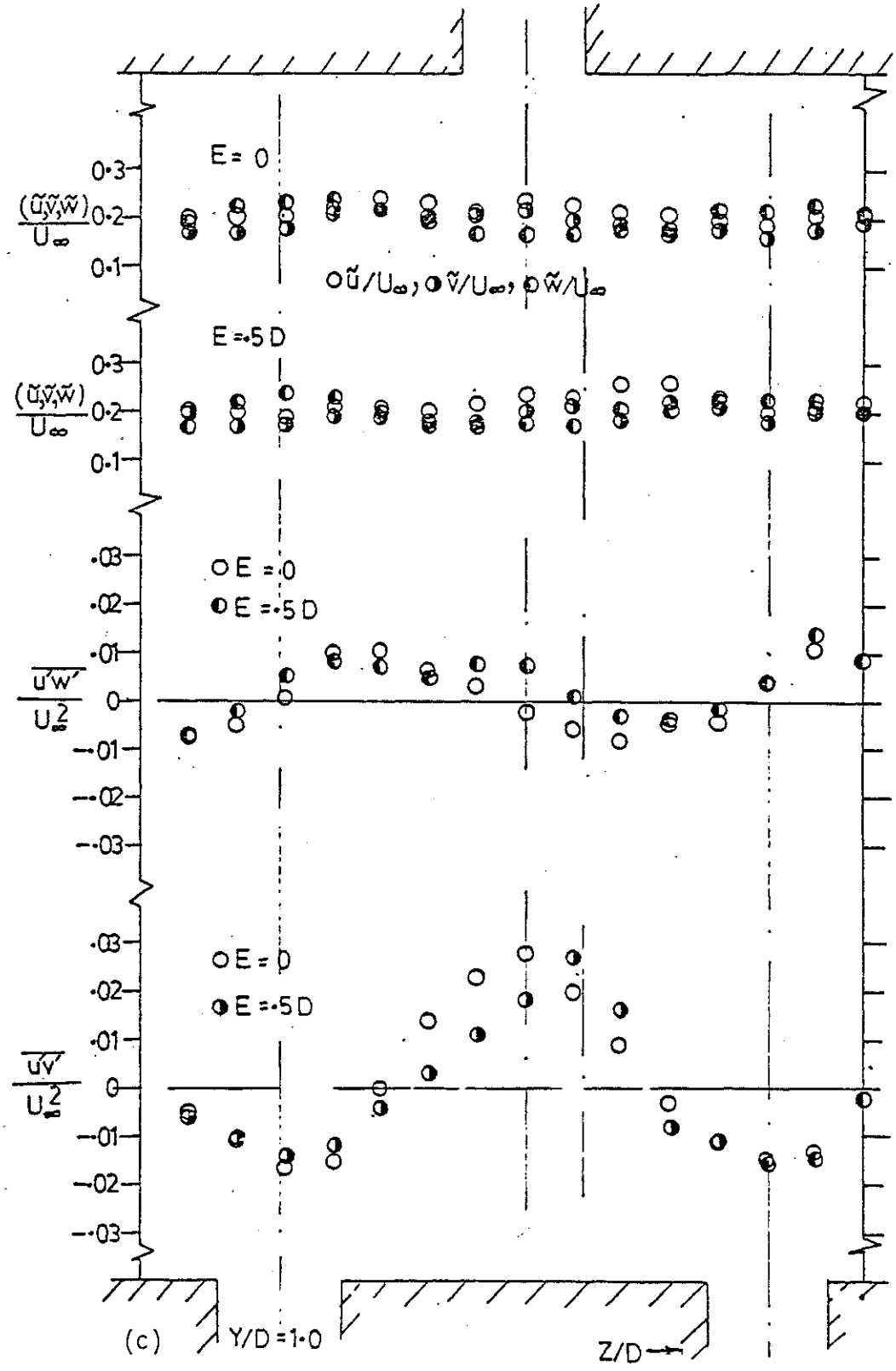
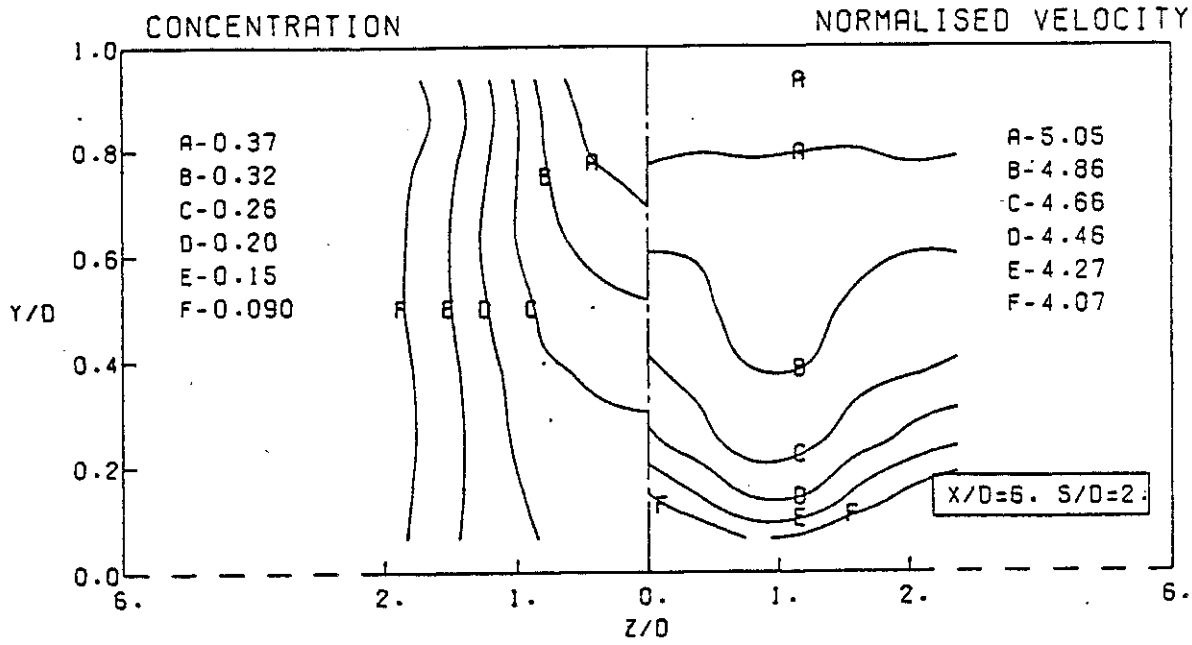
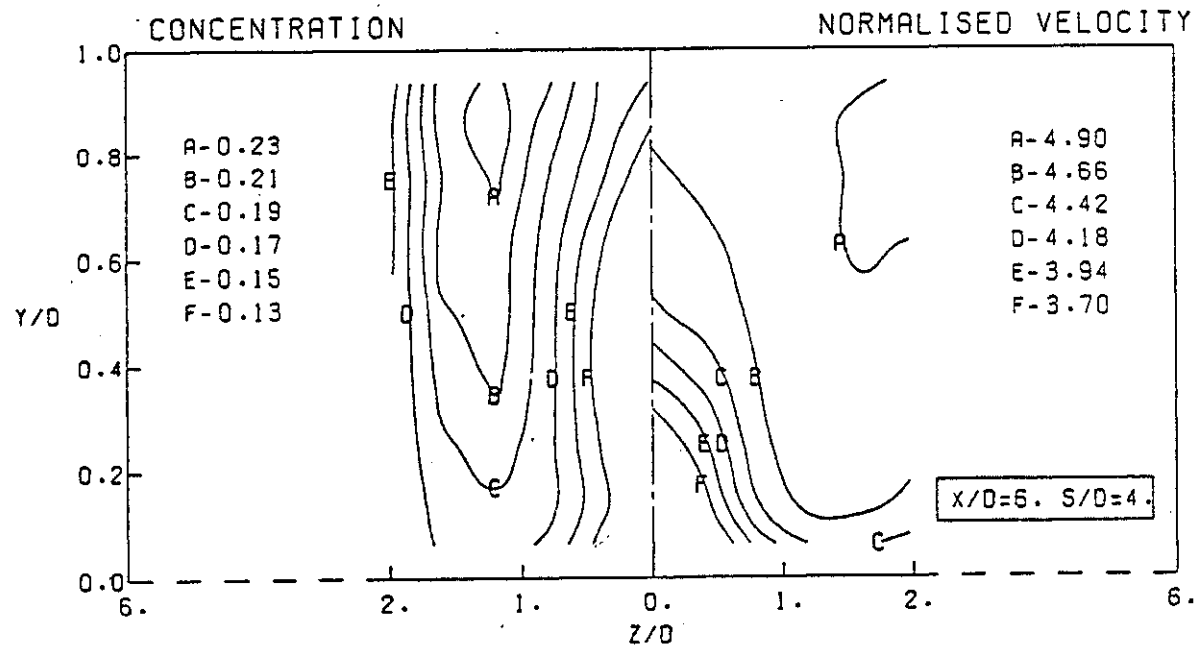


Figure 3.34 (concluded)

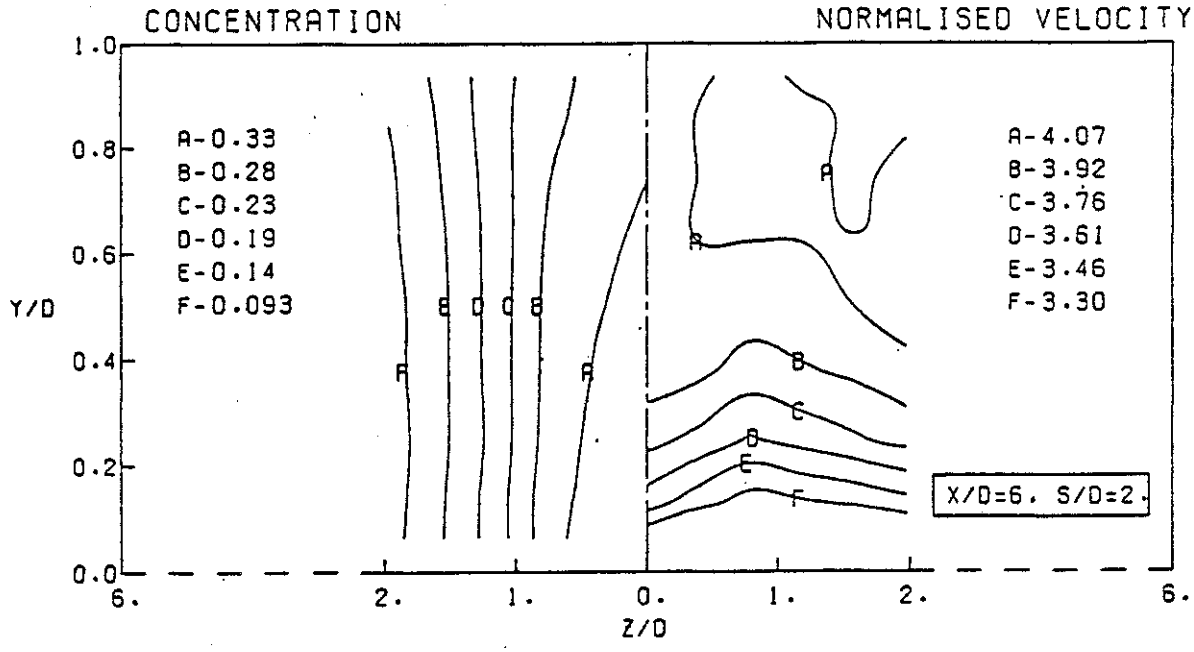


(a) S/D = 2

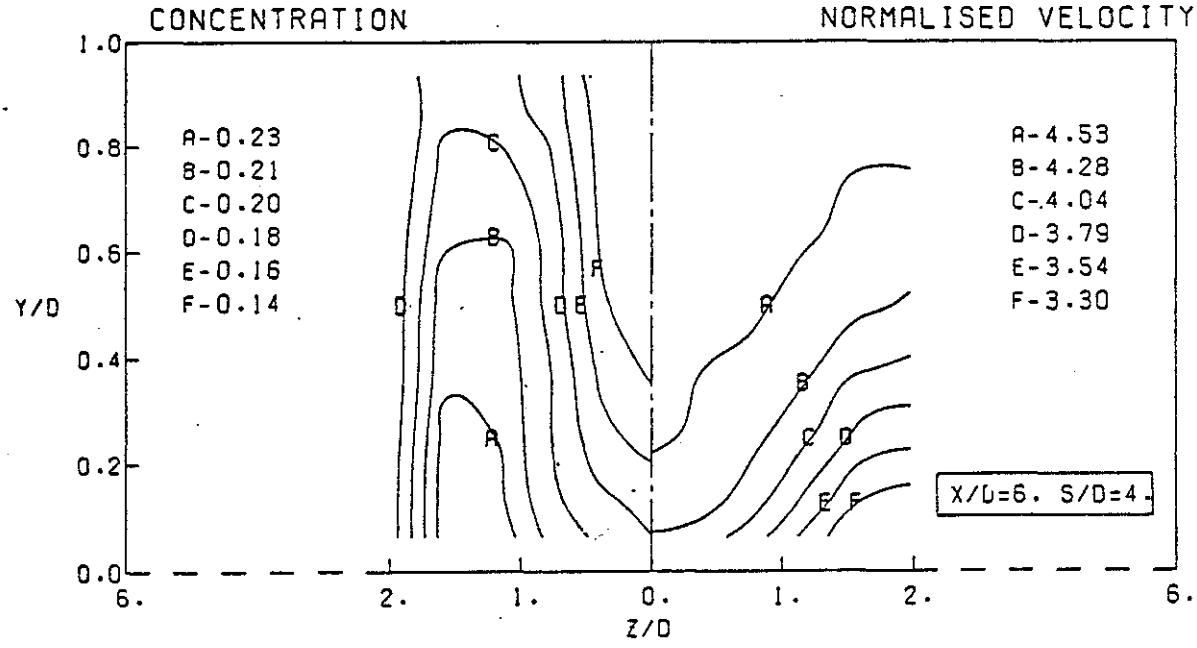


(b) S/D = 4

Figure 3.35: Normalised mean velocity and concentration contours at X/D = 6 for pitch-to-diameter ratios (S/D) of 2 and 4 and a downstream contraction with only floor jets blowing (floor central jet seeded only)

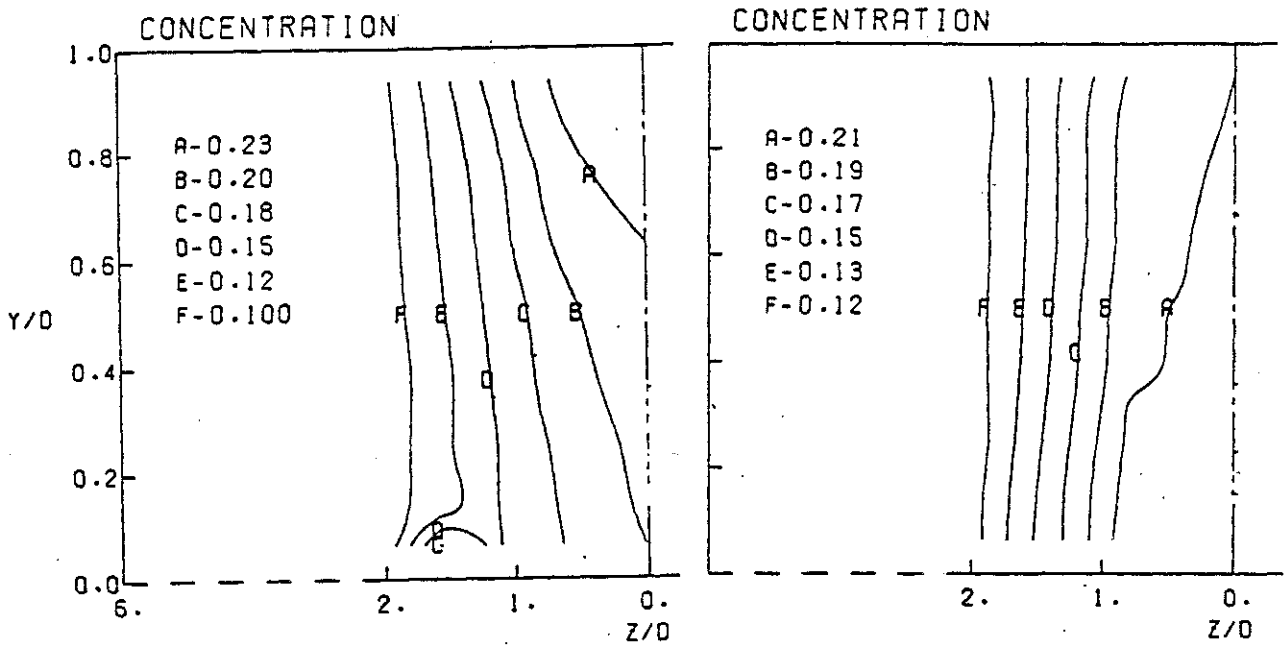


(a) S/D = 2

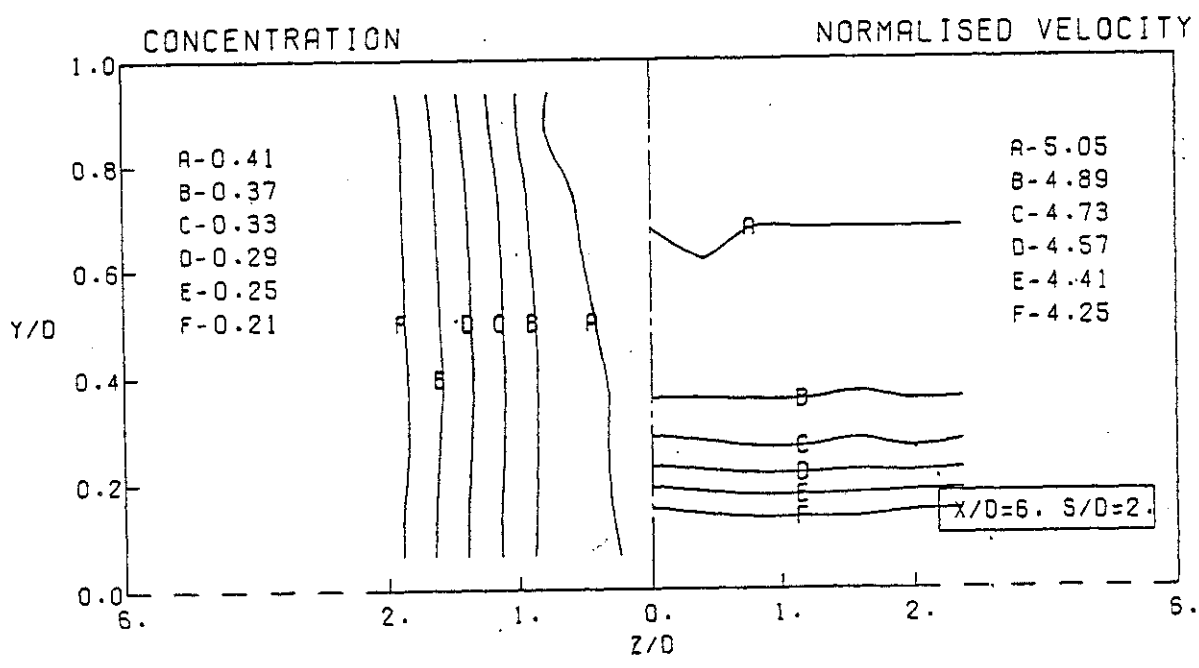


(b) S/D = 4

Figure 3.36: Normalised mean velocity and concentration contours at X/D = 6 for S/D of 2 and 4 and a downstream contraction with only ceiling jets blowing (top central jet seeded only)



(a) Central floor jet seeded only (b) Top central jet seeded only



(c) Addition of concentration contours of (a) and (b)

Figure 3.37: Normalised mean velocity and concentration contours at X/D = 6 for directly opposed jets with S/D of 2 and a downstream contraction

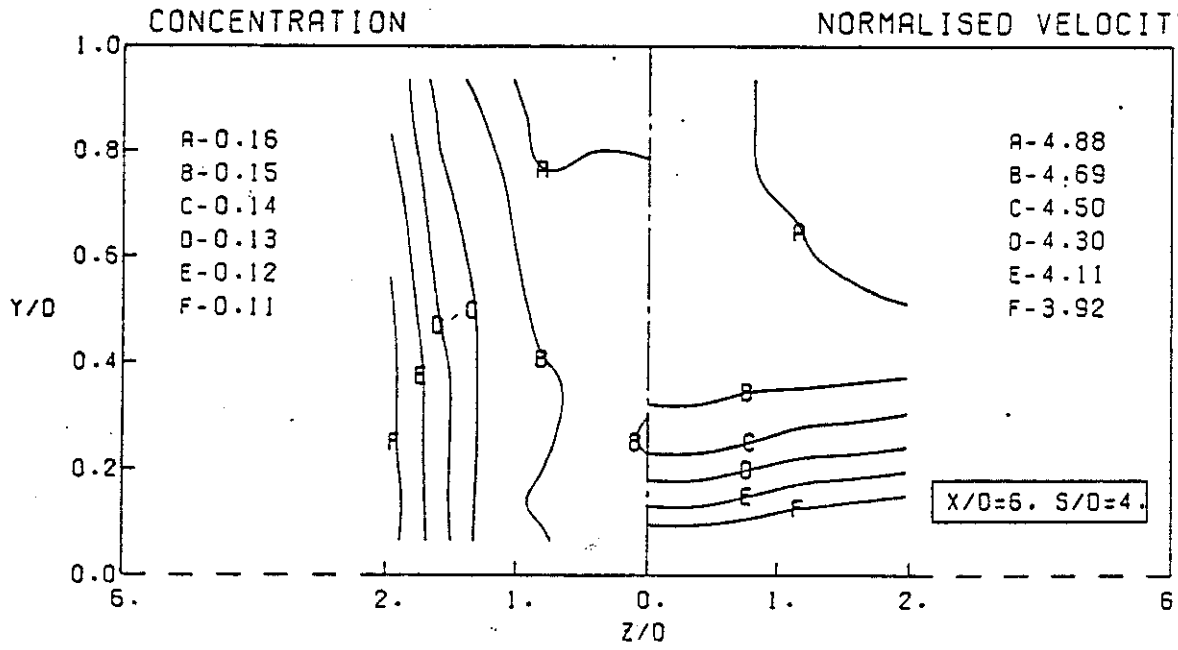
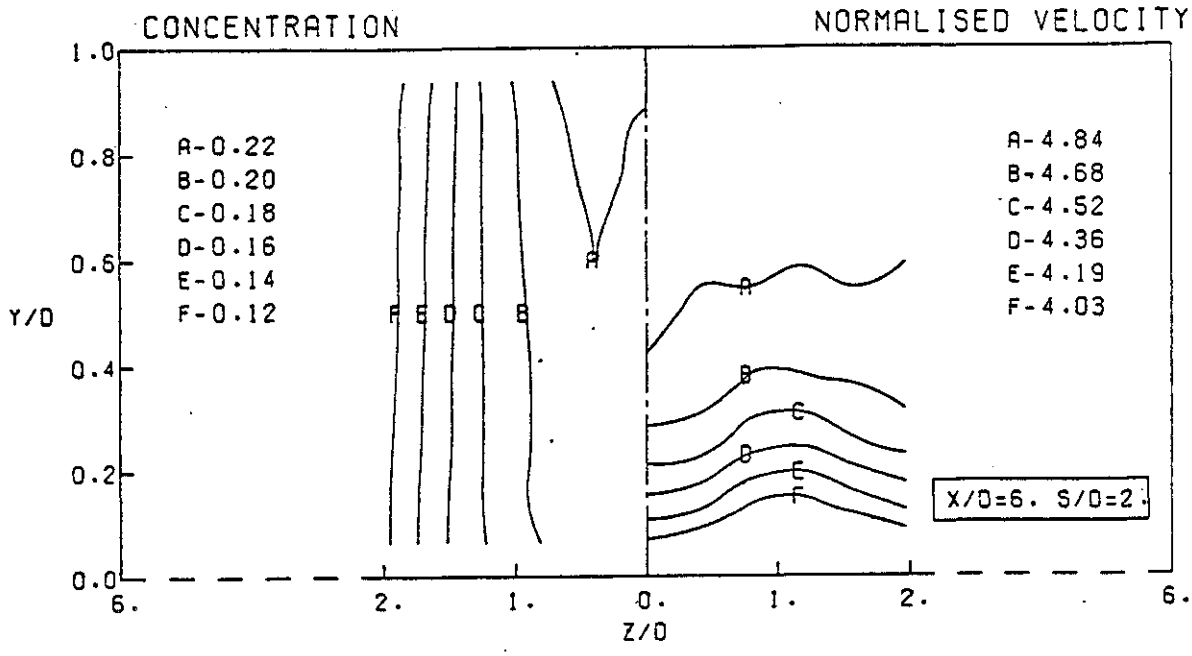
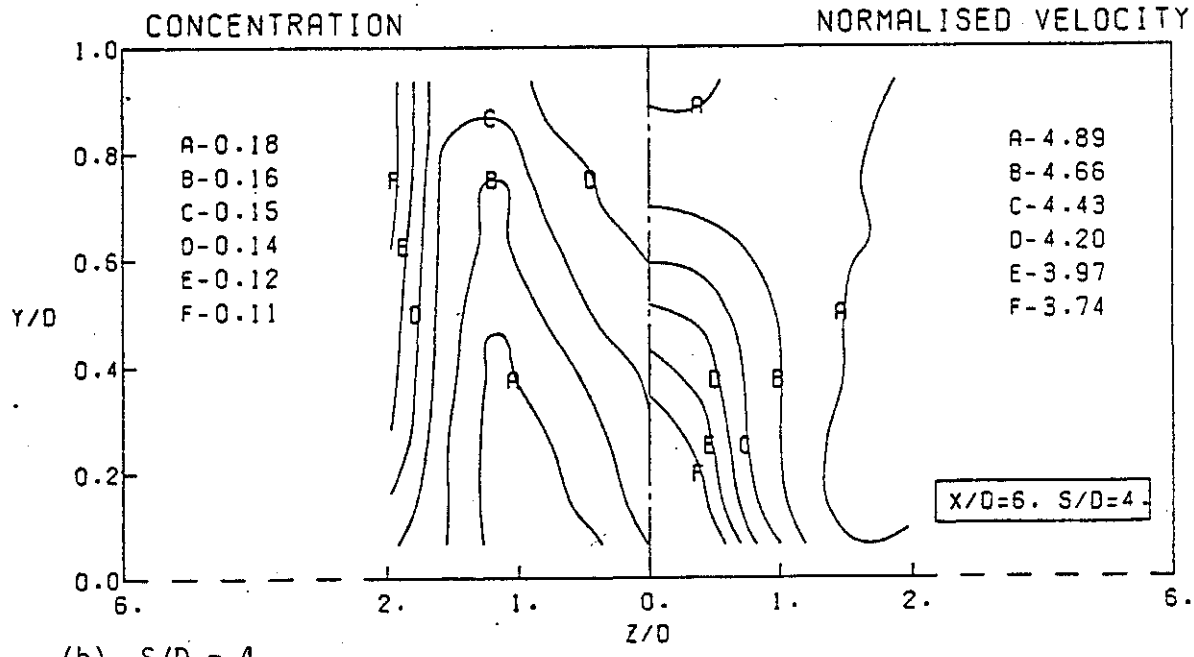


Figure 3.38: Normalised mean velocity and concentration contours at X/D = 6 for directly opposed jets with S/D of 4 and a downstream contraction (central floor jet seeded only)



(a) S/D = 2



(b) S/D = 4

Figure 3.39: Normalised mean velocity and concentration contours at X/D = 6 for the floor jets staggered laterlly and S/D of 2 and 4 with a downstream contraction (floor central jet seeded only)

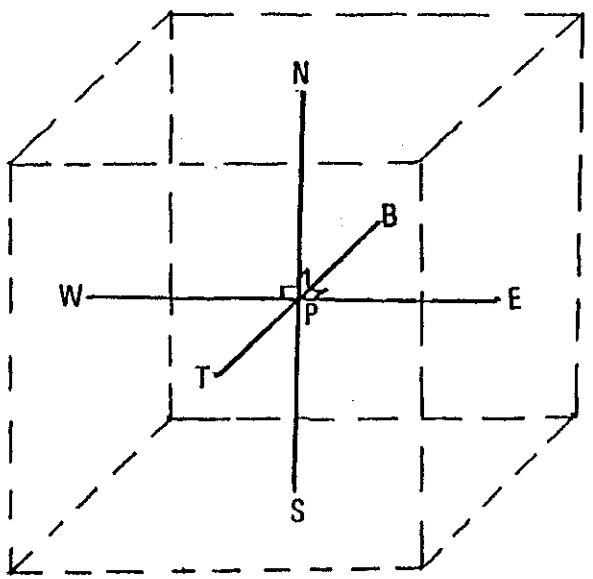


Figure 4.1: Three-dimensional control volume

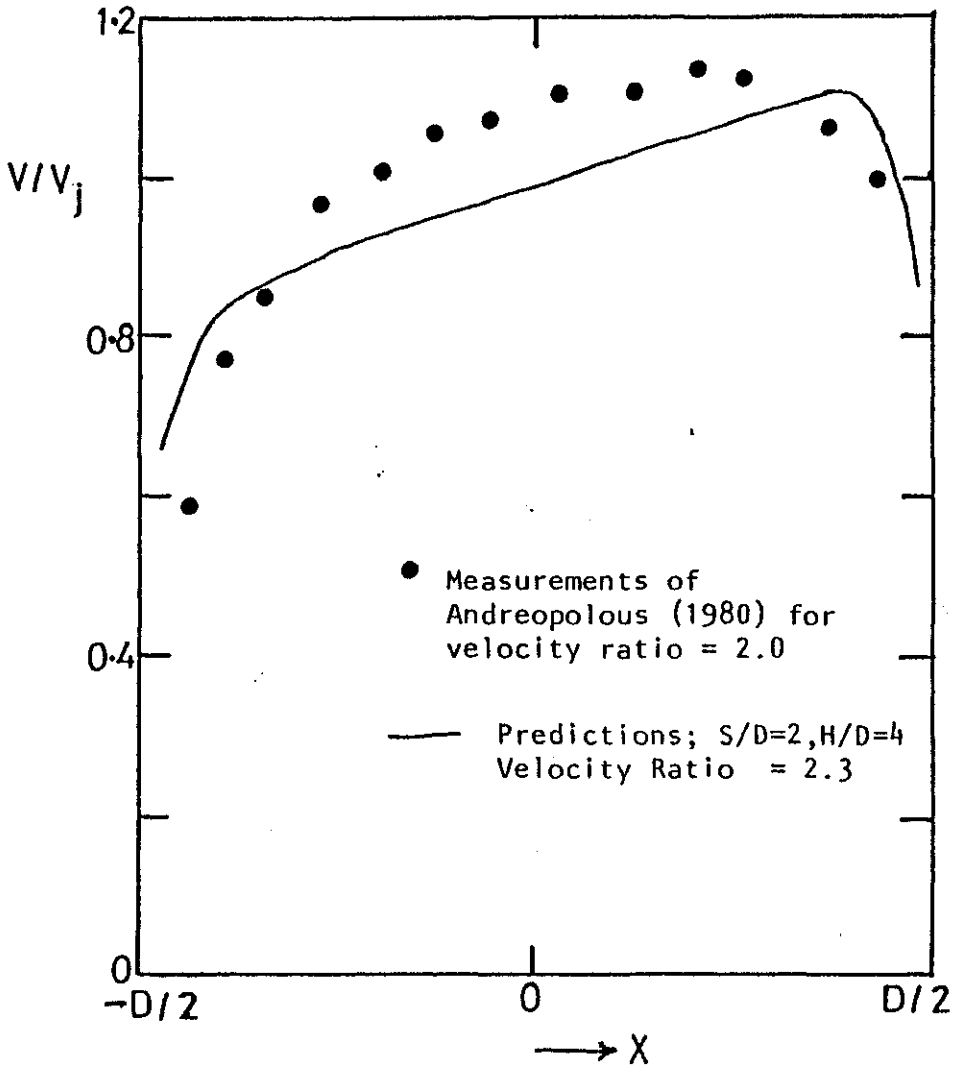


Figure 4.2: Jet exit velocity profile on centre-plane using constant total pressure condition

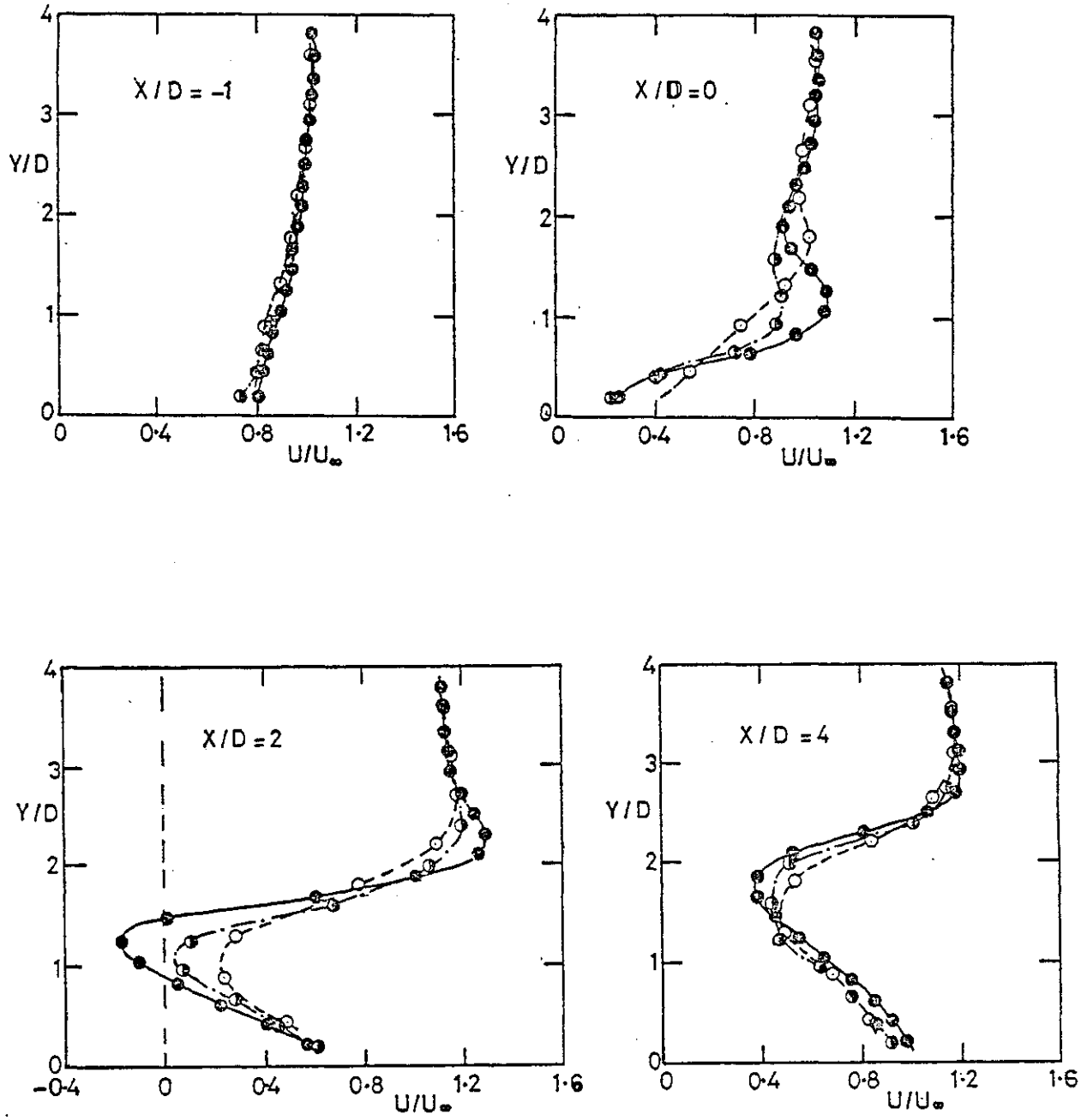


Figure 4.3: Tests for grid dependence
Centre-plane axial velocity profiles
—○— 10 x 10 x 20
—◑— 15 x 15 x 20
—●— 20 x 20 x 30

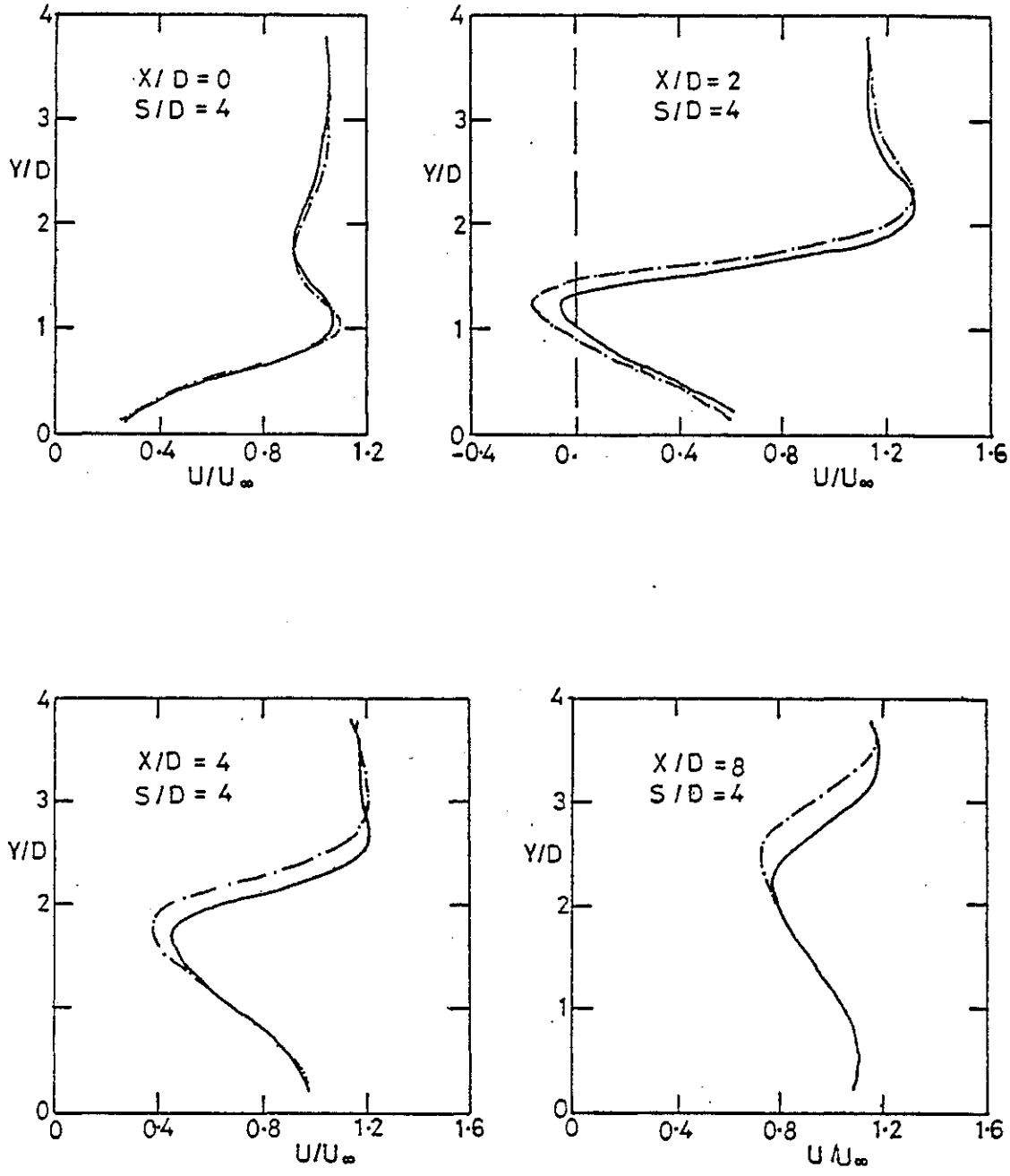


Figure 4.4: Effect of boundary conditions at jet exit, axial velocity profiles on centre-plane for H/D=4

— · — · — constant velocity, low turbulence intensity

——— constant total pressure, fully developed pipe flow turbulence intensity

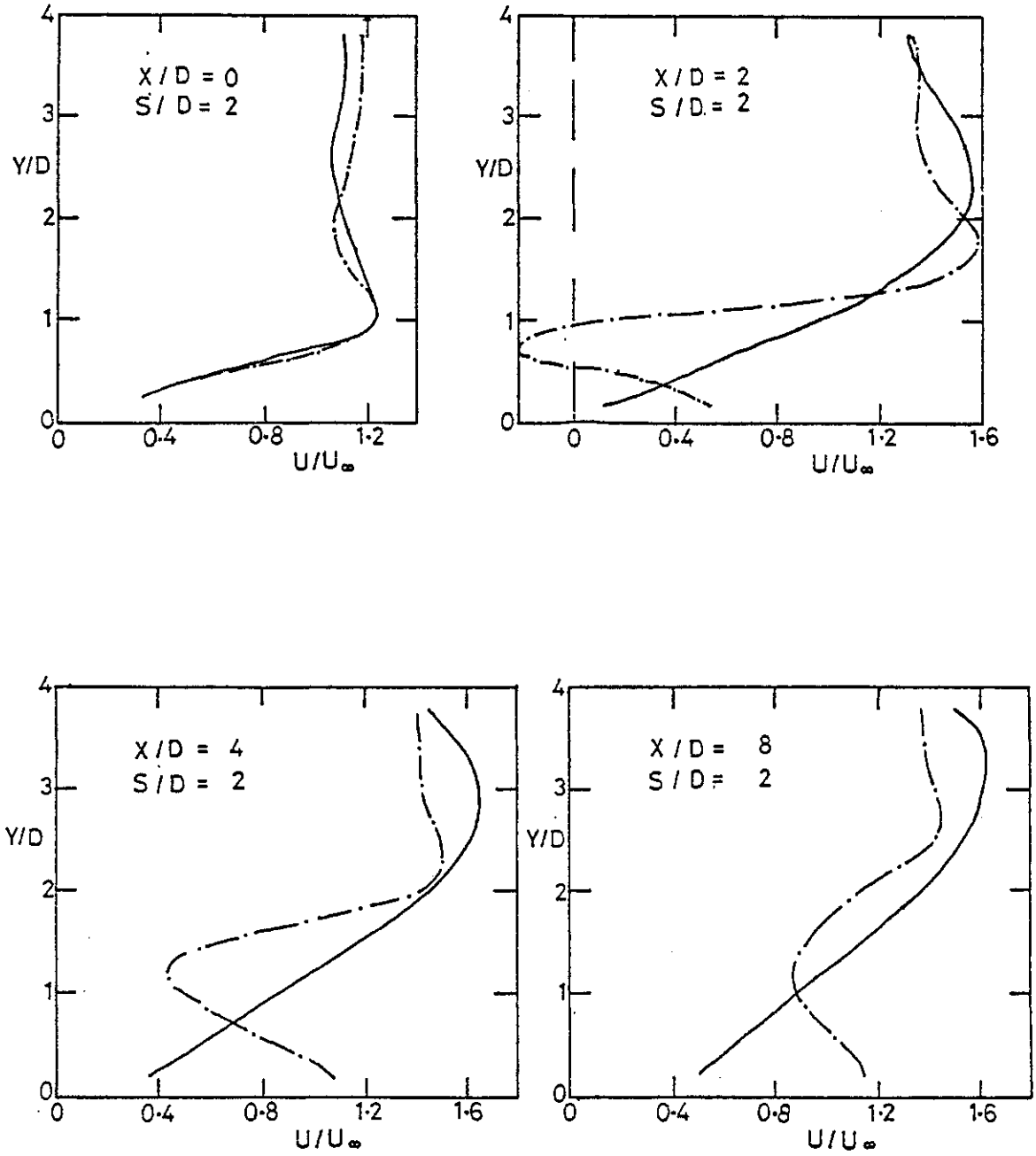


Figure 4.5(a): Effect of boundary condition at jet exit, axial velocity profiles on centre-plane (Z/D=0)

—·—·— constant velocity, low turbulence intensity

——— constant total pressure, fully developed pipe flow turbulence intensity

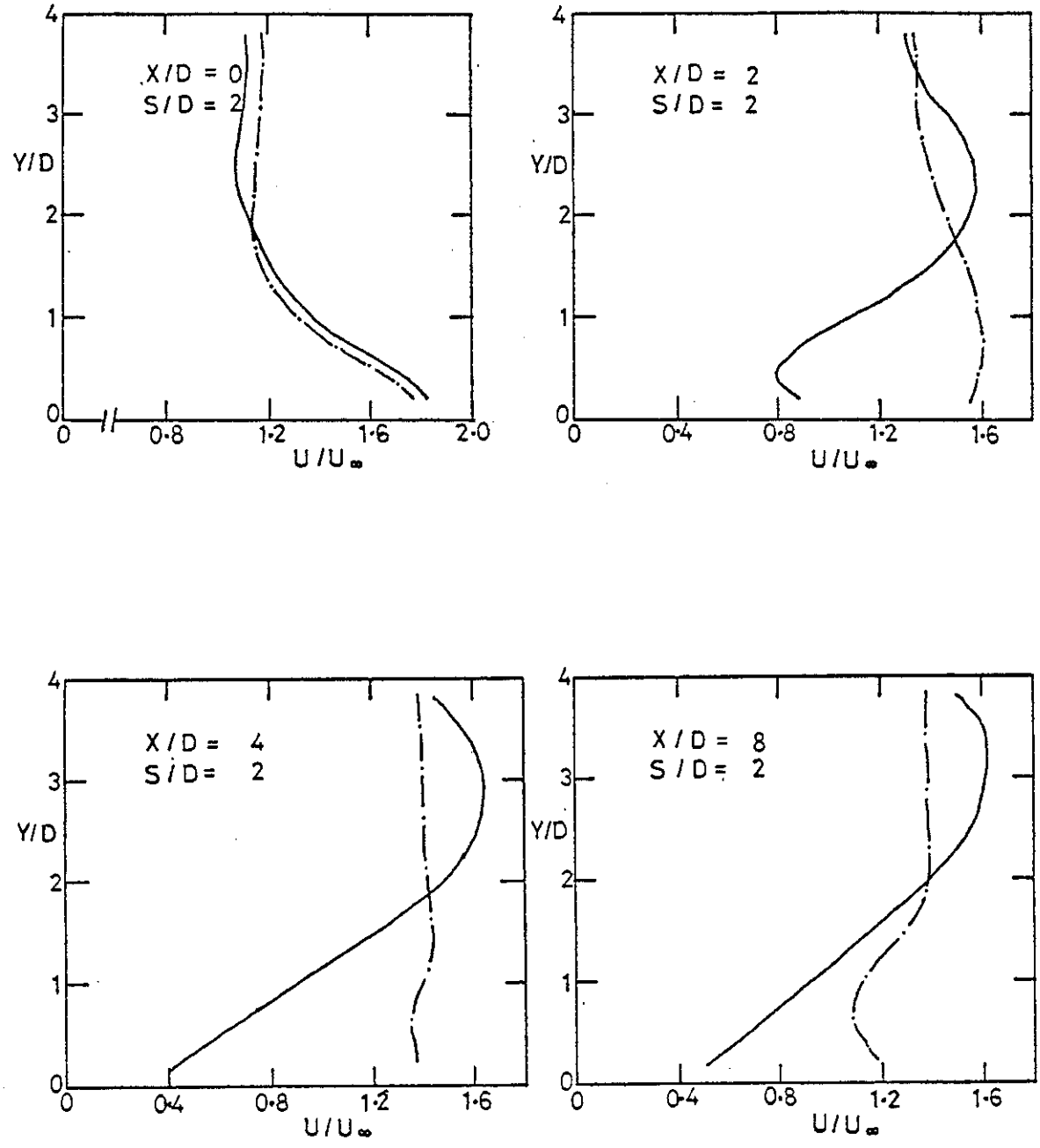


Figure 4.5(b): Effect of boundary conditions at jet exit; axial velocity profiles on mid-plane (Z/D=S/2)

——·——·—— constant velocity, low turbulence intensity

———— constant total pressure, fully developed pipe flow turbulence intensity

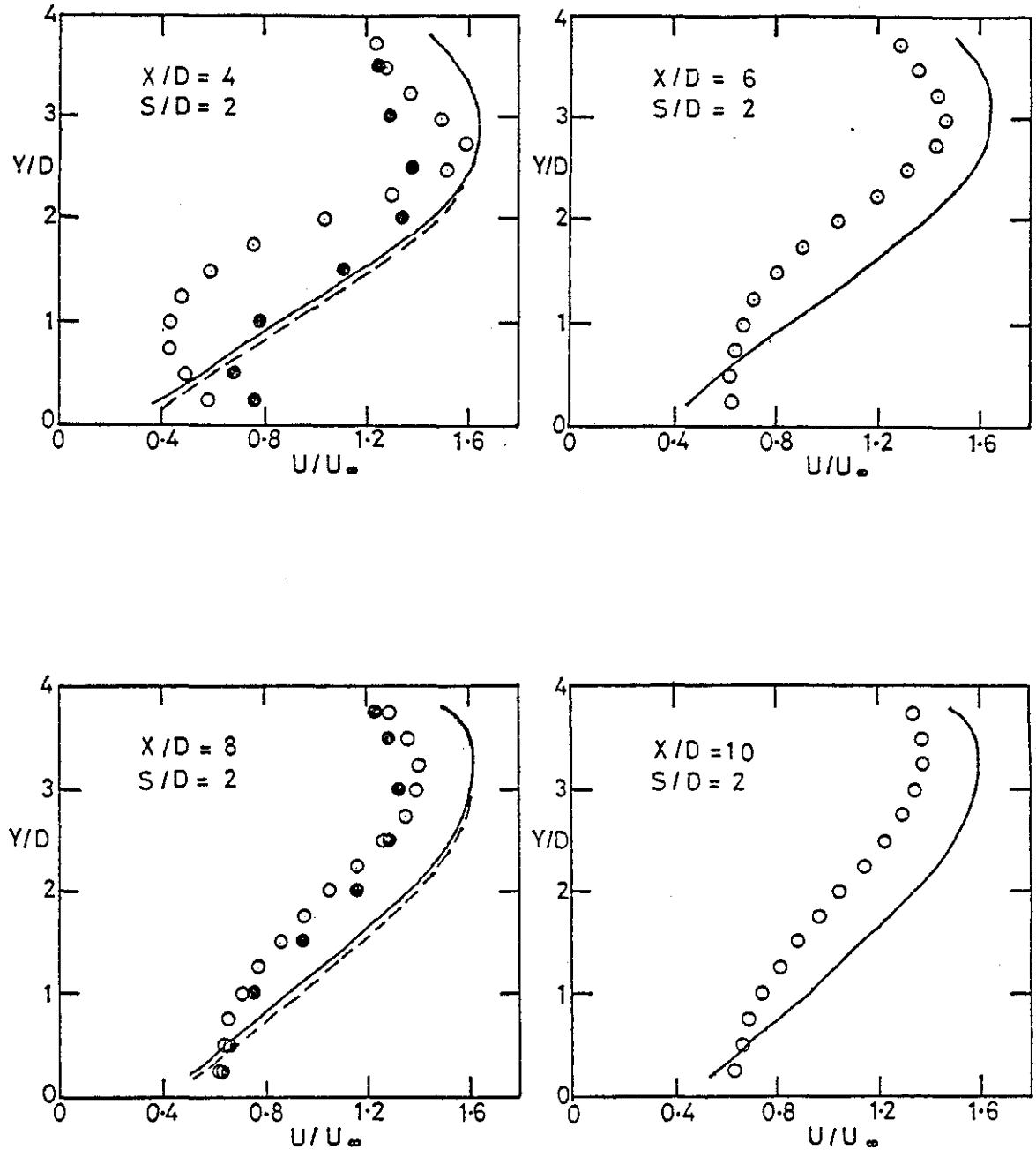


Figure 4.6 Velocity profiles along centre-plane and mid-plane for duct height 4D and jet spacing 2D

Centre-plane

○ measurements

——— predictions

Mid-plane

● measurements

– – – – predictions

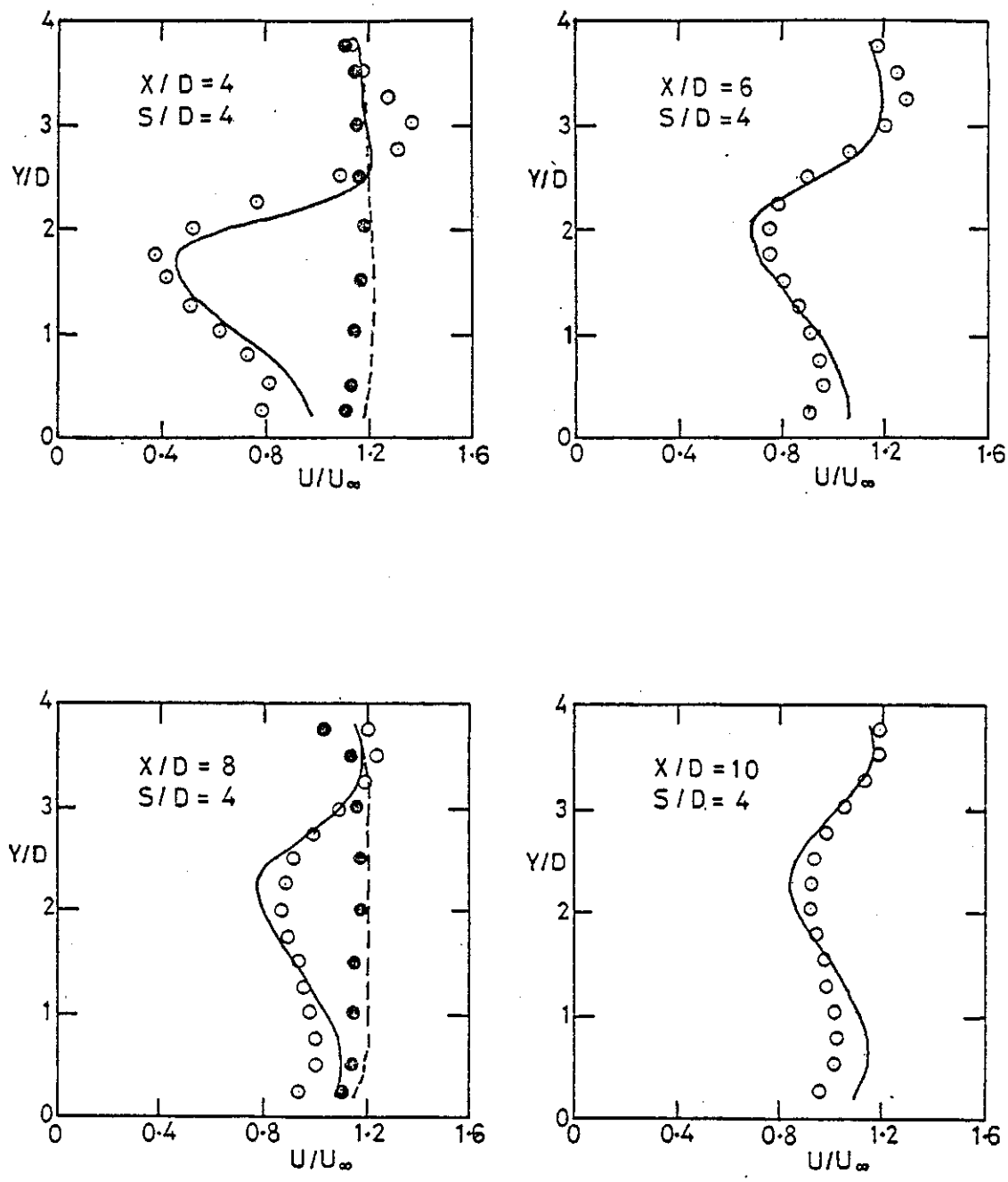


Figure 4.7: Velocity profiles along centre-plane and mid-plane for duct height 4D and jet spacing 4D

Centre-plane

○ measurements

——— predictions

Mid-plane

● measurements

– – – – predictions

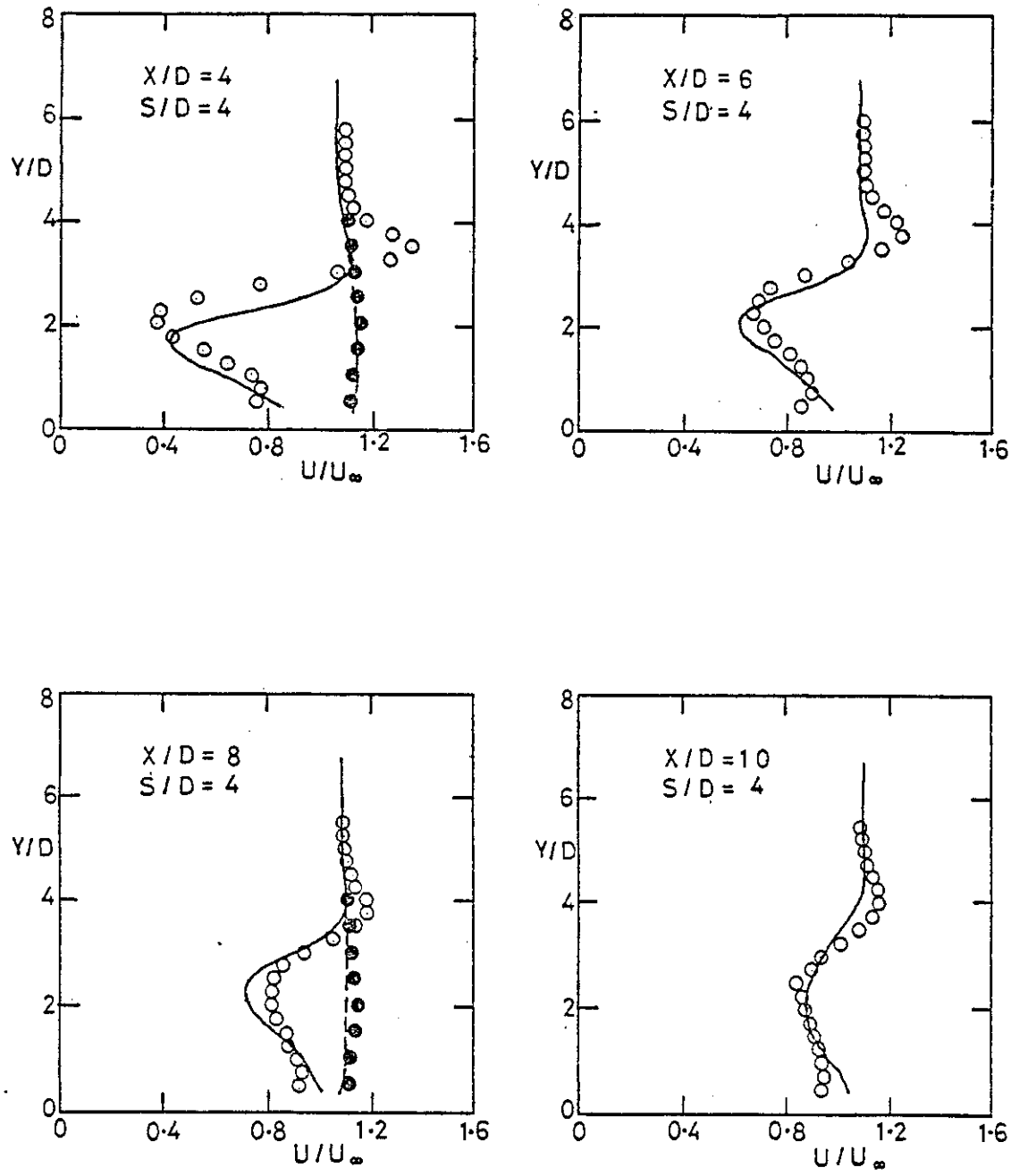


Figure 4.8: Velocity profiles along centre-plane and mid-plane for duct height 8D and jet spacing 4D

Centre-plane

○ measurements

——— predictions

Mid-Plane

● measurements

– – – – predictions

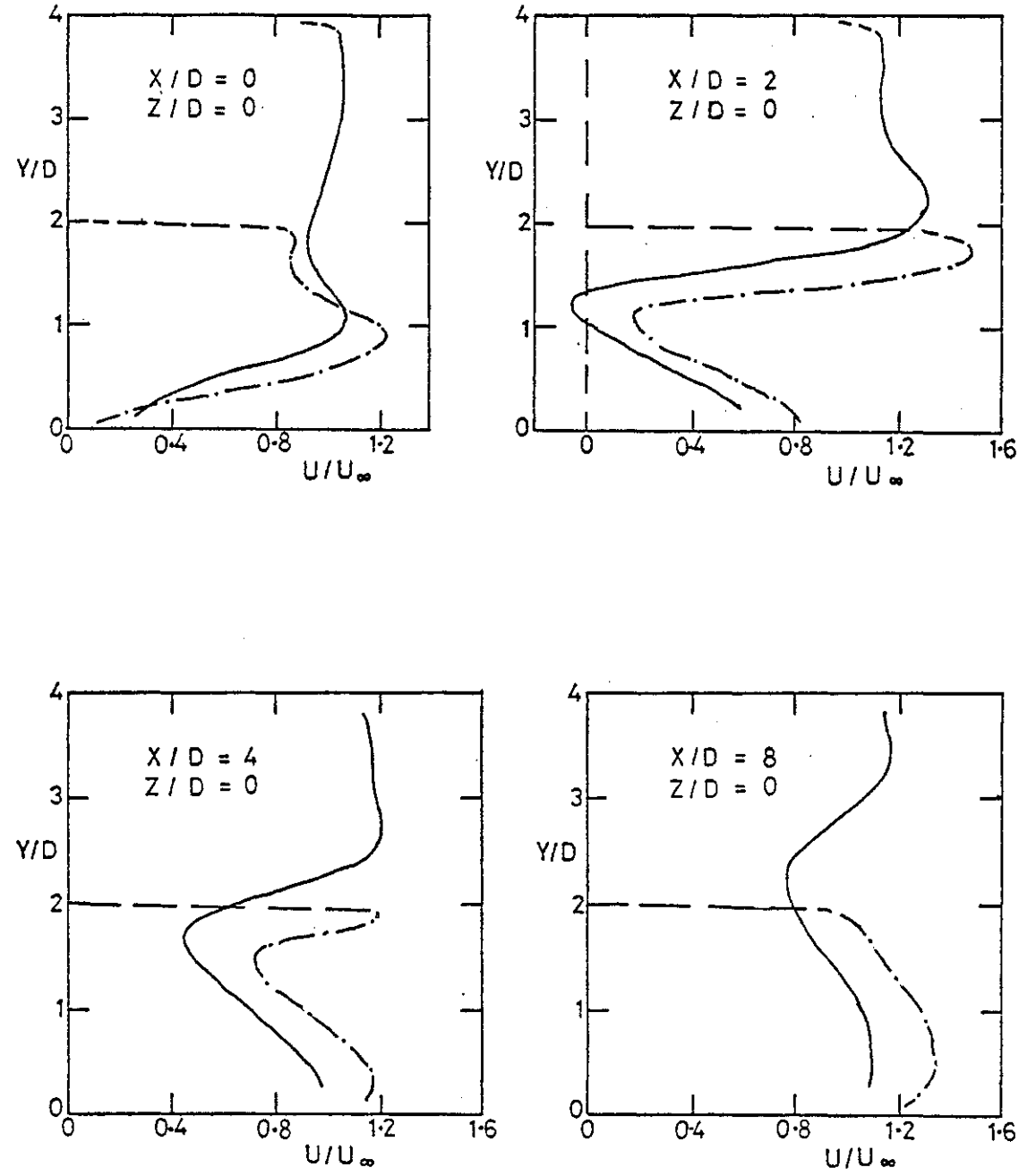


Figure 4.9(a): Axial velocity profiles on centre-plane for blockage ratios of 4 and 2

S/D=4 (——— H/D=4, —·—·— H/D=2)

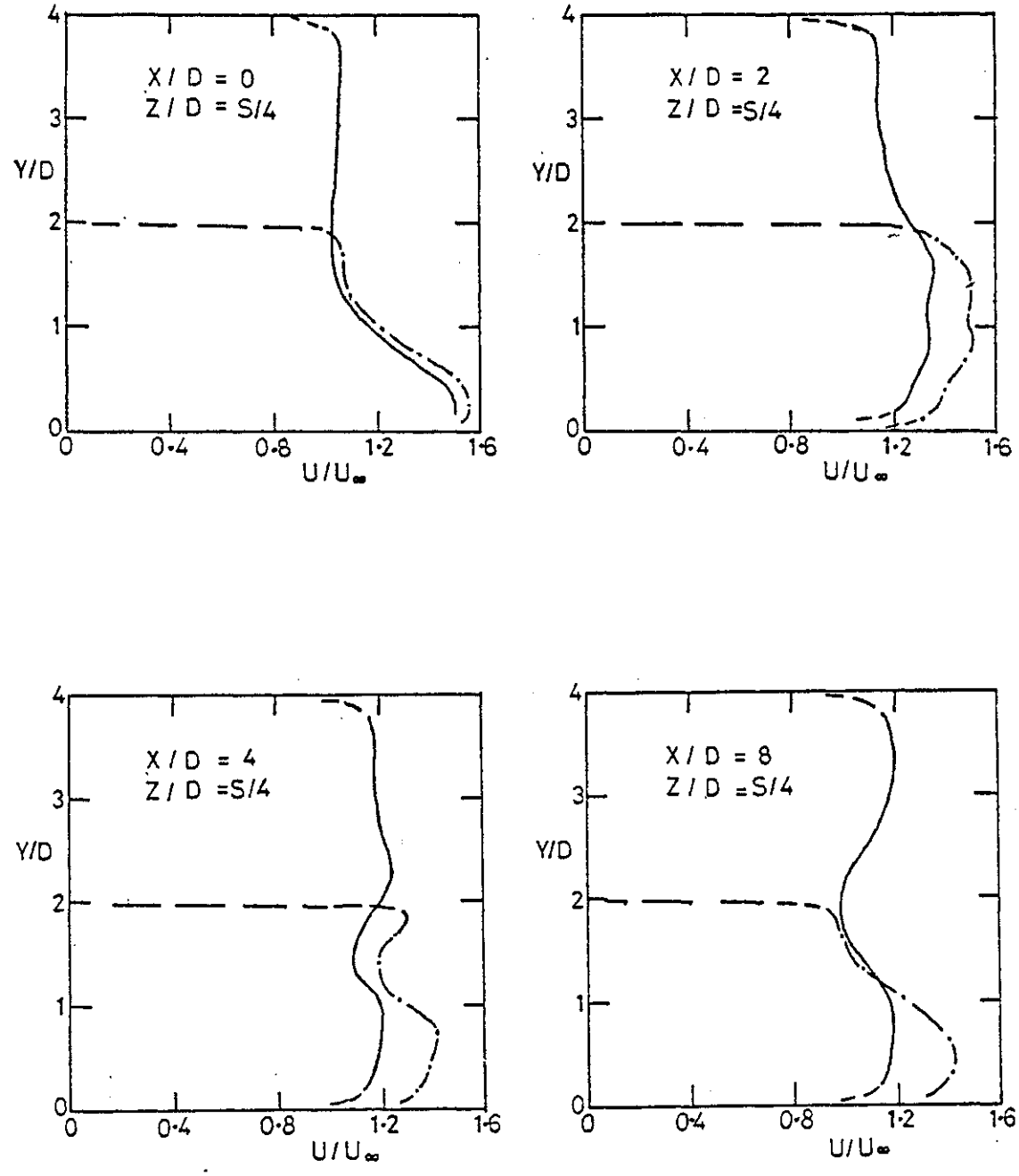


Figure 4.9(b): Axial velocity profile along Z/D=S/4 for blockage ratios of 4 and 2 with S/D=4

(——— H/D=4, —·—·— H/D=2)

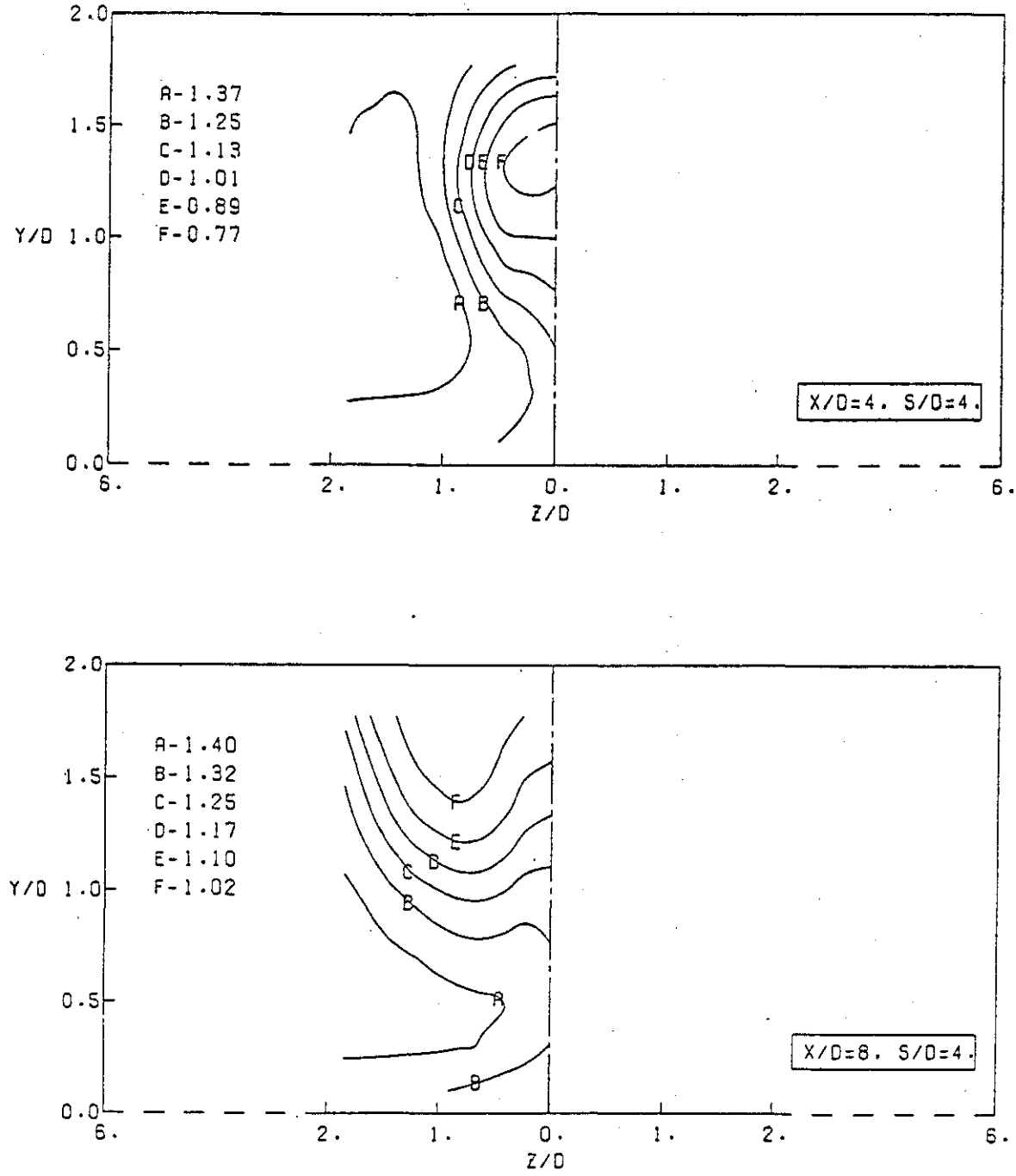


Figure 4.9(c): Velocity contours at axial positions X/D=4 and 8 for duct height 2D and pitch-to-diameter ratio 4

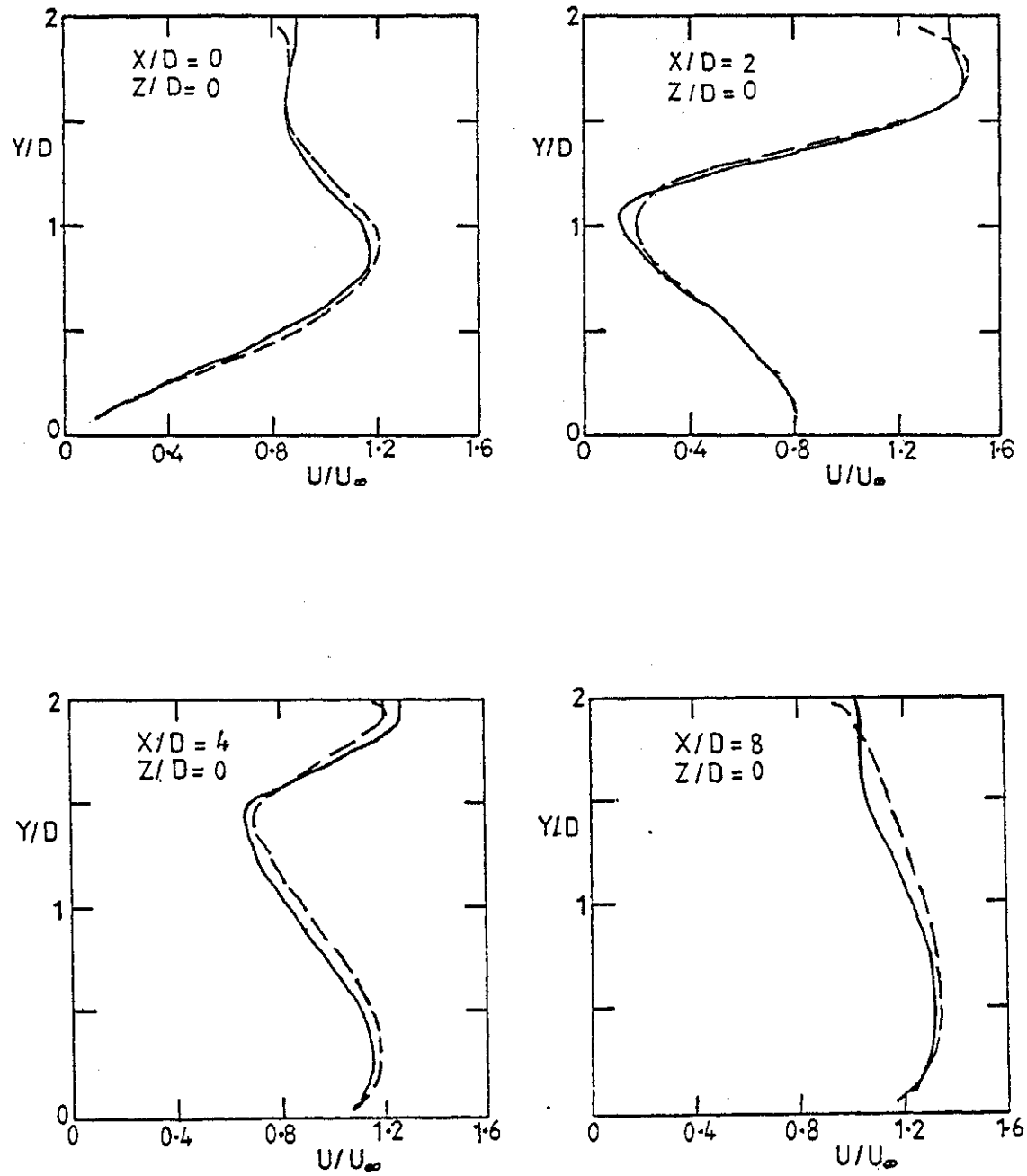


Figure 4.10(a): Axial velocity profiles on centre-plane for opposed rows of jets with H/D=4, S/D=4 and single row of jets with H/D=2 and S/D=4

(——— opposed rows, — — — single row)

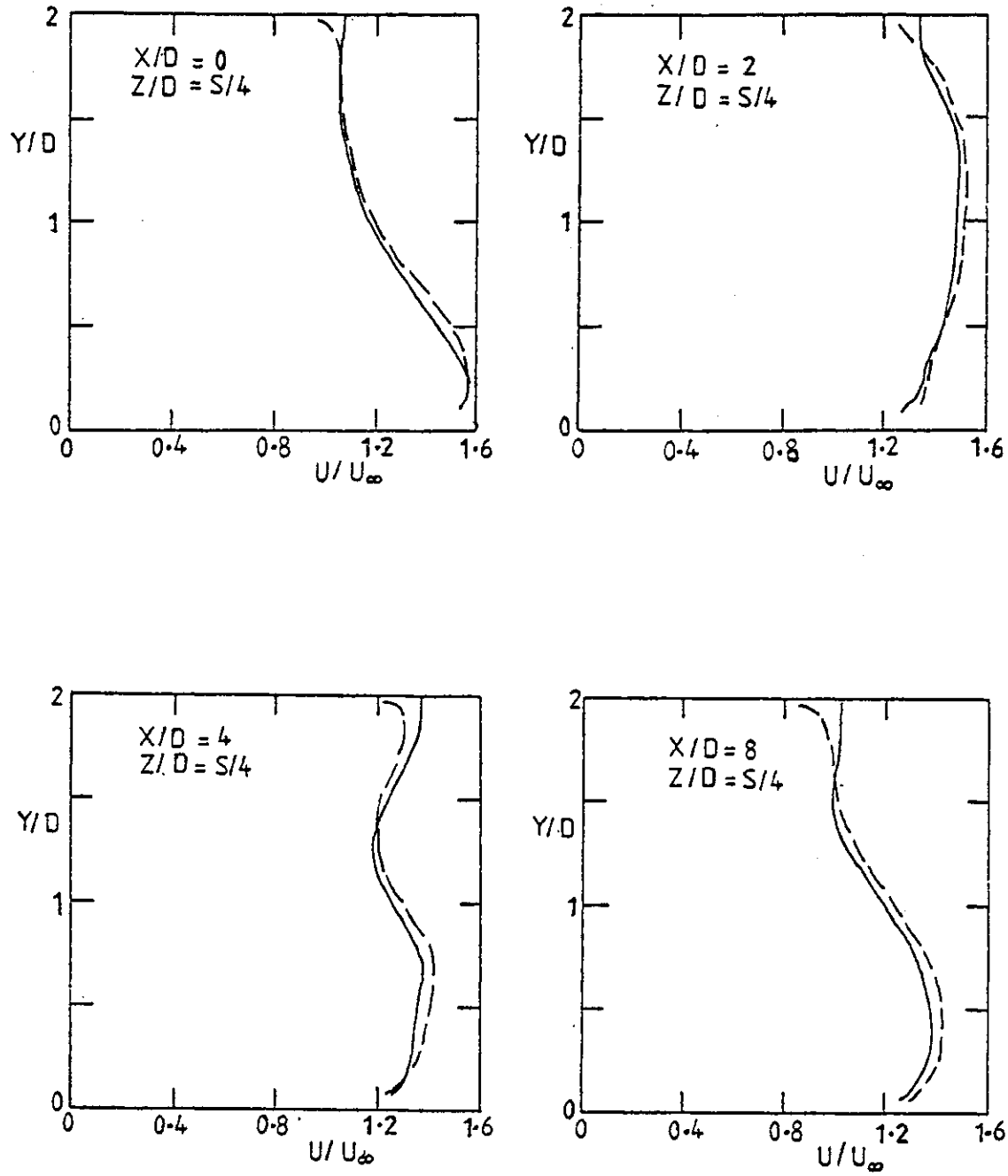


Figure 4.10(b): Axial velocity profiles along Z/D=S/4 for opposed rows of jets with H/D=4, S/D=4 and single row of jets with H/D=2 and S/D=4

(——— opposed row, — — — — single row)